AD-A118 324 NAVAL OCEAN SYSTEMS CENTER SAN DIEGO CA F/G 17/1
USE OF THEORETICAL CONTROLS IN UNDERWATER ACOUSTIC MODEL EVALUA--ETC(U)
JAN 82 M A PEDERSEN, R W MCGIRR
UNCLASSIFIED NOSC/TR-758 NL

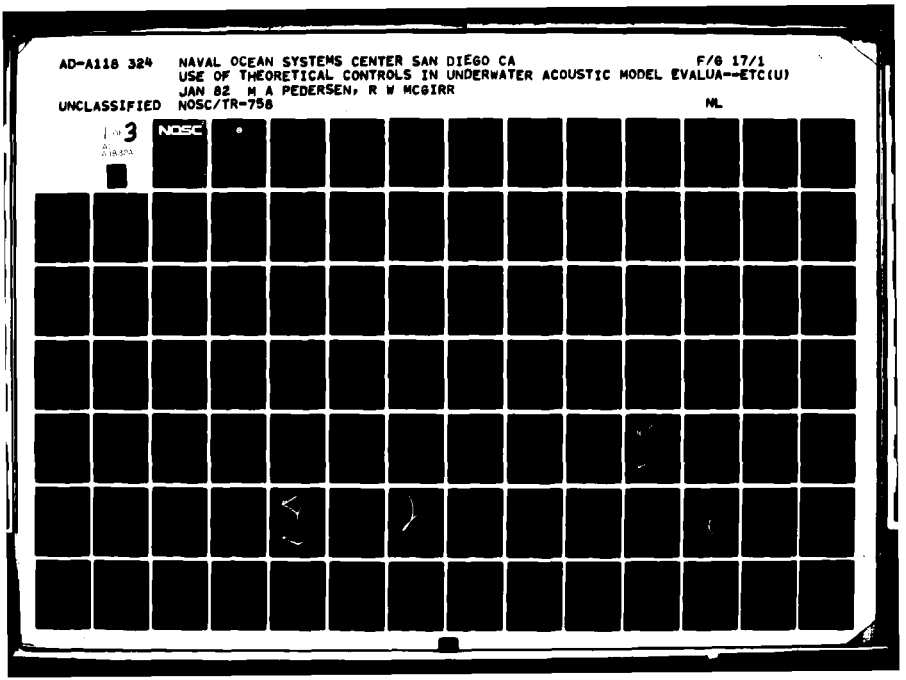

(12)

NOSC

NOSC TR 758

NOSC TR 758

Technical Report 758

USE OF THEORETICAL CONTROLS IN UNDERWATER ACOUSTIC MODEL EVALUATION

M. A. Pedersen
R. W. McGirr

4 January 1982

Prepared for
Naval Ocean Research and Development Activity
(NORDA Code 320)

Approved for public release; distribution unlimited

NAVAL OCEAN SYSTEMS CENTER
SAN DIEGO, CALIFORNIA 92152

NAVAL OCEAN SYSTEMS CENTER, SAN DIEGO, CA 92152

AN ACTIVITY OF THE NAVAL MATERIAL COMMAND

SL GUILLE, CAPT, USN
Commander

HL BLOOD
Technical Director

ADMINISTRATIVE INFORMATION

The work reported here was conducted under program element 63795N and project R0120-S4 (NOSC 724-SU48). The sponsoring activity was the Naval Ocean Research and Development Activity (NORDA Code 320). Funding was made possible jointly by SEA63D-5, NORDA 520, and NORDA 530 via the Acoustic Model Evaluation Committee (AMEC) under the auspices of OP-095E. This report covers work from October 1978 to October 1981.

Released by
M. R. Akers, Head
Systems Concepts and Analysis Division

Under authority of
E. B. Tunstall, Head
Surveillance Systems Department

ACKNOWLEDGMENT

The authors wish to acknowledge the contributions of D. F. Gordon, R. F. Hosmer, and D. White for the implementation of various test cases.

UNCLASSIFIED

SECURITY CLASSIFICATION OF THIS PAGE *(When Data Entered)*

REPORT DOCUMENTATION PAGE		READ INSTRUCTIONS BEFORE COMPLETING FORM
1. REPORT NUMBER NOSC Technical Report 758 (TR 758)	2. GOVT ACCESSION NO. AD-A11832	3. RECIPIENT'S CATALOG NUMBER 4
4. TITLE *(and Subtitle)* USE OF THEORETICAL CONTROLS IN UNDERWATER ACOUSTIC MODEL EVALUATION		5. TYPE OF REPORT & PERIOD COVERED October 1978—October 1981
		6. PERFORMING ORG. REPORT NUMBER
7. AUTHOR(s) M. A. Pedersen R. W. McGirr		8. CONTRACT OR GRANT NUMBER(s)
9. PERFORMING ORGANIZATION NAME AND ADDRESS Naval Ocean Systems Center San Diego CA 92152		10. PROGRAM ELEMENT, PROJECT, TASK AREA & WORK UNIT NUMBERS 63795N, R0120-S4, NOSC 724-SU48
11. CONTROLLING OFFICE NAME AND ADDRESS Naval Ocean Research and Development Activity (NORDA Code 320) NSTL Station MS 39529		12. REPORT DATE 4 January 1982
		13. NUMBER OF PAGES 189
14. MONITORING AGENCY NAME & ADDRESS*(if different from Controlling Office)*		15. SECURITY CLASS. *(of this report)* Unclassified
		15a. DECLASSIFICATION/DOWNGRADING SCHEDULE

16. DISTRIBUTION STATEMENT *(of this Report)*

Approved for public release; distribution unlimited

17. DISTRIBUTION STATEMENT *(of the abstract entered in Block 20, if different from Report)*

18. SUPPLEMENTARY NOTES

19. KEY WORDS *(Continue on reverse side if necessary and identify by block number)*

Underwater acoustics
Propagation modeling
Theoretical controls
Acoustic Model Evaluation Committee (AMEC)

20. ABSTRACT *(Continue on reverse side if necessary and identify by block number)*

This report supports the Acoustic Model Evaluation Committee (AMEC) by addressing one technique for the critical evaluation of underwater propagation models; ie, the use of theoretical test cases to assess model accuracy. Six advantages of a comparison with theoretical controls are discussed. Several critical environments have been identified where measurements and theory are lacking, and several unresolved theoretical questions are posed. Detailed results are presented for about 20 test cases, while definitive test environments are specified or outlined for more than 30 other test cases.

DD FORM 1 JAN 73 1473 EDITION OF 1 NOV 65 IS OBSOLETE
S/N 0102-LF-014-6601

UNCLASSIFIED

SECURITY CLASSIFICATION OF THIS PAGE *(When Data Entered)*

PROBLEM

Assist the Acoustic Model Evaluation Committee in the critical evaluation of underwater propagation models by establishing theoretical controls to test model accuracy. Specific objectives include the documentation of controls already developed, the development of new test cases, and the identification of critical propagation conditions about which little is known from either an experimental or a theoretical standpoint.

RESULTS

1. More than 50 different propagation environments are discussed. Detailed controls with results are presented for about 20 cases. In most of the remaining cases, the theoretical approaches are known but need to be implemented and investigated. In a few cases, the theoretical approach is not evident or requires extensive development.

2. Three critical controls were developed under AMEC funding: a normal mode control for convergence zone and shadow zone propagation at low frequency; a rigorous normal mode treatment of impedance boundaries; and an exact normal mode solution for range-dependent sound speed profiles. Although some results are presented here, the test cases were completed under other sponsorship and will be reported in more detail in other publications.

3. The most pressing requirement appears to be the implementation of an exact solution for a sloping bottom. There are several approximate approaches, but it is difficult to assess them without an exact solution for some simple test case.

4. Several propagation environments, about which little is known either from an experimental or a theoretical standpoint, have been identified.

5. Several fundamental questions about the general nature of theoretical solutions also have been raised. Some of these could be answered by control models; eg, Does the branch-line integral make a significant contribution when the bottom is an *absorbing* isospeed half space?

6. Six advantages of the use of test cases in model assessment have been identified and are discussed.

RECOMMENDATIONS

1. The model evaluation process should include a comparison of the model with appropriate theoretical test cases.

2. Various controls suggested here should be implemented as the need arises.

3. The use of controls should be extended to field properties other than propagation loss, which has been of primary concern here.

4. Controls should be developed by making use of techniques other than ray theory and normal mode theory.

5. The unanswered theoretical questions posed here should be resolved in an unequivocal manner.

6. Controls including other aspects of underwater acoustics (such as reverberation, noise, signal processing, etc) should be prepared.

7. After they have been prepared for environments where measurements are lacking, theoretical controls should be used to design critical experiments to determine whether the theory provides an adequate assessment of reality.

CONTENTS

ILLUSTRATIONS

TABLES

1.0 INTRODUCTION

This report has been prepared in support of the Acoustic Model Evaluation Committee (AMEC). The AMEC was chartered by OP-095E to establish a management structure and administrative procedure to evaluate underwater environmental acoustic models of propagation, noise, and reverberation. This report addresses one technique to be used in the critical evaluation of propagation models; ie, the use of theoretical test cases to assess model accuracy. Noise and reverberation test cases will not be treated here. The first step in evaluating a noise or a reverberation model is to test the propagation sub-model. Section 2.0 presents six reasons why models should be tested against theory, as opposed to the technique of comparing models with experimental data.

In addition to funding the preparation of this report, AMEC provided support for the preparation of three test cases of major importance. The first was the comparison of uniform asymptotic ray theory with normal mode theory (section 4.1.1) for convergence zone and shadow zone cases. The second was the development of a rigorous normal mode solution when the bottom boundary condition is specified as a complex reflection coefficient versus grazing angle (section 5.1.1). The third was the development of an exact normal mode solution for a sound speed profile which depends on both range and depth (section 7.1.4).

1.1 OBJECTIVES

The primary objective of this report is to prescribe a number of theoretical test cases which can be used to help evaluate environmental acoustic models. The report not only prescribes test cases (ie, critical environments), but also describes, where possible, theoretical solutions to test cases that can serve as controls against which models may be compared.

The most desirable control is an exact solution to an acceptable mathematical formulation. By 'exact', we mean that there are no mathematical approximations involved in arriving at the solution. Each theoretical approach stems from some fundamental equation. For example, normal mode theory represents a solution to the wave equation. This solution can be exact for certain sound speed profiles which depend only on depth. Geometrical ray theory represents a solution to the eikonal equation. Again, for certain sound speed profiles which depend only on depth, this solution can be exact.

Even though a method may be approximate, it may still represent an exact solution. For example, the eikonal equation is an approximation to the wave equation. Thus a normal mode solution is more accurate than a ray solution. Even though a method may be approximate, we want our control solutions to be as exact as possible. For example, a control solution for geometrical ray theory should be the most accurate solution possible as long as it satisfies some standard approximation (ie, the eikonal approximation to the wave equation).

For some control environments, we may present several solutions, each representing different standard approximations. In the case of ray theory, uniform asymptotics is a standard method which improves ray theory so that the wave equation is more nearly satisfied near caustic regions. The example of section 4.1.1 compares normal mode theory and three different standard ray theory approximations. There are also several standard approximations to normal mode theory for profile dependence on both depth and range.

Coupled mode theory represents a piecewise approximation for a profile dependence which varies continuously in depth and range. The adiabatic approximation is a further approximation to coupled mode theory in which the interaction between modes is neglected.

A second objective of this report is the comparison of different standard approximations. These comparisons allow one to determine the improvement in accuracy in going to a better approximation or the loss in accuracy in going to a worse approximation.

A third objective is to point out propagation conditions about which little is known from either an experimental or a theoretical standpoint. Examples are (1) the coupling between multiple ducts; and (2) convergence zone propagation for small depth excess.

A fourth objective is to persuade other investigators and sponsors to participate in the process of preparing control cases within their scope of interest. It will soon be apparent to the reader that this report raises as many new problems as it resolves old ones.

We invite participation at all levels of the process. Overlooked problem areas need to be specified. Some problem areas need to be investigated further. Exact solutions for proposed environments need to be determined. New control cases and new methods of solution need to be prepared. The scope of these tasks is clearly beyond AMEC resources. From our personal standpoint, the limited AMEC funding has served as an important catalyst pointing out a number of critical problem areas that we otherwise might have overlooked.

1.2 BACKGROUND

Our first use of theoretical models to test operational models dates back to the mid-1950s, when we used a focusing profile to test analogue ray tracing machines (section 3.1.3).

Our use of one theoretical model to check another theoretical model dates back to 1961. In reference 1 and in other articles that followed, the results of two ray-theory environments, which appeared similar but had different mathematical properties, were compared. The objective of some of these investigations was to expose artifacts inherent in simple sound speed profile models in common usage. These investigations demonstrated that some theoretical results did not represent a true property of ocean acoustics but were, in fact, due to a mathematical artifact of the assumed profile model. These artifacts were not the result of shortcomings of ray theory itself. We shall see other examples of the importance of modeling the environment, which is one source of error in the modeling process.

In reference 2 and other articles which followed, results of ray theory were compared to normal mode theory for an identical environment. This type of comparison between two models is a powerful tool and represents the basic approach of the present report. A good comparison under some conditions instills confidence in both models and differences under other conditions illustrate the degree of superiority of the better model. On the other hand, poor agreement indicates that at least one model is inferior or even defective.

---

1. Pedersen, M. A., Acoustic Intensity Anomalies Introduced by Constant Velocity Gradients, J Acoust Soc Am 33, 465-474, Apr 1961.
2. Pedersen, M. A., and D. F. Gordon, Normal-Mode Theory Applied to Short-Range Propagation in an Underwater Acoustic Surface Duct, J Acoust Soc Am 37, 105-118, Jan 1965.

Our first extensive use of theoretical control models was in 1971 with the development of nine distinct controls for testing RP-70, a computer program for propagation loss in use at that time by Fleet Numerical Weather Central at Monterey. These nine controls comprise the subject matter of section 3.0.

Other investigators at Navy Laboratories have used theoretical cases to test models. In 1973 Spofford, then of the Acoustic Environmental Support Detachment, selected three test cases for use in a workshop on acoustic propagation modeling (ref 3). The purpose was to provide common test cases for which some 17 different models were compared. Spofford's application differed from the approach in this report in that he used ocean environments rather than simplified environments and he did not provide the results of a control model.

The use of controls was also addressed at special sessions of the 87th Meeting of the Acoustical Society of America in April 1974, which presented advanced mathematical methods in underwater acoustic propagation. Blatstein of the Naval Ordnance Laboratory discussed the comparison of new methods with exact solutions or with previously validated methods (ref 4). Wood, then at the SACLANT ASW Research Center, discussed the comparison of computer models with exact solutions (ref 5). Indeed, Wood planned to prepare a report on the use of exact solutions. At his request, we mailed him some of our RP-70 test cases. Unfortunately, the material was sent by "slow boat" and did not arrive before he returned to the Naval Underwater Systems Center at New London. Wood apparently abandoned his plan to issue a report.

Thus the use of theoretical controls is not a new idea; indeed, the usefulness of test cases has been well established. Many of the aforementioned applications, however, have not been well documented. This report, then, documents a significant collection of test cases having known theoretical solutions and prescribes important test cases in need of theoretical solutions.

1.3 REPORT SUMMARY

Section 2.0 discusses the advantages of using controls. Section 3.0 presents in detail the control cases which were developed for testing the RP-70 model. Section 4.0 presents controls for nonbottom-reflected propagation including deep channel, surface ducts, and multiple ducts. Section 5.0 presents controls for bottom-reflected propagation with reflection coefficients specified or with sub-bottom structure specified. Section 6.0 discusses miscellaneous controls treating Murphy-Davis corrections, propagation below mode cutoff, and mode theory with doppler or special source functions. Section 7.0 presents controls for which the environment varies with range. Section 8.0 discusses acoustic properties other than propagation loss, which are desirable outputs of controls. Section 9.0 discusses models based on concepts other than ray theory or normal mode theory. Section 10.0 is a summary.

---

3. Spofford, C. W., A Synopsis of the AESD Workshop on Acoustic-Propagation Modeling by Non-Ray-Tracing Techniques, 22-25 May 1973, Washington, DC, Acoustic Environmental Support Detachment (AESD) TN-73-05, Nov 1973.
4. Blatstein, I. M., Evaluation of Methods for Comparing Propagation Models, J Acoust Soc Am 55S, S34 (A), Apr 1974.
5. Wood, D. H., Comparison of Models with Theoretical Examples, J Acoust Soc Am 55S, S44 (A), Apr 1974.

Most of the controls discussed in detail here are based on either ray theory or normal mode theory. These are commonly used methods and represent those with which the authors are most familiar. Other types of propagation models which might be useful for developing controls are discussed in section 8.2. The parabolic equation method and the fast field program are two of the methods which will be referred to on occasion.

Many of the detailed controls address only one characteristic of the acoustic fields: propagation loss. Some of the controls are limited to depth versus range trajectories of ray theory, since these represent important intermediate results. Ancillary outputs of other field characteristics (such as travel time, arrival angle, etc), which may be important for special applications, are discussed in section 8.0.

The discussion of specific controls for range-dependent environments is limited to section 3.2 and 7.0. In all other report sections, the environment is taken to be independent of range, with the exception of section 9.0, where some models can treat range-dependent environments. It should be pointed out also that the ray theory controls of section 7.0 are limited to ray tracing, or at best, propagation losses of geometrical ray theory. The application of uniform asymptotic or Murphy-Davis corrections to range-dependent environments is possible but somewhat difficult. Our controls have been chosen to isolate the effects of a single factor. The compounding of single factors, such as uniform asymptotics and range dependence, may not be simple and may require considerable effort.

The status of controls discussed here varies considerably. At one end of the scale, controls which have already been implemented and compared with other models are presented. In some cases, the comparison between the control and the model (RP-70) is given. At the other end of the scale, the discussion may be a vague statement on the desirability of a general type of control. In some cases, all that is necessary for the implementation of the control is available. In others, one or more critical elements are missing. Details of the theory may need to be worked out or the general theoretical approach may need to be developed. In some cases, the theory is available but we need more experience before we can prescribe a good control. Indeed, the preparation of this report has revealed several important propagation conditions about which little is known, even though the tools to investigate them have been available for some time. Among these are propagation characteristics of multiple ducts (section 4.3) and of convergence zones under marginal depth excess conditions (section 4.1.5).

This report is not meant to be all-inclusive. The scope of the effort limits the authors to a discussion of material with which they are readily familiar.

Detailed test cases are prescribed only for areas where we have direct knowledge. In other areas, we discuss only some of the general characteristics of controls, leaving the detailed prescription to other investigators more familiar with the subject area. Funds were not available to make an exhaustive survey of published results. This report undoubtedly has overlooked some good control cases, some theoretical approaches which could lead to controls, and some areas in need of good controls.

2.0 ADVANTAGES OF COMPARISONS WITH CONTROLS

The first question addressed by this report is: Why test models against theoretical controls rather than against experimental data which represent the real world? We first need to clarify that the use of theoretical controls is meant to complement the comparison against experimental data rather than to replace it. We next present a discussion of six advantages in testing models against theoretical controls.

2.1 ENVIRONMENTAL INPUTS ARE EXACT

In many cases, the failure of an acoustic model to reproduce experimental results can be attributed to problems with environmental inputs such as sound speed profiles, bathymetry, and sub-bottom characteristics. All too often, the accompanying environmental data are of poor quality compared to the acoustic data. In comparison with controls, no model is ever erroneously faulted because of inadequate input parameters. Moreover, if the model fails, the modeler cannot seek refuge in erroneous environmental inputs or classic environmental imponderables such as internal waves or thermal microstructure.

2.2 ACOUSTIC OUTPUTS ARE EXACT

Let's face it: errors do creep into experimental data. There are often source level problems and occasionally receiver system calibration problems. Source and receiver depths are often estimated and not really measured. There are errors in travel time measurements due to low resolution or recording pen parallax. Ranges are obtained by navigation methods of low reliability. The unexpected sources of error present the greatest problem and often remain undetected until glaring differences show up when the experimental data are compared to model results or to other experimental data.

Three examples, taken from the author's experience, illustrate such unexpected sources of error. These remain fixed in memory because of the analysis problems they caused. In one case that comes to mind, the symptom was excessively high propagation losses at short ranges where even a simple dipole model produces reasonable results. In this case two sources, one at 530 Hz and the other at 1030 Hz, were alternately pulsed. Later analysis showed that the switching equipment had malfunctioned and that the sources were switched properly but not the driver frequency, which remained at 530 Hz. Thus the 530-Hz data were correct. However, the 1030-Hz source, when driven at 530 Hz, oscillated at 1060 Hz. This received frequency was some 15 dB down on the skirts of the receiver system filters centered at 1030 Hz and produced the excessively high experimental propagation losses.

In a second sample, isoloss contours of experimental propagation loss as a function of receiver depth and range showed inexplicable anomalies. In this experiment, more than 20 receiver depths were employed with a spacing as close as 25 feet. Considerable diagnostic effort revealed that a technician had wired the receiver string improperly and had interchanged a shallow and a deep receiver. Thus the results of a deep receiver well below a surface channel had been contoured in with the low-loss results of other receivers in the surface channel, while the results of a shallow receiver in the surface duct had been contoured in with the high-loss results of the deep receivers. Since the difference in loss between in-channel and below-channel results was some 15 dB, there was clearly a problem.

In yet another example, comparisons between experiment and model showed a monotonically greater difference with increasing frequency and a progressively greater difference with time in a succession of acoustic events. The personnel who reduced the data finally became concerned when other independently obtained experimental data did not display similar characteristics. Subsequent investigation of the analogue tape recordings revealed that the tape drive had an instability which did not show up at the beginning of the tape and became progressively worse as the sea tests continued. The data were then reprocessed with a filter bandwidth wide enough to accommodate the tape drive instability. This reprocessing yielded propagation loss results which were comparable with both the models and the other independent experimental data.

These examples illustrate why we are somewhat conservative in accepting "novel" experimental results. Unless confirmed by theory or substantiated by independent measurements, there is a possibility that the result may be an experimental artifact.

All these problems of possible experimental errors are avoided when we compare model results with accurate theoretical controls.

2.3 OVERCOMES INADEQUATE EXPERIMENTAL DATA

There are cases where the experimental data do not cover a wide enough span in the variation of input parameters to allow meaningful comparisons with models. More specifically, measurements are often confined to a limited set of parameters, although our interest may extend to a wider range of values. For example, a model is verified by experimental results measured at, say, 100 Hz and we wish to assess the model at a frequency of 10 Hz. Theoretical controls are not inherently subject to such limitations and can be used to assess models over a much wider range of parameters (such as frequency, receiver and source depth, range, etc) than will ever be available in experimental data.

New propagation effects are sometimes first discovered as a result of theoretical investigation rather than of experimental measurement. In such cases, there may be a complete lack of critical experimental data. The frequencies of maximum interaction between multiple ducts, as discussed in section 4.3.2, is one of several theoretical results where we are unaware of any suitable experimental data.

2.4 SEPARATE EVALUATION OF VARIOUS FACTORS

There are many propagation factors which impact on a given experimental measurement. Unfortunately, many of these factors cannot be systematically varied in experiments, with the consequence that their causal relationships cannot be quantitatively established. This circumstance poses no problem if model results agree with experiment. But if they fail to agree, one has little idea of why the model failed or how the model might be improved to overcome the failure. However, theoretical controls can be used to test independently specific propagation phenomena to determine whether the model responds in a satisfactory manner. Simple theoretical test cases can be formulated to avoid a compounding of effects and to eliminate features which are irrelevant to the phenomena being tested. For example, a set of experimental data may be a composite of surface-channel, convergence zone, and bottom-reflected paths. It may involve complicated environments such as range-dependent sound speed profiles and complicated bathymetric and sub-bottom structures. To agree with experiment, the model may have to treat such

diverse propagation phenomena as refraction and diffraction effects, surface image interference, boundary layer effects, impedance bottom conditions, shear waves, or even sub-bottom penetration.

Fortunately, through the use of theoretical controls each of these factors can be assessed separately. A model cannot be expected to treat the composite conditions of experiment unless it can treat the critical constituent factors. In some cases, the interaction between constituent factors represents a critical feature of the propagation. Thus, in addition to controls for individual factors, we should develop controls which compound various factors to determine whether the models properly treat the combination.

2.5 EVALUATION WITH A HIERARCHY OF CONTROLS

The above remarks suggest the need for a hierarchy of controls which represent various degrees of theoretical sophistication. At the top of this hierarchy we have a wave theory control solution, which for our purposes represents ground truth. At the bottom of this hierarchy we have a control based on simple geometrical ray theory. In between these extremes lie a variety of controls based on various corrections to or extensions of geometrical ray theory. Some example corrections include: caustic boundary layer corrections using uniform asymptotics or its various approximations; a rigorous treatment of the phased combination of multipaths; the treatment of shadow zone fields by analytic continuation into the domain of complex ray parameters; and the use of Murphy-Davis corrections to rays vertexing near the ocean surface.

By matching a control to the level of theory used in modeling, one can determine whether the tested model lives up to its degree of theoretical sophistication. The control establishes an upper bound on how well the model can do. Moreover, various controls can be applied to establish a hierarchy of upper bounds on how well models of various theoretical complexity perform. By the use of controls we can, for example, estimate how much improvement there will be in a model if the theoretical approaches are improved.

2.6 UPDATE OF THE MODEL

Approaches used in the control may in some cases be used to update the model. If a control demonstrates that a model is significantly deficient in some aspect, the approach used in the control represents a potential update or replacement of the deficient aspect of the model subject to certain conditions. First, the new approach must fit within the framework of the model; eg, one cannot update a ray theory model with a wave theory control. Furthermore, execution time and storage requirements of the new approach must meet the model requirements. Finally, and most important, the control must have the flexibility of modeling real ocean conditions. This latter consideration is a primary reason why we cannot rely upon replacing models with the controls themselves.

3.0 CONTROL CASES FOR TESTING RP-70

From September 1971 to July 1973, NOSC [then the Naval Undersea Center (NUC)] was funded by ONR Code 102-OSC (LRAPP) to develop a maintenance program for the RP-70 model system. Although the objectives of this task were somewhat different from those of the present study under AMEC, most of the control cases are applicable. The results of this task have not been formally reported previously.

The RP-70 computer program was used by Fleet Numerical Weather Central at Monterey as a range-dependent ray model for predicting propagation loss. The objective of the task was to develop and supply a maintenance program to FNWC that would detect serious errors that might occur whenever a change was made to the RP-70 computer code. The maintenance program was to test adequately the RP-70 model subsequent to both small and significant changes, as well as to provide a second opinion when calculated propagation loss curves appeared unusual.

These objectives were to be accomplished by preparing diagnostic tests, providing detailed calculations for several deep ocean sound speed profiles, constructing exact solutions, and modifying various NUC programs to run on FNWC computers.

The initial deliverables were provided to the ONR Liaison Office for Acoustics at Monterey. For these test cases, RP-70 computations were made and were available for comparison with the NOSC tests and controls. About midway through the task, the Acoustic Environmental Support Detachment (AESD) was formed. The remaining deliverables were provided to AESD. There are no comparisons with RP-70 available for these tests.

During the course of the contract, it became apparent that the differences between the RP-70 calculations and the results of exact control solutions could be divided into two categories. Category 1 consists of differences caused by the use of linear segments to model the sound speed profiles. Category 2 consists of differences caused by RP-70 approximations (or possibly errors) in implementing the ray theory for linear segments. To evaluate these two categories, it was necessary to utilize the NUC linear control model. In this model, the sound speed profile is approximated by a series of layers in which the sound speed is a linear function of depth. This sound speed profile is used in RP-70 for the case of a range-independent environment.

The NUC linear model has the following description for the range traveled by any ray in each layer. For a layer with a gradient a_i

$$R_i = \frac{C_s}{\cos \theta_s} \frac{\sin \theta_i - \sin \theta_{i+1}}{a_i} \tag{1}$$

where C_s is the velocity at the source, θ_s is the angle at the source, θ_i and θ_{i+1} are the angles at the (upper and lower) interfaces of the layer and R_i is the horizontal range in the layer giving the computational form for each layer

$$R_i = \left[\left(C_m^2 - C_i^2 \right)^{1/2} - \left(C_m^2 - C_{i+1}^2 \right)^{1/2} \right] / a_i \tag{2}$$

where C_m is defined by

$$C_m = \frac{C_s}{\cos \theta_s} = \frac{C}{\cos \theta} \quad . \tag{3}$$

This form also holds for a layer in which the ray reaches either a zenith or a nadir as one of the terms in equation 2 becomes zero. The horizontal range of the ray is found by summing the incremental ranges in each layer.

The travel time counterpart of equation 2 is

$$T_i = \left\{ \ln \frac{\left[C_m + \left(C_m^2 - C_i^2\right)^{1/2}\right]}{C_i} - \ln \frac{\left[C_m + \left(C_m^2 - C_{i+1}^2\right)^{1/2}\right]}{C_{i+1}} \right\} / a_i \quad . \tag{4}$$

These equations were in all nine different controls developed for testing the RP-70. Five controls relate to range-independent environments and are discussed in section 3.1. Four controls relate to range-dependent environments and are discussed in section 3.2. All of these controls are based strictly on ray theory. Some controls address only range and travel times. Others address ray intensities and propagation loss as well.

3.1 CONTROLS FOR RANGE-INDEPENDENT ENVIRONMENTS

This section describes controls where the sound speed depends only on depth and the bottom is flat. Sections 3.1.1, 3.1.2, and 3.1.3 present test cases for which FNWC results are available for comparison with the controls. Section 3.1.4 is a summary of section 3.1.1 to 3.1.3. Sections 3.1.5 and 3.1.6 present two other controls with range-independent environments for which FNWC results are not available.

3.1.1 Three Typical Ocean Profiles

In the first example of controls, comparisons of range and travel time were made between the NUC linear control model and RP-70 for three typical ocean profiles with no horizontal changes in sound speed.

The three profiles selected by Fleet Numerical Weather Center are listed in tables 1, 2, and 3. The source and receiver depths used for all calculations were 60 ft and 300 ft, respectively. Results for only the downgoing rays at source and receiver are given. Results for other ray paths were comparable to those given here. The rays were terminated after nine bottom reflections or after reaching a maximum range specified for each profile.

Table 4 gives the range results for the profile of table 1 for 1° increments of source angle starting with 3.5°. Rays with a smaller angle are not given because of an RP-70 program requirement that rays whose maximum depth excursion is less than 225 m be excluded from further calculation. The second column of table 4 presents the range for the linear control, the third column presents the range for the RP-70 model, the fourth column presents the difference between the second and third column, and the fifth column presents 100 times column four divided by column two. Corresponding range results for the profiles of tables 2 and 3 are given in tables 5 and 6. Corresponding travel time results for all three profiles are given in tables 7 to 9. Values are tabulated only for certain source angles. At steeper angles, the results for the linear and RP-70 models were identical (to the number of digits provided by RP-70).

The horizontal line across tables 4 to 9 separate the rays which reflect from the ocean bottom from those low-angle rays which do not. Consider first the range differences for rays which do not reflect from the ocean bottom (table entries above the horizontal line). The largest difference is 0.05451%, which occurs in table 6 for the 5° angle. The second largest difference is -0.03862%. The differences may be either positive or negative, although the positive values predominate.

DEPTH (m)	VELOCITY (m/s)
0.00	1513.53
18.29	1513.63
80.00	1514.84
90.00	1512.40
91.44	1512.19
100.00	1510.94
140.00	1504.69
180.00	1499.56
200.00	1497.23
220.00	1495.54
240.00	1494.55
300.00	1490.71
400.00	1483.29
500.00	1486.46
800.00	1484.30
1200.00	1488.72
2000.00	1492.85
2200.00	1495.39
3000.00	1508.36
4000.00	1525.50
4207.00	1529.16

BOTTOM DEPTH 4286 m

Table 1. Sound speed profile for area 01, winter.

DEPTH (m)	VELOCITY (m/s)
0.00	1542.35
18.29	1542.65
29.00	1542.83
60.00	1537.62
91.44	1530.67
146.00	1519.07
180.00	1514.68
210.00	1510.55
250.00	1506.33
400.00	1495.49
480.00	1492.32
800.00	1485.16
1500.00	1486.50
2500.00	1500.10
3841.00	1522.96

BOTTOM DEPTH 3840 m

Table 2. Sound speed profile for area 12D, summer.

DEPTH (m)	VELOCITY (m/s)
0.00	1505.89
18.29	1506.21
91.44	1507.51
150.00	1508.57
300.00	1512.86
400.00	1514.29
500.00	1516.84
560.00	1516.61
600.00	1516.95
900.00	1519.95
1100.00	1523.19
1500.00	1529.75
2701.00	1549.95

BOTTOM DEPTH 2700 m

Table 3. Sound speed profile for area 60, summer.

	ANGLE (deg)	RANGE (kyd) LINEAR	RANGE (kyd) RP70	DIFFERENCE (kyd)	PERCENT ERROR
	3.5	245.134	245.067	0.067	0.02733
	4.5	243.184	243.115	0.069	0.02837
	5.5	243.549	243.476	0.073	0.02997
	6.5	245.470	245.391	0.079	0.03218
	7.5	247.616	247.581	0.035	0.01413
Bottom-	8.5	271.599	271.542	0.057	0.02099
Reflected	9.5	237.150	237.103	0.047	0.01982
Region	10.5	258.082	258.033	0.049	0.01899
	11.5	237.527	237.482	0.045	0.01895
	12.5	257.131	257.084	0.047	0.01828
	13.5	240.034	239.991	0.043	0.01791
	14.5	257.174	257.128	0.046	0.01789
	15.5	272.210	272.162	0.048	0.01763
	16.5	256.911	256.866	0.045	0.01752
	17.5	243.094	243.052	0.042	0.01728
	18.5	230.536	230.496	0.040	0.01735
	19.5	219.061	219.024	0.037	0.01689
	20.5	208.527	208.492	0.035	0.01678
	21.5	198.817	198.784	0.033	0.01660
	22.5	189.834	189.802	0.032	0.01686
	23.5	181.493	181.463	0.030	0.01653
	24.5	173.726	173.698	0.028	0.01612
	25.5	166.472	166.445	0.027	0.01622
	26.5	159.679	159.653	0.026	0.01628

Table 4. Range results for the profile of table 1.

	ANGLE (deg)	RANGE (kyd) LINEAR	RANGE (kyd) RP70	DIFFERENCE (kyd)	PERCENT ERROR
	27.5	153.302	153.277	0.025	0.01631
	28.5	147.300	147.276	0.024	0.01629
	29.5	141.640	141.617	0.023	0.01624
	30.5	136.290	136.268	0.022	0.01614
	31.5	131.223	131.202	0.021	0.01600
	32.5	126.416	126.395	0.021	0.01661
	33.5	121.846	121.826	0.020	0.01641
	34.5	117.494	117.475	0.019	0.01617
	35.5	113.343	113.324	0.019	0.01676
	36.5	109.377	109.359	0.018	0.01646
	37.5	105.583	105.566	0.017	0.01610
	38.5	101.947	101.931	0.016	0.01569
	39.5	98.458	98.442	0.016	0.01625
	40.5	95.106	95.091	0.015	0.01577
	41.5	91.880	91.866	0.015	0.01524
	42.5	88.773	88.759	0.014	0.01577
	43.5	86.777	85.763	0.014	0.01632
	44.5	82.883	82.869	0.014	0.01689
	45.5	80.085	80.072	0.013	0.01623
Bottom-	46.5	77.377	77.365	0.012	0.01551
Reflected	47.5	74.753	74.742	0.011	0.01472
Region	48.5	72.209	72.197	0.012	0.01662
	49.5	69.738	69.727	0.011	0.01577
	50.5	67.337	67.327	0.010	0.01485
	51.5	65.002	64.992	0.010	0.01538
	52.5	62.728	62.718	0.010	0.01594
	53.5	60.511	60.502	0.009	0.01487
	54.5	58.349	58.340	0.009	0.01542
	55.5	56.239	56.230	0.009	0.01600
	56.5	54.176	54.168	0.008	0.01477
	57.5	52.159	52.151	0.008	0.01534
	58.5	50.185	50.177	0.008	0.01594
	59.5	48.251	48.243	0.008	0.01658
	60.5	46.355	46.348	0.007	0.01510
	61.5	44.495	44.488	0.007	0.01573
	62.5	42.669	42.662	0.007	0.01641
	63.5	40.875	40.868	0.007	0.01713
	64.5	39.110	39.104	0.006	0.01534
	65.5	37.374	37.368	0.006	0.01605
	66.5	35.665	35.659	0.006	0.01682
	67.5	33.980	33.975	0.005	0.01471
	68.5	32.319	32.314	0.005	0.01547
	69.5	30.680	30.675	0.005	0.01630
	70.5	29.061	29.057	0.004	0.01376
	71.5	27.462	27.458	0.004	0.01457
	72.5	25.881	25.877	0.004	0.01546

Table 4. Range results for the profile of table 1 (continued).

	ANGLE (deg)	RANGE (kyd) LINEAR	RANGE (kyd) RP70	DIFFERENCE (kyd)	PERCENT ERROR
Bottom-Reflected Region	73.5	24.317	24.313	0.004	0.01645
	74.5	22.769	22.765	0.004	0.01757
	75.5	21.235	21.231	0.004	0.01884
	76.5	19.714	19.711	0.003	0.01522
	77.5	18.206	18.203	0.003	0.01648
	78.5	16.709	16.706	0.003	0.01795
	79.5	15.222	15.220	0.002	0.01314
	80.5	13.745	13.743	0.002	0.01455
	81.5	12.276	12.274	0.002	0.01629
	82.5	10.814	10.813	0.001	0.00925
	83.5	9.359	9.358	0.001	0.01069
	84.5	7.910	7.909	0.001	0.01264
	85.5	6.465	6.464	0.001	0.01547
	86.5	5.025	5.024	0.001	0.01990
	87.5	3.587	3.586	0.001	0.02788
	88.5	2.151	2.151	0.000	0.00000

Table 4. Range results for the profile of table 1 (continued).

	ANGLE (deg)	RANGE (kyd) LINEAR	RANGE (kyd) RP70	DIFFERENCE (kyd)	PERCENT ERROR
	1	165.229	165.173	0.056	0.03389
	2	154.185	154.154	0.031	0.02011
	3	148.507	148.480	0.027	0.01818
	4	143.585	143.560	0.025	0.01741
	5	138.773	138.749	0.024	0.01729
	6	133.927	133.905	0.022	0.01643
	7	161.165	161.137	0.028	0.01737
	8	155.074	155.048	0.026	0.01677
	9	149.040	149.015	0.025	0.01677
Bottom-Reflected Region	10	143.117	143.093	0.024	0.01677
	11	137.350	137.327	0.023	0.01675
	12	131.770	131.749	0.021	0.01594
	13	151.616	151.591	0.025	0.01649
	14	145.447	145.423	0.024	0.01650
	15	139.553	139.530	0.023	0.01648
	16	133.935	133.913	0.022	0.01643
	17	149.978	149.954	0.024	0.01600
	18	144.052	144.029	0.023	0.01597
	19	138.423	138.400	0.023	0.01662
	20	133.077	133.055	0.022	0.01653
	21	146.256	146.233	0.023	0.01573
	22	140.746	140.723	0.023	0.01634
	23	135.510	135.488	0.022	0.01623

Table 5. Range results for the profile of table 2.

	ANGLE (deg)	RANGE (kyd) LINEAR	RANGE (kyd) RP70	DIFFERENCE (kyd)	PERCENT ERROR
	24	130.530	130.510	0.020	0.01532
	25	141.496	141.473	0.023	0.01626
	26	136.421	136.399	0.022	0.01613
	27	131.584	131.563	0.021	0.01596
	28	126.969	126.949	0.020	0.01575
	29	122.563	122.544	0.019	0.01550
	30	118.352	118.333	0.019	0.01605
	31	114.322	114.304	0.018	0.01574
	32	110.462	110.445	0.017	0.01539
	33	106.762	106.745	0.017	0.01592
	34	103.211	103.194	0.017	0.01647
	35	99.799	99.783	0.016	0.01603
	36	96.518	96.503	0.015	0.01554
	37	93.359	93.345	0.014	0.01500
	38	90.316	90.302	0.014	0.01550
	39	87.380	87.366	0.014	0.01602
	40	84.546	84.533	0.013	0.01538
	41	81.807	81.794	0.013	0.01589
	42	79.157	79.145	0.012	0.01516
	43	76.592	76.580	0.012	0.01567
	44	74.106	74.094	0.012	0.01619
	45	71.694	71.683	0.011	0.01534
Bottom-	46	69.353	69.342	0.011	0.01586
Reflected	47	67.079	67.068	0.011	0.01640
Region	48	64.866	64.856	0.010	0.01542
	49	62.713	62.704	0.009	0.01435
	50	60.616	60.607	0.009	0.01485
	51	58.572	58.562	0.010	0.01707
	52	56.577	56.568	0.009	0.01591
	53	54.629	54.621	0.008	0.01464
	54	52.726	52.718	0.008	0.01517
	55	50.865	50.857	0.008	0.01573
	56	49.043	49.035	0.008	0.01631
	57	47.259	47.252	0.007	0.01481
	58	45.511	45.504	0.007	0.01538
	59	43.796	43.789	0.007	0.01598
	60	42.113	42.107	0.006	0.01425
	61	40.461	40.454	0.007	0.01730
	62	38.836	38.830	0.006	0.01545
	63	37.239	37.233	0.006	0.01611
	64	35.666	35.661	0.005	0.01402
	65	34.118	34.113	0.005	0.01466
	66	32.593	32.588	0.005	0.01534
	67	31.088	31.083	0.005	0.01608
	68	29.604	29.599	0.005	0.01689
	69	28.139	28.134	0.005	0.01777
	70	26.691	26.687	0.004	0.01499

Table 5. Range results for the profile of table 2 (continued).

	ANGLE (deg)	RANGE (kyd) LINEAR	RANGE (kyd) RP70	DIFFERENCE (kyd)	PERCENT ERROR
	71	25.260	25.256	0.004	0.01584
	72	23.845	23.841	0.004	0.01678
	73	22.443	22.440	0.003	0.01337
	74	21.056	21.053	0.003	0.01425
	75	19.681	19.678	0.003	0.01524
	76	18.318	18.316	0.002	0.01092
	77	16.966	16.964	0.002	0.01179
Bottom-	78	15.624	15.621	0.003	0.01920
Reflected	79	14.291	14.288	0.003	0.02099
Region	80	12.965	12.964	0.001	0.00771
	81	11.648	11.646	0.002	0.01717
	82	10.337	10.336	0.001	0.00967
	83	9.032	9.031	0.001	0.01107
	84	7.733	7.732	0.001	0.01293
	85	6.437	6.436	0.001	0.01554
	86	5.146	5.145	0.001	0.01943
	87	3.857	3.856	0.001	0.02593
	88	2.569	2.569	0.000	0.00000
	89	1.284	1.284	0.000	0.00000

Table 5. Range results for the profile of table 2 (continued).

	ANGLE (deg)	RANGE (kyd) LINEAR	RANGE (kyd) RP70	DIFFERENCE (kyd)	PERCENT ERROR
	5	108.241	108.182	0.059	0.05451
	6	150.305	150.351	-0.046	-0.03060
	7	170.877	170.943	-0.066	-0.03862
	8	162.000	161.948	0.052	0.03210
	9	170.399	170.410	-0.011	-0.00646
	10	185.190	185.242	-0.052	-0.02808
	11	159.809	159.808	0.001	0.00063
	12	172.809	172.795	0.014	0.00810
	13	186.316	186.293	0.023	0.01234
Bottom-	14	155.394	155.324	0.070	0.04505
Reflected	15	156.539	156.492	0.047	0.03002
Region	16	163.290	163.248	0.042	0.02572
	17	170.399	170.359	0.040	0.02347
	18	154.969	154.935	0.034	0.02194
	19	162.815	162.781	0.034	0.02088
	20	150.911	150.881	0.030	0.01988
	21	158.311	158.280	0.031	0.01958
	22	148.373	148.345	0.028	0.01887
	23	139.622	139.595	0.027	0.01934
	24	131.830	131.806	0.024	0.01821

Table 6. Range results for the profile of table 3.

	ANGLE (deg)	RANGE (kyd) LINEAR	RANGE (kyd) RP70	DIFFERENCE (kyd)	PERCENT ERROR
	25	124.830	124.807	0.023	0.01843
	26	118.492	118.471	0.021	0.01772
	27	112.716	112.696	0.020	0.01774
	28	107.421	107.402	0.019	0.01769
	29	102.542	102.524	0.018	0.01755
	30	98.026	98.009	0.017	0.01734
	31	93.828	93.812	0.016	0.01705
	32	89.911	89.896	0.015	0.01668
	33	86.245	86.231	0.014	0.01623
	34	82.802	82.788	0.014	0.01691
	35	79.560	79.547	0.013	0.01634
	36	76.499	76.486	0.013	0.01699
	37	73.600	73.588	0.012	0.01630
	38	70.850	70.839	0.011	0.01553
	39	68.236	68.224	0.012	0.01759
	40	65.744	65.733	0.011	0.01673
	41	63.365	63.355	0.010	0.01578
Bottom-	42	61.091	61.080	0.011	0.01801
Reflected	43	58.911	58.901	0.010	0.01697
Region	44	56.820	56.810	0.010	0.01760
	45	54.809	54.800	0.009	0.01642
	46	52.874	52.866	0.008	0.01513
	47	51.009	51.001	0.008	0.01568
	48	49.209	49.201	0.008	0.01626
	49	47.468	47.461	0.007	0.01475
	50	45.784	45.777	0.007	0.01529
	51	44.153	44.146	0.007	0.01585
	52	42.570	42.563	0.007	0.01644
	53	41.033	41.026	0.007	0.01705
	54	39.538	39.532	0.006	0.01518
	55	38.084	38.077	0.007	0.01838
	56	36.666	36.661	0.005	0.01364
	57	35.285	35.279	0.006	0.01700
	58	33.935	33.930	0.005	0.01473
	59	32.617	32.612	0.005	0.01533
	60	31.328	31.323	0.005	0.01596
	61	30.066	30.062	0.004	0.01330
	62	28.830	28.825	0.005	0.01734
	63	27.618	27.613	0.005	0.01810
	64	26.428	26.424	0.004	0.01514
	65	25.260	25.255	0.005	0.01979
	66	24.111	24.107	0.004	0.01659
	67	22.981	22.977	0.004	0.01741
	68	21.868	21.865	0.003	0.01372
	69	20.772	20.769	0.003	0.01444
	70	19.691	19.688	0.003	0.01524
	71	18.625	18.622	0.003	0.01611

Table 6. Range results for the profile of table 3 (continued).

	ANGLE (deg)	RANGE (kyd) LINEAR	RANGE (kyd) RP70	DIFFERENCE (kyd)	PERCENT ERROR
	72	17.572	17.569	0.003	0.01707
	73	16.531	16.528	0.003	0.01815
	74	15.502	15.499	0.003	0.01935
	75	14.484	14.481	0.003	0.02071
	76	13.475	13.473	0.002	0.01484
	77	12.476	12.474	0.002	0.01603
Bottom-	78	11.485	11.483	0.002	0.01741
Reflected	79	10.502	10.500	0.002	0.01904
Region	80	9.525	9.524	0.001	0.01050
	81	8.555	8.554	0.001	0.01169
	82	7.591	7.590	0.001	0.01317
	83	6.631	6.630	0.001	0.01508
	84	5.676	5.675	0.001	0.01762
	85	4.725	4.724	0.001	0.02116
	86	3.776	3.775	0.001	0.02648
	87	2.830	2.830	0.000	0.00000
	88	1.886	1.885	0.001	0.05302
	89	0.943	0.942	0.001	0.10604

Table 6. Range results for the profile of table 3 (continued).

	ANGLE (deg) (s)	TIME (s) LINEAR	TIME (s) RP70	DIFFERENCE (s)	PERCENT ERROR
	3.5	150.722	150.705	0.017	0.01128
	4.5	149.547	149.529	0.018	0.01204
	5.5	149.767	149.746	0.021	0.01402
	6.5	150.920	150.896	0.024	0.01590
	7.5	152.207	152.210	-0.003	-0.00197
Bottom-	8.5	167.590	167.581	0.009	0.00537
Reflected	9.5	147.035	147.029	0.006	0.00408
Region	10.5	160.677	160.671	0.006	0.00373
	11.5	148.488	148.484	0.004	0.00269
	12.5	161.427	161.423	0.004	0.00248
	13.5	151.364	151.361	0.003	0.00198
	14.5	162.934	162.931	0.003	0.00184
	15.5	173.315	173.313	0.002	0.00115
	16.5	164.432	164.430	0.002	0.00122
	17.5	156.450	156.449	0.001	0.00064
	18.5	149.236	149.234	0.002	0.00134
	19.5	142.682	142.681	0.001	0.00070
	20.5	136.703	136.702	0.001	0.00073
	21.5	131.228	131.227	0.001	0.00076
	22.5	126.196	126.195	0.001	0.00079
	23.5	121.559	121.559	0.001	0.00082

Table 7. Travel time results for the profile of table 1.

	ANGLE (deg)	TIME (s) LINEAR	TIME (s) RP70	DIFFERENCE (s)	PERCENT ERROR
	24.5	117.273	117.272	0.001	0.00085
Bottom-	25.5	113.301	113.301	0.000	0.00000
Reflected	26.5	109.613	109.613	0.000	0.00000
Region	27.5	106.181	106.181	0.000	0.00000
	28.5	102.980	102.980	0.000	0.00000

Table 7. Travel time results for the profile of table 1 (continued).

	ANGLE (deg)	TIME (s) LINEAR	TIME (s) RP70	DIFFERENCE (s)	PERCENT ERROR
	1	102.629	102.611	0.018	0.01754
	2	96.085	96.081	0.004	0.00416
	3	92.723	92.720	0.003	0.00324
	4	89.810	89.809	0.001	0.00111
	5	86.967	86.966	0.001	0.00115
	6	84.108	84.107	0.001	0.00119
	7	101.456	101.455	0.001	0.00099
	8	97.877	97.876	0.001	0.00102
	9	94.339	94.338	0.001	0.00106
Bottom-	10	90.877	90.876	0.001	0.00110
Reflected	11	87.515	87.514	0.001	0.00114
Region	12	84.274	84.274	0.000	0.00000
	13	97.361	97.360	0.001	0.00103
	14	93.805	93.805	0.000	0.00000
	15	90.423	90.422	0.001	0.00111
	16	87.214	87.213	0.001	0.00115
	17	98.178	98.178	0.000	0.00000
	18	94.828	94.828	0.000	0.00000
	19	91.664	91.663	0.001	0.00109
	20	88.677	88.676	0.001	0.00113
	21	98.105	98.104	0.001	0.00102
	22	95.066	95.065	0.001	0.00000
	23	92.198	92.198	0.000	0.00000
	24	89.491	89.491	0.000	0.00000
	25	97.789	97.789	0.000	0.00000
	26	95.074	95.074	0.000	0.00000

Table 8. Travel time results for the profile of table 2.

	ANGLE (deg)	TIME (s) LINEAR	TIME (s) RP70	DIFFERENCE (s)	PERCENT ERROR
	5	65.670	65.645	0.025	0.03807
	6	91.057	91.099	-0.042	-0.04613
	7	103.360	103.416	-0.056	-0.05418
	8	97.944	97.929	0.015	0.01531
	9	102.985	103.008	-0.023	-0.02233
	10	111.841	111.890	-0.049	-0.04381
	11	96.433	96.447	-0.014	-0.01452
	12	104.166	104.174	-0.008	-0.00768
	13	112.172	112.175	-0.003	-0.00267
	14	93.947	93.920	0.027	0.02874
	15	95.264	95.251	0.013	0.01365
	16	99.945	99.936	0.009	0.00901
	17	104.896	104.889	0.007	0.00667
	18	95.961	95.956	0.005	0.00521
	19	101.439	101.435	0.004	0.00394
	20	94.627	94.623	0.004	0.00423
	21	99.933	99.930	0.003	0.00300
Bottom-	22	94.320	94.317	0.003	0.00318
Reflected	23	89.411	89.409	0.002	0.00224
Region	24	85.073	85.071	0.002	0.00235
	25	81.205	81.204	0.001	0.00123
	26	77.733	77.731	0.002	0.00257
	27	74.594	74.593	0.001	0.00134
	28	71.743	71.742	0.001	0.00139
	29	69.139	69.139	0.000	0.00000
	30	66.753	66.752	0.001	0.00150
	31	64.557	64.556	0.001	0.00155
	32	62.530	62.529	0.001	0.00160
	33	60.653	60.652	0.001	0.00165
	34	58.910	58.909	0.001	0.00170
	35	57.287	57.287	0.000	0.00000
	36	55.774	55.774	0.000	0.00000
	37	54.360	54.359	0.001	0.00184
	38	53.035	53.035	0.000	0.00000
	39	51.793	51.793	0.000	0.00000
	40	50.626	50.625	0.001	0.00198
	41	49.527	49.527	0.000	0.00000
	42	48.493	48.493	0.000	0.00000
	43	47.518	47.517	0.001	0.00210
	44	46.596	46.596	0.000	0.00000
	45	45.726	45.726	0.000	0.00000
	46	44.903	44.903	0.000	0.00000
	47	44.123	44.123	0.000	0.00000
	48	43.385	43.385	0.000	0.00000
	49	42.685	42.685	0.000	0.00000

Table 9. Travel time results for the profile of table 3.

Consider next the range differences for rays which reflect from the ocean bottom. Here the differences are always positive; ie, RP-70 gives results which are smaller than the NUC linear control. For small-angle bottom-reflected rays, there is a monotonic decrease in percent error with increasing angle. This monotonic behavior maintains through the 17.5°, 6.0°, and 22.0° rays for the profiles of tables 1, 2, and 3, respectively. For still deeper angles, the percent error appears to approach a constant value of roughly 0.016 ± 0.003. This constant cannot be evaluated more precisely because of the number of digits available in the RP-70 results. The NUC results were rounded to the same number of digits as RP-70. These roundoff errors are large enough to obscure the true steep-angle behavior.

Consider the travel time errors for bottom-reflected rays. The behavior is similar to that demonstrated by the range results. It is significant that without exception the range error is larger than the travel time error. Because of roundoff error, one cannot tell exactly how much more accurate travel time is than range for steep angles. However, for the profile of table 1 at angles of around 22.5°, the range error is 20 times greater than the travel time error.

For the nonbottom-reflected rays, the results for travel time are as sporadic as those for range. For the profile of table 1, the travel time error is generally smaller than the range error for the profile of Table 3, but it is larger for five rays out of nine. There is more of a tendency for the error to be negative for travel time than for range.

These results are discussed in more detail in section 3.1.4.

3.1.2 Short-Range Epstein Profile

In this test case, the Epstein profile described on page 424 of reference 6 was used. One advantage of this profile is the short maximum range required to observe changes in range as the source angle is varied. Another advantage of this form of profile is that it possesses a closed-form solution. The five parameters in the profile allow for a variety of shapes without the problem of derivative discontinuities inherent in many of the multilayer profile models.

The Epstein profile used in these comparisons is given in table 10. This table was generated by computing values from the analytic model at depth increments of 8.2296 m from the surface to a depth of 98.7552 m. The source and receiver are placed at 108 yd depth and only rays that leave the source in the upward direction are computed. These rays are then either refracted or reflected from the surface to reach the receiver as downgoing rays. The bottom depth of 101 m in table 10 is an arbitrary choice. It means nothing in this example as only upward-headed rays at the source are considered. This depth is entered in the table only to comply with a format requirement of RP-70.

In this example, ranges and travel times were computed for three models. The first was the analytic solution of the Epstein control model. The second was the linear control profile based on the layers of table 10. The third was RP-70, based again on the layers of table 10. For all three models, upgoing rays were traced for initial angles starting from -0.015625° and proceeding to -10.5° in increments of 0.05625°. This spacing of rays was required by the RP-70 system which treats only binary fractions of ray parameters.

---

6. Pedersen, M. A., and D. F. Gordon, Comparison of Curvilinear and Linear Profile Approximations in the Calculation of Underwater Sound Intensities by Ray Theory, J Acoust Soc Am 41, 419-438, Feb 1967.

DEPTH (m)	VELOCITY (m/s)
0.0000	1487.1465
8.2296	1485.0879
16.4592	1482.8164
24.6888	1480.3887
32.9184	1477.8828
41.1480	1475.4062
49.3776	1473.0723
57.6072	1470.9961
65.8668	1469.2676
74.0664	1467.9453
82.2960	1467.0391
90.5256	1466.5234
98.7552	1466.3398
101.0000	1466.0000

BOTTOM DEPTH 101 m

Table 10. Epstein profile used in a short-range test case.

The difference in range between the NUC linear model and the RP-70 model is shown in figure 1 as a function of source angle. The RP-70 ranges were only available to the nearest yard. Hence the differences in range shown here are quantized to 1 yard. The maximum absolute difference is 8 yd. The only significant differences occur at low angles. For angles steeper than 1.8°, the maximum difference is 1 yard. As in the example of section 3.1.1, at steeper angles RP-70 gives smaller values than the NUC control.

The differences in range between the NUC linear model and the analytic solution are presented as Xs in figure 2 for ray angles up to 2°. The corresponding differences for the RP-70 model are shown as crosses. Similar data are shown in figure 3 for ray angles between 2° and 10.5°. The ranges for the NUC linear model are so close to those of the RP-70 model that they are difficult to distinguish on the range scale of figures 2 and 3. Note that the differences in figures 2 and 3 are much larger than those in figure 1. For example, the maximum error in figure 2 is 108 times that of figure 1. Thus the errors introduced by approximating the Epstein profile by linear segments (figure 2) are much larger than those (figure 1) introduced by RP-70 approximations in the ray theory.

The travel time counterparts of figures 1 to 3 are presented in figures 4 to 6. Consider first the large errors for the four smallest ray angles in figure 4. The error for these rays is from 3.6 to 14.6 times as much as the maximum error for larger ray angles. It is evident that at small angles there is a significant source of error in the travel time portion of RP-70. This problem may not be too serious since such small-angle rays are generally completely excluded in the computation.

If we exclude the four smallest ray angles, the results are quite comparable to the range errors. For example, the maximum error in figure 5 is about 108 times that of figure 4. This factor is the same as that obtained for the maximum range error between figure 2 and figure 1.

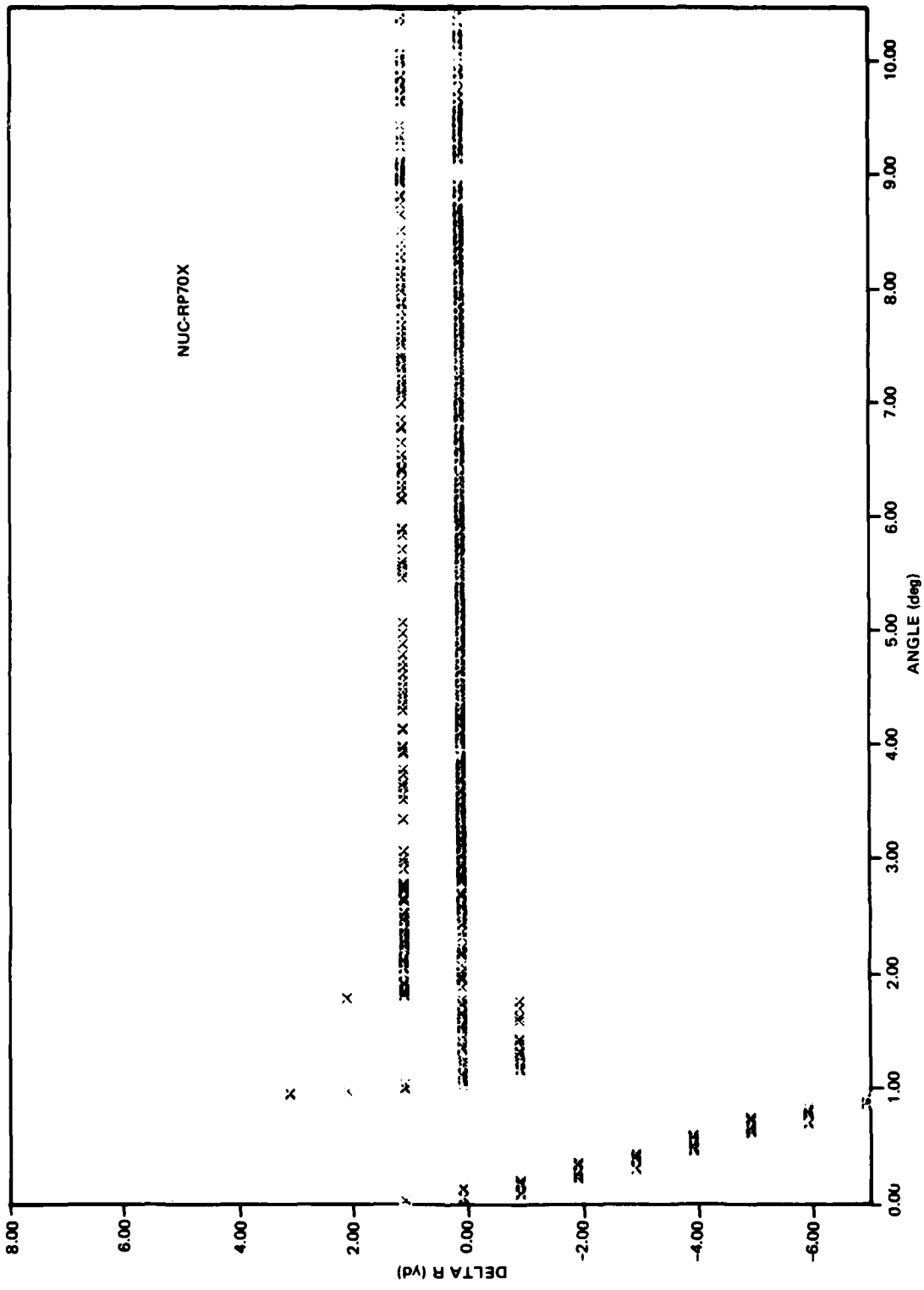

Figure 1. Range differences between the NUC linear model and the RP-70 model.

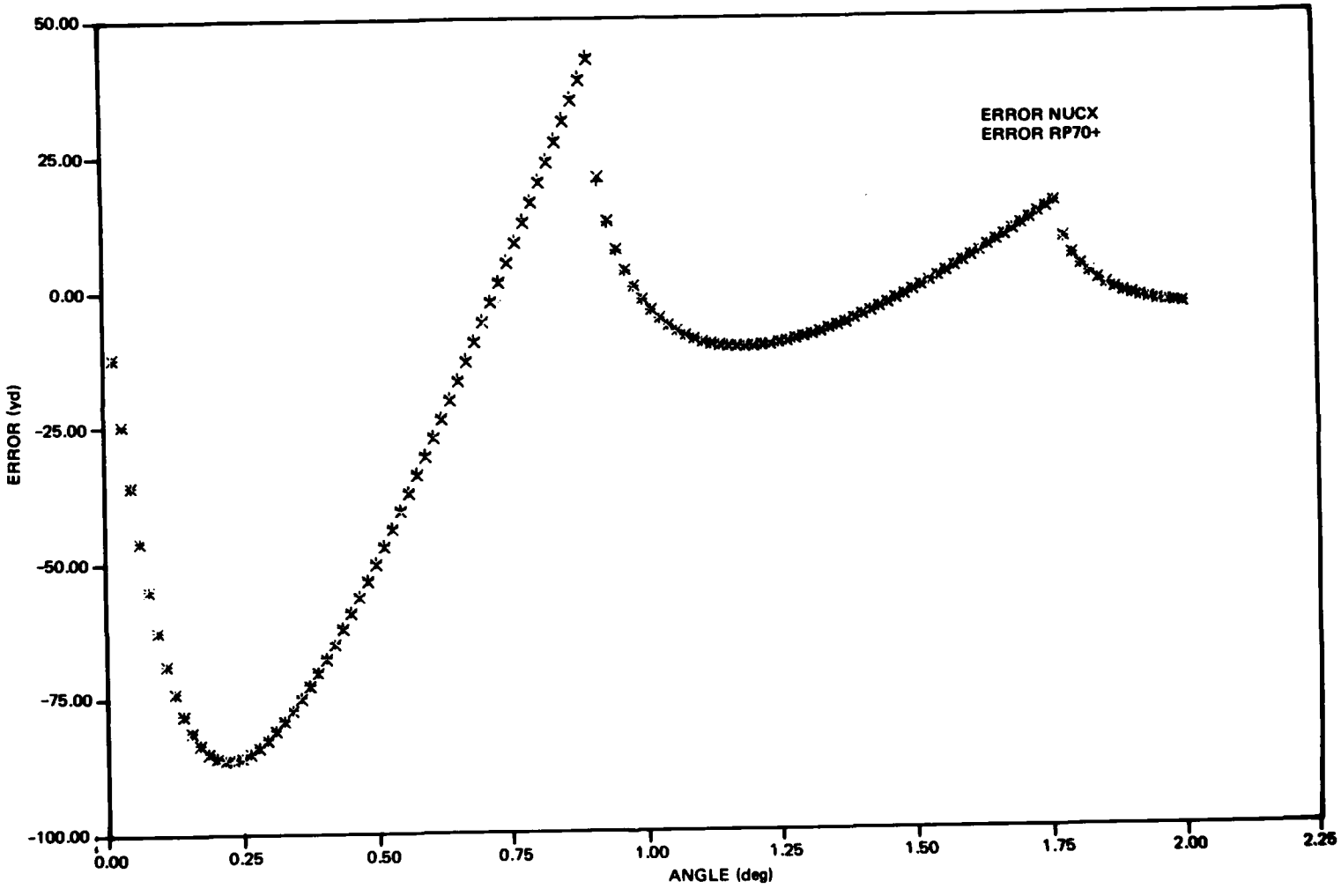

Figure 2. Range differences between the NUC linear model and the analytic solution (x), and between the RP-70 model and the analytic solution (+) for angles 0 to 2.25 degrees.

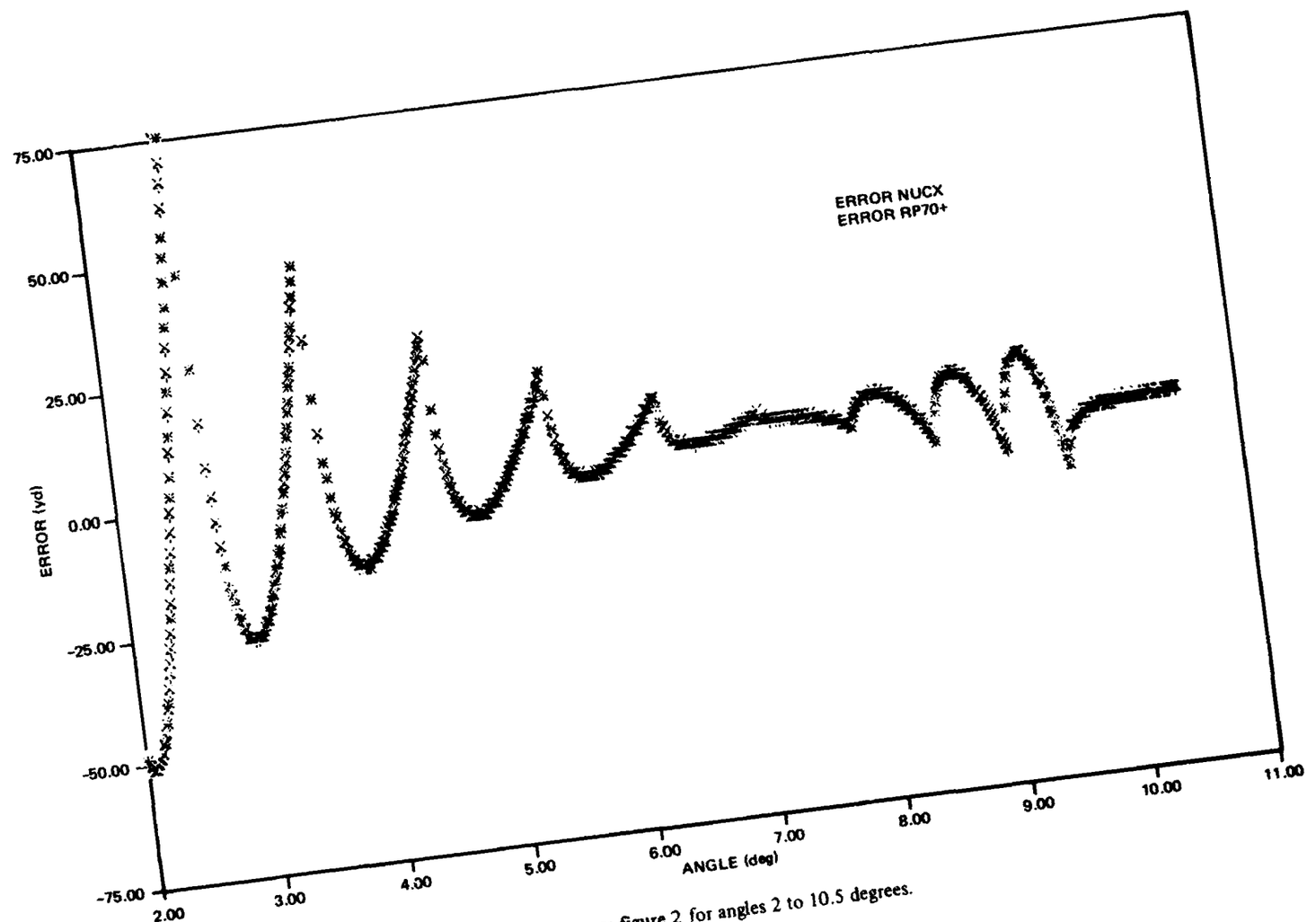

Figure 3. Same as figure 2 for angles 2 to 10.5 degrees.

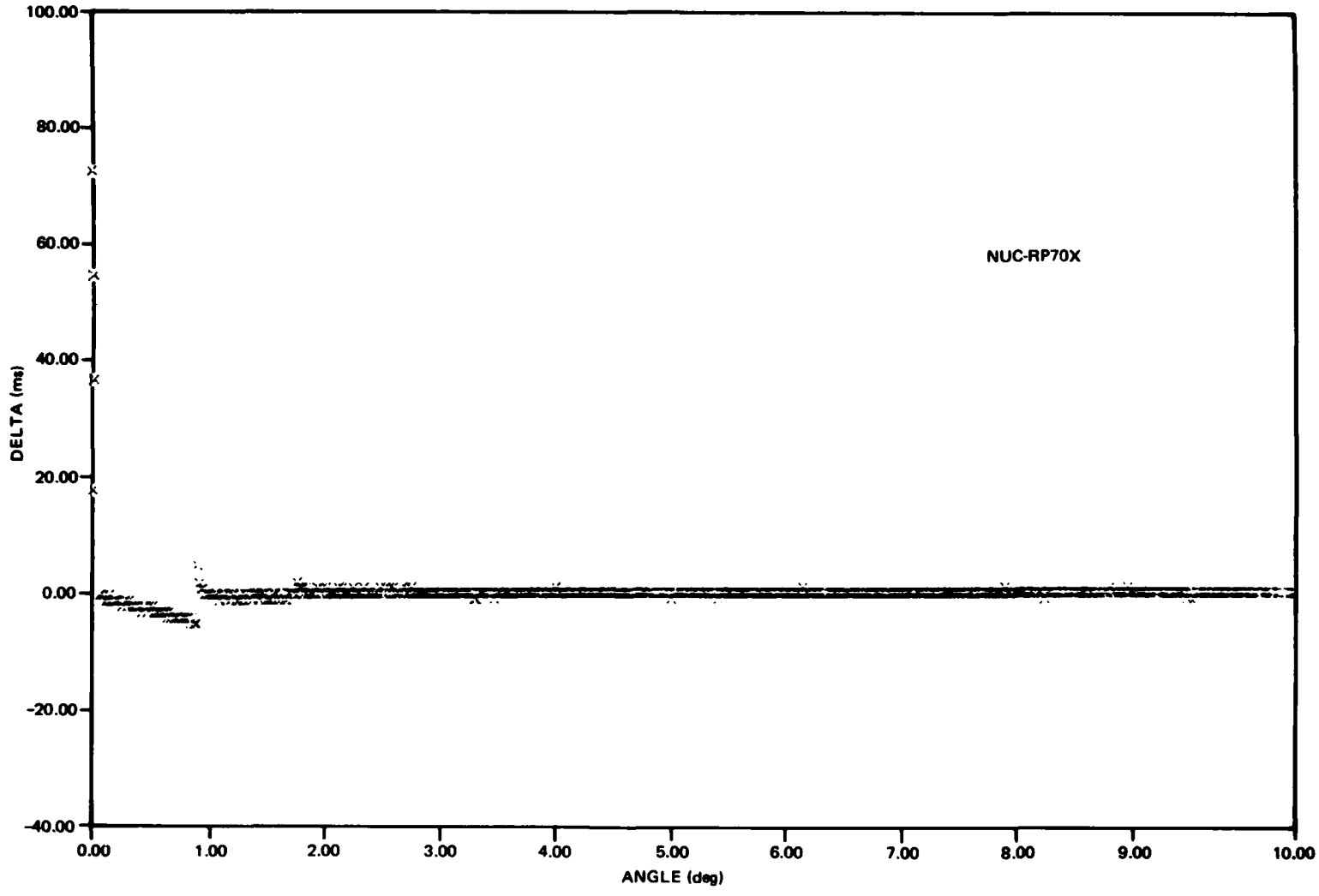

Figure 4. Travel time counterpart of figure 1.

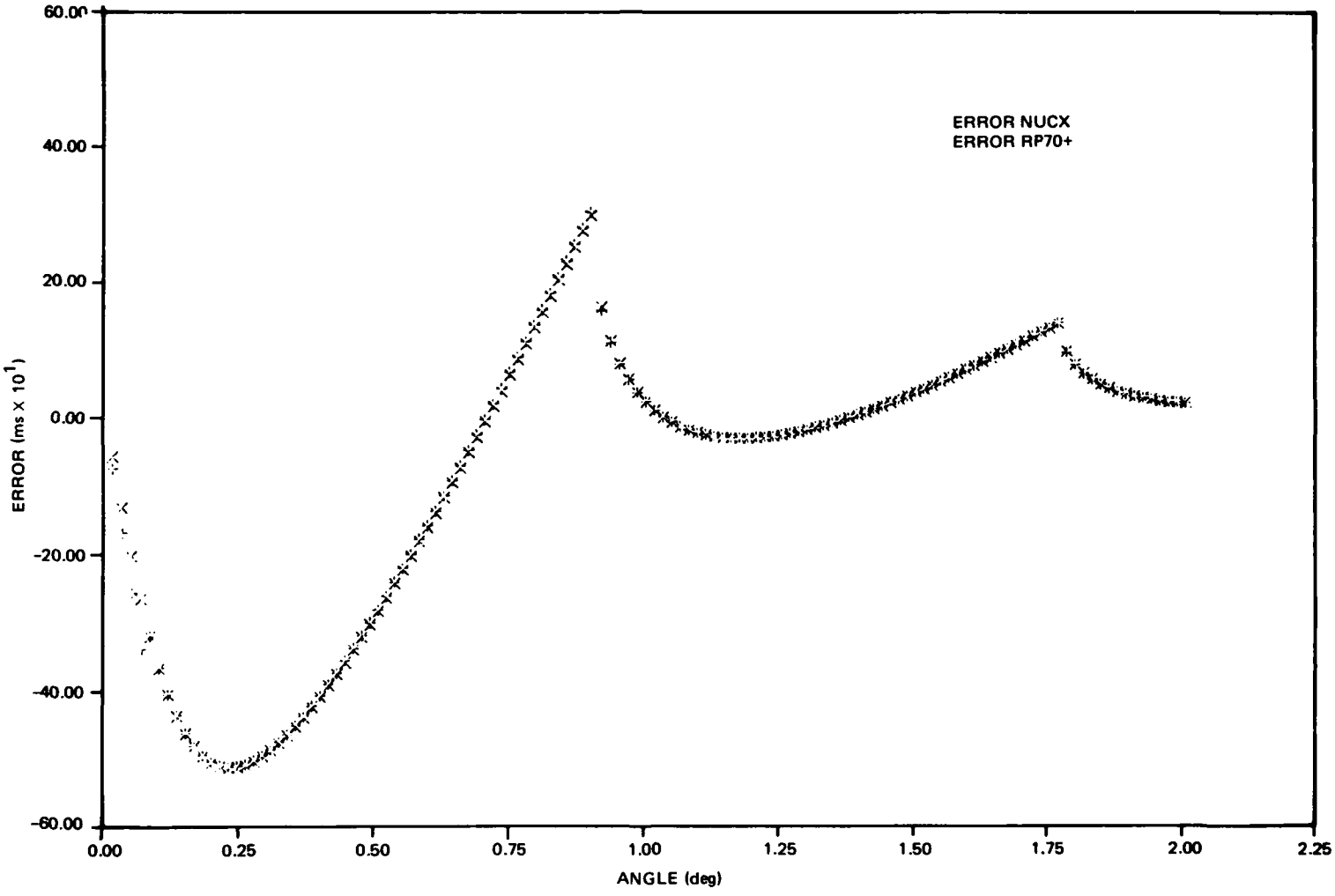

Figure 5. Travel time counterpart of figure 2.

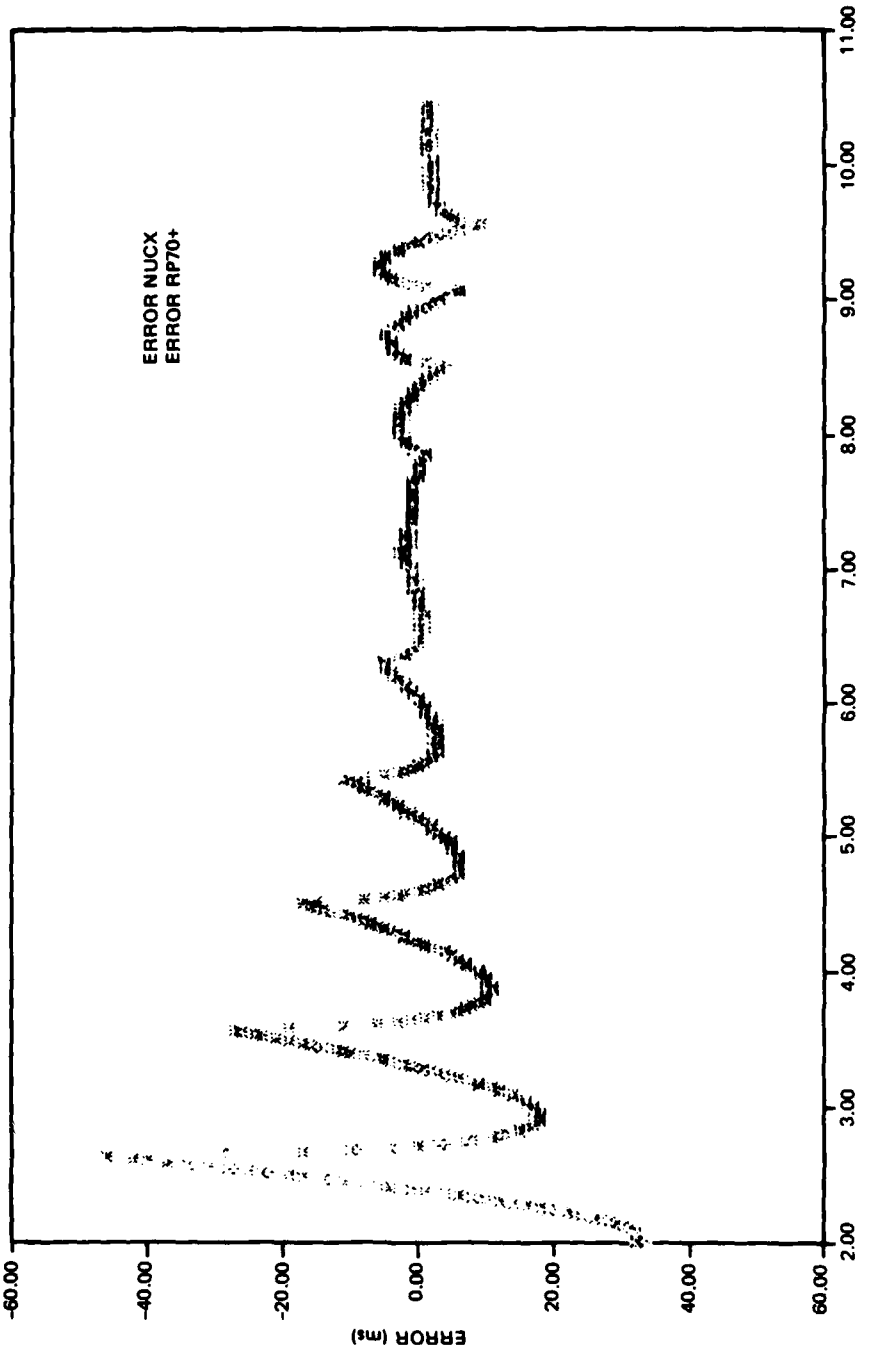

Figure 6. Travel time counterpart of figure 3.

3.1.3 Profile Focusing Rays

In this test case, a range-independent profile, which focused all rays at a range of 200 kyd, was used. Before introducing this profile, we need to provide some background. A focusing profile is one for which all rays within specified angular limits pass through a single range. The use of such a profile as a control dates back many years. In the 1950s, a number of analogue ray tracing machines were brought to the Naval Electronics Laboratory (NEL) for evaluation. We subjected them to the focusing profile test. In this test, the profile is given as:

$$C = C_0 \cosh [\pi (Z - Z_0)/R_0] \tag{5}$$

where Z_0 is the axial depth and C_0 is the axial sound speed. This profile has the property that all rays for an axial source pass through an axial receiver at a range of R_0.

The test consisted of inserting equation 5 as a sound speed profile and observing the aberrations of the ray diagram about the focal point at R_0. This simple test put the quietus on several analogue ray tracing devices. In some cases, it was found that the device could not duplicate previous results. Each time the test was repeated with the same ray parameters, the device produced a recognizably different aberration pattern.

In 1969, DeWayne White developed a theory which presented the solution of all range-independent profiles which produce focal points on an axis of minimum sound speed (ref 7). Using this approach, a profile was constructed for which all rays from 0° to 90° focused at a range of 200 kyd.

The form of the profile is given by equations 42 and 43 of reference 7. The specific parameters and functions are Z_0 = 3500 m, C_0 = 1470 m/s, $g(C) = A(1 - C_0^2 C^{-2})$, A = 37,500 m, R_0 = 200 kyd = 182.88 km, $H = R_0/2\pi$ = 29106.256 m, $n_1 = 2$, and $n_2 = 3$. The focal point occurs after three loops below the axis and two loops above. Ray diagrams are not given here. However, they may be generated with the appropriate use of equations 47, 48, 51, and 75 of reference 7.

The investigation emphasized low-angle rays which leave the source at angles of 10° and less. The idea here was to test the RP-70 model for small angles. To model the profile adequately, three linear approximations to the analytic profile were required. Each approximation consisted of a maximum number of layers (150) specified over a given depth interval. (The RP-70 program limits input at 150 layers.) The profile of table 11 presents the linear approximation used in the analysis of rays from 0 to 1 degree. This profile extends from 3182.918 m to 3722.4062 m. This depth interval contains all rays leaving the source between 0 and 1 degree. A large number of layers is required because we are attempting to approximate a parabolic-like curve with a series of straightline segments. In such a case, it is necessary to include a large number of layers near the axis.

The profile of table 12 was used in the analysis of rays from 1 to 4 degrees. For these slightly steeper angles, we do not need to space the layers so closely in depth. However, we must cover a larger depth interval – in this case, from 2561.6914 m to 4245.4062 m. Similarly, the profile of table 13 was used in the analysis of rays from

---

7. White, D, Velocity Profiles that Produce Acoustic Focal Points on an Axis of Minimum Velocity, J Acoust Soc Am 46, 1318-1332, Nov 1969.

DEPTH (m)	VELOCITY (m/s)
0.0000	2128.8008
3182.9180	1470.3691
3185.0039	1470.3652
3187.1055	1470.3594
3189.2227	1470.3555
3191.3555	1470.3496
3193.5039	1470.3457
3195.6719	1470.3398
3197.8516	1470.3359
3200.0547	1470.3301
3202.2895	1470.3242
3204.5078	1470.3203
3206.7617	1470.3145
3209.0312	1470.3105
3211.3242	1470.3047
3213.6367	1470.3008
3215.9727	1470.2949
3218.3242	1470.2891
3220.6992	1470.2852
3223.0977	1470.2793
3225.5156	1470.2754
3227.9609	1470.2695
3230.4258	1470.2656
3232.9180	1470.2598
3235.4375	1470.2559
3237.9605	1470.2500
3240.5508	1470.2441
3243.1484	1470.2402
3245.7734	1470.2344
3248.4297	1470.2305
3251.1133	1470.2246
3253.8320	1470.2207
3256.5820	1470.2148
3259.3672	1470.2109
3262.1836	1470.2051
3265.0391	1470.1992
3267.9297	1470.1953
3270.8633	1470.1895
3273.8359	1470.1855
3276.8477	1470.1797
3279.9062	1470.1758
3283.0072	1470.1699
3286.1602	1470.1641
3289.3633	1470.1602
3292.6172	1470.1543
3295.9258	1470.1504
3299.2930	1470.1445
3202.7187	1470.1406

Table 11. Focusing profile used for rays from 0 to 1 degree.

DEPTH (m)	VELOCITY (m/s)
3306.2109	1470.1348
3309.7695	1470.1309
3313.4023	1470.1250
3317.1094	1470.1191
3320.8984	1470.1152
3324.7695	1470.1094
3328.7844	1470.1055
3332.8008	1470.0996
3336.9727	1470.0957
3341.2578	1470.0898
3345.6680	1470.0859
3350.2109	1470.0801
3354.9062	1470.0742
3359.7617	1470.0703
3364.8008	1470.0645
3370.0430	1470.0605
3375.5117	1470.0547
3381.2422	1470.0508
3387.2773	1470.0449
3393.6602	1470.0391
3400.4687	1470.0352
3407.7891	1470.0293
3415.7817	1470.0254
3424.5937	1470.0195
3434.6367	1470.0156
3446.5742	1470.0098
3462.1719	1470.0059
3500.0000	1470.0000 – AXIS
3525.3906	1470.0059
3535.9570	1470.0098
3544.0859	1470.0156
3550.9492	1470.0195
3557.0078	1470.0254
3562.4961	1470.0293
3567.5469	1470.0352
3572.2539	1470.0391
3576.6797	1470.0449
3580.8711	1470.0508
3584.8633	1470.0547
3588.6797	1470.0605
3592.3437	1470.0645
3595.8711	1470.0703
3599.2812	1470.0742
3602.5781	1470.0801
3605.7812	1470.0859
3608.8906	1470.0898
3611.9180	1470.0957
3614.8672	1470.0996

Table 11. Focusing profile used for rays from 0 to 1 degree (continued).

DEPTH (m)	VELOCITY (m/s)
3617.7461	1470.1055
3620.5625	1470.1094
3623.3125	1470.1152
3626.0078	1470.1191
3628.6484	1470.1250
3631.2422	1470.1309
3633.7852	1470.1348
3636.2812	1470.1406
3638.7344	1470.1445
3641.1523	1470.1504
3643.5273	1470.1543
3645.8672	1470.1602
3648.1719	1470.1641
3650.4414	1470.1699
3652.6797	1470.1758
3654.8906	1470.1797
3657.0703	1470.1855
3659.2187	1470.1895
3661.3437	1470.1953
3663.4414	1470.1992
3665.5156	1470.2051
3667.5625	1470.2109
3669.5898	1470.2148
3671.5937	1470.2207
3673.5742	1470.2246
3675.5352	1470.2305
3677.4766	1470.2344
3679.3984	1470.2402
3681.2969	1470.2441
3683.1797	1470.2500
3685.0469	1470.2559
3686.8945	1470.2598
3688.7266	1470.2656
3690.5391	1470.2695
3692.3398	1470.2754
3694.1211	1470.2793
3695.8906	1470.2852
3697.6445	1470.2891
3699.3828	1470.2949
3701.1094	1470.3008
3702.8203	1470.3047
3704.5195	1470.3105
3706.2031	1470.3145
3707.8750	1470.3203
3709.5352	1470.3242
3711.1836	1470.3301
3712.8203	1470.3359
3714.4453	1470.3398

Table 11. Focusing profile used for rays from 0 to 1 degree (continued).

DEPTH (m)	VELOCITY (m/s)
3716.0586	1470.3457
3717.6641	1470.3496
3719.2539	1470.3555
3720.8359	1470.3594
3722.4062	1470.3652
18500.0000	2094.8086

BOTTOM DEPTH 18500 m

Table 11. Focusing profile used for rays from 0 to 1 degrees (continued).

DEPTH (m)	VELOCITY (m/s)
0.0000	2128.8008
2561.6914	1473.6992
2567.4219	1473.6504
2573.2031	1473.5996
2579.0273	1473.5508
2584.9062	1473.5000
2590.8359	1473.4492
2596.8164	1473.4004
2602.8477	1473.3496
2608.9375	1473.3008
2615.0820	1473.2500
2621.2852	1473.1992
2627.5430	1473.1504
2633.8633	1473.0996
2640.2461	1473.0508
2646.6914	1473.0000
2653.1992	1472.9492
2659.7734	1472.9004
2666.4180	1472.8496
2673.1289	1472.8008
2679.9141	1472.7500
2686.7695	1472.6992
2693.7031	1472.8504
2700.7148	1472.5996
2707.8047	1472.5508
2719.9766	1472.5000
2722.2644	1472.4492
2729.5820	1472.4004
2737.0156	1472.3496
2744.5430	1472.3008
2752.1680	1472.2500
2759.8945	1472.1992
2767.7187	1472.1504
2775.6523	1472.0996

Table 12. Focusing profile used for rays from 1 to 4 degrees.

DEPTH (m)	VELOCITY (m/s)
2783.6953	1472.0508
2791.8516	1472.0000
2800.1289	1471.9492
2808.5273	1471.9004
2817.0547	1471.8496
2825.7148	1471.8008
2834.5156	1471.7500
2843.4570	1471.6992
2852.5647	1471.6504
2861.8086	1471.5996
2871.2286	1471.5508
2880.8203	1471.5000
2890.5937	1471.4492
2900.5625	1471.4004
2910.7344	1471.3496
2921.1172	1471.3000
2931.7305	1471.2500
2942.5781	1471.1992
2953.6875	1471.1504
2965.0825	1471.0996
2976.7344	1471.0508
2988.7148	1471.0000
3001.0312	1470.9492
3013.7109	1470.9004
3026.7852	1470.8496
3040 2852	1470.8008
3054.2539	1470.7500
3068.7422	1470.6992
3083.8047	1470.6504
3099.5078	1470.5996
3115.9336	1470.5508
3133.1836	1470.5000
3151.3867	1470.4492
3170.7070	1470.4004
3191.3555	1470.3496
3213.6367	1470.3008
3237.9805	1470.2500
3265.0391	1470.1992
3295.9258	1470.1504
3332.8008	1470.0996
3381.2422	1470.0508
3500.0000	1470.0000
3580.8711	1470.0508
3614.8672	1470.0996
3641.1523	1470.1504
3663.4414	1470.1992
3683.1797	1470.2500

Table 12. Focusing profile used for rays from 1 to 4 degrees (continued).

DEPTH (m)	VELOCITY (m/s)
3701.1094	1470.3008
3717.6641	1470.3496
3733.1289	1470.4004
3747.7070	1470.4492
3761.5430	1470.5000
3774.7422	1470.5508
3787.3906	1470.5996
3799.5586	1470.6504
3811.2969	1470.6992
3822.6523	1470.7500
3833.6641	1470.8008
3844.3833	1470.8496
3854.7773	1470.9004
3864.9258	1470.9492
3874.8359	1471.0000
3884.5195	1471.0508
3893.9961	1471.0996
3903.2812	1471.1504
3912.3789	1471.1992
3921.3086	1471.2500
3930.0820	1471.3008
3938.6992	1471.3496
3947.1758	1471.4004
3955.5156	1471.4492
3963.7305	1471.5000
3971.8203	1471.5508
3979.7969	1471.5996
3987.6802	1471.6504
3995.4180	1471.6992
4003.0742	1471.7500
4010.6367	1471.8008
4018.1055	1471.8496
4025.4844	1471.9004
4032.7773	1471.9492
4039.9883	1472.0000
4047.1172	1472.0508
4054.1758	1472.0996
4061.1562	1472.1504
4068.0664	1472.1992
4074.9102	1472.2500
4081.6836	1472.3008
4088.3984	1472.3496
4095.0469	1472.4004
4101.6328	1472.4492
4108.1641	1472.5000
4114.6406	1472.5508
4121.0547	1472.5996

Table 12. Focusing profile used for rays from 1 to 4 degrees (continued).

DEPTH (m)	VELOCITY (m/s)
4127.4219	1472.6504
4133.7344	1472.6992
4140.0000	1472.7500
4146.2109	1472.8008
4152.3828	1472.8496
4158.5000	1472.9004
4164.5703	1472.9492
4170.6016	1473.0000
4176.5859	1473.0508
4182.5312	1473.0996
4188.4375	1473.1504
4194.2969	1473.1992
4200.1250	1473.2500
4205.9062	1473.3008
4211.6562	1473.3496
4217.3672	1473.4004
4223.0469	1473.4492
4228.6875	1473.5000
4234.2969	1473.5508
4239.8672	1473.5996
4245.4062	1473.6504
18500.0000	2094.8086

BOTTOM DEPTH 18 500 m

Table 12. Focusing profile used for rays from 1 to 4 degrees (continued).

DEPTH (m)	VELOCITY (m/s)
0.0000	2128.8008
1317.2617	1499.5996
1327.3477	1499.1992
1337.5645	1498.8008
1347.9121	1498.4004
1358.3926	1498.0000
1369.0137	1497.5996
1379.7754	1497.1992
1390.6797	1496.8008
1401.7344	1496.4004
1412.9375	1496.0000
1424.2969	1495.5996
1435.8164	1495.1992
1447.4961	1494.8008
1459.3437	1494.4004
1471.3633	1494.0000
1483.5566	1493.5996
1495.9316	1493.1992

Table 13. Focusing profile used for rays from 4 to 10 degrees.

DEPTH (m)	VELOCITY (m/s)
1508.4902	1492.8008
1521.2402	1492.4004
1534.1855	1492.0000
1547.3320	1491.5996
1560.6855	1491.1992
1574.2520	1490.8008
1588.0371	1490.4004
1602.0469	1490.0000
1616.2910	1489.5996
1630.7754	1489.1992
1645.5098	1488.8008
1660.4980	1488.4004
1675.7520	1488.0000
1691.2812	1487.5996
1707.0937	1487.1992
1723.1992	1486.8008
1739.6094	1486.4004
1756.3359	1486.0000
1773.3926	1485.5996
1790.7891	1485.1992
1808.5410	1484.8008
1826.6641	1484.4004
1845.1738	1484.0000
1864.0840	1483.5996
1883.4180	1483.1992
1903.1914	1482.8008
1923.4258	1482.4004
1944.1465	1482.0000
1965.3770	1481.5996
1987.1426	1481.1992
2009.4766	1480.8008
2032.4082	1480.4004
2055.9727	1480.0000
2080.2070	1479.5996
2105.1602	1479.1992
2130.8750	1478.8008
2157.4062	1478.4004
2184.8164	1478.0000
2213.1641	1477.5996
2242.5352	1477.1992
2273.0078	1476.8008
2304.6675	1476.4004
2337.6875	1476.0000
2372.1484	1475.5996
2408.2187	1475.1992
2446.1016	1474.8008
2486.0234	1474.4004

Table 13. Focusing profile used for rays from 4 to 10 degrees (continued).

DEPTH (m)	VELOCITY (m/s)
2528.2695	1474.0000
2573.2031	1473.5996
2621.2852	1473.1992
2673.1289	1472.8008
2729.5820	1472.4004
2791.8516	1472.0000
2861.8086	1471.5996
2942.5781	1471.1992
3040.2652	1470.8008
3170.7070	1470.4004
3500.0000	1470.0000
3733.1289	1470.4004
3833.6641	1470.8008
3912.3789	1471.1992
3979.7969	1471.5996
4039.9883	1472.0000
4095.0469	1472.4004
4146.2109	1472.8008
4194.2969	1473.1992
4239.8672	1473.5996
4283.3203	1474.0000
4324.9766	1474.4004
4365.0703	1474.8008
4403.7891	1475.1992
4441.2969	1475.5996
4477.7109	1476.0000
4513.1484	1476.4004
4547.6953	1476.8008
4581.4219	1477.1992
4614.4062	1477.5996
4646.6953	1478.0000
4678.3437	1478.4004
4709.3984	1478.8008
4739.9062	1479.1992
4769.8906	1479.5996
4799.3828	1480.0000
4828.4141	1480.4004
4857.0234	1480.8008
4885.2109	1481.1992
4913.0156	1481.5996
4940.4531	1482.0000
4967.5391	1482.4004
4994.2891	1482.8008
5020.7266	1483.1992
5046.8516	1483.5996
5072.6875	1484.0000
5098.2500	1484.4004

Table 13. Focusing profile used for rays from 4 to 10 degrees (continued).

DEPTH (m)	VELOCITY (m/s)
5123.5391	1484.8008
5148.5703	1485.1992
5173.3594	1485.5996
5197.8984	1486.0000
5222.2187	1486.4004
5246.3125	1486.8008
5270.1953	1487.1992
5293.8672	1487.5996
5317.3437	1488.0000
5340.6250	1488.4004
5363.7187	1488.8008
5386.6328	1489.1992
5409.3750	1489.5996
5431.9375	1490.0000
5454.3359	1490.4004
5476.5781	1490.8008
5498.6641	1491.1992
5520.5937	1491.5996
5542.3750	1492.0000
5564.0078	1492.4004
5585.5078	1492.8008
5606.8672	1493.1992
5628.0937	1493.5996
5649.1875	1494.0000
5670.1562	1494.4004
5691.0000	1494.8008
5711.7187	1495.1992
5732.3203	1495.5996
5752.8047	1496.0000
5773.1797	1496.4004
5793.4453	1496.8008
5813.5937	1497.1992
5833.6406	1497.5996
5853.5859	1498.0000
5873.4219	1498.4004
5893.1641	1498.8008
5912.8047	1499.1992
18500.0000	2094.8086

BOTTOM DEPTH 18500 m

Table 13. Focusing profile used for rays from 4 to 10 degrees (continued).

4 to 10 degrees. Here, the depth interval covered extends from 1317.2617 m to 5912.8047 m (which contains the 10-degree ray).

Each of the three approximations of tables 11 to 13 represent the same profile; ie, the points are calculated from the same analytic expression. In this example, ranges and travel times are computed for three different ray models. The answer for the analytic model is trivial. The range, 200 kyd, and the travel time is a constant (124.408 s) for all ray angles. The second ray model was the linear control model based on tables 11, 12, or 13, depending on the ray interval under investigation. The third ray model was RP-70, based again on the layers of tables 11, 12, or 13.

Table 14 presents calculated range, error, and percent error for the linear and RP-70 models. The table is divided into three groups, each corresponding to the profiles of tables 11, 12, or 13.

ANGLE (deg)	RANGE (kyd)		ERROR (kyd)		ERROR (percent)	
	LINEAR	RP70	LINEAR	RP70	LINEAR	RP70
0.5625	200.167	201.416	0.167	1.416	0.0835	0.7080
0.6250	200.136	196.848	0.136	-1.152	0.0680	-0.5760
0.6875	200.089	200.835	0.089	0.635	0.0445	0.4175
0.7500	200.071	198.264	0.071	-1.736	0.0355	-0.8680
0.8125	200.072	200.760	0.072	0.760	0.0360	0.3800
0.8750	200.033	198.819	0.033	-1.181	0.0165	-0.5905
0.9375	200.039	200.783	0.039	0.783	0.0195	0.3915
1.0000	200.055	200.286	0.055	0.286	0.0275	0.1430
1.0000	200.987	200.557	0.987	0.557	0.4935	0.2785
1.5000	200.404	200.074	0.404	0.074	0.2020	0.0370
2.0000	200.306	200.414	0.306	0.414	0.1530	0.2070
2.5000	200.141	200.203	0.141	0.203	0.0705	0.1015
3.0000	200.029	199.923	0.029	-0.077	0.0145	-0.0385
3.5000	200.058	199.822	0.058	-0.178	0.0290	-0.0890
4.0000	200.030	200.032	0.030	0.032	0.0150	0.0160
4.0000	200.963	200.911	0.936	0.911	0.4815	0.4555
5.0000	200.310	200.258	0.310	0.258	0.1550	0.1290
6.0000	200.086	200.056	0.086	0.056	0.0430	0.0280
7.0000	200.081	200.071	0.081	0.071	0.0405	0.0355
8.0000	200.049	200.024	0.049	0.024	0.0245	0.0120
9.0000	200.060	200.045	0.060	0.045	0.0300	0.0225
10.0000	200.034	199.995	0.034	-0.005	0.0170	-0.0025

Table 14. Range results for linear model and for the RP-70 model for the profiles of tables 11 to 13.

We note first that the NUC linear control gives ranges which are consistently higher than the analytic solutions. We have not investigated the source of this bias but suspect it has to do with some systematic manner in which the profile approximation differs from the analytic profile.

The errrors for both the NUC linear and RP-70 models tend to decrease with increasing angle for each of the three profiles. This effect is similar to that shown in figure 2. For linear approximations, the fewer penetrated by the ray, the larger the error.

For angles less than 1°, the NUC linear control is markedly more accurate than RP-70. For angles from 1° to 4°, the NUC linear control is somewhat better than RP-70 except for the 1.0° and 1.5° rays. For the 4° to 10° rays, the RP-70 result is somewhat better than the NUC linear control. We believe that this latter result is fortuitous, and stems from the fact that for the focusing profile the NUC linear control has a high bias. From the comparisons given for the three ocean profiles, on the other hand, we know that RP-70 is biased low relative to the NUC linear control. This low bias of RP-70 offsets the high bias of the NUC linear control and gives an apparently more accurate result.

In any case, the results of table 14 indicate that RP-70 has no serious errors in the range computation. At low angles, the RP-70 errors are about an order of magnitude greater than those for the NUC linear model, suggesting that RP-70 applies a special low-angle approximation.

Table 15 is the travel time counterpart of table 14. With two exceptions, the travel time results are very comparable to the range results just discussed. The most noteworthy exception is the RP-70 travel time for the 0.75° ray. This is completely out of line with other results, and may be a rare computer error. More likely, it is indicative of some program error which arises only under special conditions. The only other exception is that for 4° to 10° rays, the NUC linear model is more accurate than RP-70 for four out of seven cases. For the ranges and rays in table 14, RP-70 was more accurate for seven out of seven cases.

3.1.4 Summary of Sections 3.1.1 to 3.1.3

This section is a summary of the results of the previous three sections. These are the only test cases for which RP-70 results were available. The motive for presenting these results in such great detail does not arise from any abiding interest in RP-70. These results are presented here because they illustrate how control cases can be used to examine a model critically.

The following conclusions summarize the results of sections 3.1.1 to 3.1.3:

1. For typical ocean profiles without range dependence, there appears to be no serious program errors in the RP-70 ranges and travel times. The maximum errors encountered for the three typical ocean profiles were only 0.0545 and -0.0542 percent for range and travel times, respectively.
2. RP-70 appears to introduce some minor but systematic errors due to various approximations in implementing the ray theory. For rays which reflect from the ocean surface and bottom, RP-70 gives ranges and travel times which are consistently lower than the NUC linear control. The error generally decreases with increasing angle, approaching an error of about 0.016 percent at high angles. The range error for reflecting rays can be 20 times as much as the travel time error. For rays which vertex in the ocean, the error is larger and more sporadic than for reflecting rays with no obvious trends. The errors may be negative, although positive errors are more common. Negative errors are more prevalent in the travel times than in the ranges. The range error is generally larger than the travel time error.

PROFILES FOR 200-kyd FOCUS

ANGLE (deg)	TIME (s)			ERROR (s)		ERROR (percent)	
	ANALYTIC	LINEAR	RP-70	LINEAR	RP-70	LINEAR	RP-70
0.5625	124.407	124.512	125.308	0.105	0.901	0.0844	0.7242
0.6250	124.407	124.493	123.711	0.086	-0.696	0.0691	-0.5595
0.6875	124.407	124.464	124.947	0.057	0.540	0.0458	0.4341
0.7500	124.407	124.453	118.099	0.046	-6.308	0.0370	-5.0705
0.8125	124.407	124.453	124.901	0.046	0.494	0.0370	0.3971
0.8750	124.407	124.429	123.693	0.022	-0.714	0.0177	-0.5739
0.9375	124.407	124.432	124.915	0.025	0.508	0.0201	0.4083
1.0000	124.408	124.442	124.605	0.034	0.197	0.0273	0.1583
1.0000	124.408	125.021	124.774	0.613	0.366	0.4927	0.2942
1.5000	124.408	124.659	124.473	0.251	0.065	0.2018	0.0522
2.0000	124.408	124.598	124.685	0.190	0.277	0.1527	0.2227
2.5000	124.408	124.496	124.553	0.088	0.145	0.0707	0.1166
3.0000	124.408	124.426	124.379	0.018	-0.029	0.0145	-0.0233
3.5000	124.408	124.444	124.317	0.036	-0.091	0.0289	-0.0731
4.0000	124.408	124.426	124.447	0.018	0.039	0.0145	0.0313
4.0000	124.408	125.004	124.991	0.596	0.583	0.4791	0.4686
5.0000	124.408	124.599	124.586	0.191	0.178	0.1535	0.1431
6.0000	124.408	124.460	124.461	0.052	0.053	0.0418	0.0426
7.0000	124.408	124.457	124.471	0.049	0.063	0.0394	0.0506
8.0000	124.408	124.438	124.442	0.030	0.034	0.0241	0.0273
9.0000	124.408	124.445	124.454	0.037	0.046	0.0297	0.0370
10.0000	124.408	124.429	124.424	0.021	0.016	0.0169	0.0129

Table 15. Travel time counterpart of table 14.

3. For low-angle rays which are generally excluded from computation by RP-70 for typical oceanic profiles, the comparison with the NUC linear control reveals that there are some significant errors in RP-70. For rays with all angles less than 1°, the range error in RP-70 can be as much as 0.9 percent, which is larger by a factor of 16 than the error encountered in the typical ocean profiles. For such low-angle rays, there is also some marked error in the RP-70 travel time computations. The travel time computations for the four rays of lowest angle for the Epstein profile of section 2 are completely out of line. The travel time for the 0.75-degree ray of the focusing profile of section 3 is in error by about 5%.

4. Comparisons with the exact range and travel time solution for the Epstein profile indicate that the errors introduced in the profile approximation by the use of linear segments are much larger than those introduced by RP-70 approximations (excluding the travel times cited in conclusion 3 above). The maximum error (for both range and travel time) due to profile approximation was 108 times larger than that due to program approximations in implementing the ray theory.

Sections 3.1.1 to 3.1.3 suggest the following recommendations:

1. The fact that the RP-70 travel time computations are generally more accurate (often much more accurate) than the range computations suggests that there should be some simple procedures which could improve the range accuracy at least to the present accuracy of the travel times. Aside from improving the RP-70 program for low ray angles, there appears little to be gained by an extensive overhauling of the RP-70 approximations used to implement the ray theory of linear segments. Instead, emphasis should be placed on improving the model of the sound speed profile.
2. The general validity of RP-70 ranges and travel times has been established for the three typical ocean profiles, an approximation to the Epstein profile, and an approximation to a focusing profile. These five profiles then should be used as test cases to help determine that RP-70 or any other program using linear segments is operating properly.
3. The 0.75° ray for the focusing profile should be rerun on the RP-70 program to determine the cause of the travel time anomaly. This anomaly in itself may appear of little significance. However, our experience has been that such anomalies, as innocuous as they may appear, should be investigated for they often provide clues to program deficiencies which could introduce serious errors in other situations.
4. For diagnostic purposes, ray theory results of RP-70 should be printed out with more significant digits than are necessary for operational use.

We can provide some insight as to why the RP-70 range errors are large for low angles. The RP-70 counterpart of equation 1 is

$$R_i = h_i \cot \frac{1}{2} (\theta_i + \theta_{i+1}) \tag{6}$$

where h_i is the thickness of the layer. Equation 6 is an exact equivalent of equation 1 and indeed appears in the early literature (ref 8). Although exact, equation 6 is a particularly poor expression for calculating ranges when the ray forms an apex or nadir in the layer. Consider, for example, the case when the ray forms an apex in layer i. Then equation 6 becomes

$$R_i = \Delta Z \cot (\theta_{i+1}/2) \tag{7}$$

where ΔZ is the distance from ray apex to interface i+1. Equation 7 represents the product of a small number, ΔZ, and a very large number, cot $(\theta_{i+1}/2)$. Indeed, if we consider the limit of equation 7 as θ_{i+1} approaches zero, equation 7 is of the form zero times infinity. If evaluated with great precision, equation 7 will yield the proper limit of zero. However, unless each of the factors is evaluated with great precision, the result will have considerable error.

8. Physics of Sound in the Sea, NAVMAT P-9675, Washington DC, 49, 1969.

The equation 1 counterpart of equation 7 is

$$R_i = \frac{-C_s}{\cos \theta_s} \frac{\sin \theta_{i+1}}{a_i} \tag{8}$$

As θ_{i+1} approaches zero, the limit of equation 8 goes to zero without any problem.

Although we cannot be certain, we suspect that the use of equation 6 contributes to the range error in RP-70 for small angles.

It is probable that the builders of RP-70 recognized the low-angle limitations and hence excluded rays with depth excursion of less than 225 m. There are two problems with this treatment. One, it assumes that the rays are of little consequence and can be excluded without affecting the result. Two, it assumes that the depth exclusion criteria always eliminate rays which might pose a problem. The latter assumption appears to be correct for the three typical ocean profiles. However, the control cases of section 3.1.2 and 3.1.3 show that it does not always eliminate problem rays. Thus RP-70 will treat rays which can produce wild and erroneous range and travel time results.

Conclusion 4 points up a general problem in the comparison of models to controls. Every propagation model is based on some input model of the environment. The lack of agreement between two propagation models may stem primarily from differences in the input model rather than from implementation of acoustic theory. For example, the errors produced by approximating the Epstein profile with linear segments was as much as 108 times as large as the differences between the NUC linear control and the RP-70 implementations of acoustic theory. In comparing the results of two acoustic models, the input models of the environment should be identical if possible. Unfortunately, this cannot always be achieved and we cannot distinguish between differences caused by profile variations and those caused by a different implementation of acoustic theory.

3.1.5 Long-Range Epstein Profile

In this example, a range-independent profile was used to serve as a control out to a range of 200 kyd. This control was an Epstein profile obtained by fitting a set of data points taken in the Java Trench. The following discussion outlines the outputs for this profile, which were furnished to AESD.

Card decks and tabulations of the sound speed profile were furnished. The profile data were obtained by evaluating the analytic profile at incremented depths similar to the example presented in table 4.

The acoustic outputs were all calculated from the analytic expression for the Epstein profile. For this example, computations were not made for the linear control model. Ray diagrams were provided for source depths of 20 and 100 yd. Tabulations of range and travel times at appropriate depths along the rays were provided. A plot of R/T versus T for a complete cycle for source and receiver both at 20-yd depths was provided, as well as a similar plot for 100-yd depth. Two plots of propagation loss for source depths of 20 yd and 100 yd were provided. Each of these plots included receivers at 20, 100, and 200-yd depths. Tabulations of these losses were also provided. The data points in these plots and tabulations were obtained by first calculating the propagation loss at 100-yd intervals and then averaging values to 1.0-kyd intervals. These losses were obtained by assuming random phase addition of ray arrivals. No bottom-reflected rays were calculated and caustic correction approaches were not included.

3.1.6 Range and Travel Time Consistency Test

This is a test which can be applied to any program for which the sound speed profile depends only on depth. It checks the consistency of range and travel time computations. This test was first described on page 166 of reference 9. It is based on the equation

$$dR/dT = C_m = C_s/\cos\theta_s \tag{9}$$

where R and T are range and travel time. C_m is the phase velocity of the ray, C_s is the sound speed at the source, and θ_s is the ray angle at the source.

Let θ_1 and θ_2 be any two adjacent ray angles at the source which have the same history (to be explained later), with ranges of R_1 and R_2 and travel times of T_1 and T_2. Using finite differences we may write

$$dR/dT \approx \Delta R/\Delta T = (R_2 - R_1)/(T_2 - T_1)\,. \tag{10}$$

Equation 10 represents a measure of the derivative midway between R_1 and R_2. The ray parameter corresponding to this midpoint is

$$C_m \approx (C_{m1} + C_{m2})/2 = \frac{1}{2}\left[(C_s/\cos\theta_1) + (C_s/\cos\theta_2)\right]. \tag{11}$$

That is, the average C_m corresponds to the midpoint. Equations 9, 10, and 11 lead to

$$\Delta R/\Delta T \approx (C_{m1} + C_{m2})/2\,. \tag{12}$$

Table 16 illustrates the use of this check. The ray calculations are taken from the linear control model for the profile of table 3 for a 60-ft source and 300-ft receiver. The first column of table 16 presents the ray angle at the source. The second column presents the phase velocity of the ray as determined from the ray angle and the source sound speed of 1647.2112 yd/s. The range and corresponding travel times are given in columns 3 and 4. Column 5 is $\Delta R/\Delta T$ as calculated by equation 10. Column 6 is the average phase velocity as calculated by equation 11. Column 7 is the difference between columns 5 and 6.

Table 16 was provided to FNWC to check their program and is not a good example of the test because, for the linear approximation of table 3, $\partial R/\partial C_m$ is discontinuous for any ray which turns around at a profile interface. Thus the test loses accuracy when the pair of ray parameters straddle an interface sound speed. The best examples of this loss of accuracy are the 13° and 14° rays which straddle the ocean bottom and the 7° and 8° rays which straddle the interface at 900 m.

The best examples of this test in table 16 are for the 9 and 10, 11 and 12, and 12 and 13° rays. These pairs do not straddle any interfaces and the test is consistent to better than 0.1 yd/s. To get this consistency, the ratios of range and travel time differences must be consistent to better than five decimal digits. This means that the ranges and travel times themselves must be accurate to better than six digits.

---

9. Pedersen, M. A., Theory of the Axial Ray, J Acoust Soc Am 45, 157-176, Jan 1969.

ANGLE	CM	RANGE	TIME	ΔR/ΔT	AV CM	DELTA
5	1653.50333	48647.5774	29.5157578			
				1654.98714	1654.89394	0.09320
6	1656.28455	75548.8896	45.7704535			
				1658.25600	1657.93303	.32297
7	1659.58152	114141.471	69.0434470			
				1659.83261	1661.49043	-1.65781
8	1663.39934	129716.243	78.4267859			
				1666.06438	1665.57164	.49274
9	1667.74394	136421.633	82.4514744			
				1670.20933	1670.18304	.02629
10	1672.62214	148243.772	89.5297124			
				1675.40364	1675.33187	.07178
11	1678.04160	159809.299	96.4328411			
				1681.00352	1681.02626	-0.02274
12	1684.01093	172808.699	104.165960			
				1687.24202	1687.27530	-0.03328
13	1690.53967	186316.143	112.171595			
				1696.72583	1694.08901	2.63682
14	1697.63836	155394.374	93.9472191			
				1700.87605	1701.47846	-0.60241
15	1705.31857	125921.569	76.2488074			
				1709.11254	1709.45575	-0.34321
16	1713.59293	1086953.284	66.6892936			
				1717.76098	1718.03407	-0.27309
17	1722.47522	97483.5796	60.0121689			
				1726.98720	1727.22781	-0.24060
18	1731.98040	88659.6687	54.9027443			
				1736.82994	1737.05254	-0.22260
19	1742.12468	81524.2520	50.7944453			
				1747.31342	1747.52514	-0.21172
20	1752.92560	75566.0264	47.3845100			

Table 16. Range and travel time consistency check for the profile of table 3.

We were provided RP-70 outputs for various profiles. However, we could not apply this test to these outputs because the values were given to only five significant digits.

In the test of table 16, the pair of C_m differed by about 5 m/s due to the 1° spacing between rays. The accuracy of the test can be sharpened considerably by spacing the C_m closer, say 0.1 m/s apart. The size of delta with such a spacing is considerably smaller than those of table 16. The values of delta can be used to provide very good estimates of how many digits of accuracy there are in range and travel time.

3.2 CONTROLS FOR RANGE-DEPENDENT ENVIRONMENTS

This section presents controls where the environment is range-dependent. Sections 3.2.1 and 3.2.2 present controls where the sound speed profiles vary with range as well as depth. Section 3.2.3 presents a single control where the depth of ocean bottom varies with range. Section 3.2.4 presents a technique for testing ray theory in any range-dependent environment. Unfortunately, there are no RP-70 results for any of these controls.

3.2.1 Range-Dependent Profile Focusing Rays

Before presenting our first example of a range-dependent sound speed profile, let us discuss the problem in more general terms. Starting in 1969, we initiated an investigation of how to develop sound speed profiles with two-dimensional variations for which the ray theory solutions could be written in closed form. A general method, developed by DeWayne White, was available for use by 1971 although a formal description of the method was not published until 1978 (ref 10).

10. White, D., Ray Theory for Wide Classes of Sound-Speed Profiles with Two-Dimensional Variation, J Acoust Soc Am 63, 405-419, Feb 1978.

In this method, the sound speed profile is expressed in terms of x and y of a transformed coordinate system in which x and y are functions of depth (z) and range (r). The transformation and sound speed function are such that the transformed eikonal equation reduces to a partial differential equation separable in x and y. The closed-form ray equations are calculated in terms of x and y; then the results are converted to and presented in depth and range coordinates. There are large classes of allowable transformations. Five specific examples of transformations are presented in reference 10. This method leads to innumerable closed-form solutions.

Fortunately, this method was available and was put to use to develop range-dependent control cases for RP-70. The first test case is discussed on pages 410 to 412 of reference 10. In this example, the profile was constructed to focus rays. All rays leaving a source at zero range and a depth of 1000 yd, with source angles between 0.143° and -89.857°, focus at a depth of 1500 yd and a range of 200 kyd. This example provides a simple check on the ray path calculations for any scheme treating two-dimensional sound speed variations.

The inputs provided AESD for this test case were 22 sound speed profiles versus depth given at 10-kyd range intervals from 0 to 210 kyd. For each profile, the sound speeds were given at 150 depths. The spacing was 50-yd increments from 0 to 2500 yd, 250-yd increments from 2500 to 4000 yd, and 1500-yd increments from 4000 to 9850 yd. A card deck, tabulations, and plots of these sound speed profiles were provided. The depth sampling was chosen to provide extensive detail in regions where the profile has the largest changes commensurate with a 150-depth limitation on the RP-70 program. Reference 10 discusses how the sound speed profiles may be generated for any spacing in both range and depth.

The outputs provided AESD were a ray diagram similar to figure 2 of reference 10. Rays were traced for 1° increments of source angle covering a cone bounded by ±9°. Tabulations of range and travel time were also provided for these rays. Values were provided for each ray crossing of the receiver depth of 1500 yd. Values of depth, range, and travel time were provided at all turning points.

3.2.2 Range-Dependent Semirealistic Profile

The second range-dependent test case for RP-70 is discussed on pages 414 to 417 of reference 10. In this example, two sound speed profiles measured in the ocean at positions 1352 kyd apart were approximated by Epstein profiles. Although the fits are rather gross, this test case approximates an oceanic condition.

The inputs provided AESD for this test case were 22 sound speed profiles given at 10-kyd range intervals from 0 to 210 kyd, and 29 sound speed profiles given at 50-kyd range intervals from 0 to 1400 kyd. For each profile, the sound speeds were given at 150 depths. A card deck, tabulations, and plots of the sound speed profiles were provided. Figure 6 of reference 10 presents the profiles at 0, 676, and 1352 kyd. The set of profiles at 10-kyd range intervals was used for a set of ray computations out to a range of 210 kyd. The set of profiles at 50-kyd range intervals was used for a second set of ray computations made out to a range of 1360 kyd.

An extensive set of outputs was provided AESD. Ray diagrams out to a range of 210 kyd were provided for source depths of 50 and 200 yd. Rays reflecting from the surface were not included in any computations. The ray tracing algorithms of reference 10 have not been implemented for surface reflections. This implementation is possible but would be quite expensive to operate because an iterative procedure is required to find where the ray intersects the surface. Figure 7 of reference 10 presents the ray diagram for the 50-yd source out to a range of 160 kyd.

Computer printouts for a much denser set of rays were also provided. For each ray, the range, intensity, and travel time were given at each receiver crossing with receiver depths at 25, 200, and 500 yd. A printout which listed each ray apex and nadir for every tenth ray was provided. Finally, a printout of random phase propagation loss versus range was provided for each receiver depth. These printouts were provided out to 201 kyd for source depths of 50 and 200 yd. Plots of propagation loss averaged over 1-kyd steps were also provided. Figure 8 of reference 10 presents propagation loss for the 50-yd source and 25-yd receiver out to a range of 140 kyd. The effect of horizontal change is apparent even at these short ranges.

Similar information was provided for the second set of ray computations carried out to long ranges. These were done for a source depth of 50 yd and a receiver depth of 500 yd. The ray listing showed crossings starting from zone sixteen. The propagation loss tabulations and plot covered the range interval from 1150 to 1360 kyd.

3.2.3 Reflection from a Curvilinear Bottom

This example provides a test case for ray tracing in a range-dependent environment where the bottom depth varies with range. The equation defining the bottom depth was chosen as

$$Z = Z_0 - \frac{3(Z_0 - Z_1)}{R_1^2} R^2 + \frac{2(Z_0 - Z_1)}{R_1^3} R^3 \qquad (13)$$

where Z is the bottom depth, R is the range, and Z_0, Z_1, and R_1 are three parameters. Here Z_0 is the depth at zero range and Z_1 is the depth at a range equal to R_1.

For the sample case presented here, the parameters were chosen as

$$Z_0 = 3500 \text{ m}, \quad Z_1 = 2000 \text{ m}, \quad R_1 = 20 \text{ km} .$$

The bottom profile for these parameters is shown in figure 7. Equation 13 is constructed so that the relative maximum of the cubic equation occurs at R = 0 and the relative minimum occurs at $R = R_1$. Thus the depth of the relative maximum is Z_0 and that of the selective minimum is Z_1. In this sample case, the source is placed at a depth of 1000 m and at a range of -10 km, while the receiver depth is 100 m.

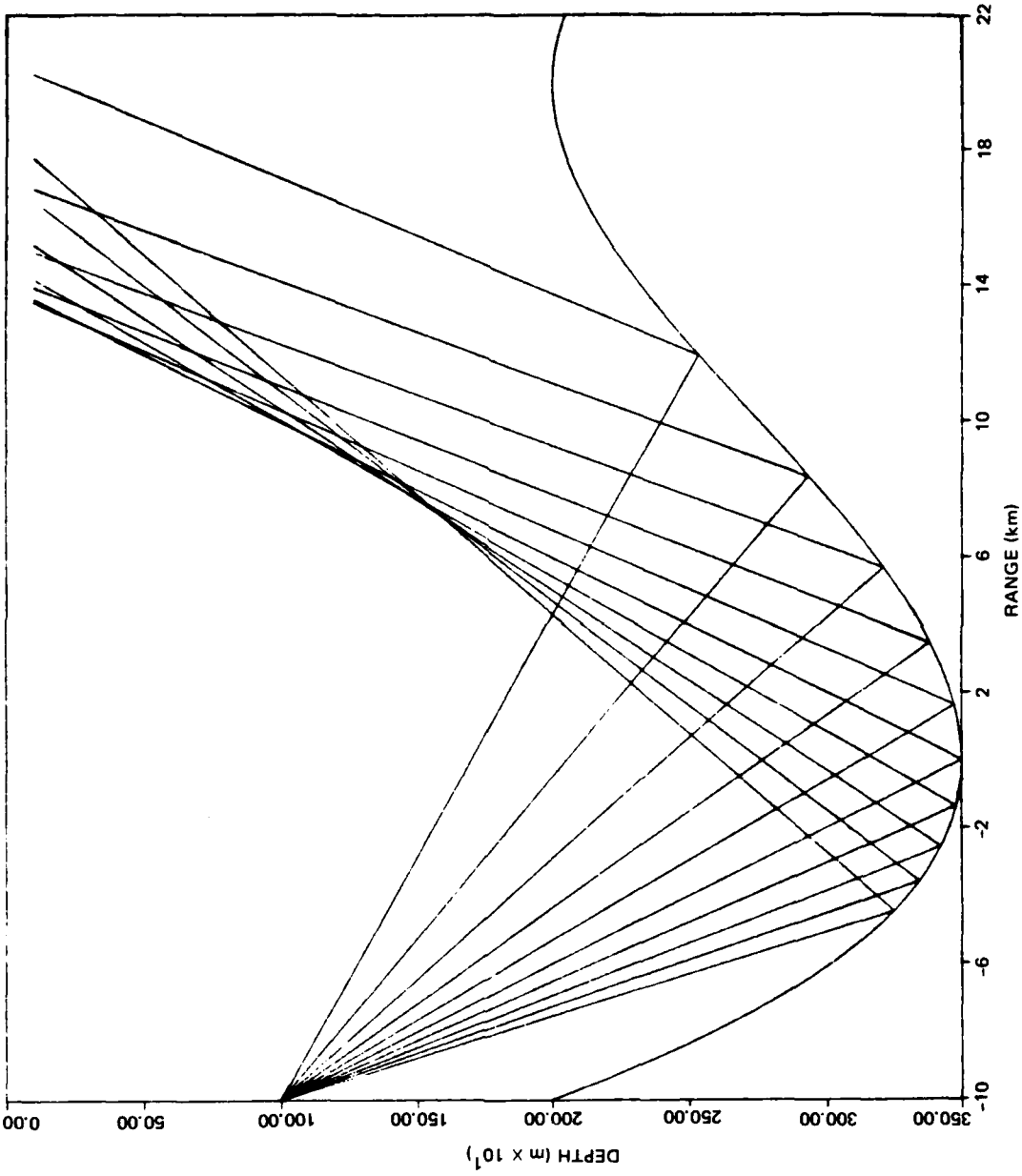

Figure 7. Ray diagram for a curvilinear bottom.

Figure 7 presents a ray diagram showing the ray paths which leave the source heading downward and arrive at the receiver heading upward. To simplify the control case, the sound speed profile was chosen to be isospeed. Thus the rays are straight lines. The equation for the downward headed ray path is

$$Z = 1000 + (R + 10\,000) \tan \theta_s \tag{14}$$

where θ_s is the source angle. The range where this ray intersects the bottom was determined in the control model by replacing Z in equation 13 with the right side of equation 14. The root of the resulting cubic equation in R was then solved by Newton's method. Once this range of intersection, R_b, is determined, the depth of intersection, Z_b, is easily determined from equation 14. The slope of the bottom at the point of intersection is then computed from

$$dZ/dR = 6R_1^{-1} (R_b/R_1)(Z_b - Z_1) [(R_b T R_1) - 1] . \tag{15}$$

The angle of the bottom slope is then

$$\theta_b = \tan^{-1} (dZ/dR) . \tag{16}$$

The equation of the upward-headed ray path then becomes

$$Z = Z_b - (R - R_b) \tan (\theta_s + 2\theta_b) . \tag{17}$$

Tabulations of each ray as well as the ray diagram of figure 7 were provided to AESD. The tabulations included the depth, range, and ray angle after reflection, as well as the bottom slope for the point where the ray intersected the bottom. The range where the ray intersected a receiver at 100-m depth was also given.

The purpose of this example is to provide a test case of a smooth concave bottom which produces a convergence zone for bottom-reflected rays. For receiver depths near the surface, the range initially decreases with increasing ray angle until a minimum in range is formed (caustic point). The range then increases with increasing ray angle. Most models approximate the bottom contour with piecewise linear sections. By comparing the results of such models with our control model, we can assess the error introduced by sloped discontinuities in the bottom contour. Our control model would also provide a good, simple test for models which fit the contour with splined parabolic sections with no slope discontinuities.

This control should probably be updated by replacing the isosound speed profile by a refractive profile. Some models to be tested do not treat isosound speeds. Moreover, the combination of depth dependence and range dependence provides a more rigorous test of the model.

Regardless of the sound speed profile used in the control, the form of equation 13 appears to be well suited for testing a model's ability to cope with curvilinear bathymetry. From equation 13 we obtain a cubic curve which forms an asymmetric trough. The bottom of the trough is at Z_0 at zero range. The top of the trough is at Z_1 at range R_1. Moreover, the bottom depth is Z_1 at a range of $-R_1/2$. The source can be placed at any range desired relative to the bottom of the trough. Since we can reflect the bottom profile about zero by letting R_1 be a negative value, we can easily simulate a variety of trough conditions.

3.2.4 Reciprocity Tests

The reciprocity test can provide an excellent test of ray tracing (range computations) for a range-dependent sound speed profile or for a nonflat ocean bottom. This test consists of tracing a given ray at angle θ_1 from the source to obtain a range R_1 and angle θ_2 at the receiver. One then proceeds to place the source at the receiver position; ie, the receiver depth is positioned at range R_1 relative to the profile or bottom range coordinate systems. Starting with the angle θ_2, one traces the ray back to a receiver depth equal to the original source depth. This ray must pass through this receiver depth at a range of zero in the profile or bottom range coordinate system; ie, when the same ray is run backwards it must return to its point of origin. Travel time should also agree.

This test is trivial for a depth-dependent-only sound speed profile and a flat bottom. However, it provides a good test of the ray algorithms in a range-dependent environment. Captain Wolfe reported that RP-70 was subjected to this test and did well (ref 11). He also noted (without verification) that most range-dependent models do not even "wind up in the same ocean" when subjected to this reciprocity test.

One caution should be observed in the use of this test. The elements must be truly interchanged. Assume the source is at $(R, Z) = (0, Z_1)$, and the receiver at (R_1, Z_2); to reciprocate, the source must be placed at (R_1, Z_2) and the receiver at $(0, Z_1)$. We cannot reciprocate by placing the source at $(0, Z_2)$ and the receiver at (R_1, Z_1). This latter placement is also reciprocal in the case of a range-independent environment. However, it is not reciprocal for a range-dependent environment.

Reciprocity may also be used as a test of the evaluation of ray intensities as well as ray paths. Some aspects of the intensities for reciprocal configurations are discussed in section 7.2.4.

4.0 NONBOTTOM-REFLECTED PROPAGATION

In this section, we discuss controls for various oceanic ducts which do not involve reflection from the ocean bottom. The sound speed profiles do not depend on range for these controls. The controls are treated in three groups. Section 4.1 treats deep-channel propagation. Section 4.2 treats surface duct propagation. Section 4.3 treats multiple ducts.

11. Wolfe, P., private communications.

4.1 DEEP CHANNEL PROPAGATION

This section is concerned with propagation associated with the deep sound channel. There are several types of propagation included here. These include convergence zone (CZ) propagation for a shallow source, RSR propagation for a deep source near the ocean bottom, and SOFAR propagation associated with a source near the axis of the deep sound channel. These have been grouped together because they share common theoretical problems. A problem solved for CZ propagation will apply to RSR propagation as well. For these types of propagation normal mode methods, the parabolic equation method (page 33 of ref 12) and the fast field method (page 90 of ref 12) work quite well. Our primary concern in this section is how well ray theory approaches can treat this type of propagation. The first four controls discussed here are concerned with various caustic structures of ray theory. Caustics pose the single greatest limitation in geometric ray theory because at such points the pressure becomes infinite. The remaining two controls of this section are concerned with other aspects of deep-channel propagation.

4.1.1 Controls for Two-Ray Caustics

This section discusses a normal mode control of convergence-zone and shadow-zone propagation. This control is compared to various state-of-the-art ray theories. It treats the superposition of simple smooth caustics to obtain the combined acoustic field for a convergence zone. These caustics are formed by two-ray systems and the geometric ray theory intensity has a single pole. This type of caustic is the most common. Other, more complicated, caustic structures are described in later sections.

When AMEC approached us about preparing some theoretical controls in FY 79, we elected this area as one of primary interest. We had just completed the work of reference 13, which presents a new method of treating caustics and shadow zones. A previous attempt at comparing the multicaustic convergence zones of ray theory, by using nonuniform asymptotics with results of normal mode theory, had met with limited success (see fig 7.6 to 7.1.6 of ref 14). We were interested in determining whether the new methods would lead to improved agreement. Work was initiated in formulating the control in FY 79 under AMEC funding. The actual implementation and examination of the control were conducted in FY 80 under another sponsor, NAVSEA 63R23, who had need of an improved model of shadow and convergence zones at low frequency.

The material presented here is taken largely from reference 15. The ray theory approach is discussed in detail by White and Pedersen (reference 13). The field in the shadow zone is evaluated by using rays with complex parameters. This approach is an analytic continuation of standard ray theory techniques for real rays. A uniform asymptotic formulation is used to evaluate the field in the boundary layer about the caustic. The

---

12. DeSanto, J. A., Ocean Acoustics, Springer-Verlag, 1979.
13. White, D., and M. A. Pedersen, Evaluation of Shadow Zone Fields by Uniform Asymptotics and Complex Rays, J Acoust Soc Am 69, 1029-1059, April 1981.
14. Blatstein, I. M., Comparison of Normal Mode Theory, Ray Theory, and Modified Ray Theory for Arbitrary Sound Velocity Profiles Resulting in Convergence Zones, Naval Ordnance Laboratory TR 74-95, Aug 1974.
15. Pedersen, M. A. et al, Comparison of Ray-Theory and Normal Mode Results for Convergence Zones, Tenth International Congress on Acoustics, Sydney, Australia, Jul 1980.

normal mode theory is discussed in detail by Gordon (ref 16). In this theory, the ocean is modeled by layers in which the square of the index of refraction is linear in depth. The parameters of this profile may be complex as well as real.

Figure 8 presents the sound speed profiles used in the comparison. The left panel gives the real part of the sound speed while the right panel gives the imaginary part. The first and second layers model the deep-water channel. These are the only layers used in the ray theory approach. Two different models of the sub-bottom structure are used in the normal-mode approach. In profile A, this structure is a negative-gradient half-space. As we shall see in a later example, the large slope discontinuity at the ocean bottom produces significant differences between the results of ray and mode theory. Profile B was devised to reduce effects of this slope discontinuity. Profile B has an additional positive-gradient layer below the ocean bottom. The sound speeds in this layer are complex. The imaginary parts of the sound speed introduce attenuation which strips off high-order modes. The parameters of profile B are chosen to make the sound speed continuous and to make the real part of the sound speed gradient continuous at the ocean bottom. There remains a discontinuity in the imaginary part of the sound speed gradient. However, the effect of this discontinuity and other discontinuities at the layer 3–4 interface is small compared to the effect of the slope discontinuiuty in profile A.

Figure 9 is a ray diagram for a 200-m source depth. The receiver depth chosen for investigation is 500 m. The dots designate the range of the five caustics in the first convergence zone. Counting from the left, caustics 1 and 3 are formed by purely refracted rays, while caustics 2, 4, and 5 are formed by surface-reflected rays. The range interval chosen for most of the detailed comparisons to follow is from about 35 to 56 km. This interval contains caustics 1 to 3. At low frequencies, the shadow-zone fields of caustics 4 and 5 also contribute in this interval.

Figure 10 presents the propagation loss of complex ray theory for each of the five caustic structures. The frequency is 25 Hz. The two ray arrivals for each caustic structure are combined coherently to produce these propagation loss curves. The propagation loss at the caustic ranges goes to $-\infty$ since caustic connections have not yet been applied. The shadow zone fields (ie, the regions to the left of each caustic) are evaluated with the use of complex ray parameters. Each curve is terminated when one of the two ray arrivals is the ray which grazes the ocean surface or ocean bottom. The present theory does not treat shadow zones formed by these grazing rays. The surface-grazing ray is first encountered at a range of 56 km. This is an upper range limit on the validity of this ray theory. Indeed, later examples will show that the ray theory results begin to deteriorate at ranges somewhat less than 56 km. This deterioration occurs because the present treatment of the ocean surface is not rigorous.

Figures 11a to 11d compare the normal-mode propagation loss of profile B (the most accurate control) with other propagation loss approaches. This control is repeated in all figures and is shown as a heavy solid curve. All calculations are for 25 Hz. The light solid curve of figure 11a is the result of elementary phased ray theory. In this ray approach, the shadow-zone field is not included and there are no caustic corrections. However, the various ray arrivals are combined coherently to obtain the resultant propagation loss. The

16. Gordon, D. F., Underwater Sound Propagation Loss Program, Naval Ocean Systems Center, TR 393, May 1979.

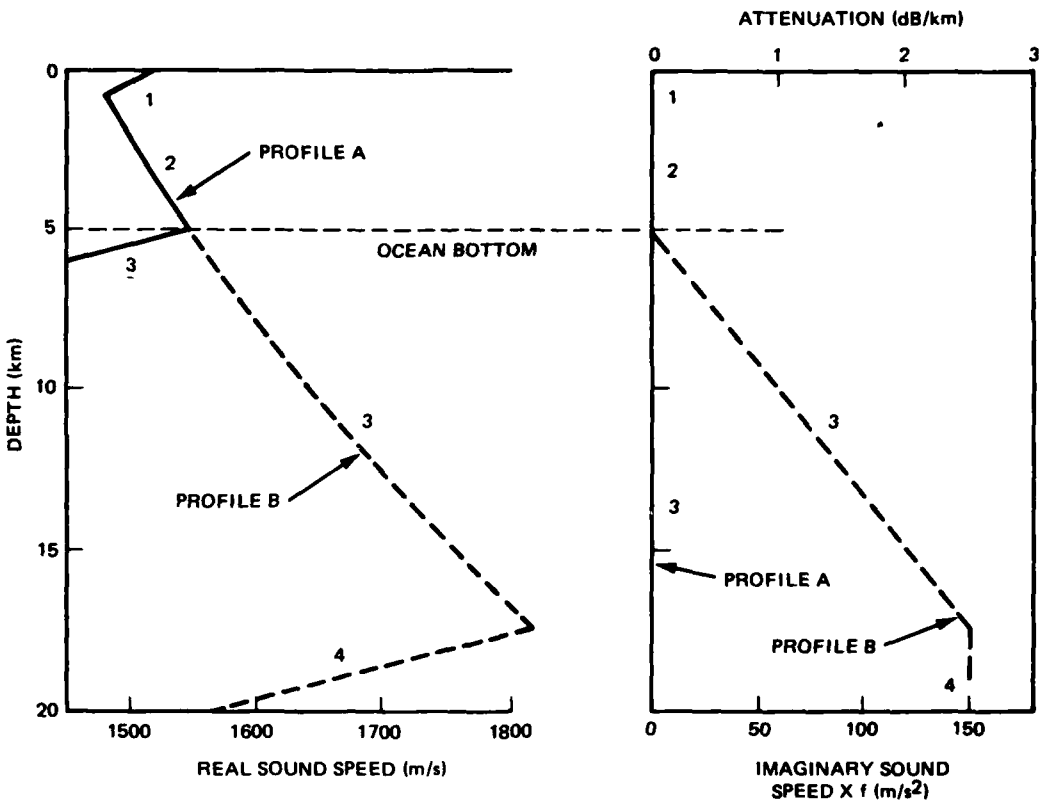

Figure 8. Sound speed profiles of convergence zone test case.

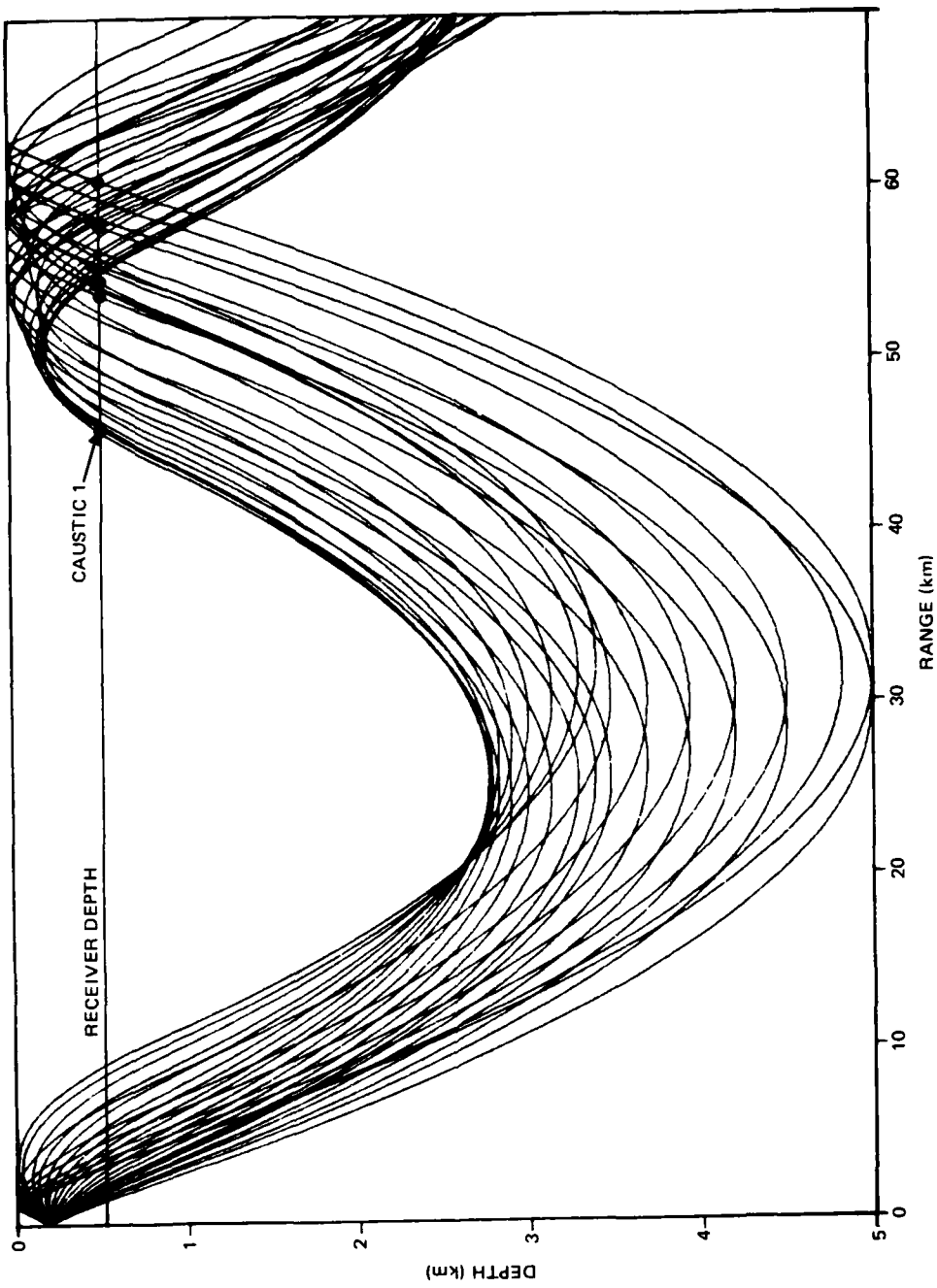

Figure 9. Ray diagram for the profile of figure 8.

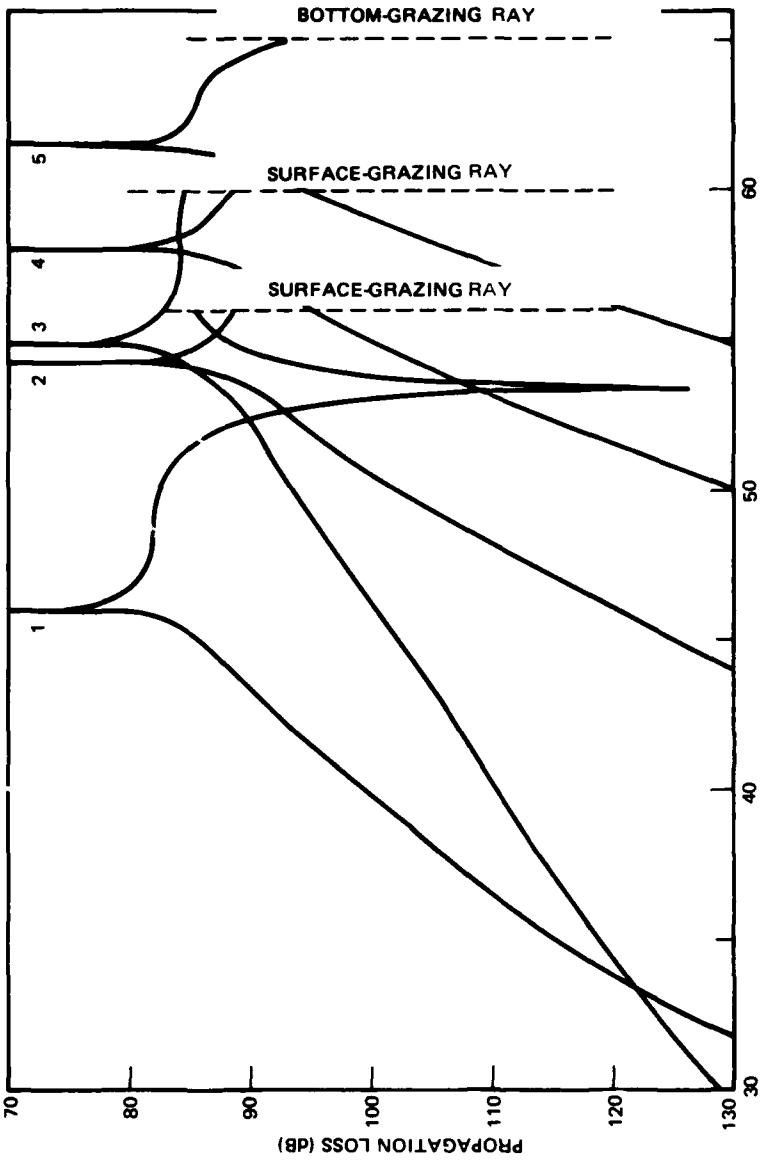

Figure 10. Propagation loss at 25 Hz for each caustic structure.

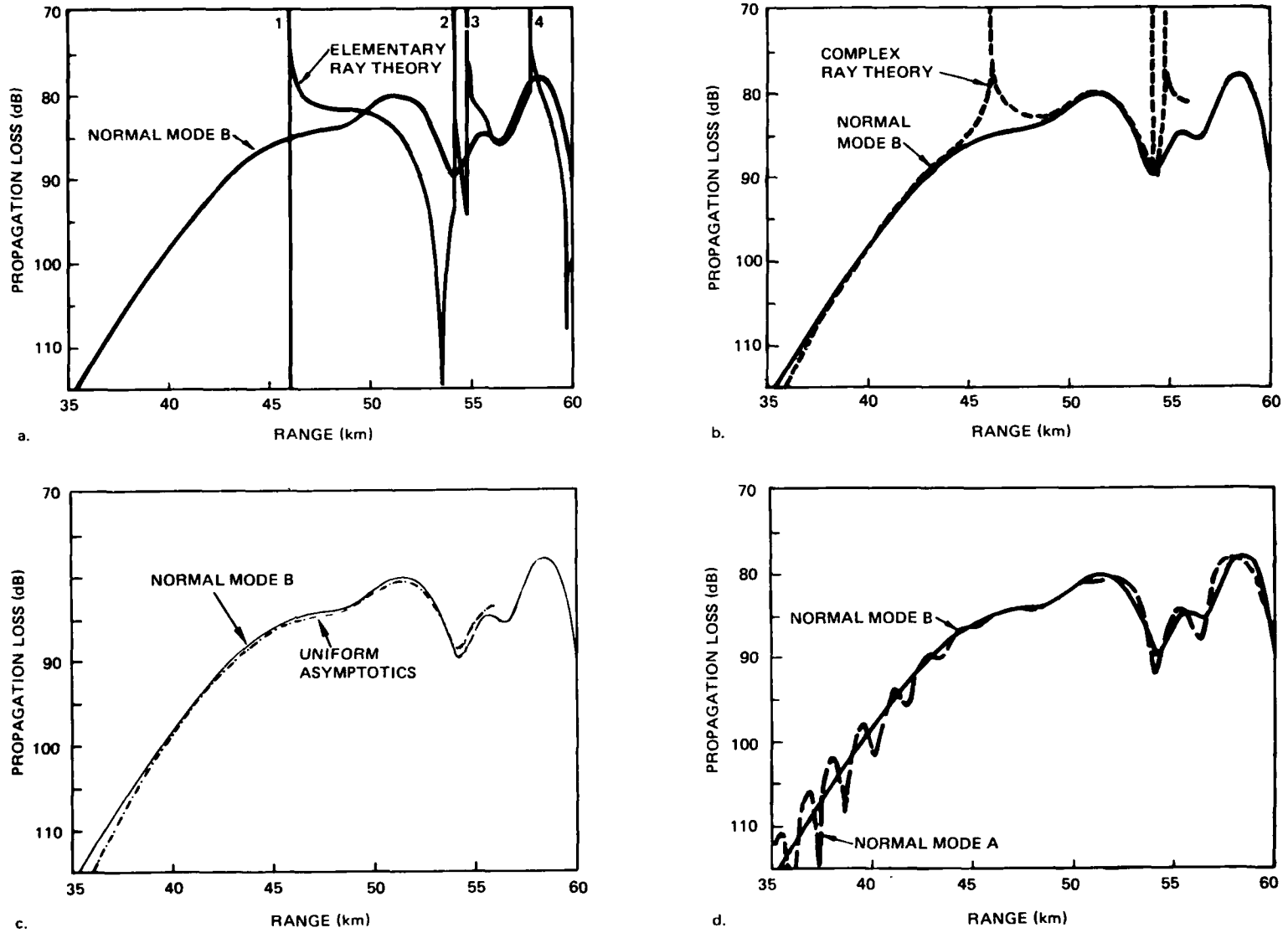

Figure 11a-d. Comparison of normal mode propagation loss at 25 Hz for profile B with that of various other approaches: (a) with elementary phased ray theory; (b) with complex phased ray theory; (c) with uniform asymptotic ray theory; and (d) with normal mode theory for profile A.

phase calculation uses travel times, a $-\pi$ phase shift each time the ray has reflected from the ocean surface, and a $-\pi/2$ phase shift each time the ray has touched a caustic curve. At this frequency, the results of elementary phased ray theory bear little resemblance to mode theory.

The dashed curve of figure 11b results from complex phased ray theory. This approach differs from elementary phased ray theory only in that the shadow-zone field is included. In this approach, the amplitudes and travel times in the shadow-zone fields are evaluated by using complex rays. There are no caustic corrections in this approach. For example, the result shown in figure 11b was obtained by combining the pressure equivalents of figure 10, by means of the same type of phase approach as in the elementary treatment. Note the relative minimum in propagation loss for the mode theory result centered at a range of about 52 km. The complex phased ray theory result models this feature very well. It is now apparent that this peak is formed by the shadow-zone fields of interior caustics 2 and 3. The combined fields are in a constructive phase relationship at this relative minimum. Here, the contribution of the shadow-zone fields reduces the resultant propagation loss by about 5 dB compared to the contribution of the insonified field associated with the first caustic.

The dot-dash curve of figure 11c is the result of uniform asymptotics. This approach combines the methods of complex ray theory and uniform asymptotics. The amplitude and travel time results of complex ray theory are treated by uniform asymptotics for each caustic structure. This treatment produces curves that are identical to those of figure 10 outside the caustic boundary layer. However, the values at and near the caustic are corrected to well-behaved, finite values. The propagation loss result is obtained through combining the various caustic structures by using the rigorous phase and amplitude calculations of uniform asymptotics. In this example, the uniform asymptotic result cannot be continued beyond 56-km range, since the method requires two arrivals for each caustic structure. At this range, one of the two arrivals associated with caustic number 1 drops out shortly after grazing the surface. The complex phased ray theory of figure 11b could be continued beyond this range, just as is done for the elementary phased ray theory. This has not been done merely for convenience, because in our computer program the complex ray theory result is produced as an intermediate byproduct of the uniform asymptotic result.

The results of uniform asymptotics compare remarkably well with mode theory. Comparison is fair even for the normal mode fade at a range of 54 km, which by chance occurs almost at the range of caustic number 2. A detailed calculation of the differences in propagation loss between uniform asymptotics and mode theory has been made. This calculation shows that the results agree to within ±0.5 dB over the 14.8-km range interval from 39.0 to 53.8 km. This result appears even more remarkable when we note that the propagation loss changes by 21.1 dB in this interval. The differences are not random but contain a bias and smooth modulation components. The mean difference over this interval is 0.19 dB, based on 75 points calculated at 200-m range intervals. If we exclude the regions near the end points of the interval, the modulation extrema lie between 0.29 and -0.03 dB.

At ranges beyond 53.8 km, the uniform asymptotic result diverges from mode theory, reaching a difference of 5.0 dB at 56-km range. Calculations at other frequencies show a similar behavior with the divergence starting at shorter ranges for lower frequencies and at a larger range for higher frequencies. We attribute this divergence to an inadequate treatment of rays, which are near to surface grazing, occurring at 56 km. Murphy and

Davis developed a correction for near-grazing rays in which the phase shift at the ocean surface is not a discontinuous jump but is a smooth continuous function of angle (ref 17). This theory is under investigation and proper application may eventually remedy the discrepancies shown here.

The uniform asymptotic result diverges from mode theory at ranges less than 39 km. Other frequencies show a similar divergence. The reason for this divergence is unknown.

A comparison of the dashed curve of figure 11b with the dot-dash curve of figure 11c shows good agreement except in the neighborhood of the caustics. This result follows from the property of uniform asymptotics, which guarantees agreement with geometric ray theory at distances well removed from the caustics.

Figure 11d presents the results of normal mode theory for profile A shown as a dashed line. For this profile, the slope discontinuity at the bottom of the water column causes reflections which produce a modulation in the profile A results which are eliminated by profile B. The amplitude of this modulation is smallest at about 48 km. This modulation amplitude increases as the range decreases below 48 km because, at shorter ranges, the ratio of the convergence zone component to the reflection component decreases. The magnitude of the reflection component can be estimated from the difference in propagation loss at the peaks or valleys of the modulation. For example, the propagation loss of the reflection component is estimated as 120 dB and 108.5 dB at ranges of 35 and 40 km, respectively.

Reference 15 also discusses results at 100, 25, 10, and 5 Hz. Agreement between uniform asymptotic and normal mode model B is best at 100 Hz, is good at 25 Hz, is marginal at 10 Hz, and is poor at 5 Hz.

Consider now some of the excellent features of this example of control. The first of these features is the use of two independent methods – ray theory and normal mode theory. The good agreement observed in figure 11c reassures us that the controls are correct and can indeed serve as controls. In establishing controls for new and complicated situations, there is always the nagging possibility that there is some error in the prospective control. This control illustrates the advantage of considering both ray and normal mode solutions. Over the years, in modeling nonbottom-reflected propagation, we have always terminated the sound speed profile of normal mode models by a negative gradient half-space starting at the ocean bottom. This scheme seemed to work quite well, and to our knowledge posed no problem. Thus the first normal mode control we considered was profile A of figure 8. However, in comparing the normal model results of this profile (fig 11d) with the results of uniform asymptotics (fig 11c), we noticed that the mode theory solution had a detailed beat structure that was not present in the ray solution. We speculated that these beats might result from reflections caused by the slope discontinuity at the ocean bottom. Dave Gordon then devised profile B of figure 8 to eliminate the slope discontinuity. The good agreement of figure 11c then convinced us that profile B was the better model to use as a control. The point is that in the absence of a good ray solution, we may well have settled for the normal mode result of profile A as a control.

The second excellent feature is the use of the same environmental input in comparing controls to models. Consider how much more complicated a comparison is when the control and the model use different functional forms to fit the environmental

17. Murphy, E. L., and J. A. Davis, Modified Ray Theory for Bounded Media, J Acoust Soc Am 56, 1747-1760, Dec 1974.

data points. In this case, the environmental inputs have only a discrete number of points in common. This example illustrates the care with which the environmental inputs must be chosen. Even though the portion of the profile utilized by the ray theory is identical to that of the normal mode theory, there are problems. Consider how more complicated a comparison is when the control and model environmental inputs have only a discrete number of points in common.

The third excellent feature has been referred to in section 2.5; ie, the concept of a hierarchy of controls. Table 17 presents a hierarchy for this example of convergence zone caustics. At the top of the table we have the simplest and crudest of ray approximations; ie, incoherent elementary ray theory in which all arrivals are added powerwise (in random phase). At the bottom of the table we have normal mode theory, which represents an exact solution to the wave equation. In between, we have a sequence of progressively more accurate approximations which will now be described.

1. Incoherent elementary ray theory.
2. Coherent elementary ray theory.
3. Semicoherent complex ray theory.
4. Coherent complex ray theory.
5. Semicoherent nonuniform asymptotics.
6. Coherent nonuniform asymptotics.
7. Semicoherent uniform asymptotics by series expansion.
8. Coherent uniform asymptotics by series expansion.
9. Semicoherent uniform asymptotics by complex rays.
10. Coherent uniform asymptotics by complex rays.
11. Semicoherent uniform asymptotics by complex rays, Murphy-Davis corrections.
12. Coherent uniform asymptotics by complex rays, Murphy-Davis corrections.

•
•
•

Parabolic equation method

•
•
•

Normal mode theory.

Table 17. Hierarchy of progressively more accurate controls for convergence zone propagation.

Referring to table 17, the ray solution of figure 11a is an example of item 2. This solution is the coherent counterpart of item 1. The remaining ray theory approaches consist of semicoherent and coherent pairs. By semicoherent, we mean that the two branches of each caustic are added coherently, but then the caustic structures are added incoherently. An example of item 3 would be obtained by adding the results of figure 10 incoherently. The ray theory result of figure 11b is an example of item 4.

Items 5 to 10 represent three different ways of handling caustic-corrected shadow zone arrivals. In items 5 and 6, by 'nonuniform asymptotics' we are referring to the method

of Brekhovskikh (ref 18) or Sachs and Silbiger (ref 19). This method gives the correct value at the caustic but does not fair in with elementary ray theory at large distances from the caustic. Items 7 and 8 refer to a method described in reference 13. In this method, the uniform asymptotic solution is developed as a power series about the caustic. Two-term series have been developed for each Ansatz quantity. The first term of these series is the nonuniform result. Items 9 and 10 represent the combined method of uniform asymptotics and complex rays. The ray theory of figure 11c is an example of item 10.

Items 11 and 12 represent potential improvements to ray theory involving Murphy-Davis corrections (ref 17) which will be discussed in a later section. The dots in the table indicate spaces for additional improvements in ray theory – or for other approaches. The parabolic equation method is sandwiched in here.

The fast field program is not included in the list, but should be regarded as about par with the normal mode theory. An advantage of this hierarchy of controls is that we can determine whether a model lives up to its theoretical expectation. For example, in testing the FACT model an appropriate control is item 5. The FACT model can do no better than this control, since the model is based on nonuniform asymptotics and semi-coherent addition of arrivals.

The method of complex rays is published (ref 13), although the details of the series expansion method have not yet been published. It is too early to say whether these methods will be utilized in future production models. This goal was our intent in developing the methods, rather than the establishment of control cases. The work of Blatstein (ref 14) falls under item 6. There are other combinations which do not fall under table 17. For example, in some of our work we use uniform asymptotics for real ray parameters and uniform asymptotics by series expansion for the shadow-zone fields. This hybrid method works well for some applications and avoids the use of complex ray calculations.

We regard these control cases to be dynamic rather than static. There are a number of potentional improvements for ray theory. The most important of these is the evaluation of the diffraction field from the left boundary of the shadow zone of figure 9. This evaluation involves Murphy-Davis corrections, which can also be used to treat grazing rays in the convergence zone itself. Reference 15 indicates that profile B of the normal mode theory leads to some problems at high frequency, presumably from reflections from the interfaces. Thus, since the ray theory has been improved, the use of profile B may pose some limitations. Here we have two choices – one is to finagle further with profile B to reduce reflections. The other choice is to develop the ray theory so that it can rigorously treat the entire sub-bottom structure.

4.1.2 Controls for Three-Ray Caustics

In this section, we discuss the status of controls for three-ray caustics. This includes the important case of cusped caustics. In the typical situation, two caustic curves merge at a cusp and result in a double pole in the geometrical ray theory intensity. The two-ray formulation of the previous section breaks down in the neighborhood of a cusp.

---

18. Brekhovskikh, L. M., Waves in Layered Media, Academic, 474-492, 1960.
19. Sachs, D. A., and A. Silbiger, Focusing and Refraction of Harmonic Sound and Transient Pulses in Stratified Media, J Acous Soc Am 49, 824-840, Mar 1971.

The most definitive treatment on cusped caustics has been prepared by Holford under contract to AESD (ref 20). Figure 12 shows the simplest form of cusp in this example as formed in a surface duct. The two caustic curves A and B merge at point C to form a cusp which has a horizontal axis. In the caustic interior (ie, between the caustic curves), there are three real rays through each point. These are clearly illustrated in figure 12. Exterior to the caustic there is one real ray, clearly illustrated in figure 12, and two complex rays.

Figure 13, also based on reference 20, presents range-versus-source angle plots for three receiver depths. For receiver depths above the cusp in figure 13a, the rays with negative source angles form a simple caustic at a relative minimum. For receiver depths below the cusp in figure 13c, the same is true for rays with positive source angles. At the cusp depth in figure 13b, there is a relative minimum for the zero-degree ray, with an additional curve passing through. This is the hallmark of a horizontal cusp for R-versus-θ_s plots.

Another type of cusp is the inclined cusp in figure 9, which appears near the conjugate or reciprocal depth. Figure 14 is a blowup showing the rays in the neighborhood of such a cusp. The sound speed profile for figure 14 is the same as that of figure 9. However, the source depth is 400 m rather than 200 m.

Figure 15 presents range-versus-source angle plots for five receiver depths. For receiver depths above the cusp (fig 15a), there is a point of inflection in the curve. For the receiver at the cusp depth (fig 15b), there is a horizontal point of inflection at the cusp. There is also a simple caustic for positive θ_s, which corresponds to the caustic boundary on the right side of the shadow zone. For receiver depths between the cusp and the reciprocal depth (fig 15c), there are a pair of connected caustics – one at a minimum in range and one at a maximum in range. There is also a simple caustic for positive θ_s. At the reciprocal depth (fig 15d), there is a simple caustic at a relative minimum in range. However, the simple caustic at a relative maximum in range and the simple caustic for positive θ_s have merged to form two nonhorizontal curves which intersect at $\theta_s = 0$. This is the hallmark of a simple caustic which occurs at the reciprocal depth. For receiver depths below the reciprocal depth (fig 15e), there is a single simple caustic for negative θ_s.

The pair of connected caustics of figure 15c can be used to illustrate why we may need to use a three-ray formulation in the neighborhood of a cusp as well as at the cusp itself. At high frequency, the boundary layers of the two connected caustics do not overlap. Such a case is illustrated in the schematic of figure 16. The range may be divided into five regions. In region 1A, the boundary layer of caustic A, we must treat caustic A as a two-ray system. However, the third ray in this region, which lies on one branch of caustic B, lies beyond the boundary layer of caustic B. Therefore, geometrical ray theory can be used for this arrival. Similarly, in region 1B, we can treat caustic B with the two-ray uniform asymptotic formulation and the third arrival by geometrical ray theory. In regions 2B and 2A, we may use geometrical ray theory for both the real and the complex arrivals. In region 3, we may use geometrical ray theory for each of the three real arrivals. Thus for this example we have no need for a three-ray formulation.

However, consider now the same situation but at lower frequencies. Region 3 tends to disappear as the boundary layers of the caustics start to overlap. In the region of overlap the three-ray formulation must be used, because if we try a two-ray formulation, we find

20. Holford, R. L., Modifications to Ray Theory Near Cusped Caustics, Continuation of LRAPP, Ref 7, Bell Telephone Labs, Whippany, NJ, Feb 1972 (unpublished).

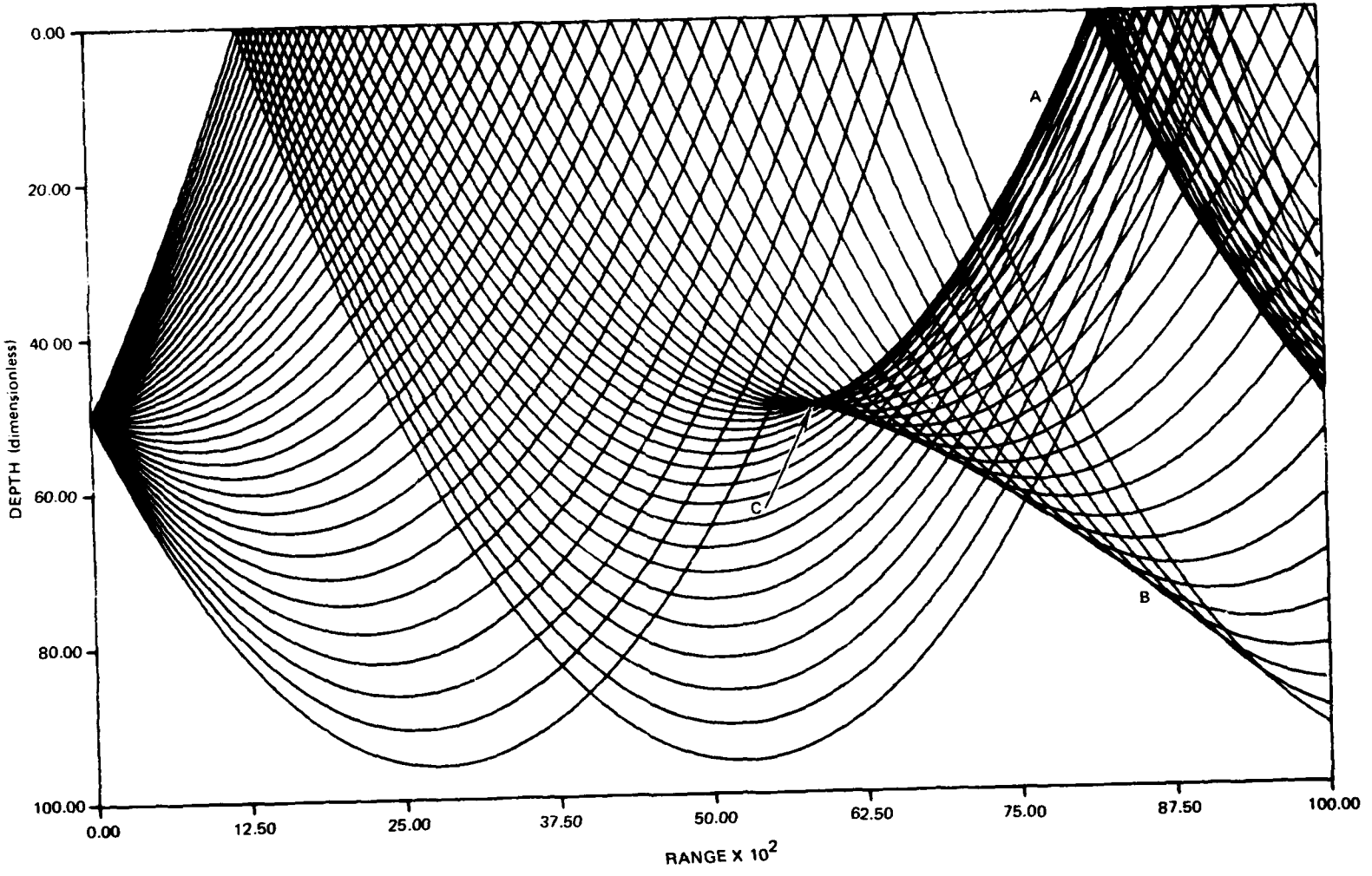

Figure 12. Ray diagram in surface duct illustrating a cusp.

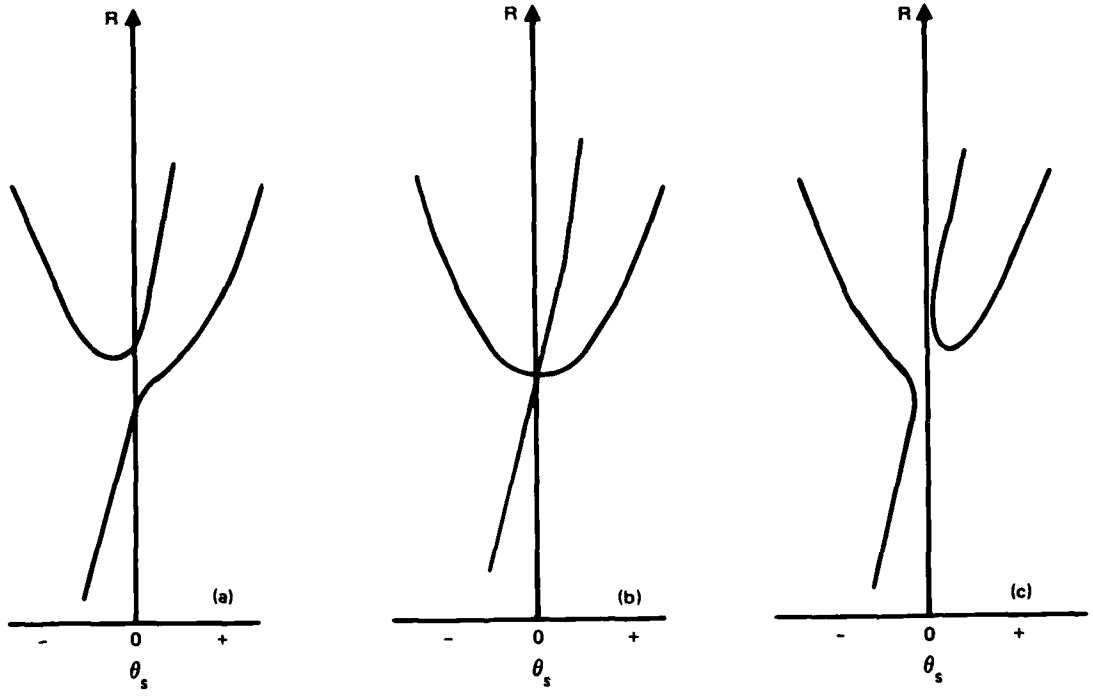

Figure 13a-c. Schematic range versus source angle plots for various receiver depths in figure 12: (a) receiver above cusp; (b) receiver at cusp; and (c) receiver below cusp.

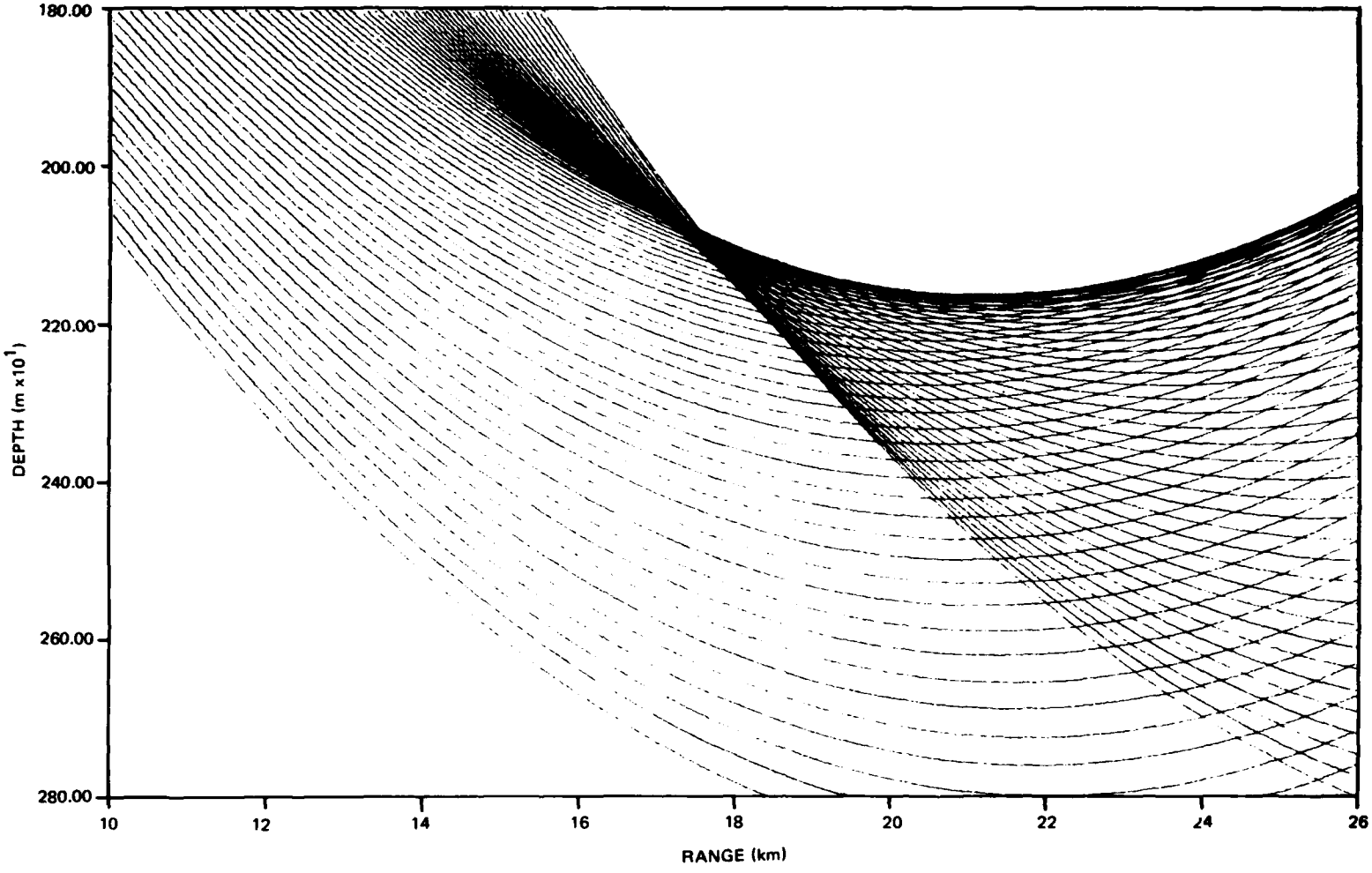

Figure 14. Expanded ray diagram illustrating an inclined cusp near the reciprocal depth.

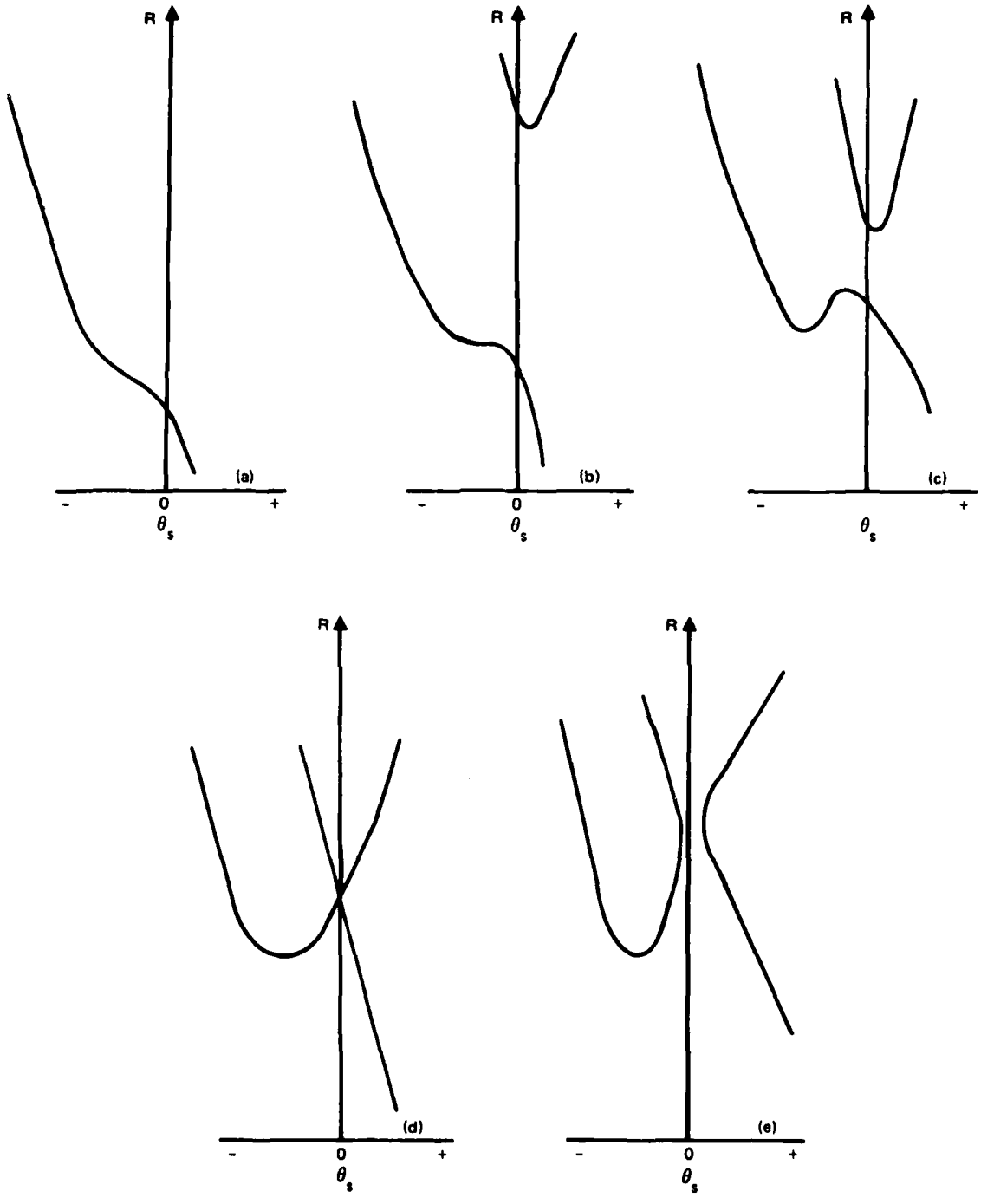

Figure 15a-e. Schematic range versus source angle plots for various receiver depths in figure 14: (a) receiver above cusp; (b) receiver at cusp; (c) receiver between cusp and reciprocal depth; (d) receiver at the reciprocal depth; and (e) receiver below the reciprocal depth.

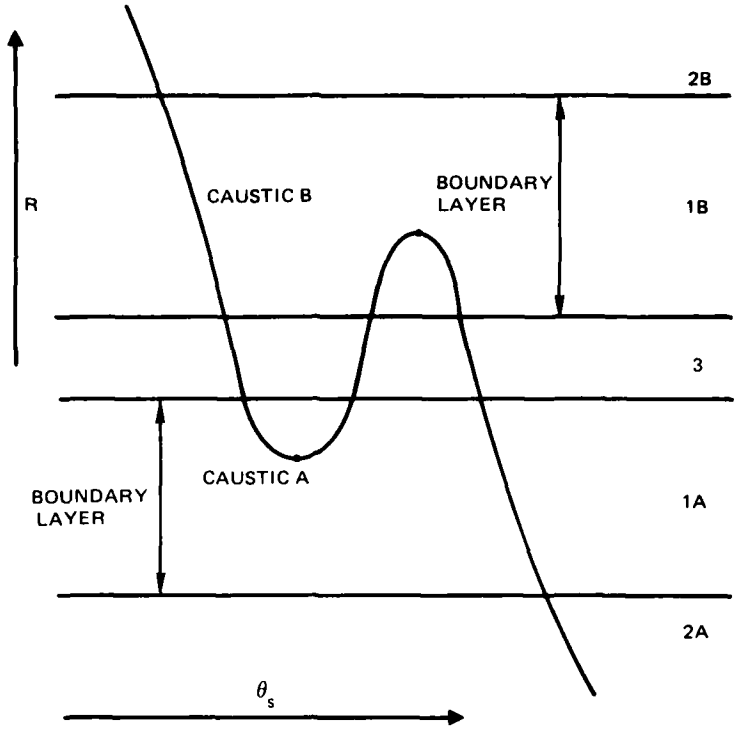

Figure 16. Boundary layers for connected caustics at high frequency.

that the common branch joining caustics A and B must be included in two separate evaluations. Thus at low frequencies a three-ray formulation is necessary wherever there is a connected caustic. As we approach the cusp, the connected caustics of figure 16 begin to merge. Thus the three-ray formulation must be used for higher and higher frequencies as we approach the cusp and must be used for all frequencies at the cusp point.

Now, in the case of the horizontal cusp it is not evident that the caustics of figure 13a and c are connected in the sense of figure 16. Moreover, figure 13b bears little resemblance to the horizontal point of inflection of figure 15b. Yet both these cases represent a cusp. The problem with figure 13 lies in the presentation of R as a function of θ_s for fixed depth. This is usually the best representation for a horizontally stratified medium. The standard computational technique is to evaluate the field as a function of range for fixed receiver depths. Unfortunately, this emulation leads to the confusion of figure 13 for a horizontal cusp.

Consider now that we hold the range fixed and plot Z, receiver depth, as a function of θ_s for fixed R. Figure 17 schematically illustrates such a plot for the case of figure 12. At ranges to the left of the cup in figure 17a, there is a point of inflection. At the cusp in figure 17b, there is a horizontal point of inflection. At ranges to the right of the cusp in figure 17c, there are a pair of connected caustics. The uniform asymptotic formulation does not depend on the fact that the receiver depth is fixed, as in figure 13. Indeed, the formulation can be used for range fixed as in figure 17 or along a curve where R is some function of Z. The point is that, mathematically speaking, the horizontal cusp is equivalent to the inclined cusp. Both have connected caustics which for low frequencies must be

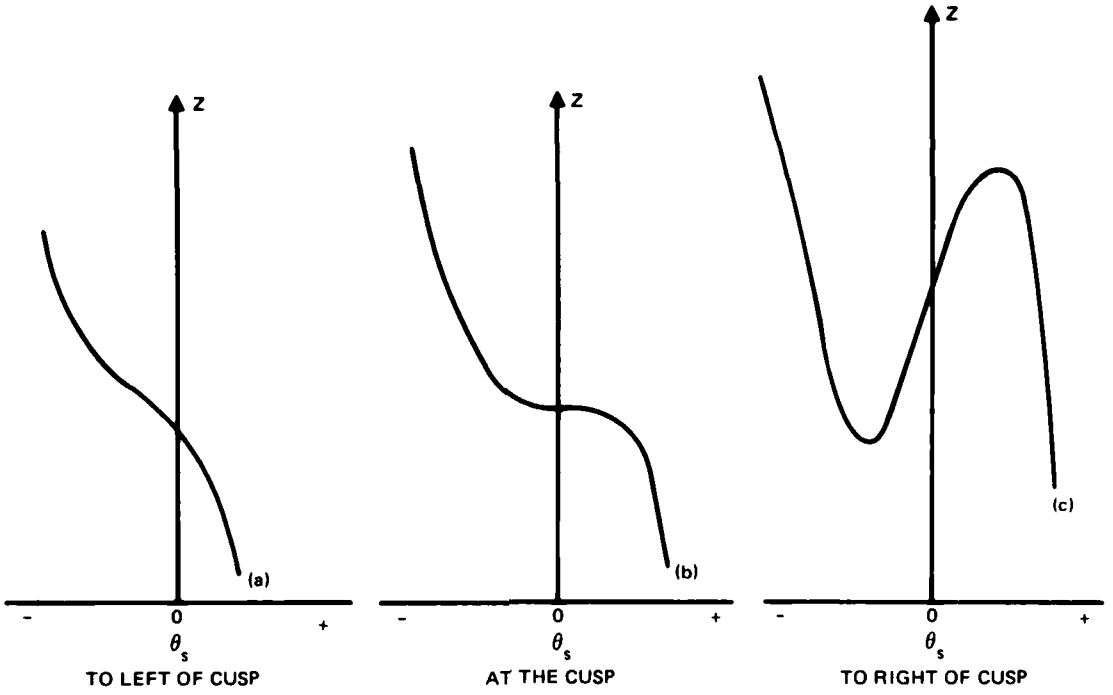

Figure 17 a-c. Schematic receiver depth versus source angle plots for various ranges in figure 12: (a) range to left of cusp; (b) range at the cusp; and (c) range to the right of the cusp.

treated by a three-ray asymptotic formulation. (In passing, we note that the Z, θ_s counterpart of figure 15d yields a simple caustic at a relative maximum in depth. Again, the strange appearance of figure 15d results from the treatment for fixed depth.)

Let us now discuss the evaluation of three-ray caustics. Fortunately, Holford (ref 20) has derived the uniform asymptotic solution in terms of the Pearcey function and its two first-order partial derivatives. He has devised the ansatz quantities which, although complicated, can be evaluated for the region of three real rays. Because of the complicated nature of the solution, the only case Holford discusses is the evaluation of a horizontal cusp along the cusp axis. The implementation of cusped caustics into models is quite limited (ref 21). In the FACT program, only horizontal cusps are treated and the field is evaluated only on the axis. This limits the evaluation to source and receiver at the same depth. Only the Pearcey function itself is included. The portions of the solution involving the first-order partial derivatives are deleted. Finally, only the nonuniform asymptotic formulation is used. Thus the formulation used in present Navy models is of the most rudimentary type.

We have made some preliminary ivestigations which indicate that the approach of reference 13 can be applied to the three-ray uniform solution of Holford (ref 20). Unfortunately, we have not been successful in obtaining funding to complete the rigorous

21. Spofford, C. W., Implementation of Cusped Caustics in the FACT Program, LRAPP Final Report, Ref 4, Bell Telephone Labs, Whippany, NJ, Apr 1973 (unpublished).

evaluation of three-ray systems utilizing complex and real rays. When and if this approach is implemented, we plan to use normal mode theory to produce a control for three-ray systems similar to those discussed in the previous section for two-ray systems. The chief goal again is the development of improved techniques for use in models, with the controls being a useful byproduct.

4.1.3 Controls for Four-Ray Systems

This section outlines the status of controls for a four-ray system. The horizontal cusp shown in figure 9 for the receiver at the source depth is part of a four-ray system. Figure 18 presents a blow-up of this critical region except for a source depth of 400 rather than 200 m. Four rays are evident in the region between the cusped caustics of figure 18. The system is characterized by the simple caustic curve A which appears at a range somewhat short of the cusped caustics. The four-ray system was first recognized by both Holford (ref 20, pages 7-22) and Spofford as posing a problem. Spofford (ref 21, figure 4-4b) illustrated a four-ray system in a range-versus-θ_s curve for a receiver at the cusp depth similar to the schematic shown in figure 19.

Again, the picture is clarified if we sketch the Z-versus-θ_s counterpart of figure 19. Far to the left of the cusp in figure 20a, a simple caustic (A) at a relative minimum in depth is formed. This caustic persists at all ranges. Slightly to the left of the cusp in figure 20b, a point of inflection forms on the right branch of caustic A. At the range of the cusp in figure 20c, a horizontal point of inflection forms on the right branch of caustic A. This point is the cusp. At a range to the right of the cusp in figure 20d, we see three connected caustics. These are the simple caustic A and the pair of caustics B and C, which merge to form the cusp.

A four-ray system is necessary whenever the boundary layer of caustic A overlaps the boundary layer associated with the caustic pair B and C. This overlapping always occurs for sufficiently low frequencies. At higher frequencies, where the boundary layer of A does not overlap boundary layers of B and C, the field may be evaluated in terms of the three-ray formulation or of the two-ray formulation and geometrical ray theory.

The question now arises as to how prevalent the four-ray systems are. The answer is that four-ray systems appear to be the rule, whereas the three-ray systems of figures 12 and 14 appear to be the exception. The only cases where we have observed the three-ray structures are the first cusp formed by the ray paths after leaving the source. For the case of an asymmetrical duct, this cusp occurs on the opposite side of the axis and is an inclined cusp. Figure 14 shows such a case for an above-axis source. For a below-axis source, a similar inclined cusp forms above the channel and again is a three-ray structure. Holford's example of a half duct in figure 12 is a special case. It is equivalent to propagation for a source on the lower branch of a symmetric channel. Mathematically, Holford's example corresponds to a below-axis source in a symmetric channel and yields the cusp which appears above the axis. Normally, this cusp is inclined since it is on the opposite side of the channel. However, a symmetric channel represents a degenerate case in which the cusp is horizontal.

It appears that all cusps after the initial one have a companion caustic associated with them. In some cases, this caustic is rather far-removed in range. Nonetheless, all of the noninitial cusps should be treated as a four-ray structure at low enough frequencies.

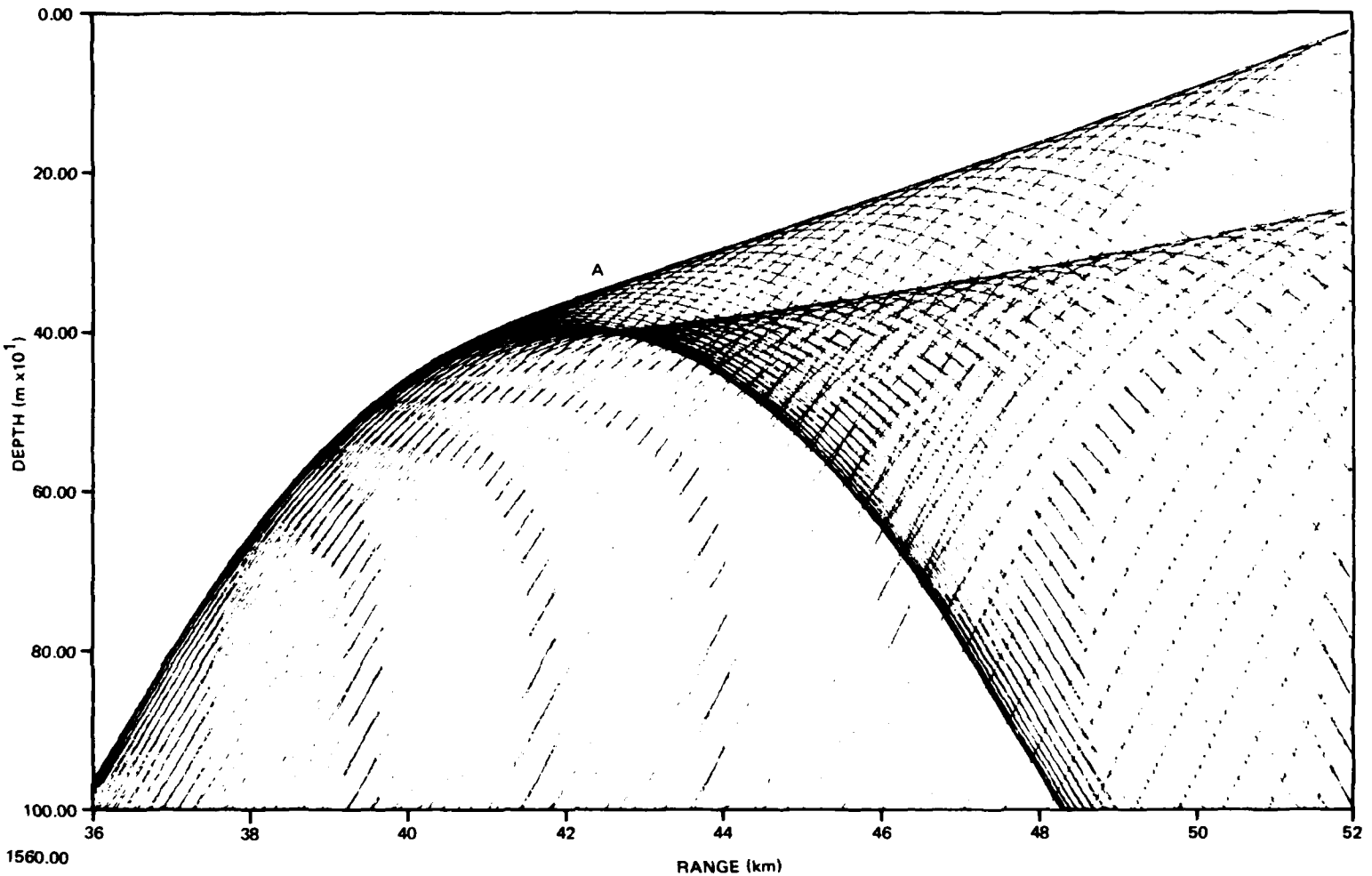

Figure 18. Expanded ray diagram illustrating a four-ray system.

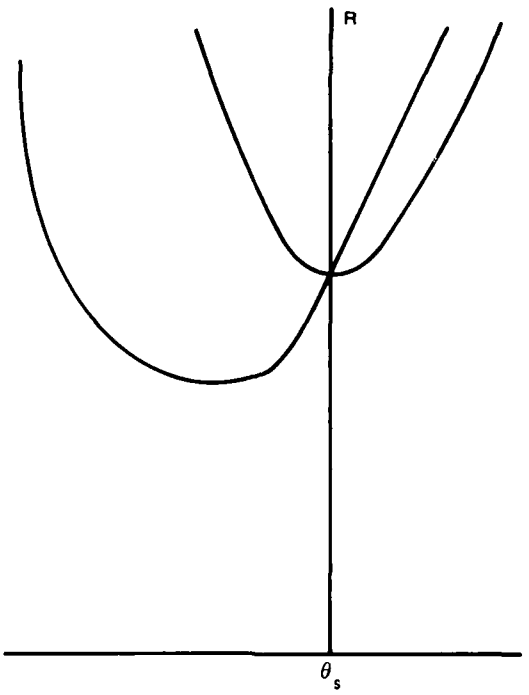

Figure 19. Schematic range versus source angle plot for figure 18 with receiver at cusp depth, illustrating a four-ray system.

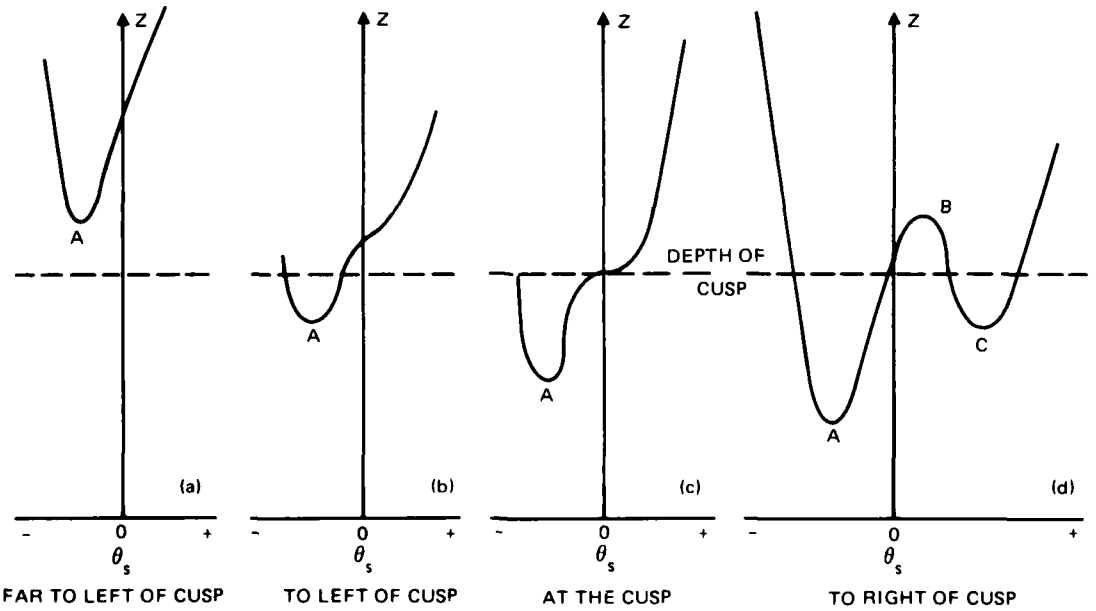

Figure 20a-d. Schematic receiver depth versus source angle plots for various ranges in figure 18: (a) range far to left of cusp; (b) range slightly to left of cusp; (c) range at the cusp; and (d) range to right of cusp.

The reason that the initial cusp has no companion caustic is that no caustic can form until after the first nadir or apex of a ray. The consequence is that for the initial ray structure there will be one less caustic than for longer-range structures.

Four-ray structures also appear in convergence zones. Figure 21a illustrates a plot of R-versus-θ_s for the first convergence zone in figure 9. This schematic is for a receiver above the source depth with rays headed down at the receiver. Caustic A is formed by refracted rays, while caustic B is formed by surface-reflected rays. The surface-grazing ray forms an end-point maximum range. The slope R is discontinuous and is $-\infty$ on the right side of the surface-grazing ray. Several such structures can form in convergence zones – one corresponding to each grazing ray configuration.

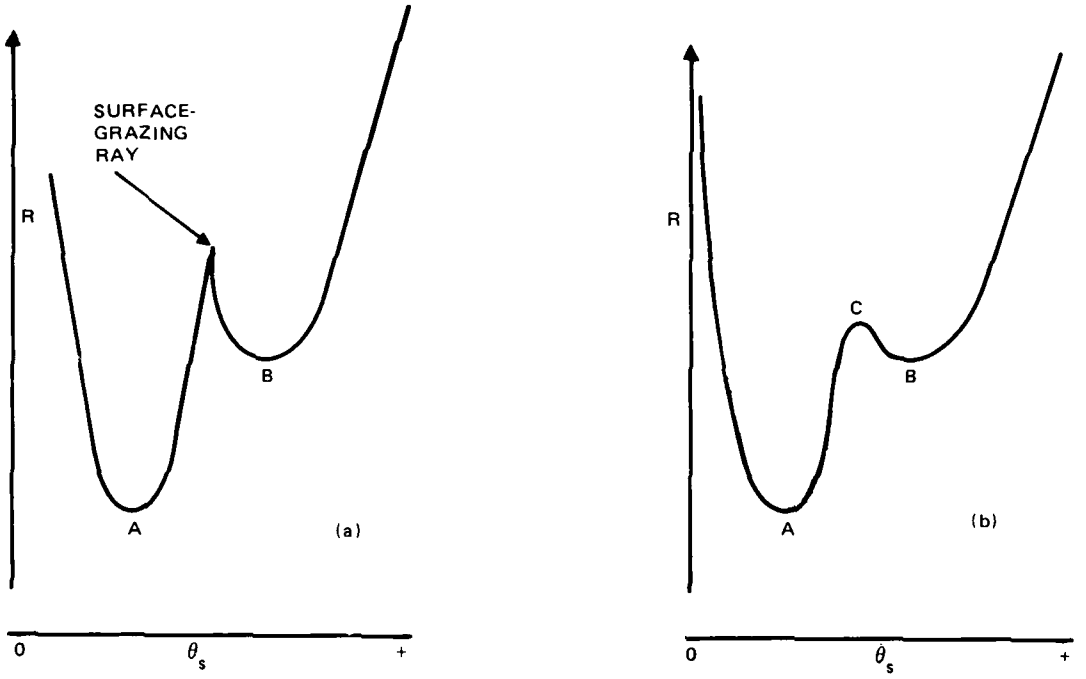

Figure 21a-b. Schematic range versus source angle plot in the first convergence zone of figure 9. Part (a) illustrates standard ray theory; part (b) illustrates the structure after Murphy-Davis corrections.

Murphy-Davis corrections can be applied to correct the surface-grazing ray structure into a smooth, well-behaved caustic. This caustic is designated in figure 21b as C. We see then that figure 21b represents a four-ray system at low frequencies.

Consider now the present status of four-ray systems. Doctor Marion Orton (ref 22) is developing a uniform asymptotic representation for such systems under sponsorship of ONR Code 486. The numerical application of these representations for improving models and generating controls is no doubt several years away. Before the four-ray evaluation can be implemented, we need to become more familiar with the three-ray systems in the previous section.

22. Orton, M., Underwater Sound Propagation in the Presence of Caustics Formed by Four-Ray Systems, Ocean Acoustics Program (ONR 486), Program Summary for FY-79, Nov 1979.

4.1.4 Controls for Hypercusps

This section introduces the concept of hypercusps, in which the geometrical ray theory intensity has a triple pole. As background, we first present a brief classification of caustic points on the basis of ray intensity. Although these are, for the most part, new results, proofs will not be presented here.

The ray intensity for a unit source may be written as

$$I/F = C_s/RC_m\,(\pm\partial Z/\partial\theta_s) \tag{18}$$

where

$$\partial Z/\partial\theta_s = -\tan\theta_h\,\partial R/\partial\theta_s = -C_m\tan\theta_h\tan\theta_s\,\partial R/\partial C_m\ . \tag{19}$$

Here, the subscript s designates the sound speed (C) or ray angle (θ) at the source. Similarly, the subscript h designates values at the receiver. R is the horizontal range, while Z represents the receiver depth. The phase velocity of the ray is C_m. The sign in equation 18 is chosen so that I/F is positive in the region of real rays. The derivative of equation 18 represents the partial derivative of the receiver depth with respect to angle at the source holding the range constant. (In all cases, the source depth is fixed.) This partial derivative is seldom evaluated by a consideration of how Z varies with θ_s for a fixed range. It is usually evaluated by equation 19 with either $\partial R/\partial\theta_s$, which represents the partial derivative of R with respect to θ_s for a fixed receiver depth, or $\partial R/\partial C_m$, which is the partial derivative of R with regard to C_m for fixed receiver depth.

Now the definition of a caustic point can be considered as those points where

$$\partial Z/\partial\theta_s = 0. \tag{20}$$

One manner of classifying caustics is by the order of a pole of I/F; ie, the order of zeros in $\partial Z/\partial\theta_s$. From equation 19, we see that there are three factors in $\partial Z/\partial\theta_s$ which can be zero: $\partial R/\partial C_m$, $\tan\theta_s$ and $\tan\theta_h$.

Consider first the case of

$$\partial R/\partial C_m = 0. \tag{21}$$

Equation 21 holds for all nonhorizontal caustics. For most of these caustics, equation 21 has a single zero. However, the case of an inclined cusp such as illustrated in figure 14

$$\partial^2 R/\partial C_m^2 = 0 \tag{22}$$

holds as well as equation 21, which has a double zero (and the intensity of a double pole).

Consider now the case of the zero-degree ray at the source. This ray never touches a caustic except at the apex or nadir of the ray: ie, the ray angle at the receiver is zero. (The case of both source and receiver on an axis of minimum sound speed is an exception and will not be discussed here.) Moreover, each apex and nadir for the zero-degree ray (at the source) represents a caustic. These are the horizontal caustics. The remaining problem is to determine the order of the pole.

Horizontal caustics can be divided into two cases. The first is where source and receiver are on opposite sides of the axis. For the usual case

$$(dC/dZ)_s \neq -(dC/dZ)_h \tag{23}$$

a simple caustic with a pole of order 1 is formed. The caustic in figures 9 and 14 at the reciprocal depth is such a caustic. For this case, $\partial R/\partial C_m$ is infinite. This infinity is canceled by the zero in $\tan \theta_s$, leaving the single zero in $\partial Z/\partial \theta_s$ due to $\tan \theta_h$.

Equation 23 represents a condition that the slope of the sound speed profile at the source is not the negative of the slope at the receiver (ie, at the ray apex or nadir). If this condition does not hold, then the caustic on the opposite side of the axis is a pole of order 2 (ie, a cusped caustic). For this case, $\partial R/\partial C_m$ is finite and a double zero in $\partial Z/\partial \theta_s$ results from $\tan \theta_h$ and $\tan \theta_s$, both zero. The cusp of figure 12 is considered to be of this type. This case is equivalent to that of a symmetric channel, for which equation 23 is trivially violated for all source depths. Equation 23 can also be violated for asymmetric profiles, although such a circumstance pretty well has to be contrived.

The second case of horizontal caustics occurs when both source and receiver are on the same side of the axis. For this case, R may be written as

$$R = n \tilde{R} \tag{24}$$

ie, the range is a multiple of the cycle range which represents twice the range from ray apex to nadir.

Moreover,

$$\partial R/\partial C_m = n \, \partial \tilde{R}/\partial C_m \, . \tag{25}$$

For this case, $\partial R/\partial C_m$ of equation 25 is finite and a double zero in $\partial Z/\partial \theta_s$ results from $\tan \theta_h$ and $\tan \theta_s$ both being zero. The cusp of figure 18 is of this type.

Under most circumstances, the result of equation 25 is nonzero and a two-pole cusp is formed. However, it is possible to select source depths such that equation 25 is zero. In this case, a cusp which has three poles is formed. We shall refer to this as a hypercusp.

To construct a hypercusp, we first make a plot of $\tilde{R}$ versus C_m for the channel. If this plot has either a relative minimum or a relative maximum, then the placement of the source at the sound speed corresponding to phase velocity of the relative minimum or maximum results in a hypercusp. Indeed, we can exhibit three examples of hypercusps for the sound speed profile of figure 8.

If we examine $\tilde{R}$ versus C_m for rays which reflect from the ocean surface, we find that there is a relative minimum. The source depth, which has a sound speed equal to the C_m of this minimum, is 3580.226 m. Figure 22 is a ray diagram for this source depth and shows the hypercusp. It looks very much like the cusp of figure 12, but has in fact one more pole.

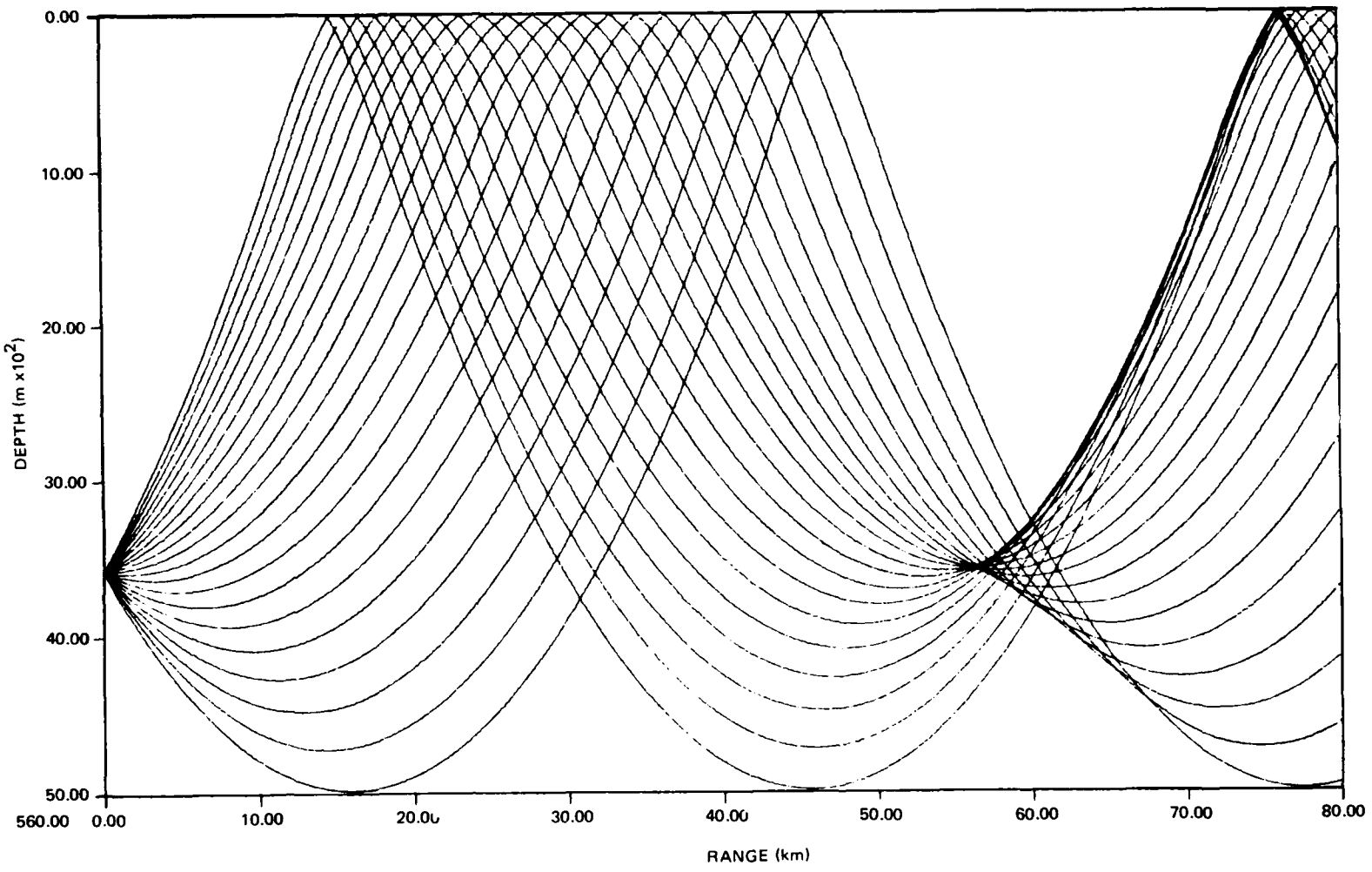

Figure 22. Ray diagram of surface reflected rays for the profile of figure 8, illustrating a hypercusp.

There is also a relative maximum in the $\tilde{R}$ of refracted rays for the profile of figure 8, if we remove the surface and bottom and extend layers 1 and 2. For this type of profile, $\tilde{R}$ has a maximum for the ray which forms an angle of 45° at the axis. Figure 23 is a ray diagram for a source above the axis at the apex of the 45° ray. The hypercusp appears at a range of about 130 km. This hypercusp bears little resemblance to the cusp of figure 9. Indeed, it points in the opposite direction. Figure 23 is not a realistic situation because the depths are about ten times greater than usually encountered in the ocean. However, figure 23 points up the possibility of radically different structures than those with which we may be familiar. Another hypercusp may be constructed by placing the source at the nadir of the 45° ray. This leads to a hypercusp below the axis, which will not be illustrated here, but again appears quite different from familiar cases.

The nature of the uniform asymptotic formulation for a hypercusp is unknown. It may be a simple extension of that for a cusp or it may be much more involved. Perhaps the best approach is to delay further ray theory work and pursue a normal mode approach. For example, the field of figure 22 could be evaluated by mode theory. Ray theory predicts exceptionally high intensities. Mode theory could be used to verify this prediction. There is also the question of whether there is any way in which hypercusps may be exploited in Navy operational models. Until this question is answered, it does not appear desirable to spend additional effort in the ray theory analysis of hypercusps.

4.1.5 Convergence Zones with Small Depth Excess

We have recently had occasion to analyze experimental acoustic data measured under conditions of small depth excess. The value of depth excess fell between 0 and 263 m. The acoustic results were remarkable. There was little evidence of convergence zones at 25 Hz. However, there were, in general, prominent convergence zones at 290 Hz. Occasionally at 290 Hz, convergence zones were missing or greatly diminished, corresponding to occasions when or where the depth excess was very small. For one experimental run at 42 Hz, there was a definite convergence zone structure. At 50 Hz, there appeared to be convergence zones for some runs but not for others.

These results suggest that the dependence of propagation loss on frequency is very complicated under conditions of small depth excess. We suspect that the dependence on frequency is not monotonic. For certain frequency bands, the phase velocity of a normal mode can fall between the bottom sound speed and the surface sound speed. Under these conditions, there should be a convergence zone structure. On the other hand, for other frequency bands no normal modes will have phase velocities which fall between the bottom sound speed and the surface sound speed. Under these conditions, one would expect less prominent convergence zones.

We have submitted proposals to use normal mode theory in a thorough theoretical analysis of convergence-zone propagation under conditions of small depth excess. If this analysis is funded, we will be in a position to prepare some control cases for this critical situation.

Controls are definitely needed. We do not believe that any present ray model can treat this case. Moreover, when the RAYWAVE and ASTRAL models, which represent improvements over ray theory, were applied to the analysis of the experimental data, they did not agree with the data. Controls for small depth excess will provide a severe test which many standard models are likely to fail.

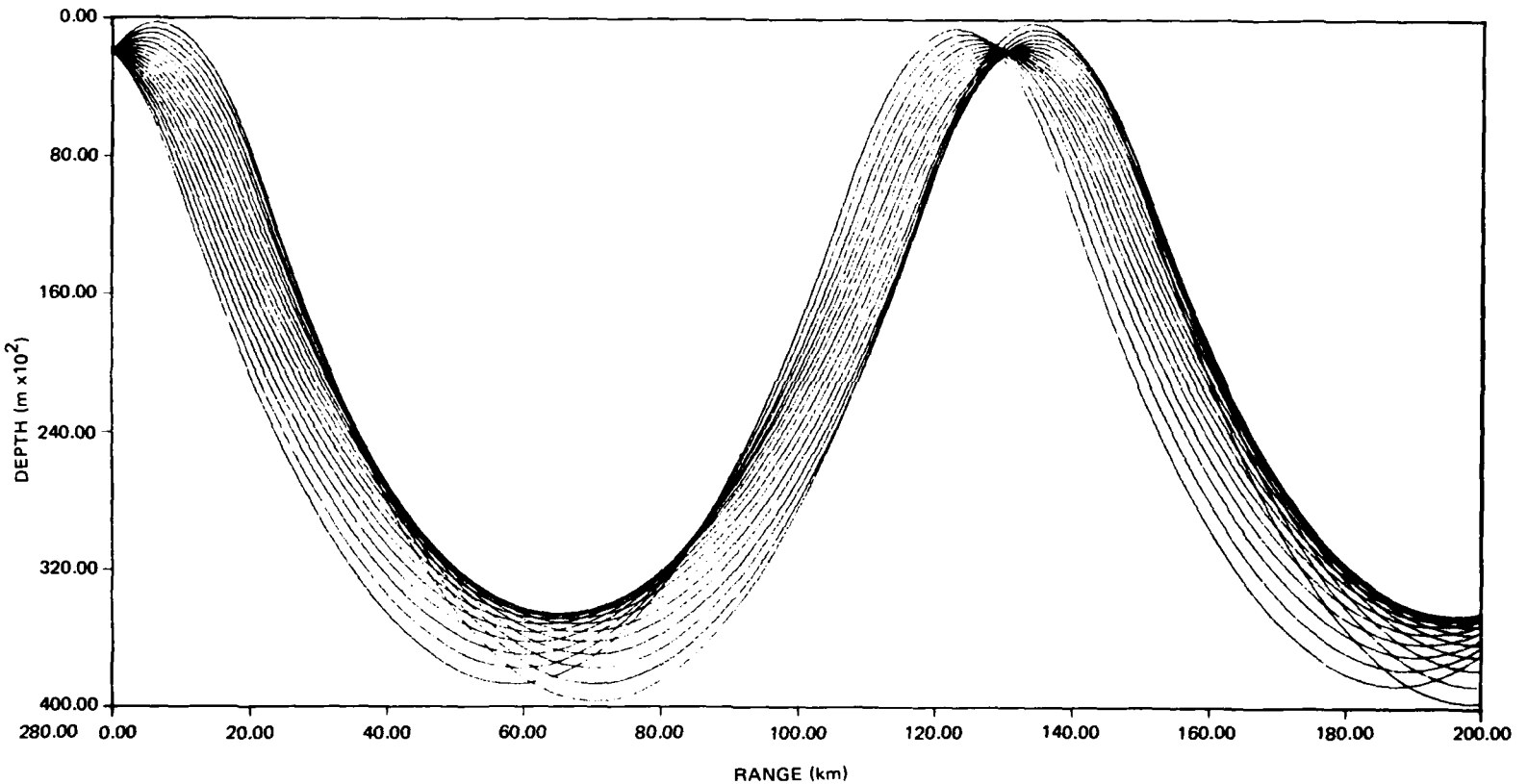

Figure 23. Ray diagram for the unbounded profile of figure 8, illustrating a hypercusp for an above-axis source.

4.1.6 Near-Axial Propagation

The nature of propagation for sources and receivers at or near the axis of minimum sound speed is quite complicated. Although there has been extensive investigation of this topic, the natures of the near-axis caustic structure, group velocity, and dispersion curves are not adequately known for realistic ocean profiles.

For example, for many years it has been generally thought that the slowest ray is the axial arrival. Indeed, the standard procedure for obtaining range was to measure the longest travel time for a near-axis shot and multiply it by the axial sound speed. However, in our experience we have encountered a number of sound speed profiles for which the axial ray was not the slowest. In one example, the slowest ray was 1 yd/s slower than the axial ray and occurred for the ray which formed an angle of 8° at the axis.

The uncertainties associated with near-axial propagation are certainly not due to neglect. Indeed, the subject has been very popular. The problem is that most analyses are carried out with simple profile forms. The ray theory results of these forms are critically dependent on their nature. Thus the results are, in many cases, an artifact of the profile form rather than a statement of propagation in a realistic ocean.

The theory of the axial ray from arbitrary profiles (ref 9) and the ray theory for axial source and various simple profiles (ref 23) have been analyzed in detail. For example, symmetric profiles represent a degenerate case. A realistic treatment of profiles requires a model in which asymmetry can be adequately modeled.

As an example of our concern, consider the ray theory and the mode theory of the model of figure 8. Even with many more layers, we would not consider the results of this model meaningful for sources and receivers on the axis of minimum sound speed. The reason is that, for this model, the slope at the axis, dC/dZ, is not zero. Ray theory analysis shows that the axial ray for all zones collapses to zero range. Moreover, the axial ray is always the slowest.

In contrast, ray analysis for a profile for which dC/dZ at the axis is zero shows that the axial ray forms periodic caustics along the axis. In most cases, they appear at a spacing of

$$R = (C_0/D_2)^{1/2}\,\pi \tag{26}$$

where C_0 is the axial sound speed and D_2 is d^2C/dZ^2 evaluated at the axis. In the case of symmetric ducts, these periodic caustics are poles of order 2. However, in the case of asymmetric ducts, the odd crossings are poles of order 1 while only the even crossings are poles of order 2. Ray analysis also shows that the axial ray may be either faster or slower than neighboring rays, depending on the relationships between various order derivatives evaluated at the profile axis.

Because the ray theory of the model of figure 8 disagrees radically with the ray theory for dC/dZ continuous, we could not consider the normal mode results of the profile model to be a good representation of the acoustic field near the axis. Normal mode models

---

23. Pedersen, M. A., and D. White, Ray Theory for Sources and Receivers on an Axis of Minimum Velocity, J Acoust Soc Am 48, 1219-1248, Nov 1970.

based on the simple profile of reference 23 would be an improvement, but since all of them are symmetric and thus exhibit a very limited and stereotyped ray theory behavior, we do not consider them to be good representatives.

In our opinion, what is needed is a critical analysis of several controls based on the general Epstein profile (ref 24). This profile has five parameters and is tractable from either a ray theory or a normal mode approach. There are five types of asymmetrical Epstein profiles with a relative minimum in sound speed. There are three types of symmetrical profiles with a relative minimum in sound speed.

The first step in the development of controls is to apply the analysis of reference 24 to the Epstein profile. This task is not easy, although it is straightforward. One needs to invert the general Epstein profile and then apply the analysis of reference 24. We expect that the flexibility afforded by the general Epstein profile will lead to a number of cases in which the near-axis acoustic properties are radically different. For some cases, the axial ray will be slower than neighboring rays and for others it will be faster. (The "cosh" profile is a special case of the Epstein profile for which all rays focus. For this case, the axial ray and all other rays have the same group velocity.) For some cases, the group velocity may increase or decrease monotonically, as is the case for the simple examples of reference 24. However, for other cases we anticipate that relative maxima or minima, or both, may be formed. Finally, some of these control cases will apply to asymmetric profiles and others to symmetric profiles.

Based on these cases with radically different acoustic properties, a set of control cases for an axial source should be developed by using ray theory, whereupon propagation loss, caustic structures, range, group velocity, and dispersion curves could all be exhibited.

The next step in the development is to evaluate these cases by means of normal mode theory. The normal mode solution for the case of two vertical asymptotes is presented in reference 25. With a minor modification, this solution also applies to some profiles with one vertical asymptote. However, the normal mode solution has not been worked out for other cases. A number of years ago, we contacted ONR Code 432 to determine whether one of their mathematical contractors could provide the desired solutions. For a variety of reasons, the desired solutions have not been developed. It appears that the case treated by Deavenport (ref 25) is the most clear cut. For some reason, the remaining cases appear to be more difficult. Thus these solutions remain to be developed before the complete set of test cases can be evaluated by normal mode theory.

The next step is to evaluate the ray theory solutions against their normal mode counterparts. We have no guarantee, for example, that the good agreement observed in the case of section 4.1.1 will apply to near-axial propagation. Ray theory appears to be critically dependent upon minute details of the mathematical properties at the profile axis. It is not clear that this sensitivity will carry over to the normal mode counterpart.

---

24. Pedersen, M. A., and D. White, Ray Theory of the General Epstein Profile, J Acoust Soc Am 44, 765-786, Sep 1968.

25. Deavenport, R. L., A Normal Mode Theory of an Underwater Acoustic Duct by Means of Green's Function, Radio Science, vol 1, no 6, Jun 1966.

The next step is to compare the controls against other acoustic models, which will approximate the appropriate Epstein profiles. Based on our ray analysis, we anticipate that this test will be severe, as these approximations in most cases will not match the desired mathematical properties at the profile axis. The real problem is to assess quantitatively how well the models compare with the controls. The differences could be insignificant, although our ray theory analysis suggests that large differences can be expected.

4.2 SURFACE DUCT PROPAGATION

This section outlines various controls for surface duct propagation. By surface duct propagation, we mean propagation which involves the near-isothermal surface layer in deep water.

4.2.1 Bilinear Control

The normal mode approach to surface duct propagation was applied to electromagnetic propagation by Furry (ref 26) and later to underwater sound by Marsh (ref 27). References 2 and 28 discuss the application of this model to short-range propagation, which is in fact a more difficult application than that of larger ranges in a duct.

In 1979, under sponsorship of NORDA Code 530, NOSC made a number of computations for a test case. In developing a WKB-approach surface duct model for NORDA Code 530, Spofford of SAI had made a number of comparisons with the parabolic equation (PE) method. In some cases, there was good agreement between the WKB approach and PE. In other cases, there was poor agreement. NOSC was asked to prepare computer outputs for the exact solution for the bilinear model. Mode eigenvalues, mode depth functions, and propagation loss were provided to SAI so that any deficiencies in the WKB approach could be identified and corrected.

The environmental parameters designated by Spofford were as follows: C_0 (surface sound speed) 5000 ft/s; γ_0 (in layer gradient) 0.018 s^{-1}; γ_1 (below layer gradient) -0.1; and Z_a (layer depth) 1000 ft. The frequencies requested by Spofford were 25, 100, 250, 500, and 1000 Hz. The in-layer gradient is the nominal isothermal value for surface ducts. The 1000 ft layer is somewhat deeper than usually encountered in the ocean. The frequencies were chosen so that a variety of propagation conditions are represented. At the highest frequency, there are 22 trapped modes. The onset of trapping for the first mode occurs at a frequency of about 33 Hz. Thus 25 Hz is below cutoff.

These test cases proved to be useful to SAI in improving their model. Thus we think this set of computations could be useful to others as a control case for this type of propagation.

---

26. Kerr, D. E., Propagation of Short Radio Waves, McGraw-Hill, NY, 140-174, 1951.
27. Marsh, H. W., Theory of the Anomalous Propagation of Acoustic Waves in the Ocean, Naval Underwater Sound Laboratory, Report 111, 1950.
28. Pedersen, M. A., and D. F. Gordon, Theoretical Investigation of a Double Family of Normal Modes in an Underwater Acoustic Surface Duct, J Acoust Soc Am 47, 304-326, Jan 1970.

For the bilinear model, there are two families of modes (ref 28). The first represents propagating waves reflecting from the ocean surface. These are the modes that contribute to long-range propagation. The second family of modes has phase velocitites less than the sound speed at the bottom of the layer. This family has high attenuation coefficients and does not contribute at long ranges. However, in the image interference region, this second family of modes may be important. In the examples of reference 28, the second family makes a significant contribution for ranges less than about 7 kyd. In the example of reference 2, the second family of modes was neglected and apparently made contributions only at ranges less than 0.5 kyd. The contribution of the second family of modes depends strongly on the parameter ρ, where

$$\rho = (\gamma_0/\gamma_1)^{1/3} . \tag{27}$$

For the example of references 2 and 28, the values of ρ were -0.860 and -0.320, respectively. The value of ρ for Spofford's test case is -0.565, and hence for short ranges the second family of modes could make a significant contribution.

In any case, the second family of modes should be included in any control case which is used for propagation at short ranges.

4.2.2 Bilinear Control for Negative Gradients

This section discusses the bilinear model for the case of downward refraction. Although extensive work has been done with the bilinear model of section 4.2.1, very little work has been done with the bilinear model with negative gradients (illustrated in fig 24).

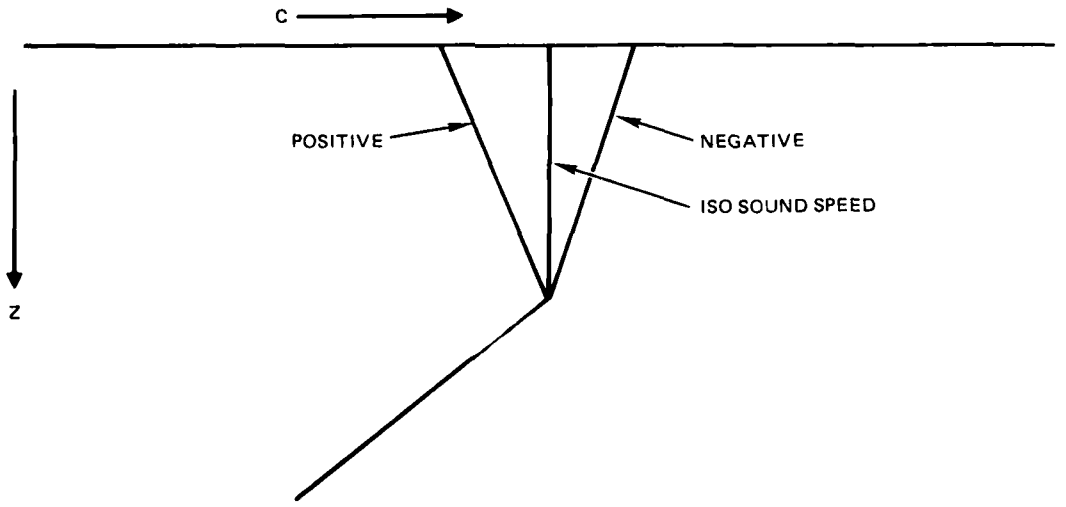

Figure 24. Schematic illustrating surface duct profiles with positive, zero, and negative gradients.

The case of negative gradients contains a number of pitfalls. It should provide a good test case for models which attempt to treat this type of propagation. In the first place, there are a number of investigators who do not believe that this problem can be solved by discrete modes. (Evidently, the analogous problem in quantum mechanics is treated by a continuous spectrum.)

We first tackled this problem in the early 1960s, when we were developing the theory of surface duct propagation. Our guide was Furry (ref 26), who presents a single formulation which treats both positive and negative γ_0. Indeed, the eigenvalue equation, as given by equation 1 of reference 28, applies to both cases and is a function of two mathematical parameters, M and ρ, which have the same sign as γ_0.

The chief procedural difference between γ_0 positive and negative is the use of different approximations for eigenvalues. Furry gives a series expansion for small M for the second family of modes which applies to γ_0 negative as well as positive. He also gives expressions for large M. These fall into four distinct cases – first and second families for γ_0 positive and first and second families for γ_0 negative.

The procedures for finding eigenvalues for γ_0 positive is discussed in detail in reference 26. One must start at high (or low) M, where the approximations apply. By means of these approximations, the exact eigenvalue is found by iteration. Using the property that the eigenvalues, for a given mode, are continuous functions of the parameter M, one can proceed to map the eigenvalues for a mode into parametric regions where the approximations are not valid. This general procedure has been designated as an eigenvalue follower and has been prepared as a computer routine (ref 16). It does not have to be used for simple channels when there are many modes trapped. However, it is used in all cases where simple rules of thumb about eigenvalues do not apply. For example, for the case of γ_0 positive, it is used for the first family of modes when below cutoff and for the second family of modes whenever short ranges are evaluated. It has to be used for both families of modes for the case of γ_0 negative. As indicated in the next major section (4.3), it is nearly always used in the case of multiple ducts.

For many of these cases, it takes detailed searching to ferret out the eigenvalues. Unless special provisions have been made, it seems very likely that routine models will fail to find all of the eigenvalues. Control models are desirable for these cases, so that we can assess where routine models fail and the conditions for which they are no longer reliable.

We have evaluated only one case of the bilinear model with γ_0 negative. Unfortunately, the results were loaned to another Navy laboratory and were never returned, so the example is no longer available. However, the general character of the results can be recalled. The value used for γ_0 was -0.018 s. The mode of minimum attenuation was not mode 1, as is the usual case. It was mode 3 or 4. This nonmonotonic behavior makes the problem of finding eigenvalues more difficult. The contours of propagation loss below the layer appeared to run parallel to the path of the limiting ray. There appeared to be some vestigial channeling effects in the layer. As expected, both families of modes showed fairly large attenuation loss. The conditions under which the first or second family of modes made the dominant contribution were not clearcut. This example was not thoroughly analyzed because it was investigated before we accumulated much experience with the bilinear model.

The only case which has been thoroughly investigated is presented in reference 29. This case is for a single negative-gradient layer where $\gamma_0 = -1.2286762\ s^{-1}$. This gradient is extreme. For example, it is about 12 times the thermocline gradient of the Spofford example of section 4.2.1 and about three times that of reference 2. Because of the extreme gradient, the results of the model of reference 29 bear little resemblance to those cited for $\gamma_0 = -0.018\ s^{-1}$. Both represent cases of downward refraction, but that is as far as the similarity goes. Reference 29 shows excellent agreement between normal mode theory and ray theory. This level of congruence assures us that, contrary to the belief in some quarters, the case of downward refraction can be handled by discrete mode theory.

The single-layer case can be thought of as a degenerate case of the bilinear model where $\rho = -1$. For this case, only the second family of modes contributes. The contribution of the first family goes to zero as $\rho \rightarrow -1$.

It appears that there is a definite need for a control case for the bilinear model with a negative value for γ_0. This control case should be thoroughly analyzed. It should include the corresponding ray theory as well as the normal mode results. The ray theory controls discussed in section 6.1.3 will serve this need. The mode theory control recently has been solved by McDaid, as discussed in section 9.0.

4.2.3 Bilinear Control for Near-Isosound Speed Conditions

The solution for the bilinear model can be expressed in terms of Airy functions or modified Hankel functions. However, this formulation breaks down when $\gamma_0 = 0$, the isosound speed case of figure 24. In this special case, the solution can be expressed in terms of trigonometric functions. An analysis of this solution is presented in reference 30, which could serve as a control for this special case.

Perhaps of equal importance would be controls for small positive and small negative values of γ_0. As $\gamma_0 \rightarrow 0$, the formal bilinear solution exhibits rather wild behavior with eigenvalues running off to infinity. These cases have never been evaluated. It is not clear, for example, that the numerical solution for small γ_0 will smoothly tend to the special isosound speed solution.

We recommend that an investigation be made of the acoustic field as the surface gradient varies from slightly positive through zero and into the slightly negative regime. This study would not only serve as a control case but would also provide information on how sensitive the propagation loss is to channel gradient in this area.

This area of investigation is important for two reasons. First, there have been reports from the Fleet that surface duct propagation is better under conditions of a small positive surface gradient rather than under conditions of a large positive surface gradient. This result is contrary to what one would expect. A possible explanation is that there are fewer reflections from the surface for the weak gradient case, which results in less scattering out of the layer. We can better assess this circumstance once we determine the propagation characteristics of weak gradients. The second reason for such an investigation is the experimental difficulty of measuring the gradient. The seriousness of errors

29. Pedersen, M. A., and D. F. Gordon, Normal-Mode and Ray Theory Applied to Underwater Acoustic Conditions of Extreme Downward Refraction, J Acoust Soc Am 51, 323-368, Jan 1972.
30. Au, W. W. L., An Investigation of a Double Family of Normal Modes in an Isovelocity Underwater Acoustic Surface Duct, J Acoust Soc Am 50, 286-299, Jul 1971.

in gradient depends on whether there is a radical change in propagation loss as the gradient varies from slightly positive to slightly negative.

4.2.4 Comparison of Bilinear Model with Complete Model of Ocean

As previously stated, the bilinear model represents the standard way of treating surface ducts. However, based on a study conducted at the SACLANT Center, Dr Ed Murphy (ref 31) has expressed a concern about the application of the model. Referring to the profile of figure 25, Murphy asks: How does the result of the bilinear model, consisting of layers 1 and 2, compare with that of the entire ocean model consisting of layers 1 to 4? For the bilinear model, the sound speed in the second layer is extrapolated to large depths. For this study, we are interested in propagation only in the surface layer or immediately below it. In the example of figure 25, the profile below a depth of 300 m is identical to profile B of figure 8. The channel depth is 100 m, the value of γ_0 is 0.01597 s^{-1}, and the surface sound speed is 1513.4245 m/s.

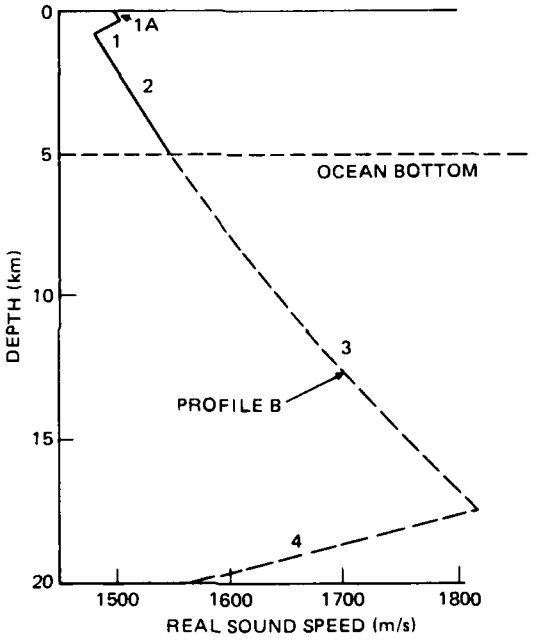

Figure 25. Modified profile B of figure 8 with surface layer.

The first step of this comparison has been carried out. Propagation losses have been compared for a 50-m source and for receivers at 50, 100, 150, and 200 m at a frequency of 300 Hz. The results for both models agree to better than 0.1 dB out to a range of 50 km. This range represents the onset of the convergence zone for the complete profile model.

---

31. Murphy, E., Supplement to Informal Notes on Surface Duct Propagation, prepared for Second Session of the International Workshop on Low Frequency Propagation and Noise, Monterey CA, Nov 1975 (unpublished).

Only three modes were used to obtain the result for the bilinear model, whereas 474 modes were used to obtain the result for the complete model. The advantage of being able to use the bilinear model is obvious.

At 300 Hz, the first mode of the bilinear model is fully trapped but not the second. (The parameter M equals 3.2). The good comparison is gratifying because it indicates that the bilinear model provides an excellent result for large M. The question which remains to be answered is: How good is the comparison when the frequency is lowered below cutoff? The suspicion and concern is that the rolloff response below cutoff for the bilinear model will not agree with the corresponding acoustic result for the entire model. Now the question to be answered is: Below what frequency (value of M) must we use the complete model rather than the bilinear model?

This question has a direct application to current Navy models. For example, in the NISSM model the low-frequency rolloff characteristics are based on the results of the bilinear model.

4.2.5 Refractive Surface Ducts

The first application of normal mode theory to underwater acoustics was the bilinear model. The next extension of this theory was to three-layer ducts (ref 32). Figure 26 presents examples of such ducts. Profiles A and F represent refinements of the bilinear duct. Profiles B through E represent examples of refractive surface ducts, which are the subject of this section.

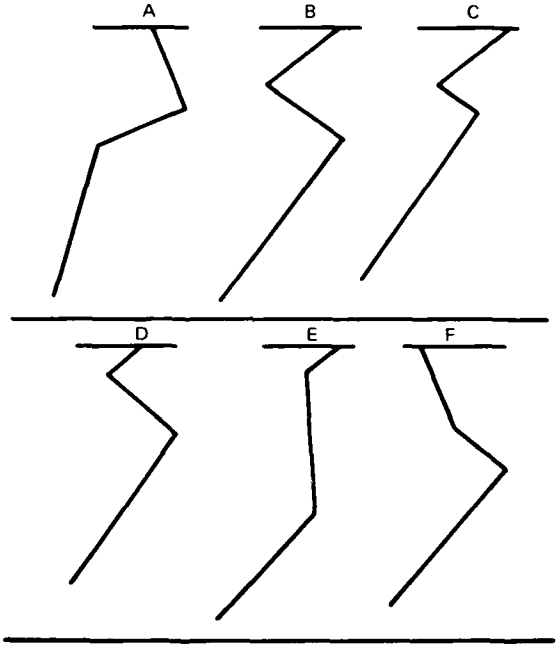

Figure 26. Examples of three-layer surface or near-surface refractive ducts.

32. Available to authorized requestors.

The eigenvalue equation for an n-layer normal mode solution requires finding the roots to a determinant of order $2n - 1$. For a large n, these are evaluated numerically by matrix methods. The problem is not as severe as it appears at first sight. For large n, most of the matrix elements are zero. No row contains more than four nonzero elements.

In the case of the bilinear model, the determinant is of order three. The algebraic expansion of this determinant leads to the eigenvalue equation of reference 28 already discussed. In the case of the three-layer examples of figure 26, the determinant is of order five. Reference 32 represents an algebraic expansion of this determinant and approximations to eigenvalues for trapped modes.

The value of reference 32 does not lie in the explicit expanded form given for the determinant. The expressions comprising the expansion are numerous, lengthy, and quite messy. Indeed, we no longer use this formulation. For three-layer cases, we use the n-layer computer program which evaluates the determinant by numerical methods. The chief value of reference 32 is the discussion of trapped modes for a refractive duct. In the case of the bilinear model, the eigenvalues for trapped modes are related to the roots of $Ai(-x)$. In the case of the refractive duct, the eigenvalues of even-order trapped modes are related to the roots of $Ai(-x)$, whereas those of odd order are related to the roots of $Ai'(-x)$.

Profile B of figure 26 is a symmetric case, in which the eigenvalues take on a simpler form than for asymmetric channels. Two examples similar to profile C of figure 26 are evaluated in reference 33. These examples represent profiles taken at sea during surface duct propagation experiments. Profile D is also a type encountered at sea, although reference 33 does not evaluate this example. Profile E is a very common type encountered at sea. An example is evaluated in reference 33. This example illustrates the afternoon effect. Under low wind-speed conditions, the thermal heating of the surface produces a negative gradient layer at the surface.

It appears that a control case for a refractive surface duct could be useful. The control would be set up by using the n-layer formulation. However, the theory of reference 32 could be used to help interpret results. As previously mentioned, Spofford has been developing a WKB approach to the bilinear duct. Using the theory of reference 32, it would be possible to extend this WKB approach to the treatment of refractive surface ducts. In this event, a control case for the refractive duct would be indispensable.

The refractive surface duct model can be used for much more sophisticated control. Consider figure 27 taken from reference 32. This plot presents eigenvalues as a function of the parameter M derived from profile B of figure 26. The dashed curve represents the actual eigenvalues of mode theory. The solid curve represents their estimates based on the phase integral method of ray theory. The change in M was achieved by allowing the refractive duct to get smaller. For the case of $M = 0$, there is only a half-duct. The region to the left of the inclined line corresponds to rays which have reflected from the ocean surface. The region to the right corresponds to rays which are confined to the refractive channel. Now the discontinuity in the phase integral in crossing the inclined line is caused by a jump in ray phase at the ocean surface. For rays which reflect from the surface, a phase shift of $-\pi$ is assumed; for refractive rays, a phase shift of $-\pi/2$ is assumed. Thus in the simple ray approach, there is a jump of $\pi/2$ in the phase for a ray just reflecting from the surface, as compared to a ray which does not quite reach the surface. Now the normal mode result of figure 27 smoothly goes through this discontinuity because the normal mode formulation results in a contin-

33. Anderson, E. R., and M. A. Pedersen, Surface-Duct Sonar Measurements (SUDS) [illegible], Undersea Center TP 463, Nov 1976.

AD-A118 324 NAVAL OCEAN SYSTEMS CENTER SAN DIEGO CA F/G 17/1
USE OF THEORETICAL CONTROLS IN UNDERWATER ACOUSTIC MODEL EVALUA--ETC(U)
JAN 82 M A PEDERSEN, R W MCGIRR
UNCLASSIFIED NOSC/TR-758 NL

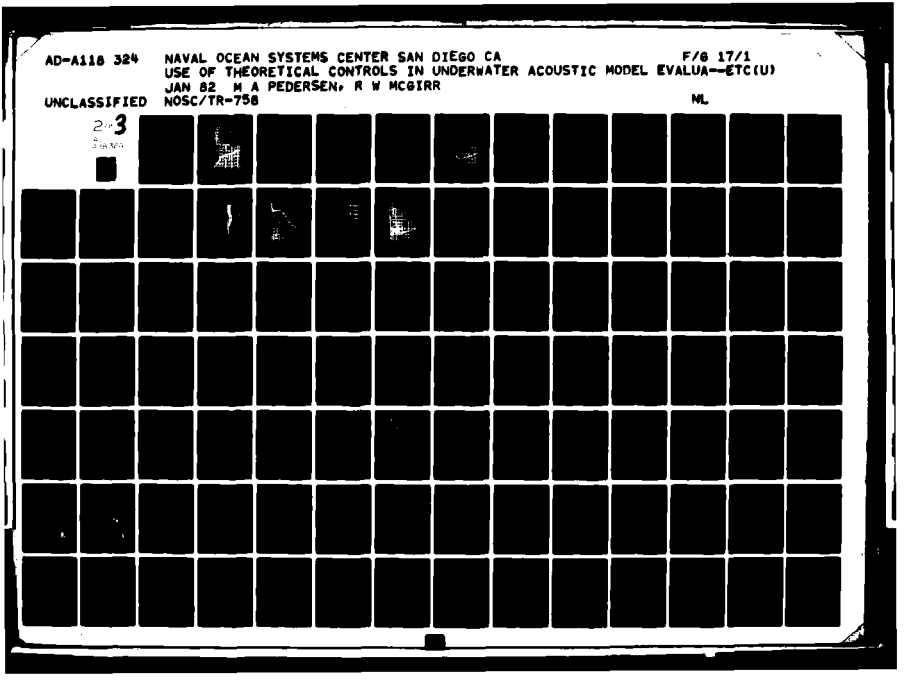

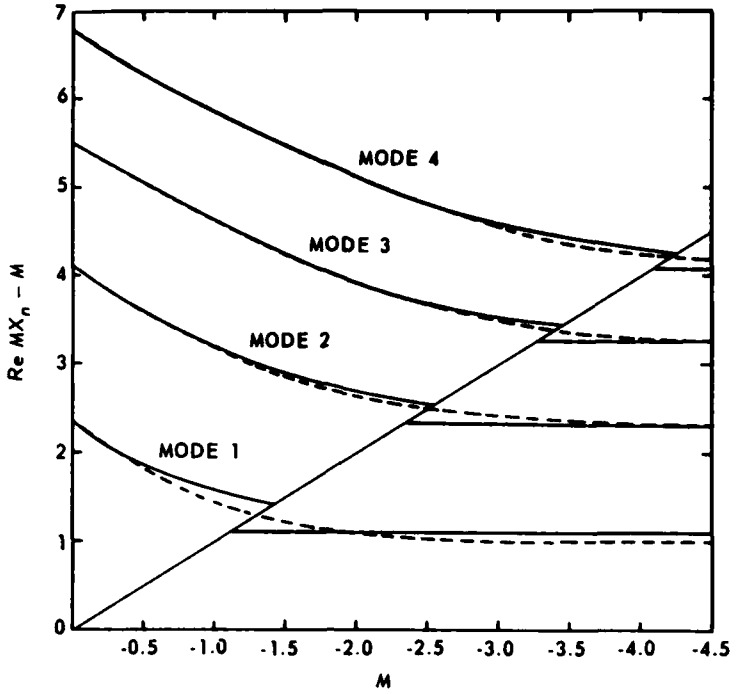

Figure 27. Comparison of eigenvalues and phase integral approximations for profile B of figure 26 as a function of M.

As will be explained later, Murphy-Davis (ref 17) corrections make the ray phase shift at the ocean surface a continuous smooth function.

The case of figure 27 then represents a test case of Murphy-Davis corrections. The mode result is the control. When Murphy-Davis corrections are applied to ray theory and when these corrected ray theory results are used in the phase integral method, a smooth continuous curve should result. This smooth curve should be in substantial agreement with the result of normal mode theory.

In obtaining figure 27, Gordon allowed the physical parameters to vary. We would recommend the application to a refractive duct similar to that of figure 26d, but where the sound speed at the bottom of the duct is much higher than that at the surface.

We would then vary the acoustic frequency but hold the sound speed profile constant. This produces a plot similar to figure 27 as the parameter M varies with frequency. At high frequencies, the phase velocity of the mode will be less than the surface sound speed. At low frequencies, the mode phase velocity will be greater than the surface sound speed, corresponding to rays which reflect from the surface. At some intermediate frequency, the mode phase velocity will be the surface sound speed. Although the result of this control would be similar to that of figure 27, it would be much easier to interpret.

4.2.6 Extremely Deep Surface Ducts

In northern latitudes during the winter, the sound speed is often a minimum value at the surface and monotonically increases to the ocean bottom. Figure 28, taken from

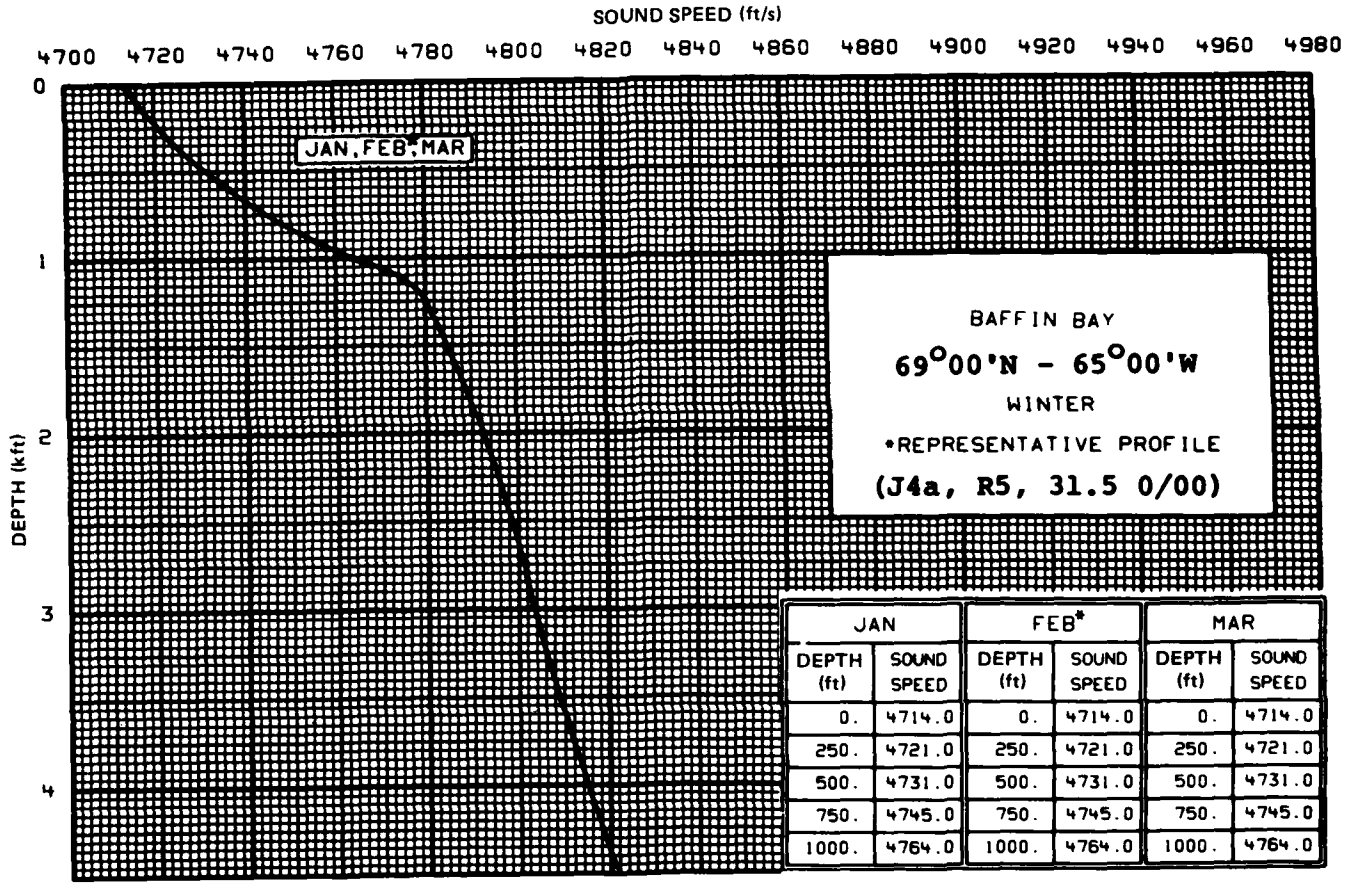

JAN		FEB*		MAR	
DEPTH (ft)	SOUND SPEED	DEPTH (ft)	SOUND SPEED	DEPTH (ft)	SOUND SPEED
0.	4714.0	0.	4714.0	0.	4714.0
250.	4721.0	250.	4721.0	250.	4721.0
500.	4731.0	500.	4731.0	500.	4731.0
750.	4745.0	750.	4745.0	750.	4745.0
1000.	4764.0	1000.	4764.0	1000.	4764.0

Figure 28. Winter profile in Baffin Bay illustrating a profile with positive gradients.

reference 34, presents the upper 4500 ft of a winter profile taken in Baffin Bay. The sound speed continues to increase for depths greater than those shown in figure 28. Profiles with similar characteristics occur in the North Pacific, the Bering Sea, and the North Atlantic. In some cases, the sound speed gradient is more nearly constant than as illustrated in figure 28.

In other cases, the near-surface gradient extends even farther than shown in figure 28.

As far as we know, the characteristics of propagation in these huge ducts have not been investigated in detail. In many cases, the water may be quite deep so that many modes will be trapped. Thus, as is the case for convergence-zone propagation in deep water, one may prefer to use ray theory rather than mode theory. One cannot infer the propagation characteristics in huge surface ducts from the behavior in small surface ducts for a few trapped modes. On the other hand, one also cannot infer the propagation characteristics in huge surface ducts from propagation about the SOFAR axis in deep water.

We recommend that a thorough investigation of extremely deep surface ducts be made and that a control case be prepared. The techniques of complex ray theory and uniform asymptotics, as presented in section 4.1.1, are directly applicable to this type of propagation. Thus this study is within the present state of the art. A comparison of normal mode and ray theories should be carried out, as discussed in section 4.1.1. This example could also serve to treat the three-ray caustics of section 4.1.2. The initial cusp formed for these profiles should resemble that of figure 12, but on a greater scale.

4.2.7 Surface Duct Models Containing Scattering

Thus far we have been concerned only with models that treat a flat surface. The transport equation has been used by Wilson (ref 35) to evaluate surface duct propagation. To test this method, NOSC provided both ray theory and normal mode results. Agreement between ray theory and the transport equation with no scattering was good. A comparison of the below-layer field by using normal mode theory, the transport equation, and experimental results suggests that at 530 Hz the contributions of diffracted arrivals and scattered arrivals were comparable. However, at 1030 Hz the contribution of scattered arrivals was more prominent than the diffracted field. This comparison was made under low sea-state conditions.

It is apparent, then, that surface scattering can be an important element in surface duct propagation. A good control case would be useful. However, this appears to be beyond the present state of the art. The biggest problem exists in properly modeling the ocean surface. A second problem is: How does one measure and characterize the ocean surface?

At NOSC, there are at least two normal mode models under development which include surface scattering. These differ somewhat in implementing scattering effects. No doubt other Navy activities have similar scattering models, using mode theory, ray theory, transport equation, etc.

Perhaps the best that can be done within the present state of the art is to evaluate these models against each other and against various data sets.

---

34. Podeszwa, E. M., Sound Speed Profiles for the Norwegian Sea, Naval Underwater Systems Center TD 6035, Jun 1979.
35. Wilson, H. L., and F. D. Tapport, Acoustic Propagation in Random Oceans Using the Radiation Transport Equation, J Acoust Soc Am 66, 256-274, Jul 1979.

4.3 MULTIPLE DUCTS

Multiple ducts occur in the ocean in a wide variety of contexts and represent an area where theoretical controls can play a vital role. The chief problem with multiple ducts is the interaction effects between the ducts. Models may do a good job of evaluating the fields associated with single ducts and yet be unsatisfactory when two simple ducts are involved. For example, ray diagrams generally provide a reasonable approximation to single-duct propagation, but are almost useless in addressing interaction effects.

An additional problem is that, at present, we do not have a clear picture of what critical test cases are necessary. We do not know the right questions to ask of models in this area. We do not know the impact of a model's failure to treat interaction effects. Here is an area where critical experimental data are sparse. The chances of useful data from a general experiment are almost nil.

In the case of multiple ducts, there is a particular problem with finding eigenvalues in a normal mode formulation. The modes are not uniformly spaced, as is usually the case for a single duct. Thus controls will be useful in testing a normal mode model's ability to locate eigenvalues under trying circumstances.

The remainder of this section presents the results of some limited work on multiple ducts and some suggestions for additional investigation. The material is organized under various types of multiple ducts.

4.3.1 Surface Duct and Deep Channel Interaction

This interaction is probably the one most commonly encountered in the ocean and occurs whenever a deep surface duct, say 300 ft deep, exists in the deep ocean. The interaction between convergence zones and such surface ducts was measured extensively (ref 36) during the early 1950s. When there is a deep surface duct, the convergence zones are extended in range. For example, the first convergence zone, which may ordinarily be only several miles wide, can extend out to perhaps a hundred miles in the presence of a deep surface channel. In this case, the increased coverage represents energy which has traveled in the surface duct by varying amounts and has taken one convergence-zone loop through the deep channel. Since there is about 0.5 s difference in travel time between the surface duct and convergence-zone loop, the number of convergence-zone loops in the combination path can clearly be distinguished in the experimental data. Furthermore, the lowest propagation losses are associated with the combination paths rather than with the direct surface duct propagation.

This elongation phenomenon has not been adequately modeled, if at all. We suggest the evaluation of a test case by normal mode theory, using two sound speed profiles. The first is profile B of figure 8; the second, profile C, is a near-surface modification of profile B, which is slightly different from that of figure 25. As in figure 25, profile C has a 100-m-deep surface layer with a gradient of 0.01597 s^{-1}. However, the sound speed at the bottom of the layer is the same as the surface sound speed for profile B. Thus profiles B and C have the same depth excess. Profiles B and C are the same, starting at the axis of minimum sound speed. This suffices to completely describe profile C, which has a slightly different gradient in layer 2 than has profile B and the profile of figure 25.

---

36. Arase, T., Some Characteristics of Long-Range Explosive Sound Propagations, J Acoust Soc Am 31, 588-595, May 1959.

The normal mode results of profiles B and C should be compared. Some depths in the layer and immediately below the layer should be investigated. Frequencies below as well as above surface duct cutoff should be examined.

This example would also provide an excellent test case for transient solutions, as opposed to steady-state solutions. Half-second CW pulses resolve the surface duct from convergence zone paths as well as the various combination CZ and surface duct paths. A proper transient solution should do the same.

There are several other interesting aspects to this problem. The steady-state solution superimposes the convergence zone and surface duct paths. We would like to separate these propagation effects without the use of the transient solution. For example, can it be done with partial mode sums, by using the method of Guthrie (ref 37)? Another possibility that should work for frequencies above surface duct cutoff is to subtract the acoustic field for the bilinear representation of profile C from the acoustic field for profile C. This procedure strips off the direct surface duct contribution and should leave us with the convergence zone and convergence-zone surface duct interaction contributions.

Another question arises with regard to group velocity and dispersion. The group velocity and dispersion curves for the modes of profile B have a completely different character from those associated with the bilinear surface duct of profile C. For example, the group velocities of convergence zone propagation are typically about 1625 yd/s, whereas those in surface ducts are slightly greater than the surface sound speed. Is there a method for obtaining group velocity and dispersion for surface duct propagation based on normal modes for profile C?

In the next section, we present an example where there is a substantial interaction between channels. In the case of profile C, which represents a more-or-less typical ocean situation, the coupling between channels is minimal. This condition comes about because the strengths of the two channels are radically different. In contrast, the profile of figure 29 represents a case where there can be a substantial interaction between the surface duct and the deep channel. The profile of figure 29, taken from reference 38, is for the winter in an area south of Newfoundland. Profiles of a similar nature are found during the winter in other northern latitudes such as the Norwegian Sea or the Greenland Sea. The profile of figure 29 is shown only to 1500 yd. It increases monotonically below this depth.

A 400-ft-deep isothermal surface channel is a substantial surface channel by ordinary standards. Here the change in sound speed from the surface to the bottom of the layer is about 7 ft/s. The corresponding value in figure 29 is 95 ft/s. It is clear that surface duct propagation in figure 29 is radically different than in what we would normally regard as an excellent surface channel. Indeed, we expect that there are more modes trapped in the surface duct of figure 29 than there are trapped in the refractive channel. The profile of figure 29 should be an excellent candidate for a mode analysis of coupling between channels. It should provide a good control case.

4.3.2 Multiple Near-Surface Ducts

Figure 30 presents the various types of sound speed profiles measured during the SUDS I experiments (ref 33). Type A represents the most common type of multiple

37. Tindle, C. T., and K. M. Guthrie, Rays as Interfering Modes in Underwater Acoustics, J Sound and Vibration 34, 291-295, 1974.
38. Podeszwa, E. M., Sound Speed Profiles for the North Atlantic Ocean, Naval Underwater Systems Center TD 5447, Oct 1976.

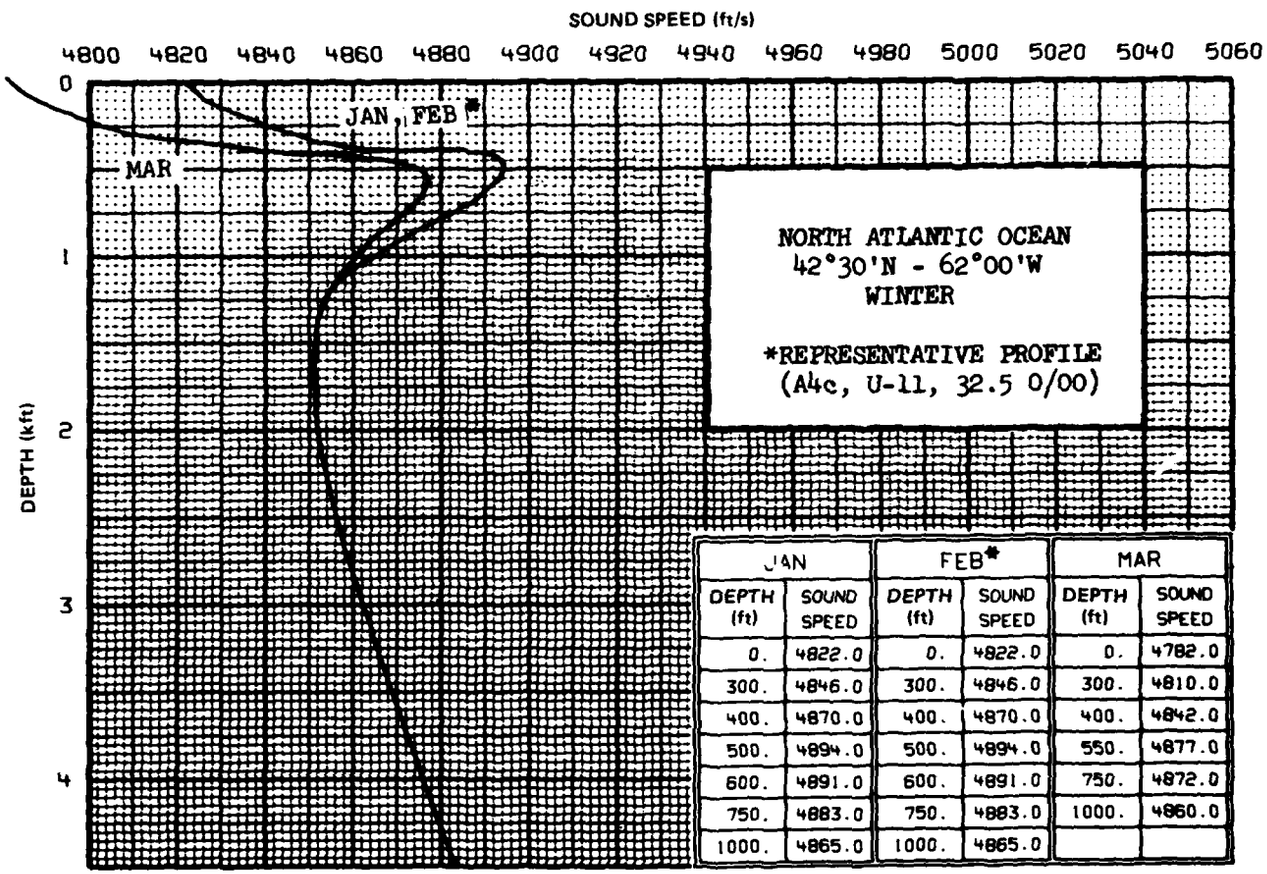

JAN		FEB*		MAR	
DEPTH (ft)	SOUND SPEED	DEPTH (ft)	SOUND SPEED	DEPTH (ft)	SOUND SPEED
0.	4822.0	0.	4822.0	0.	4782.0
300.	4846.0	300.	4846.0	300.	4810.0
400.	4870.0	400.	4870.0	400.	4842.0
500.	4894.0	500.	4894.0	550.	4877.0
600.	4891.0	600.	4891.0	750.	4872.0
750.	4883.0	750.	4883.0	1000.	4860.0
1000.	4865.0	1000.	4865.0		

Figure 29. Winter profile in North Atlantic illustrating a strong surface duct and a deep channel.

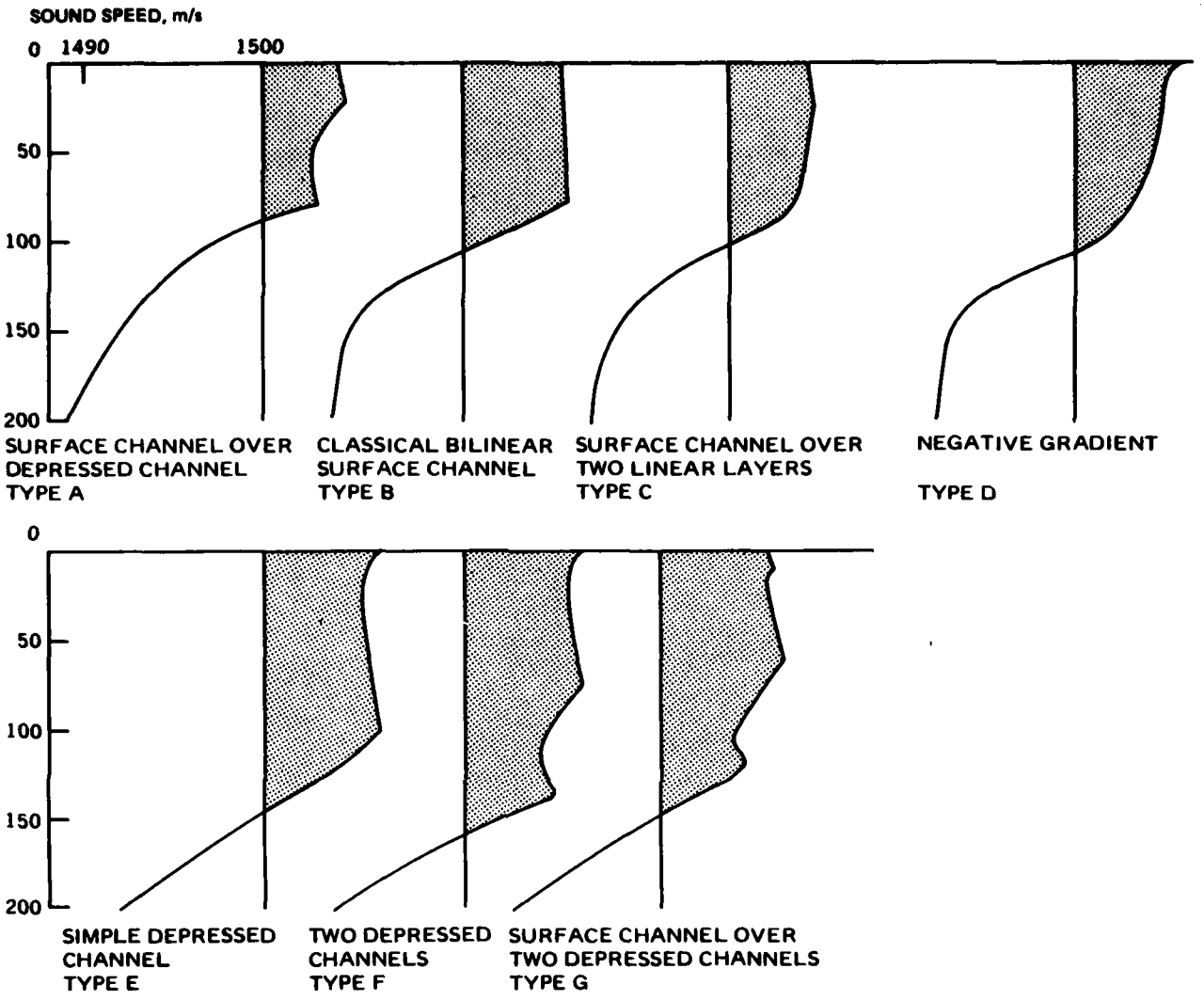

Figure 30. SUDS I sound speed profile types.

near-surface duct; ie, a surface duct overlaying a refractive duct. In the SUDS I experiments, this was the most prevalent type and occurred for 34% of the measurements. The next most prevalent type (B, the classical bilinear surface channel) only occurred for 17.6% of the measurements.

The type A duct is the chief subject of this section. There are other slightly different forms of this profile, although the form shown in figure 30 appears to be the most common. For example, the surface sound speed can be smaller than that of the axis of the refractive channel, or the sound speed at the bottom of the refractive channel can be larger than that at the top of the refractive channel. We will not make a distinction between these forms in the discussion of this section.

Before continuing, we should note in figure 30 two other types of multiple near-surface ducts. Type F, consisting of two refractive channels, occurred during 1.1% of the SUDS test period, whereas type G, consisting of a surface duct overlaying two refractive channels, occurred during 0.4% of the test period. These ducts appear to occur rather rarely and a detailed examination of these cases should be delayed until the analysis of the more important multiple ducts has been completed.

The multiple surface duct of type A has been analyzed in several reports. Reference 33 presents normal mode computations for three different ducts of this type. For one of the three ducts, the parabolic equation method was also used. Reference 39 presents a detailed modal analysis of a double duct of this type. However, there is poor coupling between the ducts since they are separated in sound speed by much more than illustrated in figure 30.

The most thorough analysis of a multiple near-surface duct is presented in reference 40, which gives four examples of this type of profile as measured during four of the Lockheed surface duct experiments of the 1960s. A stylized model of this profile was subjected to a thorough mode analysis. This duct is illustrated in figure 31. The two positive-gradient layers have a gradient of 0.018 s^{-1} (isothermal) and each is 33-1/3 yd deep. The two negative gradients are -0.2 s^{-1}. The second layer is permitted to vary in thickness from 0 to 7 yd. The analysis of these profiles provides an excellent illustration of the problems encountered when there is a strong interaction between multiple ducts.

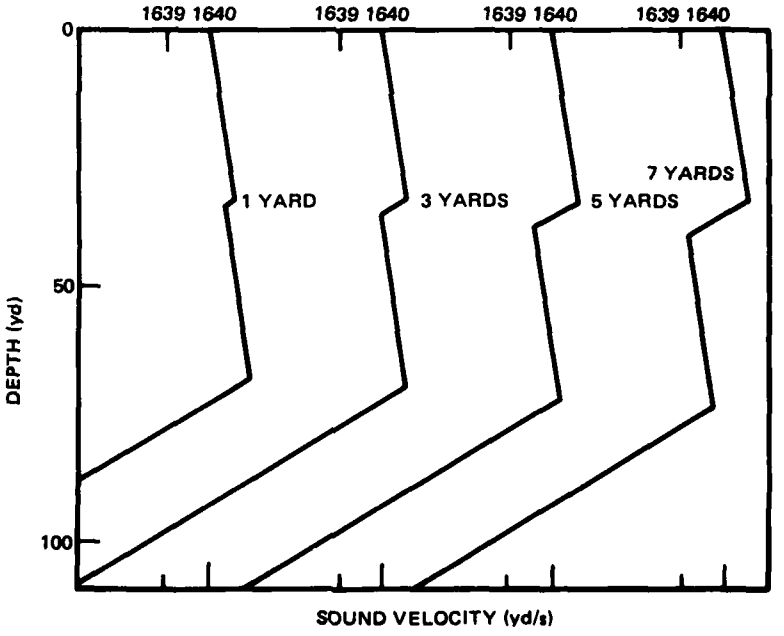

Figure 31. Double duct profiles with different thicknesses in the second layer.

39. Gordon, D. F., Normal Modes in a Pair of Ocean Acoustic Ducts, Royal Australian Navy Research Laboratory AR-001-021, Sep 1978.
40. Available to authorized requestors.

The first problem is the determination of eigenvalues and the identification of modes. In single ducts, the modes are relatively easy to find and to identify, with the possible exception of modes below cutoff. The eigenvalues, though discrete, appear to lie along smooth curves at semiregular intervals. Thus, given a few lowest-order eigenvalues, higher-order eigenvalues can be readily estimated and solved for by iteration. In the process of finding eigenvalues, the computer program calculates

$$\tilde{R} = 2\pi[\mathrm{Re}(\lambda_{n+1}) - \mathrm{Re}(\lambda_n)]^{-1} \tag{28}$$

where $\mathrm{Re}(\lambda_{n+1})$ and $\mathrm{Re}(\lambda_n)$ are the real part of the wave numbers for two adjacent modes. Here, $\tilde{R}$ represents the interference distance between adjacent modes and corresponds to the loop length of a ray with phase velocity midway between that of two modes. For single channels, successive values of $\tilde{R}$ step along in a smooth manner and agree reasonably well with the ray theory counterpart. An unreasonable behavior of $\tilde{R}$ is a sign that an eigenvalue has been missed or there is some other error in the eigenvalues. Furthermore, for single channels the mode attenuation usually increases with increasing mode number.

However, in the case of multiple ducts the duct interaction can perturb the eigenvalues so that they do not behave as anticipated for single ducts. They do not always occur at semiregular intervals, and equation 28 fails completely, although (as discussed below) it can be modified to give reasonable approximations. The mode attenuation, which is related to the imaginary part of the eigenvalue, is not monotonic with mode number, but can jump about wildly.

The behavior of eigenvalues is so startling that we need to present them for the profiles of figure 31 as a function of a second-layer thickness. Figure 32 presents the phase velocity of the first 12 modes. The phase velocity of mode n is given by

$$v_n = 2\pi f/\mathrm{Re}(\lambda_n) \tag{29}$$

where $\mathrm{Re}(\lambda_n)$ is the real part of the mode eigenvalue.

The profile of figure 31 reduces to a standard bilinear model when the thickness of the second layer is zero. Thus the eigenvalues (as characterized by the phase velocity) at the left of figure 32 are easily identified. They lie at semiregular intervals. As we increase the thickness, they no longer occur at semiregular intervals. Indeed, the real parts of the eigenvalues cross or appear to cross each other. Now, the proper way to number modes is to order them according to increasing phase velocity in the combined duct system. In figure 32, the modes are numbered according to this system at the left of the figure and also at the right. The important thing to note is that the designation has changed for those modes for which the real parts of the eigenvalue have crossed. For example, mode 4 crosses mode 3 at point D and the mode designated mode 4 at the left is designated mode 3 at the right. Mode 7 at the left ends up as mode 5 at the right, while mode 3 at the left ends up as mode 6 on the right.

Note that in some cases such as points A, B, E, F, and G, the modes do not cross but veer away from each other as if avoiding a collision. It is not clear why some veer away and others cross. Cases such as points A and B require a very fine analysis to determine whether crossing or veering occurs. The mode follower program will not, in general, distinguish crossings and veerings because the estimation based on extrapolation will jump onto the crossing branch.

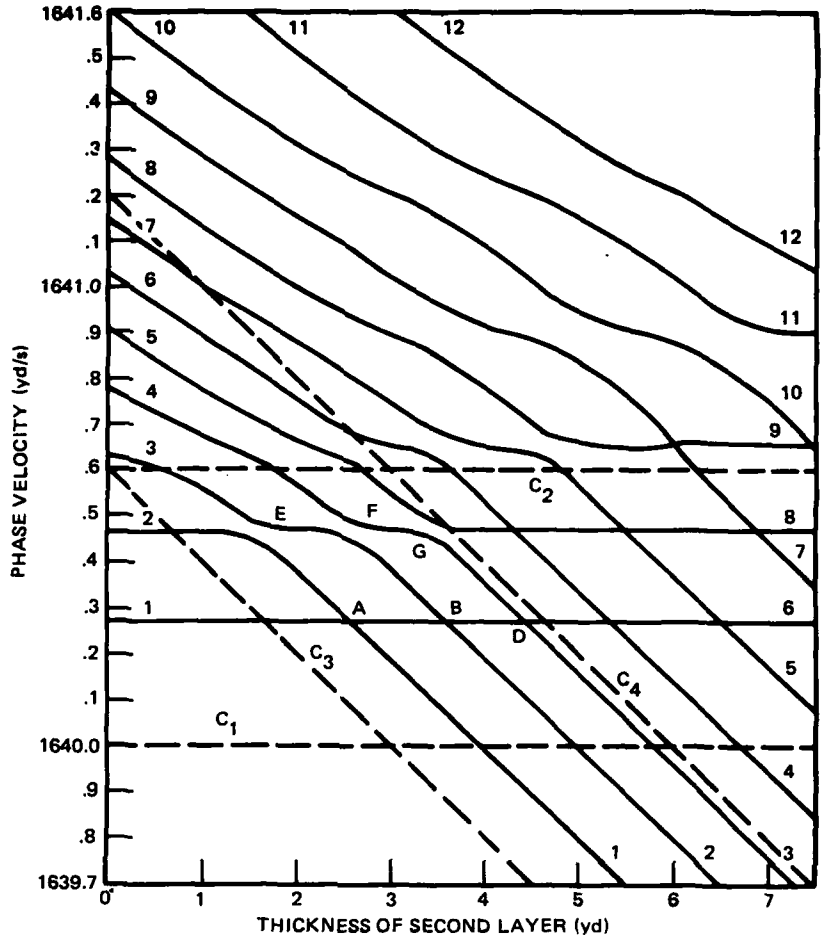

Figure 32. Phase velocity of the first 12 modes as a function of second-layer thickness. The sound speed C_i at layer interface i is shown by the broken lines.

The picture becomes even more complicated if we look at the imaginary parts of the eigenvalues. Figure 33 presents the mode attenuation for various layer thicknesses. Attenuation a_n for mode n is given by

$$a_n = -8686 \, \mathrm{Im}(\lambda_n) \, \mathrm{dB/kyd} \, . \tag{30}$$

The first thing to note is that at the left of the figure, the attenuation increases monotonically with mode number as expected. However, this behavior changes drastically for the double duct. For example, for thick layers mode 6 has smaller attenuation than modes 2 to 5. Such wild behavior in attenuation greatly increases the difficulty in finding and identifying modes. The behavior of figure 33 is correlated in an interesting manner with that of figure 32. In the case of figure 32, we noted that the curves veer away at points A, B, E, F, and G. In figure 33, we note that for these points the attenuation curves cross each other. In contrast, where the real values cross in figure 32 at points D and H, the attenuation curves in figure 33 do not even come close to each other.

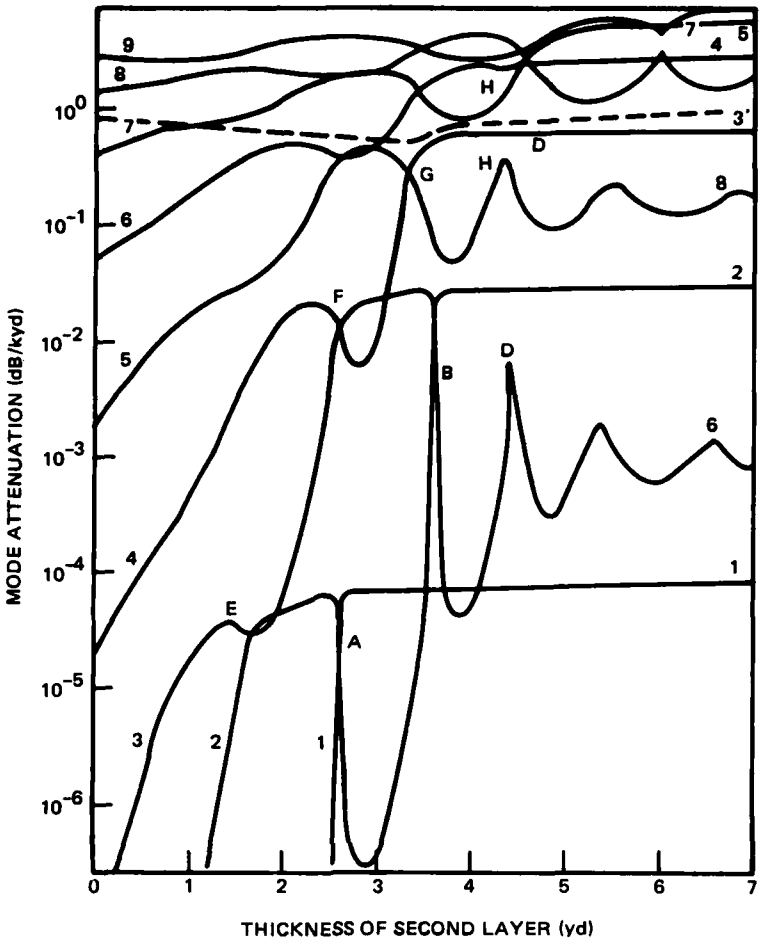

Figure 33. Imaginary part of the first nine eigenvalues expressed as mode attenuation as a function of second-layer thickness.

The major point of this example is to indicate the problems of finding and identifying modes for multiple ducts. Whenever there is a strong interaction between ducts, a wild behavior similar to that of figures 32 and 33 can occur. Even for cases of weak interaction, the problem occurs to some extent. For example, figure 4 of reference 39 presents evidence of the perturbation of mode eigenvalues, although there the problem is much easier to unravel.

In dealing with multiple ducts, we often find it necessary to prepare plots similar to figures 32 and 33, in which the frequency or some profile parameter is varied in a continuous fashion. We find that we cannot locate or interpret the discrete eigenvalues for a given modal problem with any confidence unless we can put it into a continuous context. Nor can we prescribe guidelines. Each multiple duct has its own special problems and behavior.

The phase integral method of ray theory (ref 41) can be of help in finding modes. One estimates approximate real eigenvalues for each duct independently and then iterates the combined duct system with these estimates. These approximate eigenvalues may be very good estimates, although the numbering must be according to the combined system. Figure 32 is an excellent example. The phase integral method for the first mode in the upper duct of figure 31 yields a phase velocity of about 1640.27 yd/s. Note that in figure 32, an eigenvalue for the combined duct always lies close to this value. However, the mode number may be any value from 1 to 6, depending on the duct width. Similarly, for mode 2 this method yields the eigenvalue which lies near 1640.47. Equation 3 of reference 40 gives the phase integral approximation for modes trapped in a refractive duct, such as that of figure 31. This approximation gives eigenvalues that correspond to those of figure 32, which lie parallel to the C_3 and C_4 loci.

There is a further interest in the points where the modes cross or veer off. Reference 40 discusses the response for a receiver located in the lower duct when the source is in the upper duct. A maximum response or coupling occur at points where the modes cross or veer off. Maximum coupling occurs at points E, A, F, B, D, and H, in that order. This ordering is apparently related to the attenuation of figure 33. A similar result holds for a receiver located in the upper duct when the source is in the lower duct. It appears, then, that maximum coupling between ducts occurs when the phase velocities of the modes come near crossing. This occurs when the phase integral method yields the same approximate eigenvalue for both ducts. For example, reference 40 develops an equation based on this algorithm which yields the crossing points of the trapped modes to two decimal places. Thus the crossing points represent an important physical phenomenon and not just some aberration which impedes our determination of eigenvalues.

We should say something more about the identification of modes. The importance of identifying eigenvalues with a certain numbering of the modes lies in making certain that no modes have been left out. (The order in which modes are summed make no difference in the resultant field).

In complicated eigenvalue relationships such as those of figures 32 and 33, it would be advantageous to be able to identify a mode number with an eigenvalue. For example, if one can identify some eigenvalue λ as belonging to mode 10, say, then one knows that there are nine other eigenvalues with smaller $\mathrm{Re}(\lambda)$. If nine such values have not been found, one knows that there are missing modes.

The manner in which we have identified a mode in the past is to plot the absolute value of the depth function versus depth. The mode number is the number of antinodes or nodes in the depth function. Thus the mode number is usually the number of relative maxima (antinodes) or the number of relative minima (nodes) plus one. The mode number is one more than the number of relative minima because there is a node at the surface. This scheme fails when mode eigenvalues are near the crossing or veering locations. As illustrated in reference 40, a spurious extra maximum or minimum may occur. A more sensitive test of mode number is to calculate the phase of the depth function versus depth. The

41. Bucker, H. P., Normal-Mode Sound Propagation in Shallow Water, J Acoust Soc Am 36, 251-258, Feb 1964.

phase changes rapidly by π at a node in the depth function. The mode number can then be related to these phase changes. According to Gordon (ref 40), the phase change can be used to distinguish a spurious relative minimum from a true node.

We recommend that the eigenfunction phase be examined in detail at crossover points in multiple ducts. It may be possible to implement a computer algorithm which would identify the mode number. Such an algorithm would be of considerable help in making certain that no mode has been omitted.

There is another important problem which may arise in multiple ducts. Reference 42 extends the analysis of reference 40 to the consideration of degenerate or nearly-degenerate modes. Degenerate modes are two (or more) independent modes with the same eigenvalue. Degeneracy does not usually occur because, as figures 32 and 33 demonstrate, when the real parts of the eigenvalues cross, the imaginary parts do not and vice versa. However, by varying two parameters, the second layer thickness and the lower gradient in the third layer, Gordon (ref 42) was able to come very close to obtaining degenerate modes.

At and near this point, the amplitude functions for each of the modes become exceedingly large. These amplitude functions are expressed as

$$U_m(Z)\, U_m(Z_0) = F_m(Z)\, F_m(Z_0)/D_m \tag{31}$$

where $F_m(Z)$ and $F_m(Z_0)$ are eigenfunctions evaluated at the source and receiver, respectively, while D_m is a normalization factor which assumes the form

$$D_m = \int_0^\infty F_m^2(Z)\, dZ \ . \tag{32}$$

The quantity D_m changes the orthogonal function F_m into the orthonormal function U_m. Gordon (ref 42) determined that near the point of degeneracy, two of the $F_m(Z)$ were almost identical. The same was true of $F_m(Z_0)$. However, the two normalizing factors approached zero in such a fashion that their phase difference approached 180°.

The reason that D_m of equation 32 approaches zero can be rationalized as follows: Since F_m is orthogonal

$$\int_0^\infty F_m(Z)\, F_{m+1}(Z)\, dZ = 0 . \tag{33}$$

When modes m and m+1 are nearly degenerate, the integral of equation 32 is almost identical to that of equation 33. Thus the value of D_m goes to zero.

42. Available to authorized requestors.

Gordon (ref 42) points out that the opposite sign of D_m and D_{m+1} causes a cancellation in the sum of the amplitude functions of the two modes. Indeed, in the limit of degeneracy, the sum of the two modes is of the form

$$\text{mode sum} = \infty - \infty \tag{34}$$

which, if evaluated properly, should lead to a finite answer. This answer would be the evaluation of the residue for a double pole, which represents the degenerate case.

In normal mode analysis we often sum the modes in random phase. This process, for example, strips off the scintillations exhibited by phased mode addition and exhibits more clearly the dependence on other factors such as depth and frequency. Gordon (ref 42) points out that whenever mode eigenvalues cross each other, there is a danger in random phased addition. In such a case the two crossing modes should first be added coherently, and then this resultant should be added incoherently with the remaining modes. Gordon shows, for example, that at point B of figure 32, the coherent and incoherent additions of the modes differ by 1.2 dB. However, this difference increases to a value of 35.5 dB for the most nearly degenerate case.

The impact of this result as a control arises in two contexts. First, such a control would illustrate the pitfall of random phase addition. Second, for conditions close to degeneracy the result of summing the two modes is extremely sensitive to computational methods. That is, any errors or carelessness in either the eigenvalue location process or the normalization process are exposed.

Of course, one may argue that near-degeneracy is a condition that seldom occurs. However, the coupling between multiple ducts appears to be a maximum under these conditions. Thus, it may be that this case is the one of maximum importance and interest.

We recommend, for example, that the coupling between double ducts, such as those of figure 29, be thoroughly investigated as a function of frequency. The analysis of Gordon (ref 40) should be extended to determine optimum frequencies and receiver depths for selected source depths. As a result of this investigation, some control cases should be prepared. These should not only be used as controls for normal mode models but for other models as well. For example, it would be very interesting to see results of the parabolic equation method or the fast field program (both ref 12) under conditions of optimum coupling between multiple ducts.

We have previously mentioned that in double-duct cases, the interaction between the two sets of modes causes the eigenvalues to be perturbed from their single-duct values. This effect is not unique to underwater acoustics, as we shall demonstrate by two examples of other modal phenomena.

Reference 43 discusses the mechanical vibration of plates, which involves two sets of modes. These are the thickness-shear mode and the flexural mode. Lee (ref 43) presents four different plots of resonant frequency of various modes as a function of the ratio of plate width to thickness. These plots bear an astonishing likeness to figure 32. However, in contrast to figure 32, the two sets of modes never cross each other; they always veer away from each other. Some come very close, as at point A in figure 32, whereas others remain well separated, as at point E.

---

43. Lee, P. C. Y., and S. S. Chen, Vibrations of Contoured and Partially Plated Contoured, Rectangular AT-Cut Quartz Plates, J Acoust Soc Am 46, 1193-1202, Nov 1969.

The second example is discussed on pages 153-155 of reference 44. It treats the crossing of energy bands for two closely spaced energy levels of the isolated potential well. The solution for the individual levels cross each other. However, the solution for the combined pair do not cross but steer clear of each other.

These examples further illustrate that, in the case of multiple channels (sets of modes), there is some underlying physical principle which contorts the mode eigenvalues to avoid degeneracy. In the examples of references 32 and 33, the eigenvalues are real and the modes never cross each other. Our mode theory is more complicated, in that the eigenvalues are complex. Here, the real parts or the imaginary parts (but not both) of the eigenvalues may cross.

This complication suggests another problem in modeling double ducts. As will be discussed later, there are normal mode programs which are formulated for real eigenvalues only. It would be interesting to determine whether these programs can deal with the coupling between multiple ducts.

4.3.3 Depressed Channel and Deep Channel

This section presents several examples of two refractive ducts. These examples are all taken from references 34 and 38. One of the ducts is the familiar deep or SOFAR channel. The other is a secondary refractive duct which occurs in or below the thermocline.

Figure 34 presents a series of refractive ducts for the North Atlantic. In these examples, the shallower refractive duct is attributed to high saline water flowing out of the Mediterranean Sea. Figure 34 applies to regions near the Straits of Gibraltar. The ducts persist over much of the North Atlantic, although the shallower refractive duct weakens considerably and becomes shallower.

Figure 35 is an Atlantic profile at 36°30'N, 67°00'W, which is somewhat east of Cape Hatteras. In this case, the refractive duct is high in the thermocline. This type of profile also occurs in the North Pacific, but is not as prevalent as in the Atlantic. The channels are well separated and coupling effects may be rather minimal.

Figures 36 and 37 are examples of double ducts which occur at higher latitudes in both the Atlantic and Pacific. Figure 36 is a Pacific profile at 45°N, 155°W. Figure 37 is an Atlantic profile at 42°30'N, 62°00'W. These profiles illustrate a common phenomenon in northern latitudes. There is a refractive channel at or near the bottom of the thermocline and the deep sound channel lies immediately below. Figures 36 and 37 represent more or less extreme types. For example, the minimum sound speeds of the two ducts are generally much closer. Moreover, in many cases the difference between minimum and maximum sound speeds between the ducts is much smaller. For more northern latitudes than those of figures 36 and 37, ducts become shallower and become of more equal strength. Even farther north, the two ducts merge and become one shallow duct.

We suspect that there might be strong coupling between many of these double ducts. There are so many variations, however, that considerable effort may be required to establish a "typical" situation along with upper and lower bounds. Meaningful controls cannot be established until we have a better understanding of multiple ducts.

---

44. Smith, R. A. Wave Mechanics of Crystalline Solids, Chapman and Hall, London, 1961.

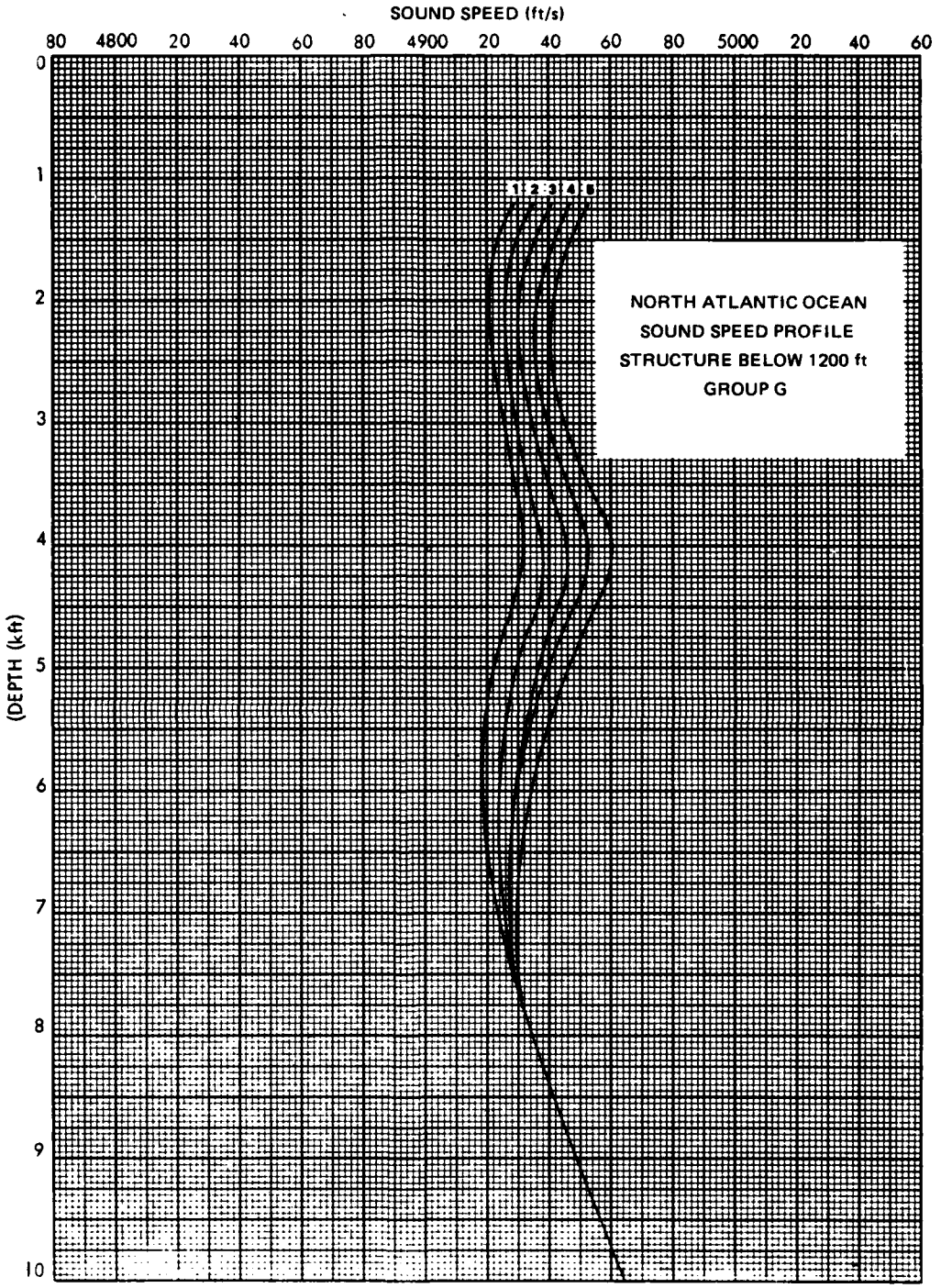

Figure 34. Five Atlantic sound speed profiles illustrating two refractive ducts near the Straits of Gibraltar.

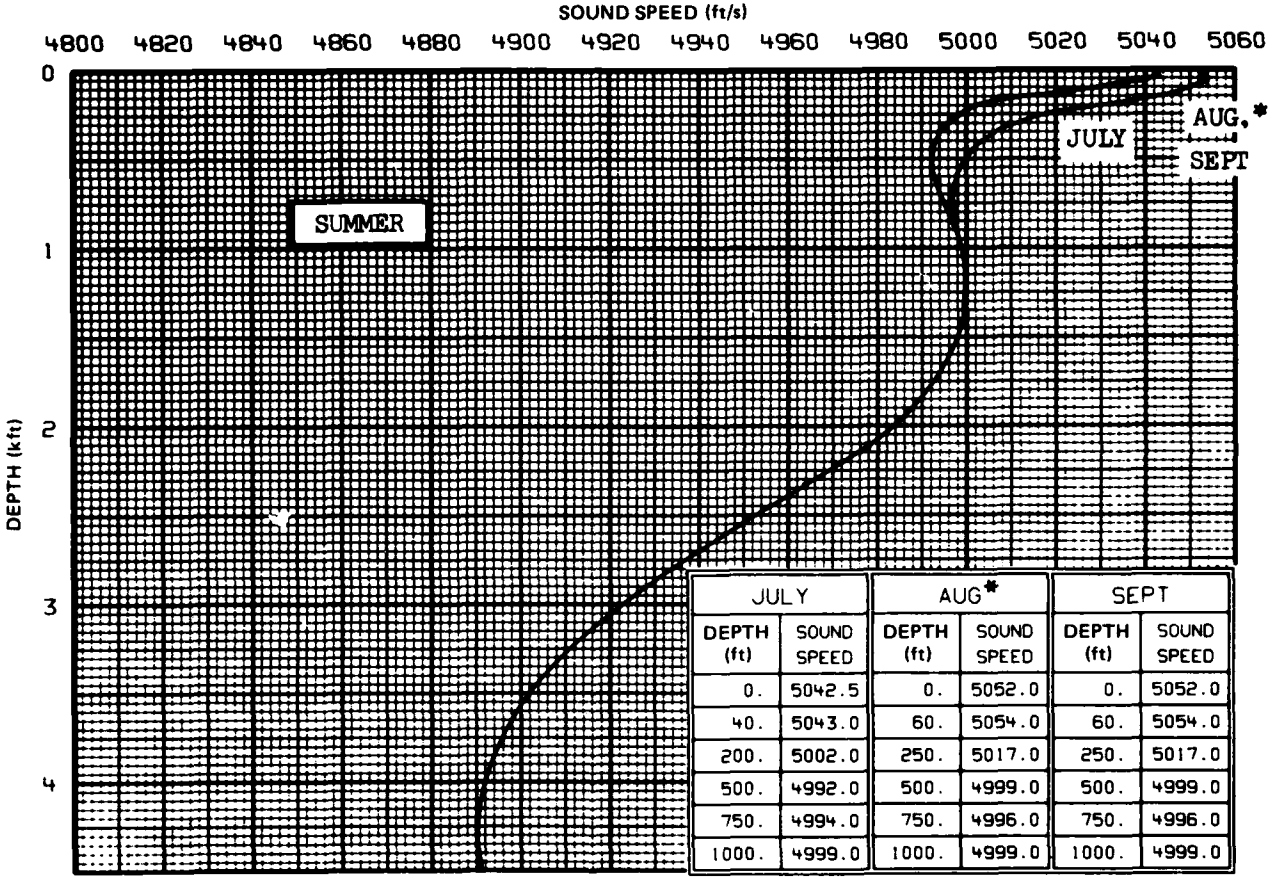

JULY		AUG*		SEPT	
DEPTH (ft)	SOUND SPEED	DEPTH (ft)	SOUND SPEED	DEPTH (ft)	SOUND SPEED
0.	5042.5	0.	5052.0	0.	5052.0
40.	5043.0	60.	5054.0	60.	5054.0
200.	5002.0	250.	5017.0	250.	5017.0
500.	4992.0	500.	4999.0	500.	4999.0
750.	4994.0	750.	4996.0	750.	4996.0
1000.	4999.0	1000.	4999.0	1000.	4999.0

Figure 35. Atlantic sound speed profile illustrating a refractive duct high in the thermocline.

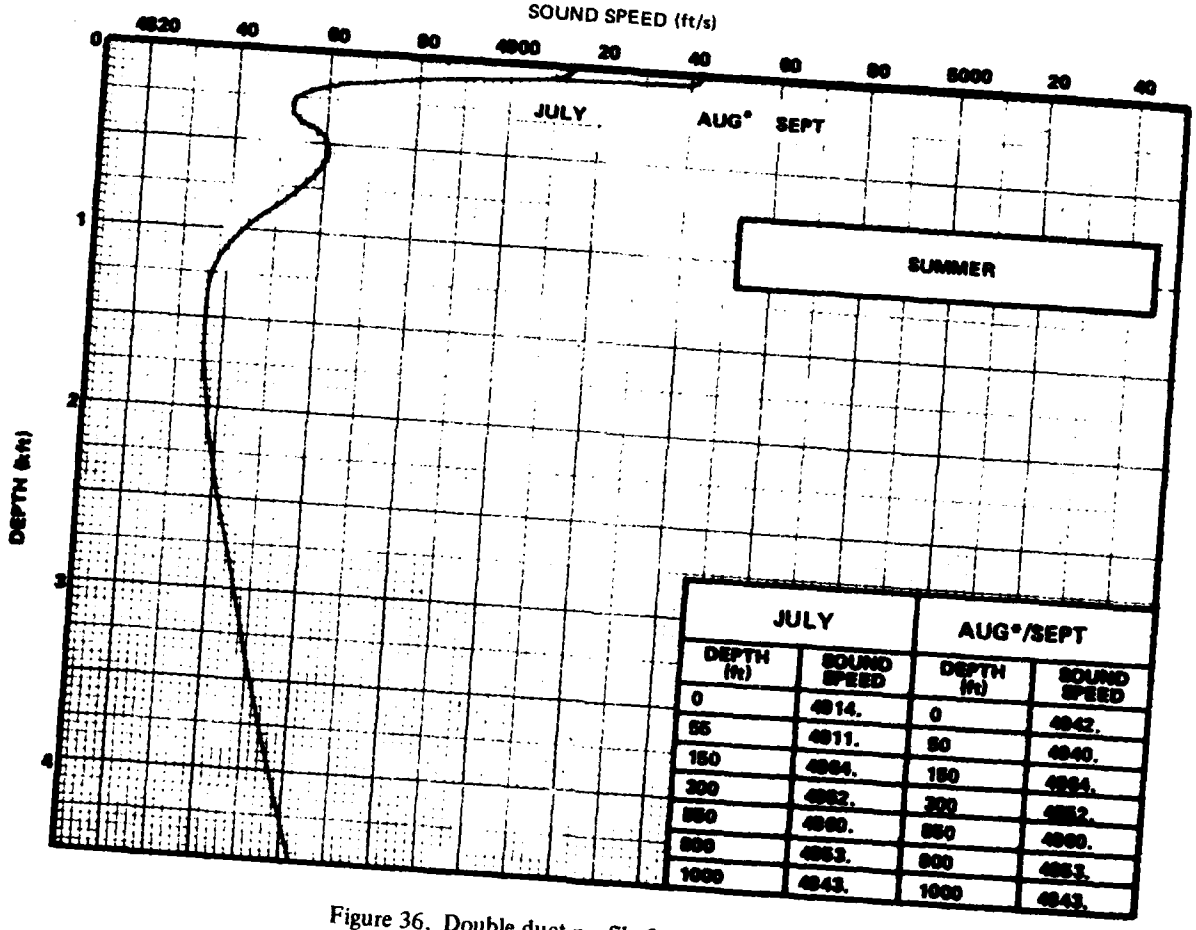

JULY		AUG*/SEPT	
DEPTH (ft)	SOUND SPEED	DEPTH (ft)	SOUND SPEED
0	4914.	0	4942.
55	4911.	50	4940.
150	4904.	150	4934.
200	4902.	200	4932.
850	4860.	850	4860.
900	4863.	900	4863.
1000	4843.	1000	4843.

Figure 36. Double duct profile from the Pacific.

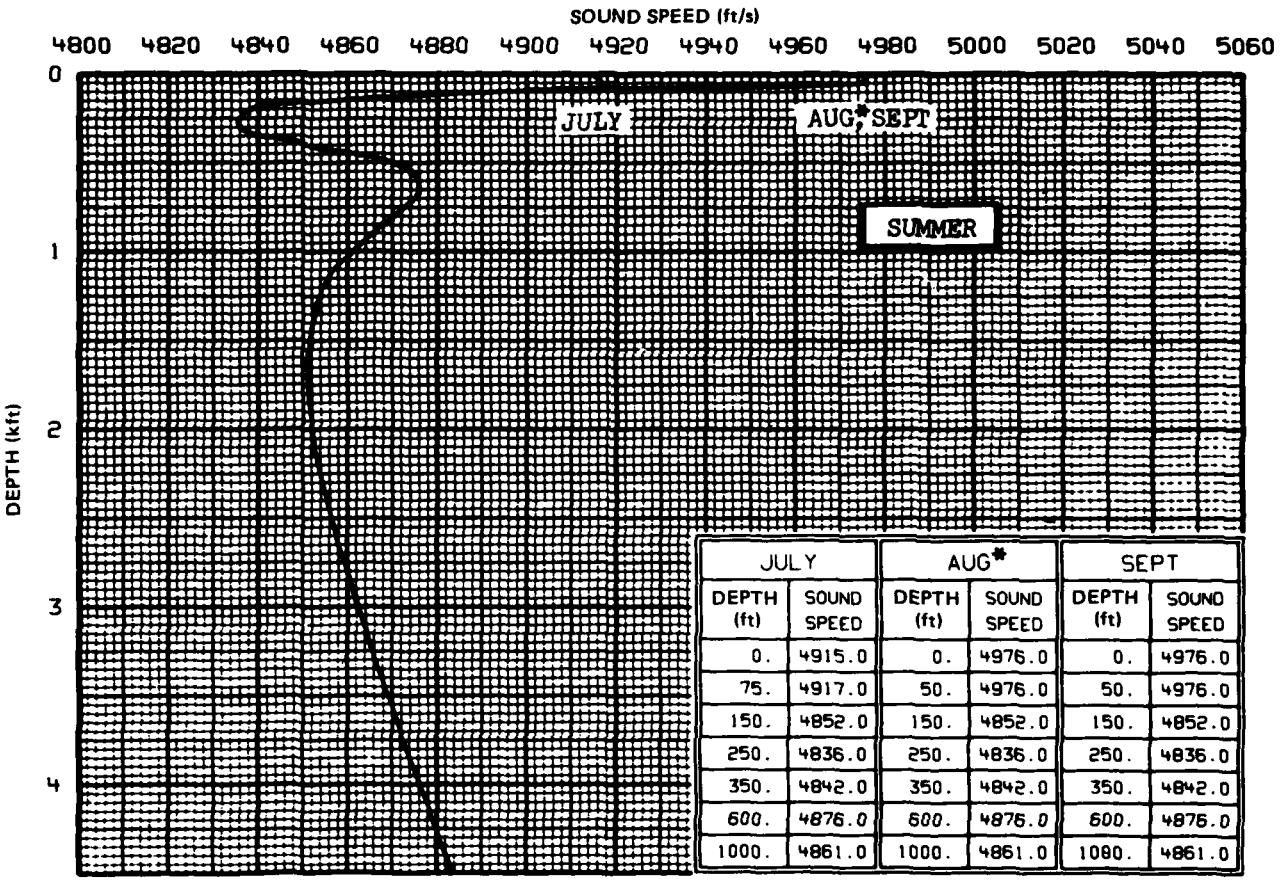

JULY		AUG*		SEPT	
DEPTH (ft)	SOUND SPEED	DEPTH (ft)	SOUND SPEED	DEPTH (ft)	SOUND SPEED
0.	4915.0	0.	4976.0	0.	4976.0
75.	4917.0	50.	4976.0	50.	4976.0
150.	4852.0	150.	4852.0	150.	4852.0
250.	4836.0	250.	4836.0	250.	4836.0
350.	4842.0	350.	4842.0	350.	4842.0
600.	4876.0	600.	4876.0	600.	4876.0
1000.	4861.0	1000.	4861.0	1080.	4861.0

Figure 37. Double duct profile from the Atlantic. This is the summer profile corresponding to the winter profile of figure 29.

5.0 BOTTOM-REFLECTED PROPAGATION

In this section, we discuss controls for bottom-reflected paths. The sound speed profile does not change with range and the ocean bottom is treated as perfectly flat. The controls are discussed in two groups. Section 5.1 treats controls where the bottom characteristics are described in terms of the impedance at the water–bottom interface. Section 5.2 treats controls where the bottom characteristics are described by a sub-bottom sound speed structure.

5.1 BOTTOM REFLECTION PROPERTIES SPECIFIED

This section discusses controls where reflection properties are specified at the water-bottom interface. These conditions are given as bottom loss and bottom phase shift or as the equivalent complex reflection coefficients.

5.1.1 Rigorous Normal Mode Solution

One of the first problems we addressed, when requested to prepare controls by AMEC, was a rigorous normal mode solution where the complex bottom reflection coefficients are given. From a ray theory standpoint, these coefficients completely specify the boundary conditions. The first question to ask is whether this specification is adequate in terms of normal mode theory.

This question was first addressed by looking at the normal mode solution for a layered bottom and determining whether one could replace the sub-bottom structure by specifying characteristics at the water–bottom interface. These characteristics and the water-column structure then would serve as inputs to a normal mode solution which would be identical to the original solution for the layered bottom. The characteristics of the water–bottom interface contain, in effect, all the information needed about the sub-bottom structure as long as our interest is only in the acoustic field in the water column or at the water–bottom interface.

It has been known for some time that the complex reflection coefficients at the ocean bottom could be calculated from the mode solution for the layered bottom. Using these coefficients, together with a specification of the water column, one could calculate the same eigenvalues for the original layered bottom. It was then found this procedure was not sufficient to specify the modal solution. The normalization factor in the solution for the layered bottom contained contributions from the sub-bottom layers. The problem then became to determine this contribution.

The solution to this problem is summarized and illustrated in reference 45, which was prepared under AMEC funding.

The result of reference 45 for the normalization factor is

$$D_n = \int_0^{Z_B} U_n^2(Z)\, dZ + D_{sn} + D_{bn} \quad . \tag{35}$$

---

45. Gordon, D. F., and D. White, Bottom Interaction Represented by Impedance Conditions in Normal-Mode Calculations, Conference on Bottom-Interacting Ocean Acoustics, SACLANT ASW Centre, LaSpezia, Italy, Jun 1980.

The first term of equation 35 represents the contribution to D_n between the ocean surface and bottom. The quantity D_{sn} represents a surface contribution and is equal to zero for a perfectly reflecting surface. The quantity D_{bn} is a contribution at the bottom interface and may be written as

$$D_{bn} = U_n^2(Z_B)/2\lambda_n \, V_n^2(Z_B) \, D_{cn} \quad . \tag{36}$$

Reference 45 notes that $U_n(Z)$ and $V_n(Z)$ are both eigenfunctions which differ only by a constant. Thus their ratio is constant. The most convenient place to evaluate this ratio is at the bottom Z_B.

The quantity D_{cn} in equation 36 is

$$D_{cn} = -i \, W^2 \left[2\ell_n \, (\partial R/\partial\lambda)_{\lambda=\lambda_n} + \lambda_n/\ell_n \, (R_n^2 - 1) \right] \tag{37}$$

where W is a known constant,

$$\ell_n = (k_B^2 - \lambda_n^2)^{1/2} \quad , \tag{38}$$

and R_n is the complex reflection coefficient.

Given the complex reflection coefficients, which of the expressions in equations 35 to 38 can be evaluated? We note first that R_n and the water-column characteristics are sufficient to calculate the eigenvalues λ_n and the eigenfunctions $U_n(Z)$ and $V_n(Z)$. Thus all expressions except $\partial R/\partial\lambda$ in equation 37 can be evaluated. Thus, in addition to the given reflection coefficients, the slope of the reflection coefficients must be given.

This slope can be evaluated in terms of more familiar quantities if we first express R in polar form

$$R = |R| \, e^{i\phi} \tag{39}$$

and note that

$$\lambda = \omega/C_p - i\alpha/8686 \tag{40}$$

where C_p is the phase velocity and α is the mode attenuation in dB/km. Application of equations 39 and 40 leads to

$$(\partial R/\partial\lambda)_{\lambda=\lambda_n} = \frac{-C_p^2 \left(R \frac{d|R|}{dC_p} \frac{1}{|R|} + \frac{d\theta}{dC_p} \right)}{\omega + i \, C_p^2 \, (d\alpha/dC_p)/8686} \quad . \tag{41}$$

Thus, for a control case we should specify $|R|$ and ϕ as given functions of the phase velocity. These functions can be differentiated and, when evaluated at the eigenvalues, yield the numerator of equation 41. The derivative in the denominator of equation 41 may be estimated from plots of mode attenuation versus phase velocity.

Reference 45 estimates the contributions of various terms to D_n for an example where a structured bottom was given and the discrete reflection coefficients were calculated at the eigenvalues for the structured bottom. The D_n for the structured bottom were compared to the D_n for a second modal calculation by using these discrete reflection coefficients and the foregoing equations. Values of $d|R|/dC_p$ and $d\phi/dC_p$ were estimated from the discrete reflection coefficients plotted as a function of phase velocity. Estimates based on an 11-point fit to R yielded the D_n, which were in error by less than 0.5% for modes 2 to 10 and 1.6% for mode 1. The error that resulted from neglecting D_{bn} in equation 35 was as much as 1.2%. However, there was more error when the second term of equation 37 was included in the computation, but not the first term. Thus, setting $\partial R/\partial\lambda = 0$ leads to errors of from about 5% for mode 1 to 1.4% for mode 10. In this case, the error was less when D_{bn} was ignored completely than when only the second term in D_{cn} was used.

In making these estimations, reference 45 ignored the imaginary component in the denominator of equation 41. Evaluation of this component shows that magnitude was about 0.6% of that of ω. We estimate that this component affects D_n by about 0.02%. If numerical methods are used to estimate the numerator of equation 41, this component can be ignored. However, it should be included in the computation of a rigorous solution in which the numerator of equation 41 can be evaluated from given functional forms.

In the case of the mode calculation for the structured bottom, $\partial R/\partial\lambda$ can be evaluated exactly from other expressions involving the bottom structure. When these values were used in equation 37 in lieu of those values estimated from the reflection coefficients by the use of equation 41, the D_n obtained from equation 35 agreed to at least three decimal digits with those obtained from the structured bottom as calculated by

$$D_n = \int_0^\infty U_n^2(Z)\, dZ \quad . \tag{42}$$

Thus the formulation of equations 35 to 38 has been verified.

The derivation of equations 36 to 38 is a truly formidable task, which is only hinted at in reference 45. It involves two sets of depth functions U and V. U satisfies the surface impedance condition and all the interface conditions below it. It does not necessarily satisfy the bottom impedance condition. V satisfies the bottom impedance condition and all interface conditions above it except the surface. If one of these satisfies both impedance conditions, then it is an eigenfunction. That is, an eigenvalue has been found. In this situation, U and V differ by only a multiplicative constant, as discussed in connection with equation 36. The use of both U and V is a critical part of the derivation of equations 36 to 38.

In the course of this derivation, a number of different formulations of the eigenfunctions were investigated. For example, the D_n may be evaluated from the theory of residues. It was quite difficult to demonstrate the relationships between these formulations. There is, for example, a completely different method for evaluating D_n than the use of equation 35. In this method, the normalization factor is written as a function of the

derivative of the eigenvalue determinant with respect to the eigenvalue. Otsubo (ref 46) has presented a method for computing this derivative, which he used to iterate into the eigenvalues. The implementation of Otsubo's method may lead to an improved method for evaluating D_n. However, as expected, this method also requires $\partial R/\partial \lambda$.

A formal report on the derivation of equations 35 to 38 and on the various formulations of eigenvalues and normalization factors would be extremely valuable. The basic work has been carried out under AMEC funding, which was insufficient for a complete final report. Such a report will require additional funding from AMEC or some other interested sponsor. Experience may prove that other formulations are superior to that of equations 35. However, for the present we believe that a rigorous normal mode solution for the case of a specified bottom impedance condition has been established and that it could be used to develop a control case against which other models could be tested.

5.1.2 Semicoherent Ray Model

A coherent ray model is one in which the ray paths are combined, taking all phase relationships into account. An incoherent ray model is one which ignores phase and adds power intensity, and hence assumes that the arrivals are in random phase relationships. The incoherent summation generally yields a satisfactory result, except when either source or receiver is near an ocean boundary. In this case, pairs of rays which are up and down-going at the boundary are in a phase relationship which is strongly biased. For example, as a source or receiver approaches the ocean surface, the phase relationship between the pair of arrivals approaches 180° and the signals cancel each other. It is apparent that the incoherent summation breaks down in this case.

This problem is resolved by using a semicoherent model. In this case, the ray pairs are first summed coherently and these resultants are then summed incoherently. In practical applications, the calculation involving the exact phase and amplitude relationships is not used. The exact effect can be approximated by the use of surface decoupling loss. This loss is defined as the propagation loss for some near-surface receiver (or source) minus the minimum propagation loss for all near-surface receivers. This minimum propagation loss occurs at a depth called the surface-decoupling depth. Various expressions for the decoupling depth are given in references 47 and 48.

The FACT propagation model is semicoherent and is based on the surface-decoupling loss for an isospeed medium. Other semicoherent propagation models use the surface-decoupling loss expression of reference 47, which can treat arbitrary sound speed profiles. Control models to test how models treat near-surface sources or receivers are highly desirable.

---

46. Otsubo, H., et al, Normal-Mode Solution in the Ocean with Absorbing Bottom Sediments Which Have a Sound Speed Gradient, J Acoustic Soc Japan (E) 1, 47-57, 1980.
47. Pedersen, M. A., et al, Low Frequency Propagation Effects for Sources or Receivers Near the Ocean Surface, Naval Undersea Center TP 488, Sep 1975.
48. Bannister, R. W., and M. A. Pedersen, Low Frequency Surface Interference Effects in Long Range Sound Propagation, article submitted to J Acoust Soc Am 69, 76-83, Jan 1981.

The primary control should be a model in which the pairs of rays are summed coherently by using exact phase relationships with the resultants then summed incoherently. Other secondary controls would be based on approximations such as those used in FACT, FACT Extended, and RAYWAVE. Comparison of the various controls would establish the degree of confidence in each of the approximations.

The simplest control would be for convergence-zone propagation in deep water. This case is simple because the surface-decoupling depth is almost independent of range. The surface-decoupling depth depends on the angle of the ray and, since the angles of the dominant arrivals lie within fairly narrow bounds, the surface-decoupling depth is a weak function of range. Under these circumstances, the approximations to surface decoupling are generally regarded as satisfactory, although they probably have never been subjected to comparison with our proposed primary control.

The reader may now be wondering why this discussion is under a bottom-reflection category. The answer is that we can specify a control case for which the surface-decoupling effect is range-dependent.

Figure 38 presents propagation loss measurements made in a deep-water, bottom-limited environment. The circles represent a source depth of 91 m and the crosses (joined together) represent a source depth of 18 m. The receiver is located on the ocean bottom. The upper panel presents results at 20 Hz and the lower panel at 140 Hz.

For the discussions here, our interest is in ranges out to only 600 km. The region beyond this range is discussed in a later section. Observe that the behavior with range at 140 Hz is almost identical for 18 and 91-m sources. However, at 20 Hz it is radically different. As explained in reference 48, the difference between the results for the 91 and 18-m source at 20 Hz is a measure of the surface decoupling loss at 18-m source depth and 20 Hz. Note that at close range this difference is small and that it increases with increasing range to a limit of about 12 dB.

This range dependence is caused by the interaction between the surface decoupling loss and the bottom loss. At close ranges, the dominant arrivals have steep angles which have a low surface decoupling loss. The bottom loss per bounce is high for these rays. However, there are only a few bounces at close range, so the propagation loss remains low. At long ranges, the many bottom bounces have stripped off the steep-angled arrivals. In this case, the dominant arrivals have very low angles with minimum bottom loss per bounce. However, the low-angle rays are the very ones which have the highest surface-decoupling loss. For this example, the propagation loss-versus-range curve represents a complicated and delicate interplay between the surface decoupling loss and the bottom loss. This interplay requires a stringent control. For example, it is not clear that the simple surface decoupling algorithms which appear to be satisfactory for convergence-zone propagation will be adequate for bottom-limited regimes. The differences are that in the bottom-limited regimes both shallow and steep rays come into play. Consequently, the surface-decoupling effect interacts with the bottom characteristics, and hence the total effect is range-dependent rather than range-independent.

We recommend that the various semicoherent ray theory controls, previously discussed, be implemented for a bottom-limited case and that these controls include the source and frequency combinations of figure 38. Moreover, we recommend that the identical environment be modeled by mode theory. This result can then serve as a primary control against which the various ray theory controls may be compared. The normal mode theory

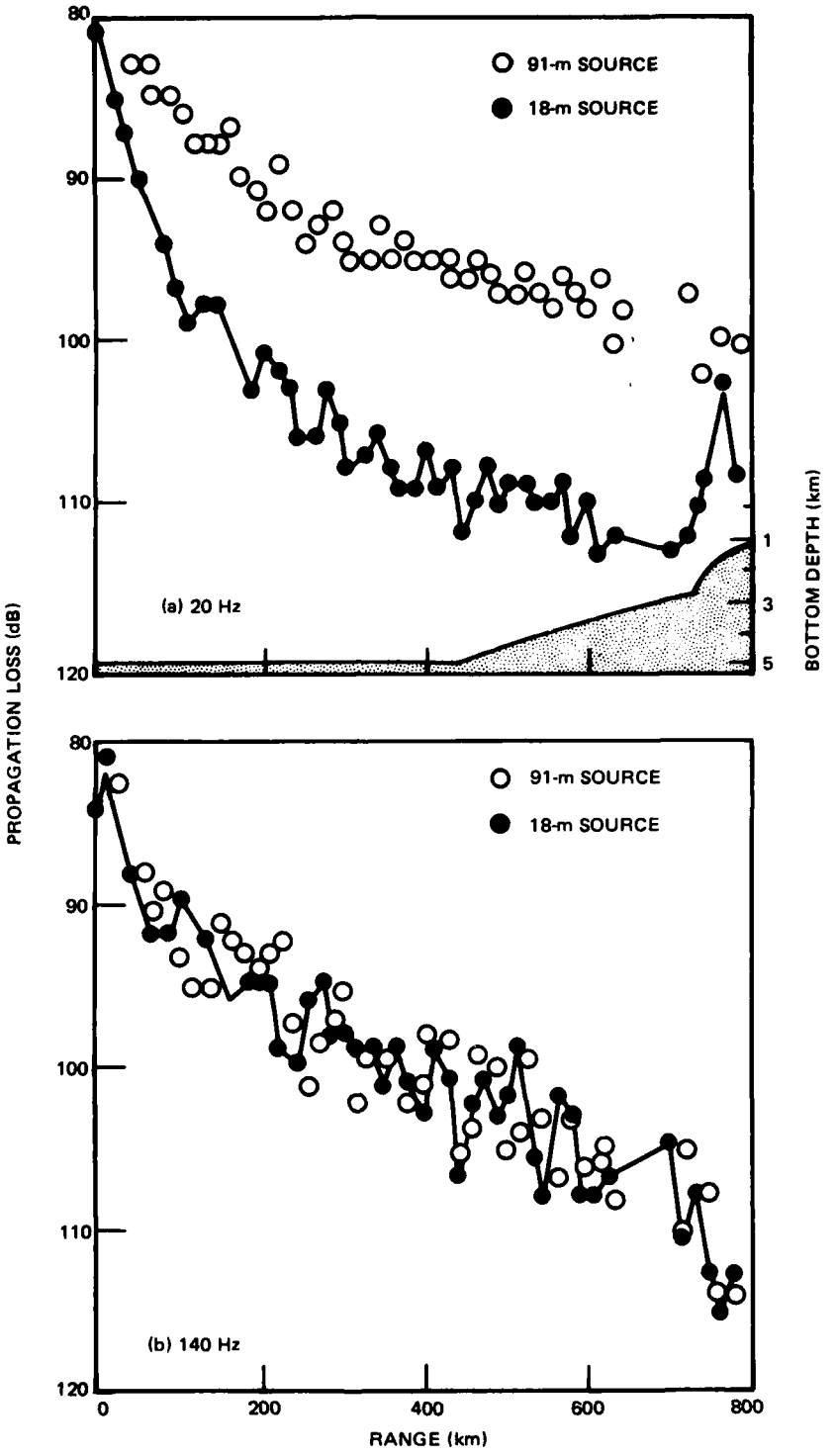

Figure 38. Propagation loss for two frequencies and two source depths, illustrating the surface decoupling loss for a low-frequency shallow source.

will be based on the results of the rigorous normal mode solution of section 5.1.1. Indeed, one reason that this mode solution was developed was so that it could serve as a control for ray theory calculations formulated in terms of bottom-reflection loss and bottom-phase shifts.

Figure 39 illustrates some important features of the normal mode results for a deep-water, bottom-limited environment. Propagation loss is presented as a function of receiver depth for fixed ranges of 50, 100, 200, 500, and 1500 km. In these computations, the normal modes are added in random phase at the given ranges. This procedure averages out the detailed structure of the phased acoustic field and produces a good representation of the depth structure. This structure is the incoherent combination of the depth structure of individual normal modes.

The frequency is 25 Hz, while the source depth is 18 m. Note the near-surface minimum in propagation loss, which coincides with the surface-decoupling depth. In this example, the decoupling depth increases from about 30 m at 50-m range to a value of about 55 m at 1000-km range. The reason for this increasing depth has already been discussed in explaining figure 38. At short ranges, the steeper angles dominate and these have shallower decoupling depths. At long ranges, the steeper angles are stripped off by bottom loss. Thus the shallow angles dominate and these have deeper decoupling depths. For any fixed receiver depth shallower than 30 m, the decoupling loss increases with increasing range because the receiver is further up from the surface-decoupling depth as the decoupling depth increases.

In figure 39, the scale breaks at 500 and 2900 m. The region between these breaks shows very little detail and is not plotted. However, near the ocean bottom there is again evidence of an interference pattern. The propagation loss is a minimum at the bottom, increases to a relative maximum somewhat off the bottom, and then decreases slightly to a value somewhat typical of most of the water column. The difference between the maximum loss and the loss at the bottom varies from 3.0 dB at 50 km to 4.0 dB at 1000 km. The depth of maximum loss varies from 29 m off the bottom at 50 km to 49 m off the bottom at 1000 km.

The chief reason for presenting figure 39 is to note the interference pattern near the ocean bottom. The up- and downgoing waves apparently reinforce each other. However, as the receiver is moved up from the bottom, the up- and downgoing waves change from a situation of reinforcing each other to one of cancelation. This cancelation is achieved more rapidly at shorter ranges with steeper angles, and somewhat more slowly at longer ranges with shallower angles.

Although figure 39 represents the incoherent addition of modes, the interference effects due to the ocean surface and bottom interfaces extend several wavelengths into the medium. Incoherent addition still displays this interference effect because the individual modes all satisfy the boundary conditions. Thus the interference is contained in the constituent modes. For example, each mode has zero amplitude at the ocean surface. The power addition of modes does not destroy this feature. However, at distances over several wavelengths from the surface, the location of nodes and antinodes becomes more randomly distributed. Here, the power addition of the modes smoothes out their depth structure.

In contrast to mode theory, the interference at the boundaries is not built into individual rays. We must accomplish this by the semicoherent addition of rays discussed earlier. Thus the pattern exhibited in figure 39 near the surface should also be reproduced by the semicoherent ray models previously discussed.

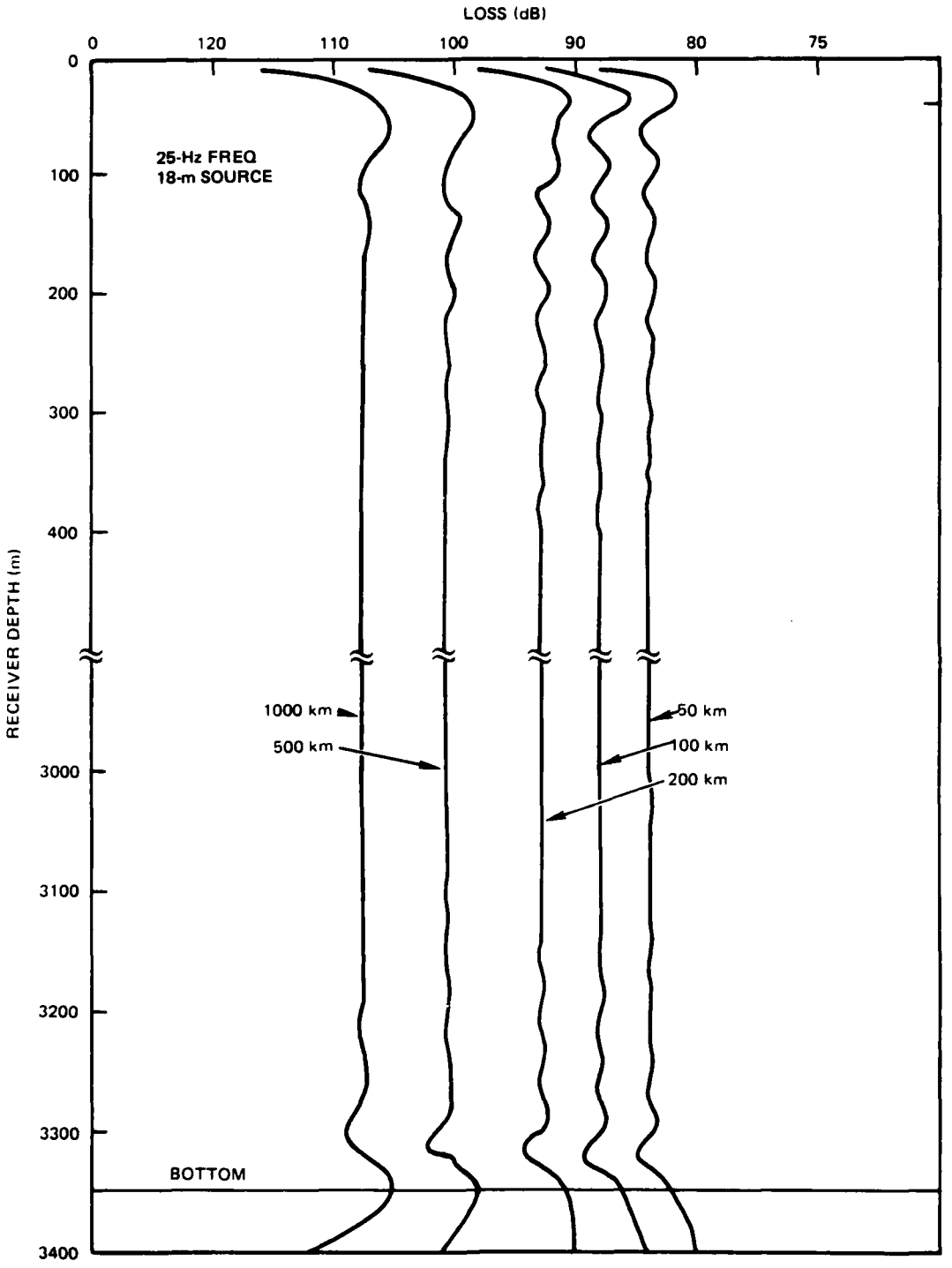

Figure 39. Propagation loss versus receiver depth for various fixed ranges.

In contrast, the interference patterns in figure 39 near the ocean bottom will not be reproduced by present semicoherent ray models because these models treat the near-bottom arrivals in an incoherent fashion. The output of these ray models, if applied to the condition of figure 39, would be a single continuation directly to the bottom of the prosaic, almost-constant behavior we observe between 3000 and 3100 m.

It may be possible to develop a "fix" to incoherent ray theory which would treat near-bottom interference. Such a treatment would be more complicated than the surface-decoupling theory for the ocean surface in several ways. First the phase shift is not fixed at 180° but varies with grazing angle. Second, the up- and downgoing arrivals are not of equal amplitude because one of them has suffered an additional bottom loss. If such a "fix" is possible, it should be incorporated into the semicoherent ray theory. This "fix" would correct the near-surface and near-bottom source or receiver and would allow the use of incoherent ray addition for all other situations.

Another approach is the use of a coherent ray theory, which is the subject of the next section. However, before continuing we should note that the model on which figure 39 is based had a layered sub-bottom. Indeed, in figure 39 the acoustic structure is shown to 50 m into the sub-bottom. In contrast, a normal mode control should be constructed for an impedance bottom condition. Such a control will, in fact, have more flexibility since the functions describing bottom loss and bottom phase shift are arbitrary. Care must be taken in selecting these functions because the resulting interference pattern should be realistic and should resemble those of figure 39, which is the model of a measured ocean environment.

5.1.3 Coherent Ray Model

By a "coherent ray model," we mean that the various ray arrivals are combined coherently to obtain the resultant propagation loss. The phase calculation is similar to that discussed in section 4.1.1, in that it uses travel times, a $-\pi$ phase shift for each time the ray reflects from the ocean surface, and a $-\pi/2$ (or uniform asymptotic treatment) for each time the ray touches a caustic curve. However, in addition, the phase shift for each bottom bounce must be included.

There are two major regimes where a coherent ray model may be necessary as compared to present semicoherent models. The first regime has just been discussed. It is the interference region near the ocean bottom. Given the same input parameters, a coherent ray theory should be as effective in portraying this region as a coherent mode theory.

The second regime is that formed by caustics. Most readers associate caustics with convergence-zone propagation. However, caustics are also formed in the bottom-limited case. There are no caustics for rays which reflect from the surface. However, every ray which does not reflect from the surface touches a caustic curve between successive apexes. The caustic structures for bottom-limited areas have never been examined in detail. However, it is evident that for the zero-degree ray at the source, a horizontal cusp exists for a receiver at each apex.

We have not investigated the problem of extending the uniform asymptotic approach to bottom-reflected propagation. Bottom phase shifts, which vary with angle, must be included in the problem and it is not evident that this is a simple extension of the present problem. Moreover, the calculation of complex rays may pose some unanticipated problems.

In any case, we recommend that this extension be carried out and that various ray theories and coherent normal mode theory be compared for an environment similar to that of figure 39. The comparison in the caustic regime would be similar to that of section 4.1.1 except that there would not be so many caustic structures. A second difference would be that the shadow zone for the initial caustics would not be so deep because there would also be ensonification by bottom-reflected rays.

5.1.4 Control for Mode Stripping Simulation

The recommended controls of the previous two sections were for bottom-limited propagation. This choice was made because the effects to be modeled were most pronounced for this case. Moreover, it would be best to prepare these controls without the additional complication of convergence-zone propagation, in much the same way as we designed the model of section 4.1.1 to avoid the effects of bottom-bounce propagation.

Once the controls of the previous two sections have been prepared and verified by comparison of mode and ray theories, the next step is to prepare a control for RSR or convergence-zone propagation in deep water in which the bottom is included. This control should provide a rigorous test of models because it will involve the phased superposition of bottom-reflected and purely refracted paths. This should pose no new problems for the controls in most cases; if the controls properly treat each type of path separately, they should handle the combination.

An exception of considerable interest will pose new problems. In the case of convergence-zone propagation to long ranges, the normal mode theory exhibits the phenomenon of mode stripping near the ocean bottom.

Figure 40 presents propagation loss contours as calculated by the incoherent addition of normal modes. The calculation is for a Pacific Ocean profile with a depth excess of about 2000 m. In this example, a layered structure was used for the sub-bottom. The frequency is 50 Hz and the source depth is 91.4 m. The method of summing modes is the same as that shown in figure 39. The method of display is different. Figure 39 presents loss versus receiver depth for fixed ranges, whereas figure 40 presents contours of propagation loss in the range-receiver depth plane.

Note in figure 40 how the propagation loss contours cut back in range for receiver depths below 3000 m. For example, the 110-dB contour reaches almost out to 10^4 kyd. whereas at the bottom it only reaches out to about 300 kyd. This phenomenon is known as mode stripping. The incoherent addition of normal modes averages out the convergence-zone structure but well illustrates this stripping.

An explanation of mode stripping involves two mechanisms. The first is mode attenuation. Those modes with phase velocities larger than the sound speed will suffer attenuation due to the bottom loss. At long ranges, these modes will be stripped off by bottom loss and will not contribute to the field. Moreover, modes with phase velocities smaller than the bottom sound speed also have some attenuation. For phase velocities close to the bottom, this attenuation can be large enough to cause some mode stripping here, too. Thus the phase velocity of the highest-order mode which has not suffered appreciable stripping can be significantly smaller than the sound speed at the bottom.

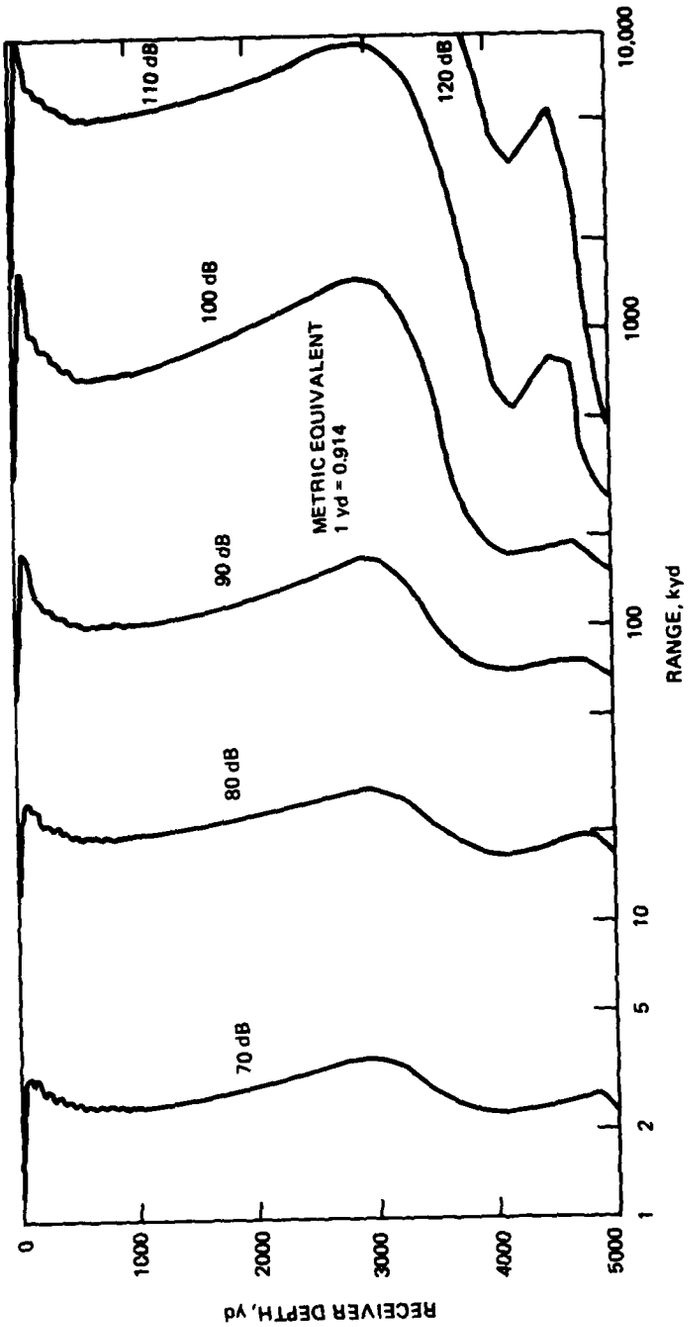

Figure 40. Propagation loss contours for convergence zone propagation, illustrating mode stripping near the bottom.

The second mechanism is diffraction. The depth where the mode phase velocity equals the sound speed of the water column corresponds to zero argument of the Airy functions, Ai. This is the main contribution to the mode depth function because, for modes with low attenuation, the complementary Airy function Bi contributes very little. Depths with sound speeds greater than the mode phase velocity correspond to the region of exponential decay of Ai (diffraction region). The rapid rolloff near the bottom in figure 40 is the result of exponential decay.

The question now arises as to whether the coherent ray model can duplicate this effect. The example of figure 40 would not be suitable as a control for the ray model, because there was a layered bottom. However, one should be able to develop a normal mode control with an impedance bottom condition which displays mode stripping.

Any ray model of mode stripping will involve additional problems and considerations. One of these is the specification of the bottom loss characteristics for phase velocities below that at the bottom. One of the reasons for selecting a bottom-limited environment for the two previous sections is that the refractive problem does not arise since only bottom-reflected rays are involved. In any case, it appears that the introduction of some bottom loss for below-grazing rays could introduce the desired stripping for near-bottom-grazing rays. However, one would then have to modify present ray theory concepts because otherwise there is no point in specifying a bottom loss for rays that do not reflect from the bottom.

The answer lies in the formulation of a Murphy-Davis (ref 17) correction for an impedance condition at the bottom. In this theory, near-grazing rays will still be affected by the impedance condition. Moreover, the bottom-grazing rays of simple ray theory will be transformed into caustics. These caustic structures then may provide for the diffraction effects which are observed in the mode formulation.

Even if this full treatment works well in describing mode stripping, it would be highly desirable to develop some approximate methods. One then could develop a series of controls based on mode theory and provide approximate ray theories to assess their limitations.

5.2 SUB-BOTTOM STRUCTURE SPECIFIED

This section discusses controls where there is a sub-bottom structure specified rather than an impedance boundary condition. The first four subsections discuss the case of a fluid sub-bottom, while the last subsection briefly outlines some of the problems involved in rigid bottom structures.

The controls discussed here for the fluid sub-bottom are based on the normal mode model of reference 16. Other normal mode models may serve equally well. However, this model is the one with which we are familiar. To place the model of reference 16 in proper perspective, we provide details of the model. This review points out the strengths, limitations, and weaknesses of the model.

The normal mode program of reference 16 is based on a fluid sub-bottom structure. The sound speed in each layer is of the form

$$C^{-2} = a_i + b_i Z \qquad (43)$$

For layers in the ocean column, a_i and b_i are real and are constrained so that there are no discontinuities in C at layer interfaces. For sub-bottom layers, a_i and b_i are allowed to become complex. This model achieves several goals. It leads to attenuation, which is the mechanism that leads here to bottom loss. Moreover, the sound speed and the attenuation have gradients in the bottom.

The absorption in the bottom is taken to be proportional to frequency; ie,

$$\alpha = hf \ . \tag{44}$$

Here, α is the attenuation in dB/km, f is the frequency in Hz, and h is the coefficient provided from a geoacoustic model. We now define the parameter A:

$$A = h/(20{,}000\ \pi \log e) \ . \tag{45}$$

The imaginary sound speed, corresponding to A, is given by

$$\text{Im } C = 1/A - [1/A^2 - (R\ell\ C)^2]^{1/2} \ . \tag{46}$$

The justification for equations 44 to 46 is given in reference 16.

For each sub-bottom layer, four coefficients are available in equation 43. The coefficients can be determined from a specification of the real sound speed at the upper and lower interfaces and the attenuation at the upper and lower interfaces. In modeling the sub-bottom layer, both the sound speed and the attenuation are discontinuous at each interface for the typical case.

The particular form, equation 43, is chosen so that the reduced Helmholtz equation is Stokes' or Airy's differential equation. This equation is the simplest to treat when the sound speed varies with depth.

A different density may be used in each layer, although it is constant for a given layer. In practice, the density in each water column layer is specified as unity and in the bottom sublayers by whatever density is given by the geoacoustic model.

The bottom structure is always tied off with a negative-gradient half-space, as in figure 8. This feature dates back to the bilinear surface duct model. The advantages are that the solution in this last layer is h_2, the modified Hankel function of order one-third. This boundary condition is convenient. Moreover, according to Towne and Wilson (ref 49), the use of such a half-space eliminates the need to consider a branch line integral. In modeling bottom-reflected propagation, care is always taken to see that the modes are stripped off by attenuation before the last interface in the model is encountered. If this is not the case, this interface is moved farther down in the sub-bottom until the modes are stripped off. This ensures that the unrealistic attenuation introduced by the negative gradient layer (or high-order mode) has no significant effect on the results.

We now consider some controls which make use of this model.

---

49. Towne, D. H., and K. G. Wilson, Refraction and Diffraction of Explosive Pressure Pulses by Gradients in the Propagation Velocity, part II, Woods Hole Oceanog Inst, ref no 57-45, 1957.

5.2.1 Multiple Ducts in Shallow Water

This normal mode model has been used in the investigation of propagation in shallow water (ref 50). In many of the shallow-water areas examined, there is a positive-gradient surface duct, which leads to a double duct. Figure 41 is the simplest schematic sound speed profile, which illustrates this configuration.

The profile of figure 41 presents all the multiple duct problems discussed in section 4.1 with some others to boot. The cases discussed in section 4.1 were half-ducts, full ducts over full ducts, or a half-duct over two full ducts. Figure 41 is a case of two half-ducts. The upper duct is a half-duct formed by the surface interface. The lower duct is a half-duct formed by the bottom interface, although there may also be some ducting due to refraction in the bottom layer.

A normal mode assessment of shallow-water areas has been prepared, but not completed and published (ref 50). This work evaluates the normal modes for downward refraction cases as well as cases similar to figure 41. Finding the eigenvalues is an involved task. What makes it more difficult than the case of nonbottom-reflected propagation is that the imaginary part of the eigenvalues is implicitly determined by the attenuation in the bottom. This problem, when combined with those discussed in section 4.3 for multiple ducts, makes this case one of the most difficult in which to find eigenvalues. One of the cases of reference 50 could serve as a valuable example or control for the case of a multiple shallow-water duct. However, the bottom models of reference 50 contain multiple sub-bottom layers. Perhaps a better approach is to prepare an initial test case based on a simple stylized profile such as that of figure 41. This could be followed up with other more realistic test cases which contained more layers in the water and in the sub-bottom.

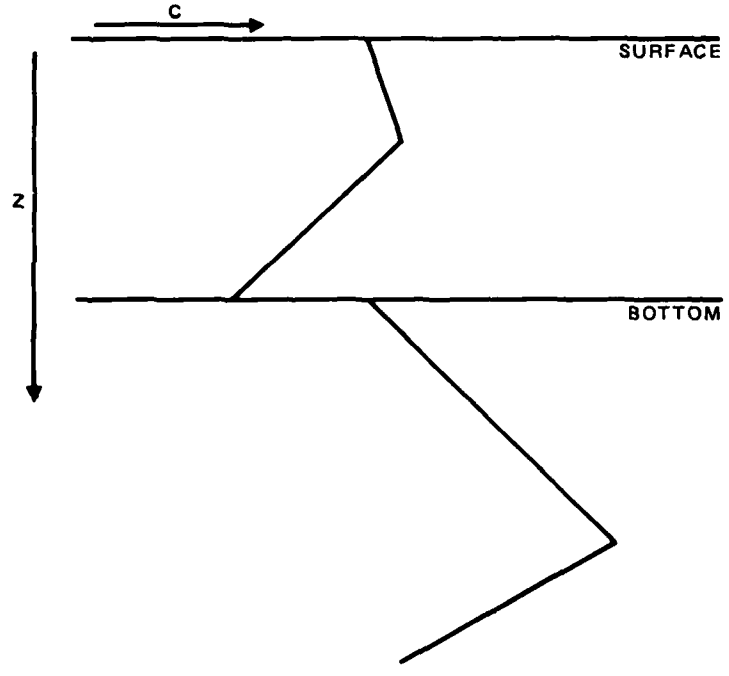

Figure 41. Schematic sound speed profile, illustrating a double duct in shallow water.

50. White, D., Normal Mode Evaluation of FASOR Shallow Water Areas, unpublished.

5.2.2 Assessment of Ray Theory Use of Normal Mode Reflection Coefficients

Assume now that we have a mode theory control in which the sub-bottom structure is specified. From these mode theory results, we can compute reflection coefficients at the bottom interface; from the theory of section 5.1.1, we can construct a second modal solution based on various mathematical properties at the bottom interface. This is essentially what was done in reference 45, and the second model solution was a reasonable approximation to the critical mode solution.

The question that now arises is: How well can a ray theory work which is based on complex reflection coefficients at the ocean bottom? This is the standard way to use ray theory, but does it work? Consider, for example, the case of low attenuation in a positive gradient sediment. Rays will penetrate into the bottom, turn around in the bottom, and return into the water column. If the attenuation is low, this contribution could be appreciable. Under those circumstances, it is difficult to see how a ray theory, which only deals with reflection from the water–bottom interface, can adequately treat components which return from the sub-bottom.

The controls proposed can assess this problem, although something of a paradox remains. In section 5.1.1, we noted that we could specify an exact mode solution for the case in which the bottom reflection coefficients are given as analytic expressions. If the ray theory gives a good approximation for this problem, how is it possible that, if we determine the reflection coefficients from a structured bottom, it may not? We believe that the apparent inconsistency lies in the difference between a discrete and a continuous representation of the bottom reflection coefficients.

In the case of the analytic expressions, values are available for continuous functions of phase velocity (grazing angle). Thus the ray theory has an exact representation of bottom reflection coefficients for all of the required angles. However, in the case of the reflection coefficient as determined by the structured bottom, we only have discrete values corresponding to each mode. If these discrete values appear to lie on rather smooth curves, we can approximate them with continuous functions as required for the ray theory.

In contrast, when there is considerable energy refracted in the bottom or reflected from sub-bottom discontinuities, the reflection coefficients will not lie on smooth curves. Indeed, the interference often produces a series of reflection losses which at all but low grazing angles jump up and down in an unpredictable manner. Under these circumstances, it is impossible even to guess, let alone estimate, how to approximate correctly with a continuous function. In our estimation, the capability of the ray theory will depend directly on our ability to fit simple continuous functions to the discrete coefficients determined from individual modes.

5.2.3 Comparison of Plane Wave and Wave Theory Reflection Coefficients

The usual manner for treating sub-bottom structures is to calculate plane wave reflection coefficients. Given the sub-bottom structure, one first calculates the plane wave reflection coefficients. These coefficients and a sound speed profile for the water column are then used as inputs for some propagation loss model such as normal mode or ray theory.

The question that now arises is: How accurate is the use of plane wave reflection coefficients? Can the bottom be treated separately from the water column as an acceptable approximation?

There is general acceptance that plane wave reflection coefficients provide good answers. However, it is interesting to note that for certain refractive conditions in the bottom substructure, caustics can be formed in the water column. Indeed, figure 162 of reference 18 shows the simple example of a homogeneous medium overlaying a refractive medium. The point source in the homogeneous medium, together with the refracting medium which could be a sub-bottom structure, produce a caustic structure in the homogeneous medium. It turns out that in the case of plane waves impinging on a refracti medium, the caustic curve is a horizontal line which remains in the refractive media. Also there is a fundamental difference between the point source and plane waves. We believe that for this example, plane wave reflection coefficients would not be a good approxi ation.

With the theory of section 5.1.1, we are able to prepare a control which would determine inaccuracies that result from using plane wave reflection coefficients. One would first run the control case, using the normal mode theory for a structured bottom. Then the plane wave reflection coefficients for the structured bottom would be determined. These characteristics and the water column structure would then be entered into the normal mode program discussed in section 5.1.1. The propagation loss results of this program would then be compared to those of the control.

Reflection coefficients could also be evaluated from the normal mode solution with the structured bottom. These coefficients could be compared directly with the plane wave reflection coefficients. This will aid in assisting the differences in the propagation loss.

Comparisons should be made for several types of bottom structures. It could be, for example, that plane-wave coefficients are a good approximation for simple bottom structures but are not for complicated structures that would form caustics.

5.2.4 Ray Calculations in the Sub-Bottom Structure

In section 5.2.2, we discussed the strong possibility that ray theory might not work with inputs of reflection coefficients derived from a sub-bottom structure. If this is the case, a ray theory approach will require ray computations in the structured bottom. Reference 51 indicates how ray theory may be used to obtain reflection coefficients for a structured bottom with fluid sediment layers.

However, the calculation of reflection coefficients is somewhat beyond what we see as an initial control for ray tracing in fluid bottoms. Indeed, as the first control we would propose the model of figure 8. This is the simplest model we could construct; that is, a single layer with simple interface conditions.

We would, however, extend the ray treatment of reference 51 in that, instead of associating an attenuation with the path length as in equation 7 of reference 51, we would calculate the attenuation from the travel time. The theory of reference 13 treats the case of complex ray parameters for real sound speeds. We would extend this theory to treat the case of complex sound speeds. The ray parameters will be complex for these rays and will lead to complex travel times which will contain the attenuation information. For this rigorous approach, all the rays penetrating into the bottom layers will have a complex range component. One would have to iterate on a complex ray parameter to make the range real.

---

51. Mitchell, S. K., and J. J. Lemmon, A Ray Theory Model of Acoustic Interaction with the Ocean Bottom, J Acoust Soc Am 66, 855-861, Sep 1979.

With this ray theory extension in hand, the propagation loss calculation for figure 8 need not be terminated at the bottom-grazing ray. Ray calculations could be continued into the bottom layers and the propagation loss calculated. These losses could then be compared with the normal mode propagation losses, similar to the comparison of figure 11 but carried out to more distant ranges. As an intermediate step, the loss calculated from the imaginary part of the travel time could be compared to that estimated from the ray path length in the bottom and the attenuation coefficient.

If this first control proves successful, various other controls for ray calculations in more complicated bottom sediments could be established. These would include discontinuities, multiple layers, etc.

5.2.5 Controls for Bottom Layers with Rigidity

This section points out the need for controls where the sub-bottom layers are rigid rather than fluid. We may not be as specific about controls here as in other sections of the report, as our familiarity with the problems involved is not first-hand. We recommend that other investigators active in this specialty make their recommendations for specific controls.

There have been many recent advances in the theory of treating rigid bottoms. Reference 52 discusses a method which evaluates plane wave reflection coefficients in a sediment for which the density, compressional wave velocities, and shear wave velocities are arbitrary functions of depth. This model also introduces compressional wave and shear wave attenuation through the use of complex velocities. This appears to be a versatile method which, once verified, could serve as an excellent control for the calculation of plane wave reflection coefficients. Vidmar (ref 52) refers to the analytic description of Gupta (ref 53), which is noted to be very restricted in its applicability. However, this model might well serve as a control against which the direct numerical approach of reference 52 could be checked.

A new ray model has been developed (ref 54) which can evaluate plane wave reflection coefficients for a rigid bottom. The recent study of reference 55 suggests that shear waves are important for thin bottom layers and for frequencies as high as 200 Hz. Reference 56 discusses the impedance of Stonely waves, while reference 57 discusses the effects of density gradients. These studies make it clear that models more complicated than the constant-density fluid model are necessary.

---

52. Vidmar, P. J., and T. L. Foreman, A Plane-Wave Reflection Loss Model Including Sediment Rigidity, J Acoust Soc Am 66, 1830-1835, Dec 1979.
53. Gupta, R. N., Reflection of Elastic Waves from a Linear Transition Layer, Bull Seism Soc Am 56, 511-526, 1966.
54. Vidmar, P. J., Ray Path Analysis of Sediment Shear Wave Effects on Bottom Reflection Loss, J Acoust Soc Am 68, 639-648, Aug 1980.
55. Vidmar, P. J., The Effect of Sediment Rigidity in Bottom Reflection Loss in a Typical Deep Sea Sediment, J Acoust Soc Am 68, 634-638, Aug 1980.
56. Hawker, K. E., The Influence of Stonely Waves on Plane Wave Reflection Coefficients: Characteristics of Bottom Reflection Loss, J Acoust Soc Am 64, 548-555, Aug 1978.
57. Rutherford, S. R., and K. E. Hawker, The Effects of Density Gradients on Bottom Reflection Loss for a Class of Marine Sediments, J Acoust Soc Am 63, 750-757, Mar 1978.

Our chief concern with these treatments has already been expressed in section 5.2.3 in the use of plane wave reflection coefficients and in the separate treatment of water and bottom columns. We would like to see someone prepare an exact analytic control solution for a nonconstant water column overlaying a bottom layer with rigidity. The propagation loss results of this model should then be compared with one which utilizes the plane wave reflection coefficients of the rigid layer.

Before closing this subject, there is one more area where a control model would be of interest. We have heard of the possibility of underwater sound entering and traveling deep in the Earth's crust only to emerge again in the water column at great distances. A rigorous assessment of this phenomenon – its extent and possible importance – would be of value.

6.0 MISCELLANEOUS CONTROLS

This section describes a number of controls which can be used with a range-independent environment but do not conveniently fit under sections 4.0 and 5.0. These controls fall under four unrelated subsections, each of which discusses an independent category of control. Section 6.1 discusses Murphy-Davis corrections. Section 6.2 deals with the special problems of very low frequency propagation, including below-mode cutoff. Section 6.3 treats normal mode theory under Doppler conditions. Section 6.4 discusses the treatment of special source functions.

6.1 MURPHY-DAVIS CORRECTIONS

The Murphy-Davis corrections of principal interest here are those associated with modified ray theory for bounded media (ref 17). Consider first the ocean surface, which is a pressure release condition. The modifications result in four significant changes in ray theory. The first is that the phase change associated with the surface is continuous with ray angle as rays go from refracting below the surface, to grazing the surface, to reflecting from the surface. This circumstance is in contrast to elementary ray theory where there is a $-\pi/2$ jump in phase for the surface-grazing ray. The second change is that the shadow-zone boundary associated with the grazing ray is corrected into a caustic boundary. Thus the grazing-ray boundary, which requires a special solution, is converted into a caustic boundary for which we have the known solution of uniform asymptotics. The third change is that the ray paths themselves are frequency-dependent. The fourth change is that the rays which vertex near the surface "feel" the effect of the surface. The first three subsections below discuss the test cases involving the ocean surface. The fourth subsection discusses a case involving the bottom, while the last discusses a correction for unbounded media.

6.1.1 Surface-Grazing Rays in Shallow Water

This case is presented first because it is a dramatic illustration of frequency-dependent ray paths; it is discussed in reference 58.

---

58. White, D., and D. F. Gordon, Analysis of Shallow Water Sound Propagation by Normal Mode Theory, J Acoust Soc Am (A) 60S, 34, Fall 1976.

Figure 42 presents the sound speed profile for a shallow-water area 73 m deep. The upper panel presents the water column. The lower panel presents the complete sound profile. The profile parameters are given in table 18. Column 2 gives the depth at the top of the layer. Column 3 gives the sound speed at the top interface of the layer. Column 4 gives the sound speed gradient in the layer. The quantity h is the attenuation coefficient in dB/hm/Hz, while ρ is the density in column 6. An explanation of the gradient column will be helpful for those who are not familiar with discontinuities of sound speed at layer interfaces. Table 18 contains no redundant information. There is no gradient listed in the first layer because the sound speed is continuous at interface 2. The given gradients provide the information to evaluate sound speed discontinuity at other interfaces. For example, application of the –0.61635 gradient yields a sound speed at the bottom of the water column of about 1523.2 m/s.

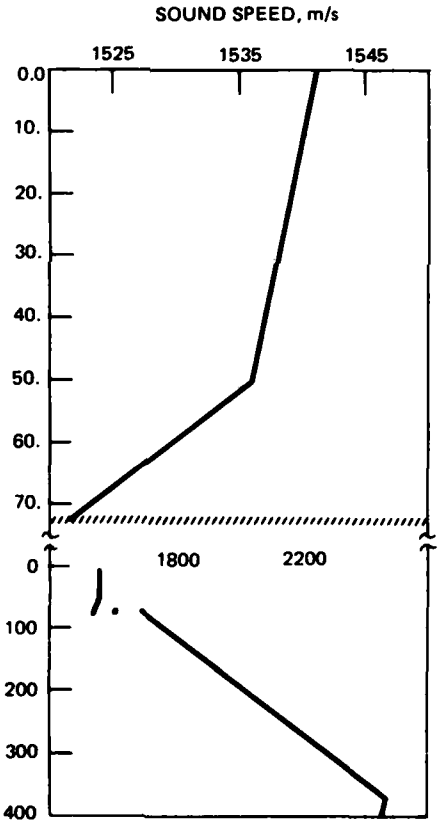

Figure 42. Shallow-water sound speed profile. The upper panel is an expanded section of the profile in the water column.

LAYER	DEPTH (m)	SOUND SPEED (m/s)	GRADIENT	h	ρ
1	0.0	1542.2	–	0.00	1.02
2	51.0	1536.8	-0.61635	0.00	1.02
3	73.0	1606.0	1.5	0.12	1.68
4	73.3	1684.0	1.5	0.73	1.91
5	373.3	2466.9	-0.1	0.73	1.91

Table 18. Parameters for the profile of figure 42.

Figure 43 presents the cycle range of the profile of figure 42 plotted as a function of phase velocity. The cycle range is the range between successive reflections from the ocean bottom. Figure 43 compares ray theory with two different mode equivalents (dots and crosses) at a frequency of 1500 Hz.

Consider first these mode equivalents. The dots represent the mode interference range given by equation 28 and are plotted at points midway between the phase velocity of adjacent modes. The scale at the top of figure 43 indicates where the various mode eigenvalues fall along the phase velocity scale.

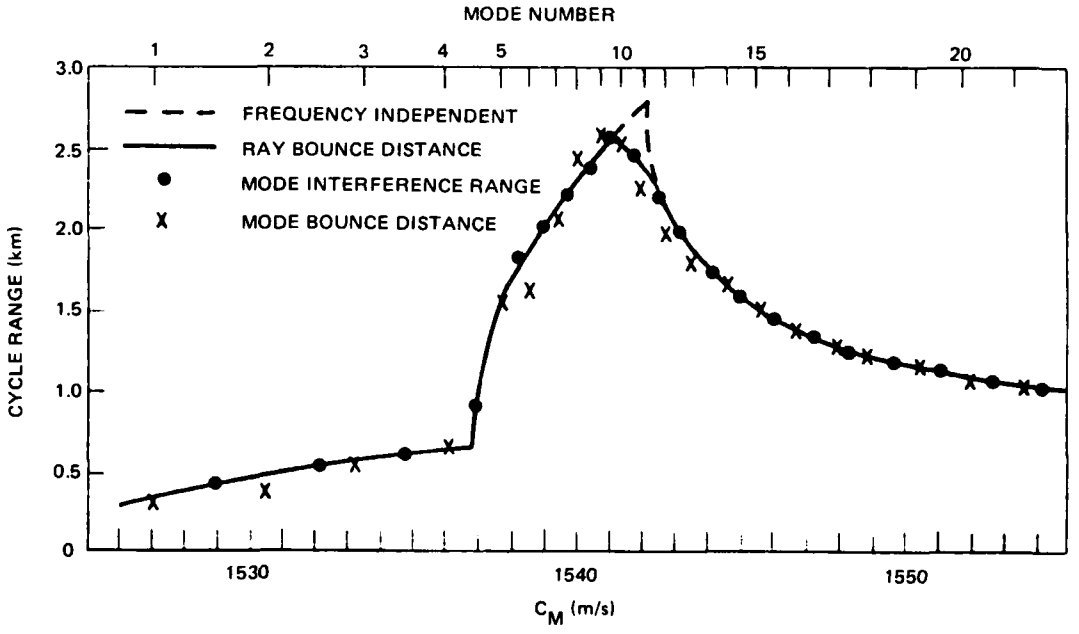

Figure 43. The cycle range for the profile of figure 42 as a function of phase velocity. Results of two-ray theories are compared to results of mode theory.

The other mode equivalent is the mode bounce distance, plotted as crosses in figure 43. These are calculated from

$$R_b = \text{mode bottom loss/mode attenuation.} \tag{43}$$

To evaluate equation 43, one first calculates the reflection coefficient at the water-bottom interface from the mode eigenfunctions for the given mode. This is then converted to bottom loss in dB. The mode attenuation in dB/km is calculated from the imaginary part of the mode eigenvalue and then divided into the bottom loss to produce the range of equation 43 in km. Equation 43 is a restatement of the fact that the loss per bounce must equal the bounce distance times the attenuation per unit distance.

The solid curve in figure 43 is the ray bounce distance or cycle range for the modified ray theory of Murphy-Davis. The dashed curve in figure 43 is the ray bounce distance for simple ray theory. The maximum range for this simple ray theory occurs for the ray which grazes the ocean surface. This is an endpoint maximum. Note in figure 43 that this endpoint maximum is converted to a smooth relative maximum by the Murphy-Davis correction. The dashed curve differs from the solid curve only for ray parameters near the surface sound speed. Observe that in this region, the modified ray theory agrees much better with the normal mode result than does simple ray theory.

Figure 44 presents a plot of how the cycle range of modified ray theory depends on frequency. The curve for 1500 Hz corresponds to the solid curve of figure 43, whereas the curve for infinity corresponds to the dashed curve of figure 43. Curves for frequencies of 500, 200, and 100 Hz are also shown. At these low frequencies, the cycle range for near-surface-grazing rays is changed drastically. For example, at 100 Hz the maximum cycle range is 1.6 km. At 1500 Hz it is 2.6 km, or about 60% greater than at 100 Hz.

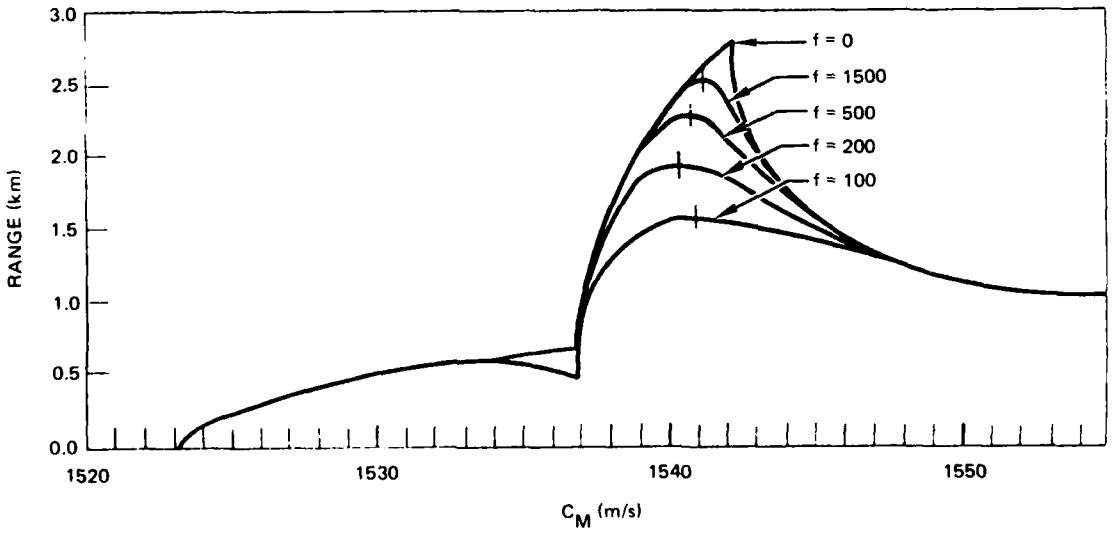

Figure 44. The cycle range of modified ray theory for various frequencies.

Reference 58 also presents normal mode results which show that the optimum frequency of propagation for mode 1 is 116 Hz and for mode 2 is 288 Hz. The surprising result is that the long-range propagation loss at 288 Hz is less than that at 116 Hz. For this example, the increased loss per bounce at 288 Hz is more than made up for by the increased number of bounces that must take place at 116 Hz.

In any case, this example indicates that Murphy-Davis corrections are important in shallow-water propagation. These corrections can make a significant percentage change in the ray cycle range.

This example or a similar simplified version would provide an excellent test case for shallow-water ray models. Models that do not append Murphy-Davis corrections are doomed to fail the test.

6.1.2 Surface-Grazing Rays in Convergence Zones

This second test case of Murphy-Davis modified ray theory has already been mentioned in section 4.1.1. Murphy-Davis modifications will allow one to continue the uniform asymptotic evaluation of figure 11c beyond 56 km and should result in improved agreement between uniform asymptotics and mode theory for ranges beyond about 54 km. However, as discussed in connection with figures 21a and 21b, such evaluation may require the uniform asymptotic formulations for either a three-ray or four-ray system.

6.1.3 Short-Range Shadow Zones for Negative Gradients

This third test case has also been mentioned in section 4.1.1. The left boundary of the shadow zone of figure 9 is determined for the most part by the ray which grazes the ocean surface. Murphy-Davis modifications will transform this boundary to a caustic boundary. The uniform asymptotic results for this caustic boundary can be compared to the normal mode solution. Thus the configuration of section 4.1.1 also provides a good test case for Murphy-Davis modifications.

A somewhat simpler test case is that of a single negative gradient layer. The modal solution is discussed in reference 29, whereas the ray theory solution is presented in reference 59.

6.1.4 Bottom-Grazing Rays

Murphy-Davis modifications can also be applied to rays which are grazing or near-grazing the ocean bottom. Again, the Murphy-Davis modification causes the rays which turn near the bottom interface to "feel" the effects of the bottom interface. Murphy-Davis (ref 17) presents the theory for a rigid bottom. This would be useful as an intermediate and clear-cut test case.

However, DeWayne White (ref 60) believes that with minor effort modified ray theory can be applied to the case of a general impedance condition at the bottom boundary. If true, these modifications could be included as part of the test case discussed in section 5.1.3. These modifications, again, would convert the shadow-zone boundary of a grazing ray to the shadow-zone boundary of a caustic.

---

59. Davis, J. A., Extended Modified Ray Theory Field in Bounded and Unbounded Inhomogeneous Media, J Acoust Soc Am 57, 276-286, Feb 1975.
60. White, D., private communication.

6.1.5 Relative Maximum in Sound Speed

This test case refers to the modifications to ray theory developed by Murphy (ref 61). This procedure modifies the rays which turn in the neighborhood of a relative maximum in a sound speed profile. This "split-beam" problem is illustrated for simple ray theory for the Epstein profile in figures 8 and 9 of reference 24. This modification represents an important first step in the development of a ray model which can treat multiple ducts, since these ducts are always separated by a relative maximum.

We need a normal mode model, which includes a relative maximum, to serve as a control and to assess the importance and effectiveness of Murphy's modifications. An initial control could be constructed by using the n-layer model of reference 16. However, this control may be deficient because of the slope discontinuity at the relative maximum. Eventually, we would want the modal solution for a relative maximum with continuous gradients.

The parabolalike profile of reference 6 is a possible candidate. However, solutions have not been developed for a relative maximum. Moreover, the profile is symmetric about the relative maximum and may present a special case.

Another test case is provided by the normal mode theory of an Epstein surface duct (ref 62). The Epstein profile can be strongly asymmetric, as exhibited by figure 3 of reference 62. For an initial test case, the ocean surface should be far removed from the relative maximum. The example of reference 62 would not be satisfactory because it involves not only the corrections of reference 61 but also surface corrections similar to those of reference 17. Note that reference 17 only treats the case of refraction away from the surface, and cannot be applied directly to a positive gradient near the surface. However, if we move the surface far away from the relative maximum, we should be able to separate the surface effect from effects associated with the relative maximum. One test case should be prepared for a source in the channel above the axis. Another test case should look at the direct field associated with a source below the axis. This should provide the simplest test case for the corrections of reference 61.

We should be on the lookout for an exact modal solution to some single-layered analytic profile which has both a relative minimum and a relative maximum. This profile avoids the problems of slope discontinuities. Such a solution would make an excellent test case for the Murphy (ref 61) corrections. The placement of a boundary on the nonchannel side of a relative maximum results in a double duct which would also make a good test case.

6.2 PROPAGATION FOR LOW FREQUENCIES

This section points out the need for controls in the region of low frequencies where there are additional problems which we have not yet addressed. The format of this section differs from others in that we shall first discuss the nature of the problems. This discussion will then be followed by subsections which describe test cases. Some of these cases may not represent controls for practical models, as they are contrived to cast light on some fundamental problems. With some trepidation, we will enter the jungle of branch line integrals.

---

61. Murphy, E. L., Modified Ray Theory for the Two-Turning-Point Problem, J Acoust Soc Am 47, 899-908, Mar 1970.
62. Bucker, H. P., and H. E. Morris, Epstein Normal-Mode Model of a Surface Duct, J Acoust Soc Am 41, 1475-1478, June 1967.

To the authors, the literature on this subject is riddled with contradictions – enough to have discouraged us from serious consideration in the past. Our knowledge of the problems might only be enough to get us into trouble. Nonetheless, we shall present our impressions, some of which could be in error, and pose a number of fundamental questions, some of which may be easily answered by those more versed on the subject.

Our concern here with normal mode theory is in frequency regimes at or below mode cutoff, which we now need to define. In the case of a representation with real eigenvalues, there is a discrete number of modes. Such representations may be referred to as "proper" modes (ref 63), "true" eigenfunctions (ref 3), etc. We define mode cutoff as the lowest frequency for which mode 1 has a real eigenvalue. At lower frequencies, there are no modes in the representation. In the case of representations with complex eigenvalues, there is an infinite number of modes. Such representations may be referred to as "improper" modes (ref 63) and residue series representations (ref 3). The n-layer model of reference 16 falls into this category. Here, mode cutoff occurs when the phase velocity of mode 1 equals the maximum sound speed in the channel. In the case of a surface duct, this is the sound speed at the layer depth; for a deep channel, it is the sound speed at the ocean bottom. At frequencies well above mode cutoff, the mode attenuation is negligibly small; the attenuation starts to increase more rapidly as mode cutoff is approached and usually increases very rapidly as the frequency is decreased below cutoff.

At low frequencies below mode cutoff, any model formulated in terms of real eigenvalues (proper modes) will not calculate any field at all unless it deals with the contribution of the branch line integral. Even at frequencies somewhat above cutoff, the discrete modal contribution may be small compared to the branch line integral.

This feature is well illustrated by Stickler's discussion (ref 63) of the shallow-water test case of reference 3. This test case includes an isospeed half-space. Stickler points out that there are two ways of taking branch cuts in the problem. In the Pekeris cut, the field is represented by a finite number of proper modes, an infinite number of improper modes, and a branch line integral contribution. In the Ewing-Jardetsky-Press cut, the field is represented by a finite number of proper modes and a branch line integral contribution.

By a comparison of various propagation models for the shallow-water test case, Stickler (ref 63) shows the following: At 500 Hz, the discrete contribution of five proper modes is in excellent agreement with the full solution. Here, the branch line integral contribution is nil. At 100 Hz, the discrete contribution of proper modes is only adequate beyond a range of 2 kyd. However, the discrete contribution plus the improper modes of the Pekeris cut is in good agreement with the full solution into at least 500 yd, the shortest range tested. The critical test is for 50 Hz, for which the first mode is quite near cutoff. Here, the discrete contribution plus the improper modes are still 4.5 dB less than the full contribution at a range of 18 kyd, with significant differences to much greater range. It is obvious in this case that the branch line integral cannot be neglected.

This example well illustrates why we present this section on problems at low frequency and why controls are required. Many normal mode models will work at high frequencies. However, at low frequencies some models can fail badly if there is not an adequate treatment of the branch line integral. Failure is almost guaranteed for proper mode representations which do not treat the integral. Models which treat an infinite number of

63. Stickler, D.C., Normal-Mode Program with Both the Discrete and Branch Line Contributions, J Acoust Soc Am 57, 856-861.

improper modes may fail under conditions such as the isospeed half-space considered by Stickler. From the standpoint of mode theory, our test cases are designed with two goals in mind: (1) To test a "proper" mode formulation for the treatment (or lack thereof) of the branch line integral under a number of conditions, and (2) to help determine those conditions under which a formulation in terms of "improper" modes is adequate without the evaluation of branch line integrals.

Part of the confusion in the literature as to when branch line integral contributions occur and when they do not is that proper emphasis is not placed on the particular formulation of the problem. If formulated in terms of proper modes, branch-line integrals are almost certainly a necessity. However, the question we want to answer is: Under what circumstances is it possible to obtain the complete solution in terms of improper modes and, conversely, under what circumstances is it impossible to avoid treating branch line integrals?

At low frequencies, there is another problem with improper modes below cutoff. The eigenvalues are more difficult to locate than when the modes are above cutoff. Although our experience with below-cutoff modes in the deep ocean is limited, we do not expect any problem with the model of reference 16. Other models may have problems, however. The previously described eigenvalue follower technique, which tracks modes from well above trapping down to below trapping, has worked well in surface ducts and should work well in other deep-water cases. For example, in reference 47 mode theory calculations were made for three deep-water profiles down to the cutoff frequency of mode 1. The values of frequency are 0.53, 0.64, and 0.65 Hz for the three profiles. Thus in the deep-water case, the cutoff frequencies are very low.

Another problem with mode theory at low frequency is the increased importance of shear waves in the sub-bottom structure. This problem was referred to in section 5.2.5 and will not be addressed here.

Our concern with ray theory at low frequencies lies in its validity. The study of reference 15 indicated that uniform asymptotic corrections in the boundary layer were effective at 25 Hz and gave results very comparable to normal mode theory. However, at 5 Hz, these corrections were not adequate. The Murphy-Davis corrections discussed in section 6.1 may further lower the frequency limit for which ray theory is valid. However, are there other corrections which must be applied at low frequency? Is there some fundamental frequency limit, below which no ray theory scheme works? Can ray theory be applied below mode cutoff and if it does work, what is the mechanism that stimulates damping?

We can also pose a number of general questions about normal mode solutions. However, these will best be given as we discuss specific test cases.

6.2.1 Isospeed Bounded Model

The simplest model of the ocean is one considered on page 21 of reference 64. This model is an isospeed ocean of constant depth. The surface is free and the bottom is rigid. The modal solution is given as a finite number of "propagating" modes with real eigenvalues and an infinite number of evanescent modes described as "nonpropagating". The eigenvalues of these evanescent modes are purely imaginary.

64. Bradley, D., and A. A. Hudimac, The Propagation of Sound in a Wedge Shaped Shallow Water Duct, Naval Ordnance Laboratory TR 70-235, Nov 1970.

According to Stone (ref 65), the appearance of a branch line integral is only a consequence of the fact that a medium is unbounded in depth and is not associated with boundary conditions at layer interfaces. Towne and Wilson (ref 49) support this view by stating that the existence of branch points is associated with the fact that the sound speed does not vanish at infinite depth. These references seem to suggest that in bounded media one does not have to deal with branch line integral contributions. Is this true for all bounded media? In particular, is it true for the model of reference 64?

We recommend this model as a test case. An excellent control for the case would be the fast field program (FFP) discussed in section 8.2. This method automatically includes the branch line integral contribution if there is one. We recommend a comparison of the modal solution with the FFP solution at several frequencies, including some below mode cutoff. This comparison will ascertain whether there is a branch line contribution. The solution to the problem in terms of "proper" modes and a branch line contribution would also be of interest.

Reference 64 also presents the geometric ray theory solution to the problem. As far as we know, no ray theory corrections are necessary. All rays except those forming a direct path between source and receiver reflect from either the surface or the bottom, or both, and, since the medium is nonrefracting, no caustics are formed. The one exception is the direct ray between a source and a receiver at the same depth. Murphy-Davis corrections are not necessary because there are no refracted rays for this problem. The ray theory for this model should be programmed and compared to the mode theory and to the FFP result. A frequency below mode cutoff should be assessed. If the ray theory agrees here, the frequency should be lowered still further to determine whether there is a fundamental limit below which ray theory fails.

6.2.2 Bilinear Bounded Model

The next case is a simple modification of the test case of section 6.2.1. This case is illustrated in figure 45. Conditions such as water depth and the boundary should be the same as those of section 6.2.1. However, there is a small bilinear channel which introduces refractive effects. Asymmetry is deliberately introduced to avoid a degenerate case. We recommend that FFP, normal mode, and ray theory solutions be compared for this model. The normal mode program of reference 16 can be easily adapted to treat this profile. The ray theory should include uniform asymptotic boundary layer corrections and Murphy-Davis corrections for the free and rigid boundaries. Reference 66 presents another ray theory correction which should be applied if possible. In brief, the method of reference 66 modifies the sound speed profile so that the eikonal and wave equations are brought into closer agreement. The idea is that standard ray methods applied to the modified profile will produce a result that is closer to wave theory than that of the original profile. One problem with this method is that the modified sound speed profiles are not soluble in closed form. Whereas numerical integration is possible, the applications of uniform asymptotics or Murphy-Davis corrections could pose a problem.

---

65. Stone, J. L., A Theoretical Analysis of Acoustic Wave Modes in Layered Liquids, Princeton Univ report no 9, contract N60NR-270 (1953).
66. Floyd, E. R., Modified Phase Integral Approximation for a More Rigorous Ray-Tracing Technique, J Acoust Soc Am 60, 801-809, Oct 1976.

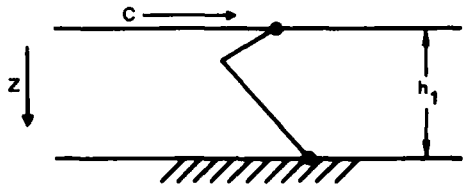

Figure 45. Bilinear bounded model.

In any case, a detailed investigation of the profile of figure 45 should provide additional insight into branch line integrals and the efficacy of ray theory at low frequencies. Calculations should be carried out for several channel widths, h_1. By moving the cutoff frequency, we should get a better assessment of the ray theory. For example, we can determine if mode cutoff poses a significant limitation to ray theory.

This model raises some other interesting questions. The mode model of reference 16 always has produced improper modes, except for a layered bottom test case. The complex part of the sound speed was set to zero to determine whether the bottom loss was associated with the bottom absorption. This was indeed true. The modes for this special test case had real eigenvalues. Thus we have no doubt that there will be real eigenvalues. It will be interesting to see if there are modes with eigenvalues that are purely imaginary. This leads to several general questions about mode theory. When do such modes arise? Do they only or always appear for a nondissipative medium with perfect boundaries? Are improper modes (ie, complex eigenvalues) always associated with some loss mechanism? Can there ever be both modes with purely imaginary eigenvalues and modes with complex eigenvalues? Are there any propagation problems for which the complete solution consists of a finite set of real eigenvalues?

6.2.3 Bilinear Channel Over an Isospeed Half-Space

The next case is a further modification of the test case of figure 45. This case is illustrated in figure 46. Conditions in the water column are identical. However, the rigid bottom has been replaced with an isospeed half-space which is an absorbing liquid; ie, the sound speed has an imaginary component. This test case is quite similar to that of Stickler (ref 63) discussed in section 6.2. The important difference is that the half-space has a definite loss mechanism other than energy dribbling off to infinity.

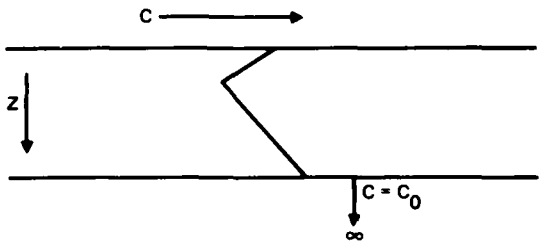

Figure 46. Bilinear channel over a dissipative isospeed half-space.

We recommend that the comparisons made in the Stickler example (ref 63) be carried out for the profile of figure 46. The normal mode program of reference 16 should be modified to treat this profile. The results of this program should be compared with those of the FFP model and also with a model which treats the branch line integral. It would be particularly interesting to determine whether the branch line integral contribution for a frequency just above cutoff of the first mode is as important for the profile of figure 46 as it was for the Stickler example.

6.2.4 Bilinear Channel Over a Negative Gradient Half-Space

Our last test case of this sequence is a further modification of the profile. Note that the profile of figure 47 is similar to that of figure 46, except that the isospeed layer is of finite width, h_2, and the half-space is a negative gradient layer. The program of reference 16 should be modified to treat this profile. The results of this program should be compared with those for figure 46, and also with the results of the FFP model. According to Towne and Wilson (ref 49), there is no branch line contribution for the model of figure 47.

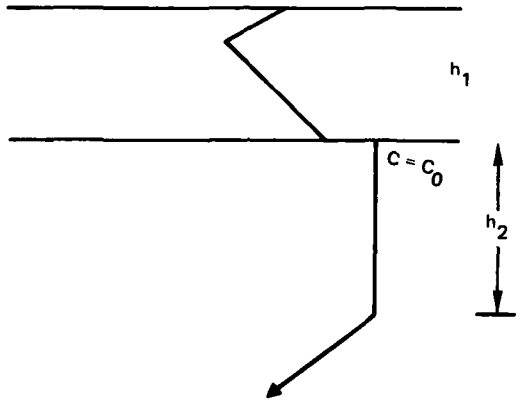

Figure 47. Bilinear channel over a negative gradient half-space.

For sufficiently large h_2, one would expect the results for the profile of figure 47 to agree with those of figure 46. The concept is that downgoing waves will be so severly attenuated by the time they reach the depth h_2 that the nature of the sound speed profile below h_2 has a nil effect on propagation in the refractive medium. However, the logical conclusion for this line of reasoning is that there is no branch line integral contribution for the model of figure 46 as long as there is some attenuation in the bottom layer.

6.2.5 Other Considerations

Before closing the discussion, we should point out that the models of figures 46 and 47 could be used as the simplest controls which address the problems raised in sections 5.2.2, 5.2.3, and 5.2.5. To refresh the reader's memory, section 5.2.2 questions the effectiveness of ray theory based on reflection coefficients at the water-bottom interface; section 5.2.3 questions the use of planewave reflection coefficients; and section 5.2.5 addresses bottom rigidity. The questions of sections 5.2.2 and 5.2.3 can be addressed without modification of the profile. The question of section 5.2.5 can be addressed by modifying the profile to also contain an isospeed complex shear velocity. The case of constant shear speeds can be solved exactly, and would provide a simple first test case of shear wave propagation.

The question of reflection coefficients and ray theory bring up some more fundamental questions about branch line integral contributions. Where does this contribution enter into a ray computation? Suppose, for example, we are treating some structured sound speed profile for which there is a branch line integral contribution. We replace the sub-bottom structure by reflection coefficients obtained either by the plane wave approximation or by the full mode treatment. The branch line integral contribution is obviously not contained in the reflection coefficients. Is it automatically contained in other aspects of the ray theory? If it is not, is it possible to deal with in some ray context? If the branch line integral does make an important contribution in practical applications, then these questions are more than academic.

6.3 TREATMENT OF SPECIAL SOURCE FUNCTIONS

The far-field pressure can be expressed as

$$p(r,z,t) = \int_{-\infty}^{\infty} S_o F_s(\omega) p(r,z) e^{-i\omega t}\, d\omega \qquad (44)$$

where $F_s(\omega)$ represents the frequency spectrum of a harmonic point source of strength S_o. In the passive sonar case, interest typically focuses on narrowband continuous wave (CW) signals. Thus $F_s(\omega)$ goes to $\delta(\omega - \omega_o)$, where ω_o is the frequency of interest, and the far field pressure nicely reduces to the time-independent expression.

In the active sonar case, a variety of signal waveforms may be of interest. However, even for a pulsed signal having a finite bandwidth, propagation loss calculations are, more often than not, given a treatment similar to the passive sonar case, where ω_o is some "center" frequency. System parameters such as integration time and bandwidth are then "neatly handled" by means of a simple processing gain calculation. If bandwidth is an important issue, then the casual treatment above can be made somewhat less casual by "proper averaging" propagation loss calculated at selected frequencies over the band.

More accurate treatments require a specification of the source spectrum $F_s(\omega)$. Waveforms generated by transient signals, broadband sources, and shock waves may require more than a casual treatment of $F_s(\omega)$ if system (eg, medium and receiver) response is important.

A few exact solutions for nonsteady-state cases are no doubt available. However, the problem goes well beyond the assessment of the effect of the medium. Propagation loss *per se* is of limited value here. Even a detailed characterization of the acoustic field from a complicated source function would be of limited value unless one could also simulate the effect of the receiver processing system and predict the output of such a system. The responsibility for this level of assessment clearly does not lie solely with the developer of environmental acoustic models.

There are several miscellaneous problems which fall under special source functions. One is a source with vertical directivity. This source is relatively easy to accomodate in a ray theory treatment. One normal mode approach is to approximate the directivity pattern by a vertical array of point sources.

A second problem is that of distributed multiple sources. For example, the sound field emitted by ships may need to be characterized by sources distributed in range as well as depth.

A third problem is the evaluation of the acoustic field in the near field of a special source. This poses a particularly complicated problem. For example, very few of the current propagation loss programs have the capability of evaluating the near field of a steady-state harmonic point source, to say nothing of other sources. A special case here is the evaluation of the source level of a parametric array which relies upon nonlinear effects to produce a high directivity at low frequency.

Controls would be obviously desirable for all these problems. Excessive concern about such controls would appear premature at this time. Our impression is that the state of the art and experience with the use of special source functions must first advance beyond the present level.

6.4 TREATMENT OF DOPPLER

Arriving at test cases for checking the validity of Doppler calculations is a tricky problem because only extremely simple geometric and environmental acoustic assumptions exist. Consider first the simple case of a source moving with velocity v toward a stationary receiver. In the case of an isospeed medium $C = C_o$, the frequency shift of a harmonic signal emitted with frequency f_o is

$$\delta = f_o \left(\frac{v}{C_o}\right) \left(1 - \frac{v}{C_o}\right)^{-1} \approx f_o \left(\frac{v}{C_o}\right) \quad . \tag{45}$$

The question now arises as to what to use when C is not constant or even when C is constant and there are boundaries involved. Our first exposure to this problem occurred some 25 years ago when we were called upon to correct the range of a frequency-modulated sonar for a moving target. Our first reaction was to use the group velocity

$$C_g = R/T \tag{46}$$

of ray theory. This approach gave answers which were not in agreement with experimental values. On further thought, we decided that the phase velocity C_m was the proper value to use. Our reasoning was that Doppler shifts were associated with incremental range and incremental travel time rather than range and travel time *per se*. As discussed in connection with equation 9,

$$C_m = dR/dT \quad . \tag{47}$$

We found that

$$\delta \approx f_o \left(\frac{v}{C_m}\right) \tag{48}$$

did indeed give results in good agreement with experiment.

Equation 48 can be "derived" from another standpoint. Let the sound speed at the source be given as C_s. If V is the speed of the source along the horizontal, the projection of this speed in the direction θ_s is given by $V \cos \theta_s$. Thus equation 45 becomes

$$\delta \approx f_o \frac{\left(V \cos \theta_s\right)}{C_s} = f_o \left(\frac{v}{C_m}\right) \quad . \tag{49}$$

We see that the Doppler shift depends upon the ray angle.

The Doppler shift is an important feature in describing propagation. However, there are several other effects which influence the ray theory acoustic field for a moving source. The effective transmitted frequency is $f_o (1 \pm V/C_m)^{-1}$. Thus each ray propagates at a slightly different frequency. This shift gives a complication when frequency-dependent effects such as bottom loss or diffraction are functions of the ray angle. However, the frequency shifts are so small that they are not likely to be of practical importance – particularly when one realizes that the frequency dependence of bottom loss is usually modeled rather crudely.

Another effect is that the travel times of the various arrivals are different. This means that the rays which arrive at the receiver at a given instant of time left the source at different times and correspond to different positions of the source in range. A rigorous ray treatment then requires that each ray have a different range between source and receiver.

Note that the problem of a moving receiver and a fixed source is somewhat easier. Were each ray propagated at the same frequency (ie, the source frequency), all rays would leave the source at the same position. It would appear, in the case of a moving receiver and a fixed source, that conventional ray calculations for the fixed source and fixed receiver apply except that the frequency to be used in combining each arrival is somewhat different. Even here, we run into another problem. How does one combine arrivals at slightly different frequencies? Again, this involves modeling the receiver processing system, as discussed in section 6.3.

Reference 67 discusses the ray theory of a moving source. It is not clear without some critical analysis that the approach of reference 67 could serve as a test model. However, the reference appears to be a good start toward the development of a rigorous ray theory control.

In our opinion, the implementation of Doppler into ray models to whatever degree desired is relatively easy. The implementation is straightforward, since ray theory fits well into the Doppler formulation.

The same is not true of other approaches to propagation. For example, phase velocity and travel times are not readily available from normal mode methods or numerical approaches such as the parabolic equation or fast field program. It is not clear that the effect of a moving source can be addressed by any of these methods as rigorously as it can be by ray theory.

A normal mode approach to the Doppler problem is presented in reference 68. This treatment appears to be more thorough than the previous work which it references. The Doppler shift can be determined from equation 39 of reference 68 to be

$$\delta_n \approx f_o (V/C_{mn} - V^2/C_{mn}C_{gn}) \quad . \tag{50}$$

Here, δ_n is the phase shift associated with mode n, while C_{mn} and C_{gn} are the phase and group velocities associated with mode n. Now, equation 50 may be expressed in terms

---

67. Clark, J. G., et al, Multipath Acoustic Propagation with a Moving Source in a Bounded Deep Ocean Channel, J Acoust Soc Am 60, 1274-1284, Dec 1976.
68. Hawker, K.E., A Normal Mode Theory of Acoustic Doppler Effects in the Oceanic Waveguide, J Acoust Soc Am 65, 675-681, Mar 1979.

of equation 48 as

$$\delta_n = \delta(1 - V/C_{gn}) \quad . \tag{51}$$

Since $V \ll C_{gn}$, there appears to be a relatively minor difference between the results of ray theory and mode theory. However, it raises an interesting point. Is equation 48 the best expression that can be derived from ray theory? For example, could one derive equation 50 from ray theory? If equation 48 is the rigorous result of ray theory, equation 50 represents an improvement resulting from a more rigorous treatment of the wave equation.

The normal mode solution of reference 68 is couched in the forms available in conventional stationary source, normal mode theory. These forms contain expansions of V/C_{gn}. Reference 68 also discusses an approach to determining Doppler broadening which makes use of the processing of the receiver system.

References 67 and 68 indicate that the Doppler problem is quite complicated. A definitive control model does not appear feasible at this time. However, some cross checks between various theoretical models appear desirable. The ray theory approach of reference 67 should be checked against the mode theory approach of reference 68 for the identical environmental model. The model of section 4.1.1 or any other environmental model that results in good agreement with the stationary source solution are good candidates. An exact normal mode solution for a moving source for some simple environment would be useful to test the general solution of reference 68. The isospeed version of the profile of figure 45 is a possible candidate. Note that for this model, the modes have different group and phase velocities even though the sound speed is constant. Thus the necessary elements of reference 68 can be tested.

Once the case of the moving source has been evaluated, the case of simultaneous moving source and moving receiver should be established. There are, no doubt, adequate treatments of Doppler in a moving medium. However, the combination of source, receiver, and medium motion has probably not yet been addressed.

7.0 CONTROLS FOR RANGE-DEPENDENT ENVIRONMENTS

Sections 4.0 to 6.0 all dealt with environments which did not change with range but were dependent on depth only. This section deals with environments which change with range. Section 7.1 presents controls for which the sound speed profiles change with range with either flat or nonexistent boundaries. Section 7.2 presents controls for which the bottom boundary (bathymetry) changes with range. Our interest here is in the rigorous (exact) solution for range-dependent environments. Because of our requirement for exact solutions, the environments will be stylized and will seldom represent realistic ocean conditions. The eventual use of these controls is to check range-dependent models such as FACT-X, ASTRAL, and the parabolic equation method. These methods can treat realistic ocean environments at the expense of employing various approximations such as adiabatic invariance, the omission of certain terms in the wave equation, etc. The purpose of the exact solution is to assess the errors introduced by these approximations and to obtain a feel for the conditions under which the approximate models break down and no longer give reliable results.

7.1 NONBOTTOM-REFLECTED PROPAGATION MODELS

Our concern here is with examples in which the sound speed profiles are range-dependent. We are not concerned with a range-dependent bathymetry; ie, we do not treat boundaries which are range-dependent. The boundaries, if present, are flat.

7.1.1 Range-Dependent Ray Models

As discussed in section 3.2.1, the method of reference 10 can be used to generate innumerable closed-form solutions which could be used as control cases. Section 3.2.1 and 3.2.2 present two examples, the latter from reference 10, which were used as controls for testing the RP-70 model. Pages 412-414 of reference 10 present a profile with multiple focal points which could also be used as a third control. However, the three examples of reference 10 are not adequate for a thorough testing of range-dependent models. At least two additional control cases should be prepared.

The first is a control case which would include reflection from the ocean surface. The profile of section 3.2.2 could serve as this control provided the ocean surface is included. The inclusion of a flat interface at ocean surface or bottom, or both surface and bottom, poses no technical problem as the solution is given on page 408 of reference 10. In brief, it requires some iteration procedure to locate the range where the ray intersects the interface. Although this procedure can be tedious and involved, it is straightforward.

The second is a control case for which the sound speed is a function of the two mathematical coordinates rather than of just one of the coordinates. For the three evaluated examples of reference 10, the sound speed depends on only one of the coordinates. For example, the profiles of sections 3.2.1 and 3.2.2 depend only on the angle, Θ, and not the range, ρ, of polar coordinates. Here, the trajectory of a ray can be expressed explicitly as $\rho = f(\theta)$ [or as $\Theta = g(\rho)$ for the case where the profile depends on ρ but not on Θ].

When the sound speed is a function of two coordinates, say ρ and Θ, then the trajectory of the ray given in reference 10 is expressed implicitly by $f(\Theta) = g(\rho)$. This implicit representation, plus other aspects of the ray computation presented in reference 10, lead to a more complicated evaluation for two-coordinate variation in sound speed.

The two-coordinate variation is important as a test case because it permits a variation in range which can be comparable to that with depth. The one-coordinate variation of sections 3.2.1 or 3.2.2 is satisfactory when the range dependence is slight compared to the depth dependence. However, it would not provide an adequate test for models which were called upon to treat strong horizontal sound speed gradients.

The case of two-coordinate variation has the complication that the ray trajectories can reverse direction in both mathematical coordinates. Comparable variation in both coordinates will lead to ray paths which can turn around in range as well as in depth.

A critical test case for range-dependent environments is one for which rays will turn around in range and head in the opposite range direction from that of initial projection. Whether this is a significant situation in terms of an oceanic environment is not known. Such a case can occur for steep rays and strong horizontal change. Such range reversals appear possible for certain configurations in ocean fronts and eddies. In any case, the practical significance of range reversals cannot be assessed without some ray models which can treat this problem.

7.1.2 Warfield-Jacobson Ray Model

A somewhat extreme but simple test of range dependence for ray trace codes is provided by a strictly range-dependent model described by Warfield and Jacobson (ref 69).

69. Warfield, J. T., and M. J. Jacobson, Acoustic Propagation in a Channel with Range Dependent Sound Speed, J Acoust Soc Am 45, 1145-1156, May 1969.

In this model, there is no dependence in depth (y), while the dependence on range (x) is linear; ie,

$$C(y, x) = C_0 + hx . \tag{52}$$

The medium is bounded by flat surfaces at y = o and y = Y.

Figure 48 is taken from reference 69, which presents work supported by Acoustic Programs, Office of Naval Research. The upper panel presents a ray path for h positive while the lower panel presents the corresponding path for h negative. The ray angles steepen with range for h positive and become less steep with range for h negative. The ray paths are circular arcs. For h positive, the radius of curvature lies at smaller ranges and above y = 0 for upward-headed sections and below y = Y for downward-headed sections. For h negative, the opposite is true. The radius of curvature lies at longer range and above y = 0 for downward-headed sections and below y = Y for upward-headed sections.

Specific ray theory expressions for range and travel time are given in reference 69 and could be used to provide a quantitative test case.

However, the qualitative nature of figure 48 was enough to establish that the range-dependent model RAY WAVE failed when subjected to this test case. Figure 49a presents an example for C° = 1400 m/s, Y = 500 m, s = 250 m, and h = 0.002. Source angles are in 0.25° steps from 0 to 1°. Figure 49b is the corresponding plot for h = -0.002. These figures appear to duplicate the salient results of reference 69 in that the ray cycle range decreases with range for figure 49a and increases for figure 49b. On closer inspection,

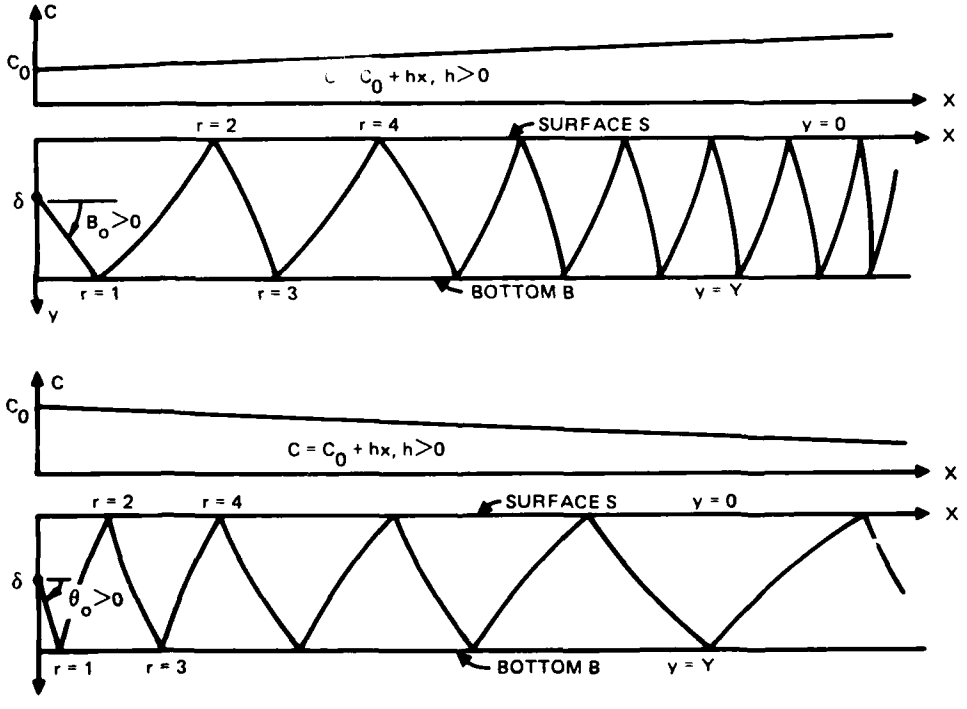

Figure 48. Ray paths for the Warfield-Jacobson model.

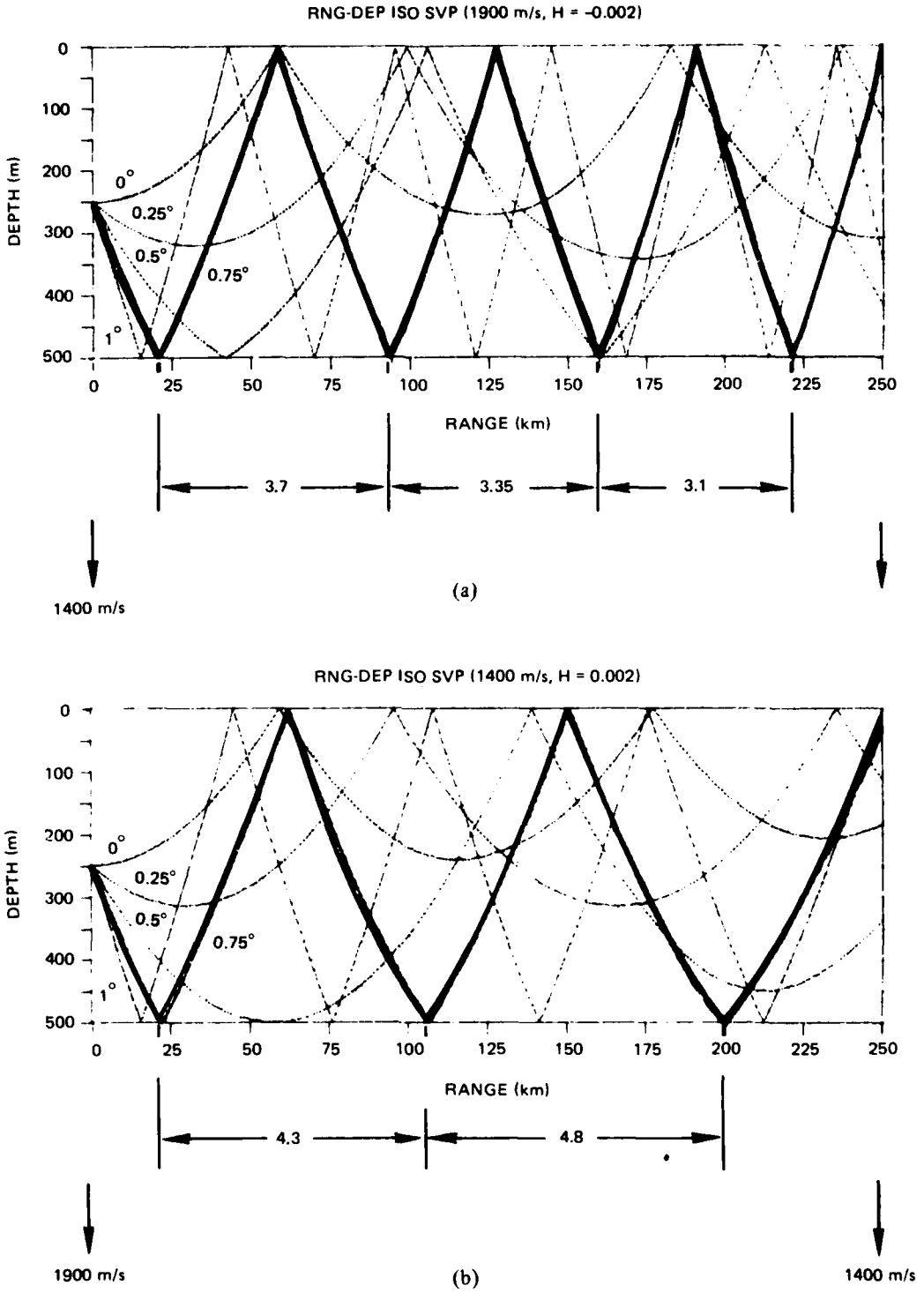

Figure 49a-b. Ray paths illustrating failure of the RAYWAVE Model: (a) positive gradient range dependence; (b) negative gradient range dependence.

there are two erroneous features. First, the curvature has the wrong sign for downward-headed rays in figure 49a and upward-headed rays in figure 49b. Second, the rays turn around in depth and form an apex. This should not happen for a profile which does not depend on depth. Indeed, for this profile the zero-degree ray should be a straight horizontal line. The precise problem with RAYWAVE has not been diagnosed. Apparently, the present RAYWAVE program will not run without a vertical sound speed gradient. The operator inserted a slight vertical gradient to make the program run. This may account for some of the problem, but not all.

We think the problem is much more fundamental than some quirk with RAYWAVE. RAYWAVE and no doubt other range-dependent models do not use a rigorous form of Snell's law. The formulation is based on the assumption that the major sound speed gradient is vertical and that the horizontal sound speed gradients are relatively small compared to the vertical. For example, angles are measured relative to the horizontal.

An even more rigorous test using the Warfield-Jacobson model is for rays near a source angle of 90°. Some of those rays will turn around in range. For example, for h positive the 90° ray will move in the negative x direction and rays with launch angles slightly smaller than 90° will start out in the positive x direction, turn around, and then move in the positive x direction. However, rays with launch angles slightly greater than 90° will start out in the negative x direction, turn around, and then move in the positive x direction. Yet, how many ray models that accommodate horizontal change make provision for negative ranges or for launch angles greater than 90°?

One may argue that the Warfield-Jacobson model is unrealistic in terms of oceanic profiles, and indeed it is over long-range intervals. However, for near-isospeed surface ducts it seems quite likely that the horizontal gradient could exceed the vertical gradient on a local basis.

7.1.3 Conformal Mapping

De Santo (ref 12) points out that by using a conformal mapping technique, it is possible to relate solutions of the Helmholtz equation with sound speed varying in range and depth to the solution of a parabolic equation whose sound speed varies in only the mapped depth coordinate. He also gives one example, although the details of the solution are not presented. De Santo notes also that this class of analytically solvable models might be useful in checking approximation methods in two dimensions. We concur and recommend that this approach be examined in more detail and that several control cases be prepared.

7.1.4 Normal Mode Model With Linear Range-Dependent Profile

In FY79, one of the NOSC tasks under AMEC was to develop tests for range-dependent models. As part of this effort, DeWayne White investigated simple sound speed variations with depth and range for which the wave equation could be solved exactly. This section presents a summary of his investigation.

He considered models of the form

$$k^2 = \omega^2/C^2 = k_{zi}^2 + k_{rj}^2 \qquad (53)$$

in which both depth and range are layered. Here, i refers to layer i and j refers to layer j.

Of various cases considered, he decided that the most desirable was one for which

$$k_{rj}^2 = a_j (r_{j-1} - r) \tag{54}$$

Here, a_j is the range gradient in range layer j and r_{j-1} is the interface between layers j-1 and j. The range dependence then is given by

$$H_j(r) \sim r^{-1/2} \left[A_j h_1(\tau_j) + B_j h_2(\tau_j) \right] \tag{55}$$

where

$$\tau_j = a_j^{-2/3} \left[\lambda_n^2 + a_j (r_{j-1} - r) \right] \tag{56}$$

and where λ_n is the separation constant (eigenvalue when a mode has been found). Here, h_1 and h_2 are the modified Hankel functions of order 1/3. One of the advantages of the dependence of equation 54 is that these Hankel functions (with different functional arguments) are used in the n-layer normal model program to evaluate depth functions. Thus the numerical routines for evaluating h_1 and h_2 are already available.

Equation 55 is exact provided that

$$4r^2(\lambda_n^2 + k_r^2)^{-1} \ll 1 \quad . \tag{57}$$

Thus equation 55 is valid except at close ranges.

The simplest type of depth dependence is

$$k_{zi}^2 = \omega^2 (a_i + b_i Z) \quad . \tag{58}$$

The solution then is the same as that for the n-layer normal mode program except that the range dependence of $H_0^2(\lambda_n r)$ is replaced by the $H_j(r)$ of equation 55. Thus the eigenvalue and eigenfunctions for the depth dependence are identical to that of the n-layer normal mode program with no range dependence.

At about this stage of development, White discovered that this was a special case of the profile considered by Nagl (ref 70). With a few minor differences, the solutions of Nagl were exactly what was wanted.

---

70. Nagl, A., et al, Adiabatic Mode Theory of Underwater Sound Propagation in a Range Dependent Environment, J Acoust Soc Am 63, 739-749.

For example, Nagl presents in detail the evaluation of A_j and B_j in equation 55. We describe the approach here because it is a significant feature of the solution. One starts with the last range layer, J, which extends out to infinity. In this layer, there is no range dependence in the sound speed profile. The reason is that if we allow the last range layer to be of the form of equation 54, we find that at infinity the sound speed is either infinite or complex. The solution for this last layer must be an outgoing wave or

$$H_j(r) = H_o^{(2)}(\lambda_n r) \quad . \tag{59}$$

Nagl uses $H_o^{(1)}$. Our use of $H_o^{(2)}$ here is consistent with our time dependence of $e^{-i\omega t}$. Nagl expresses equation 55 in terms of Airy functions. We prefer h_1 and h_2 because they represent incoming and outgoing waves, respectively. The boundary condition at each range layer interface is

$$H_j(r_j) = H_{j-1}(r_j) \tag{60}$$

and

$$\frac{\partial H_j(r_j)}{\partial r} = \frac{\partial H_{j-1}(r_j)}{\partial r} \quad . \tag{61}$$

Thus equations 59 to 61 allow us to evaluate A_{J-1} and B_{J-1}. Once A_{J-1} and B_{J-1} have been determined, we can apply equations 60 and 61 to determine A_{J-2} and B_{J-2}. The process is repeated again and again. All coefficients will have been determined when equations 60 and 61 are applied to the first range interface.

In the initial range interval, 0, Nagl chose (in essence) no range dependence with a solution of the form

$$H_J(r) = A_o H_o^{(1)}(\lambda_n r) + B_o H_o^{(2)}(\lambda_n r) \quad . \tag{62}$$

This judicious choice is dictated by the requirement of equation 57, which will be satisfied for all layers except the source layer. However, if we choose no range dependence in the source layer, equation 55 is exact and equation 57 no longer applies.

An alternate approach is to assume that equation 54 holds for the source layer and obtain higher-order correction terms to the solution of equation 55 by means of a series solution such as that described on page 451 of Abramowitz and Stegun (ref 71).

In the application of his theory, Nagl (ref 70) allows the depth function to vary with range and the range function to vary with depth. Under these conditions, the solution is not exact but falls under the condition of adiabatic approximation.

---

71. Abramowitz, M., and I. A. Stegun, Handbook of Mathematical Functions, National Bureau of Standards Applied Mathematics Series: 55, June 1964.

For our control case, we wish an exact solution. This imposes a serious restriction on the model in that a_j is the same for all i and a_i and b_i are the same for all j. Thus range dependence is identical for all layers, while the depth dependence is identical for all ranges. As a first-order approximation, the profiles at any range are translations of the profile at zero range. This results in the same change with range at the ocean surface as at the ocean bottom and is quite unrealistic from the standpoint of ocean conditions. Nonetheless, it may serve as a test case for approximate methods. It does have the advantage that it is a simple extension of existing N-layer normal mode program and thus can be implemented with relative ease. The ray theory can also be solved in closed form for this profile, which could be used as an example of ray and mode comparison for a range-dependent environment.

Figure 50 presents a model, constructed by White, which could serve as a control for a range-dependent surface duct. Values are plotted for range cuts of 0, 20, and 40 km. Beyond the last range of interest, the profile is independent of range. This channel should be stronger than a nonrange-dependent channel of the same depth and gradient. In contrast, for the case of a positive (ie, the sound speeds decreasing with increasing range), the channel would rapidly lose energy with increasing range.

A range-layered model such as figure 50 can be used to provide a test for a deficiency in the parabolic equation model. This later model does not treat incoming waves. It starts at zero range and marches outward. Thus the solution at any given range is independent of the environment at longer ranges. However, the solution for a range-layered model clearly contains both incoming and outgoing waves in all but the semi-infinite layer. It is also evident that the solution at short ranges depends upon the environment at long range because one evaluates coefficients by starting with the long-range solution and working in to short ranges.

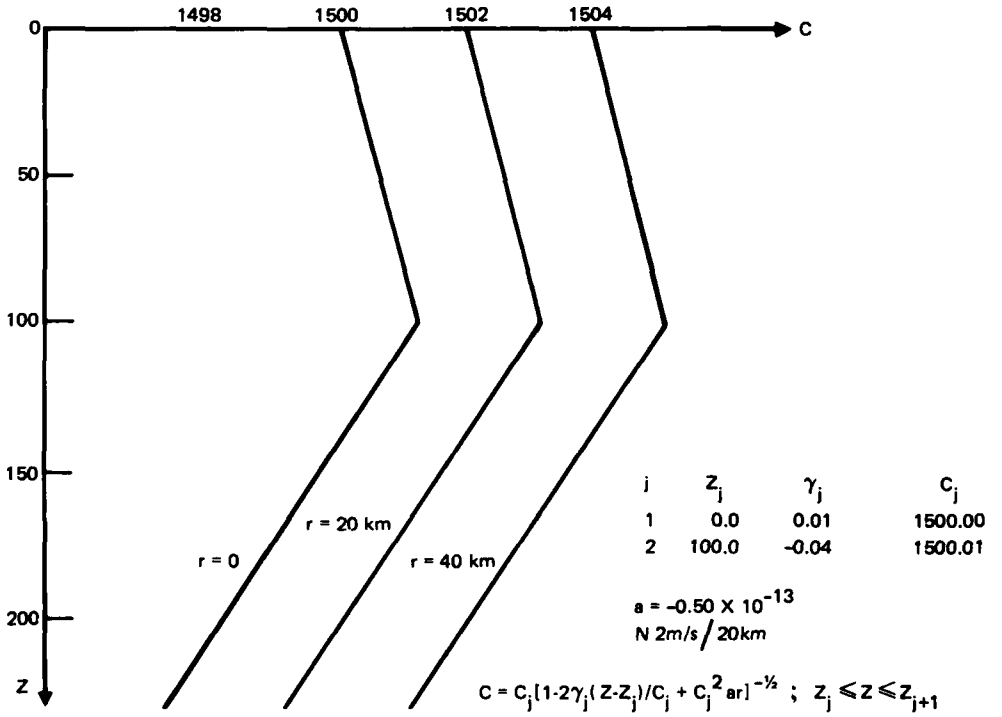

Figure 50. Model of a range and depth-dependent surface duct.

We should recognize a limitation in models with layered ranges. For the model of equation 54, there are slope discontinuities at the range-layer interfaces. This can introduce spurious reflections. The effect of slope discontinuities in depth has been recognized for some time. Indeed, the study of section 3.1.2 showed the importance of such discontinuities. The effect of slope discontinuities for layered ranges should be assessed once the first-order problems of range-dependent profiles have been resolved.

7.1.5 Range-Dependent Parabolic Velocity Profile

Reference 72 presents the normal mode solution of coupled range equations associated with an unbounded parabolic channel which opens up with increasing range. The solution includes the first-order coupling terms, but ignores higher-order coupling terms. The solution is also compared with the results of the adiabatic approximation, which was found to be quite reliable for gradual range dependence.

Even though the solution is not exact because of the neglect of higher-order coupling terms, it may serve as a useful control to compare with other types of range-dependent methods.

7.1.6 Channels Which Disappear With Range

The most significant range dependence that we can visualize is one where an acoustic channel disappears with range. For this type of propagation, trapped modes with little attenuation must be converted to untrapped modes with large attenuation. Thus, in any future investigation of exact solutions for range and depth dependence, we should be on the lookout for a model in which the channel disappears with range. By appropriate scaling, this could take place rapidly or slowly with range. Both conditions would provide good test cases.

Models of double channels which change their relative strengths as a function of range would also provide good test cases. Such conditions occur in the ocean. For example, a surface channel can disappear, leaving only the SOFAR channel, or two refractive ducts can merge to form a single duct.

7.1.7 Variation in Three Dimensions

Thus far, we have only considered profile variation in depth and range and not in three dimensions. As a matter of fact, most of our two-dimensional models are restrictive in that they assume radial symmetry; ie, we consider the ocean to be described in cylindrical coordinates where the sound speed depends on depth and range but not on the azimuth angle ϕ. This assumption leads to tractable solutions, but is not too realistic when one considers that it is equivalent to stating that the ocean environment revolves symmetrically about any arbitrary source location.

The practical approach to this problem has been to divide the ocean up into "pieces of pie" with the source at the center. The assumption is that the medium is independent of azimuth over each piece. Thus a different propagation-loss-versus-range dependence is generated for each piece. This approach would appear to be adequate from the standpoint of propagation loss. However, it does not address refraction in the azimuthal direction.

72. Chwieroth, F. S., et al, Mode Coupling in a Sound Channel with Range-Dependent Parabolic Velocity Profile, J Acoust Soc Am 64, 1105-1112, Oct 1978.

For example, a ray path headed due East in the Northern hemisphere will be bent in a northerly direction because of the tendency for sound speeds to increase slightly toward the South. Thus the azimuthal ray angle at the receiver will not correspond to the bearing of the source. However, it is probably not necessary to use a full-blown three-dimensional model to assess this effect.

The case of two-dimensional propagation in the z, x plane with no environmental variation in y is more difficult than that in cylindrical coordinates but has been addressed by a few investigators. For example, Nagl (ref 70) treats this case. It would be of interest, for example, to compare the results of an exact solution with no variation in ϕ with that for no variation in y, given that the variation in the other two coordinates were the same. This would help assess the assumption of radial symmetry.

The state of the art for treating a profile variation in three dimensions has perhaps not progressed to the point where we can recommend controls for three-dimensional variation. The simplest of such controls would be the testing of three-dimensional models with variation in only two of the dimensions. The ultimate control in three-dimensional profile variation would be an exact solution for some stylized model of an oceanic eddy or front.

7.2 BOTTOM-REFLECTED PROPAGATION MODELS

Our concern here is mainly with controls where the bottom boundary (bathymetry) changes with range. Unless stated otherwise, the sound speed profile is assumed to be independent of range.

7.2.1 Simple Parabolic Bottom Test

The parabolic bottom test is appropriate for ray trace codes that accommodate reflections off nonflat bottom boundaries. The simplest representation of arbitrary bathymetric features is provided by linear segments. That is, bottom depth is expressed as a piecewise linear function of range. The linear segments of such a profile are often referred to as facets. Representing a curved portion of bathymetry by several facets generally introduces subtle anomalies into calculations that depend on various ray path parameters.

The crux of the problem is illustrated in figure 51, where 10 uniformly spaced rays reflect off two bottom facets. The bottom facets provide a crude approximation to the smooth bathymetry (dashed line) and effectively partition the 10 rays into two distinct groups. The five shallowest rays reflect off facet two and exhibit a greater change in range than do the steeper rays that reflect off facet one. The impact on intensity calculations is difficult to quantify in general terms.

A test that is simple to implement and which graphically illustrates any frailties of a bottom depth profile model is provided by the parabolic bottom test. In this test, the bottom depth profile takes the form of a parabola (actually half a parabola) and the source is placed at the focus. For convenience, the parabola axis coincides with the surface. All rays should reflect off the parabolic bottom in the horizontal direction regardless of launch angle.

As an example, consider the parabolic bottom profile generated by $z = 0.002\, b\sqrt{r/b + 1}$, where z is bottom depth in meters, r is range in kilometers, and b is a constant. When b = 250000, the focus is located 250 m from the parabola vertex and

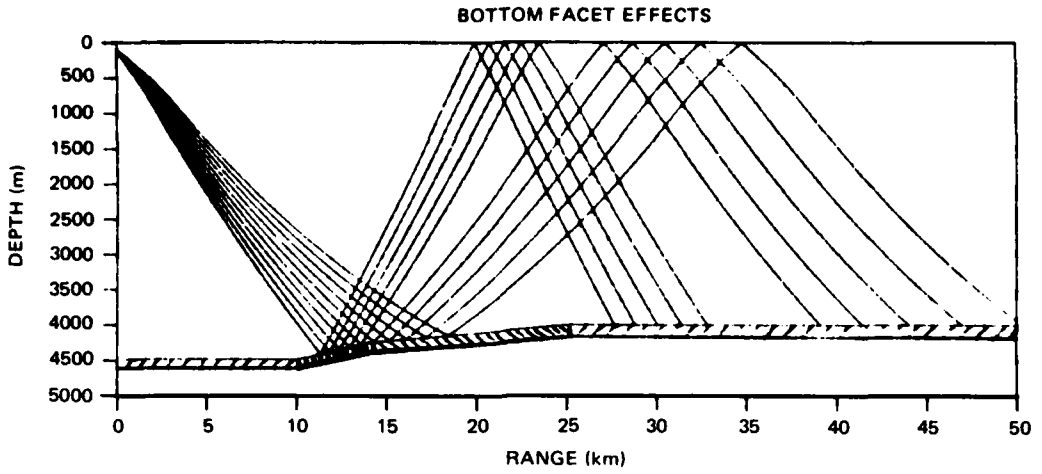

Figure 51. Ray diagram illustrating the effect of bottom facets.

the half-length of the *latus rectum* is 500 m. Since the focus is to coincide with the origin (source position) of the ray diagram, the bottom depth at r = 0 is 500 m. Figure 52 illustrates a ray diagram generated by a "ray-trace-only" version of RAYWAVE II. The rays were traced through a constant-velocity medium bounded by a parabolic bottom as approximated by 10 linear segments. The actual input values of the bottom-depth-versus-range profile are reproduced in table 19. Note in figure 52 that the less steep the ray, the closer to horizontal the rays reflect off the ocean bottom. This is proabaly not due to the RAYWAVE II model, but is due rather to the bottom profile property that the slope is modeled better by constant gradient layers as we go deeper along the profile.

Section 3.2.3 presents a similar type of control for a cubic bottom.

RANGE (km)	0	0.3125	0.75	2	3.75	6	8.75	12	15.75
DEATH (m)	500	750	1000	1500	2000	2500	3000	3500	4000
RANGE (km)	20	24.75	—	—	—	—	—	—	—
DEPTH (m)	4500	5000	—	—	—	—	—	—	—

Table 19. Linear approximation to a parabolic bottom.

7.2.2 Rigorous Ray Theory for a Piecewise Curvilinear Bathymetry

The development of an improved ray theory approach for treating variable bathymetry is in progress at NOSC. This approach can be used to produce excellent controls or test cases. The first such example is given in section 7.2.3, which provides a brief description of the method. The approach has three advantages: (1) it determines exactly where the ray encounters the bottom and does not use an iterative procedure; (2) it can treat curvilinear (parabolic) segments as well as segments of constant slope; and (3) it determines ray theory spreading from exact analytic expressions rather than from finite differences based on adjacent ray paths.

There are other ray models which do not require iteration to find the bottom. However, most if not all of these are limited to segments of constant slope and evaluate ray density by finite difference approaches.

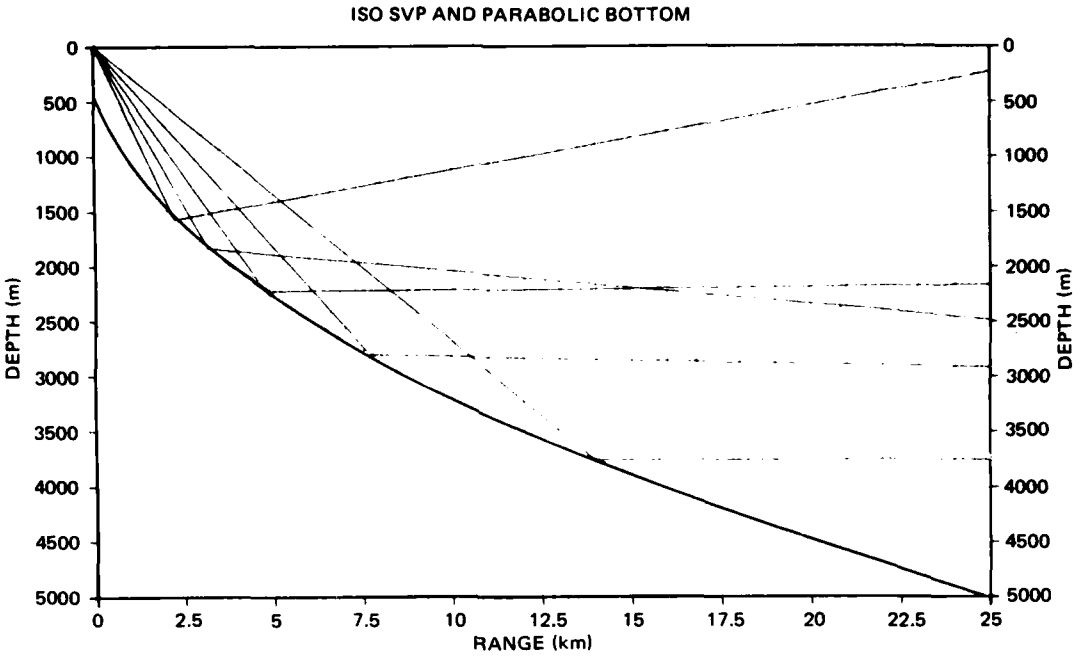

Figure 52. Ray paths for a parabolic bottom approximated by 10 linear segments.

Figure 53 presents the basic method for an improved way to treat a bottom which varies with range. The environment can consist of any depth-dependent sound speed profile including the composite profile model.* However, the deepest part of the profile, below what we will call the juncture depth, is of the special form

$$1/C^2 = a + bz \quad . \tag{63}$$

This limitation is not serious because the near-bottom profile segment has nearly constant slope and the special form will be adequate. In preparing the model of the sound speed profile, care should be taken to make the sound speed and its depth derivative continuous at the juncture depth.

The bottom profile is described by a series of piecewise segments. Any segment may be flat, sloping with constant gradient, or parabolic in form. The mathematical prescription for the bottom is

$$Z = B_o + B_1 R + B_2 R^2 \tag{64}$$

73. Pederson, M. A., and R. F. Hosmer, Combined Acoustic Propagation in Eastpac region (Exercise CAPER): Initial Acoustic Analysis, NOSC TR-276, June 1978.

*In the composite profile method, range variation is accommodated by introducing a new sound speed profile at convergence zone range intervals. The transition problem between profiles is avoided by assuming that all the near-surface changes take place between convergence zones when the rays are vertexing in the deep ocean where the profiles are taken to be independent of range. (An example of the use of this model is given in reference 73).

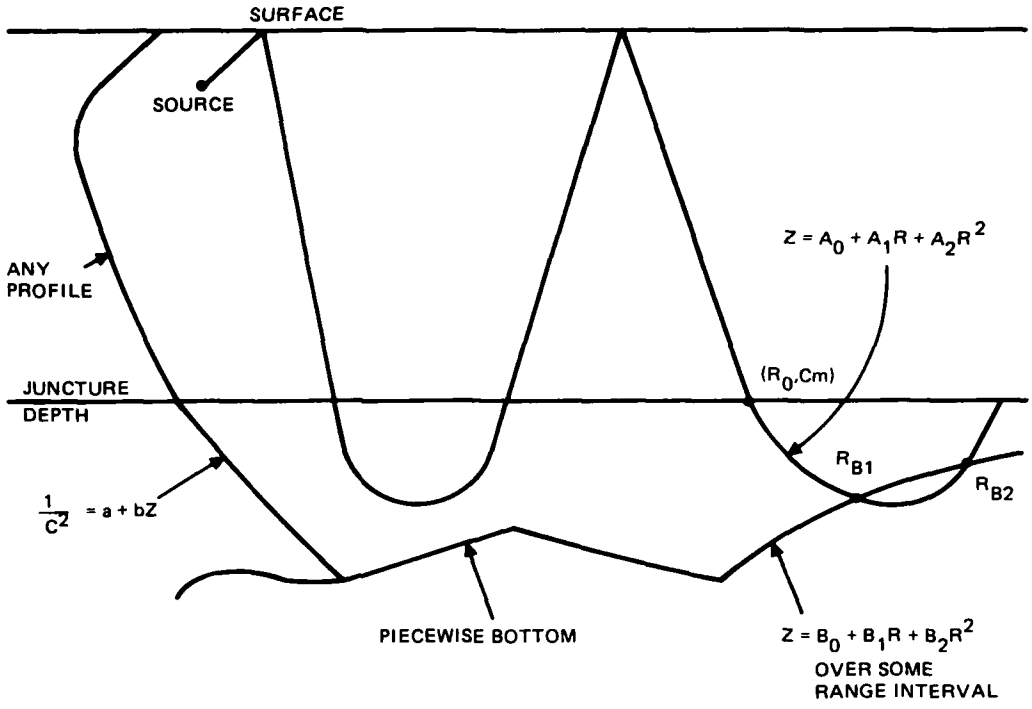

Figure 53. Schematic illustrating a ray model for range-dependent bathymetry.

which is valid over some specified range interval. The ability to use parabolic segments is desirable since they can eliminate or reduce the joints between constant gradient segments. These joints lead to the bottom facet effects described in figure 51.

Ray computations proceed in a standard fashion until at some range R_o the juncture depth is reached. We know the range R_o at the juncture depth and we know the ray parameter. Given these values and the profile parameters of equation 63, the depth of the ray in the deepest layer can be expressed as a parabola in range; ie,

$$Z = A_o + A_1R + A_2R^2 \quad . \tag{65}$$

By making equations 64 and 65 equal, we obtain a quadratic equation in R. The two real roots of this quadratic equation represent the two ranges at which the ray intersects the bottom segment. The root with the smaller range is generally the intersection of interest provided that it occurs in the range interval where equation 65 applies. If the roots are complex, the ray does not intersect the bottom. If the discriminant is zero, the ray grazes the bottom.

Having determined the range of the intersection, the depth of the intersection can be obtained from equation 65. Furthermore, the bottom slope at the point of intersection can be evaluated from

$$dZ/dR = B_1 + 2B_2R \quad . \tag{66}$$

Thus all the necessary items are available to continue the ray trace after reflection, starting at the point of intersection on the bottom.

Note that the points of intersection satisfy a quadratic equation whether the bottom is flat, of constant slope, or parabolic. Thus the curvilinear bottom is no more difficult than a sloping bottom from the standpoint of finding the intersection. However, the curvilinear bottom introduces other complications which will be discussed later.

Tappert (ref 74) has pointed out that he could not use the results of the CONGRATS ray model for a variable bathymetry. His interest was in travel time differences between various ray paths as a function of range. Whereas no travel time was seriously in error, values for successive ranges did not track sufficiently well for his purpose. A possible cause of this problem is that the points of bottom intersection for adjacent rays were slightly inconsistent, and enough to cause a significant jitter in the travel time results. For the model of figure 53, the only problem with adjacent rays is likely to occur when they straddle joints, or when one ray intersects the bottom and the other does not.

The ray tracing part of the new approach is deceptively simple. The most difficult accomplishment to date is the evaluation of the ray theory derivatives. This process involves the implicit differentiation of three simultaneous equations in four variables and at least partially explains why past models have used finite difference methods.

Present plans call for the introduction of this treatment of variable bathymetry into the semicoherent and coherent ray models discussed in sections 5.1.2 and 5.1.3. The method has been used for the analysis of simple cases such as those discussed later in sections 7.2.3 and 7.2.4. However, there are many problems that do not occur for a flat bathymetry and must be solved before an arbitrary piece-wise curvilinear bathymetry can be treated.

There is a formidable bookeeping problem. For the flat bottom and depth-dependent-only sound speed profile, a ray which reflects from the ocean surface and ocean bottom will continue to do so and ray arrival histories can only be designated by the number of loops which are directly related to the number of bottom and surface reflections. For the variable bathymetry, the number of arrival histories is horrendous because the ray may or may not reflect from the surface for any given loop. Indeed, for any given loop, the ray also may reflect zero, once, or a multiple number of times from the curvilinear bottom. The number of distinct ray histories as to surface and bottom reflections could easily be in the hundreds for general bathymetries.

7.2.3 Ray Model of Slope Enhancement

This section discusses controls for the phenomenon of slope enhancement. It is well known that the sound field from a source located above a sloping bottom shows enhancement.

Such an enhancement is illustrated in the upper panel of figure 38, which was introduced in section 5.1.2. Note that the propagation loss for the 18-m source at 20 Hz decreases by about 10 dB at a range of about 750 km where the source is over the steepest part of the slope. Note further that there appears to be little or no enhancement for the 91-m source at 20 Hz or for either the 18 or 91-m source at 140 Hz, as shown in the lower panel of figure 38. Bannister (ref 48) has explained this result in terms of surface decoupling.

74. Tappert, F. D., private communication.

The shallow source at low frequency has a large surface decoupling loss for the low-angle rays which propagate with relatively small loss associated with low grazing angles at the bottom. When this source passes over a slope, steeper-angle rays with a smaller surface decoupling loss can propagate across the bottom with low grazing angles. These steeper angles are changed to less-steep angles by slope conversion. Thus the slope enhancement here is not an enhancement but a decrease in the surface-decoupling loss. Observe in the upper panel of figure 38 that the "enhanced" levels for 18 m still have greater loss than those for the 91-m source. Thus the "enhancement" merely returns levels to values they would have had, had there been no surface decoupling.

Slope enhancement has not been dealt with adequately from a quantitative standpoint. Part of this problem is that reliable experimental data are sparse. Figure 38 is a typical example. There may be only two or three shot measurements for the entire slope. Moreover, models such as ASTRAL have not shown great success in modeling slope enhancement.

In response to this problem, the SEAS program (NORDA 520) funded NOSC in late FY 80 to implement a rigorous ray model for a very simple slope enhancement configuration. Of particular interest is the detailed dependence of propagation loss as a function of the range up the slope, and the dependence of this range pattern on various frequencies.

The bathymetry of figure 38 was too complicated for a first attempt at slope enhancement. To properly model this case would require three segments. The first segment is a flat bottom out to about 430 km. The second segment has a constant slope of about 0.5°. The third segment, starting at a range of about 725 km, is a parabolic section with a maximum slope of about 5°. Apparently, the 0.5° slope is not enough to produce a detectable enhancement, whereas the steeper slopes over the parabolic section produce enhancement at 20 Hz for an 18-m source depth.

In our initial attempt at slope enhancement, the bottom of figure 38 was assumed to be flat at 5100 m depth to a range of 630 km, and then to have a constant slope of -0.03, which corresponds to an angle of 1.7°. This slope was extrapolated to the surface although the bottom contour of figure 38 does not shoal to the surface.

Table 20 presents the model of bottom loss as a function of grazing angle. Linear interpolation was used between tabular values. The same values were used on the flat bottom as well as the slope. The values were assumed to be frequency-independent. For a more realistic model, the bottom loss should vary with frequency and a different table should be used for the flat bottom, as compared with the slope. However, our purpose is to produce a simple test case. Additional refinements can be added in subsequent test cases.

The sound speed profile used in this study is given in table 21, and is a simple bilinear model of the form of equation 63 fitted to the data points of table 21.

The source of the test case is located on the ocean bottom at zero range. Only rays headed up initially at the source are considered. The ray theory described in section 7.2.2 has been implemented; ie, the intersection of rays with the bottom slope is solved exactly. In this case, the juncture depth of figure 53 is taken as the axis of minimum sound speed.

For simplicity, the sound speed at the bottom and at the surface are taken to be identical. Thus we only need to deal with rays which reflect from the ocean surface.

GRAZING ANGLE (deg)	BOTTOM LOSS (dB)
0	0.0
5	3.0
10	5.0
15	7.0
20	8.0
25	8.5
30	9.0
40	10.5
50	12.0
60	12.0
90	12.0

Table 20. Bottom loss table for slope enhancement study.

DEPTH (m)	SOUND SPEED (m/s)
0	1543
1100	1481
5100	1543

Table 21. Sound speed profile for the slope enhancement study.

The ray program is coherent; ie, both phase and amplitude are Interpolated to the desired range point and all arrivals are combined coherently to product propagation loss. The phase computation includes the travel time and a 180° shift at each reflection from the ocean surface. The phase shift at the ocean bottom is assumed to be zero for all angles.

The profile and bottom topography have been stylized to simplify the problem. Our interest is in the first-order effects involved in slope enhancement. In this initial investigation, we are not interested in a detailed depth-dependent sound speed, changes in sound speed profile with range, or minor details in the bathymetry between the source and the toe of the slope. These cause second-order effects. Factors causing first-order effects are frequency, receiver depth, angle of slope, and bottom loss characteristics.

The dashed curve of figure 54a presents the propagation loss for the slope enhancement model for an 18-m receiver at a frequency of 25 Hz. The bathymetric profile is also presented so that the loss pattern can be seen relative to the bathymetry. The solid curve represents the propagation loss for a flat bottom at all ranges. At ranges of less than about 652 km, the dashed curve becomes indistinguisable from the solid curve because all arrivals at shorter range do not intersect the slope.

The difference between the solid curve and the dashed curve represents the slope enhancement. In this example, there is enhancement (with the exception of some narrow gaps) from about 652 to 713 km. Beyond this range, the loss for the sloped bottom is greater than that for the flat bottom. If we ignore the spikes in propagation loss due to the caustics, the largest enhancement is about 13 dB.

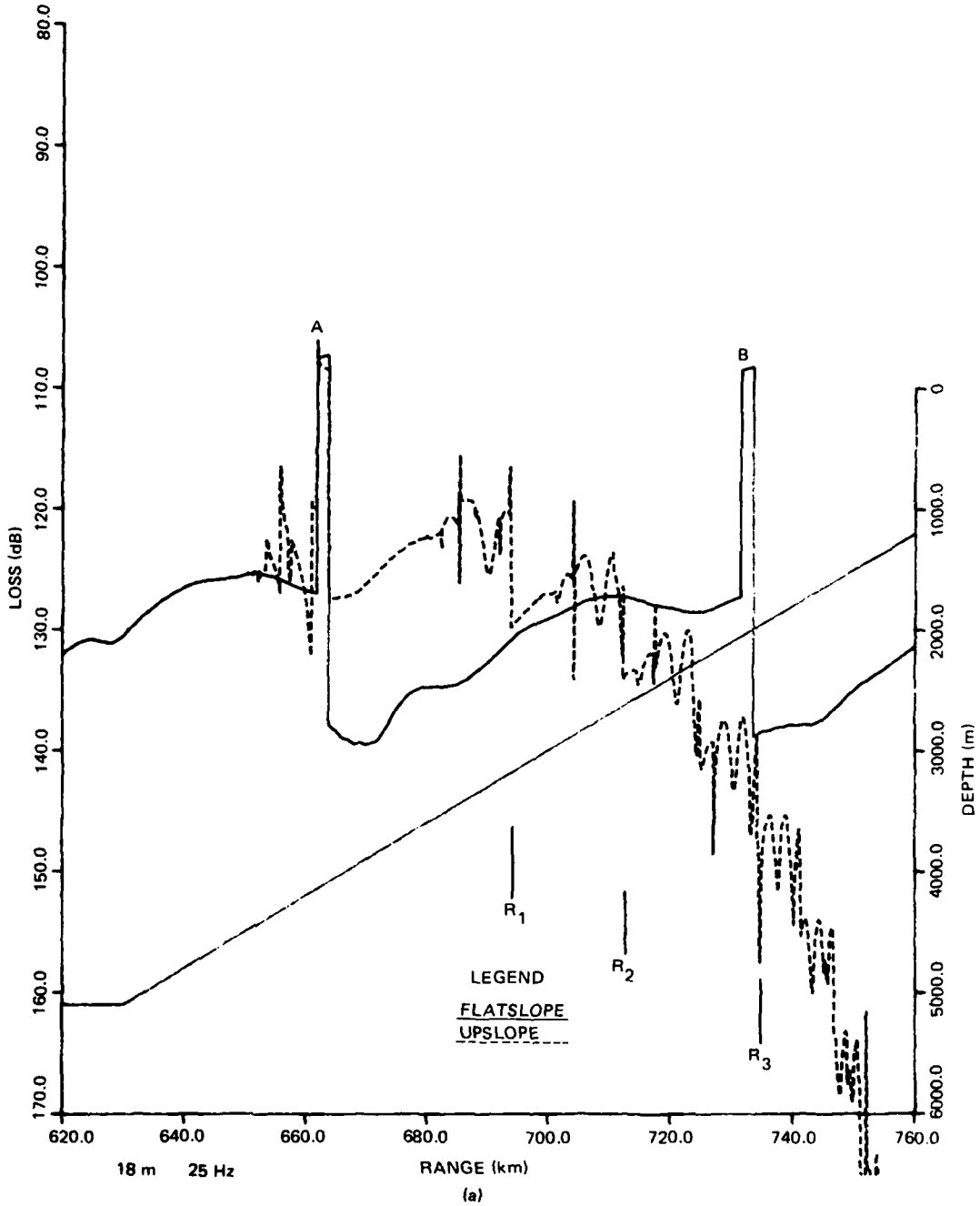

Figure 54a-d. Propagation loss for the slope enhancement model: (a) frequency 25 Hz, receiver depth 18 m: (b) frequency 25 Hz, receiver depth 91 m: (c) frequency 100 Hz, receiver depth 18 m; (d) frequency 100 Hz, receiver depth 91 m.

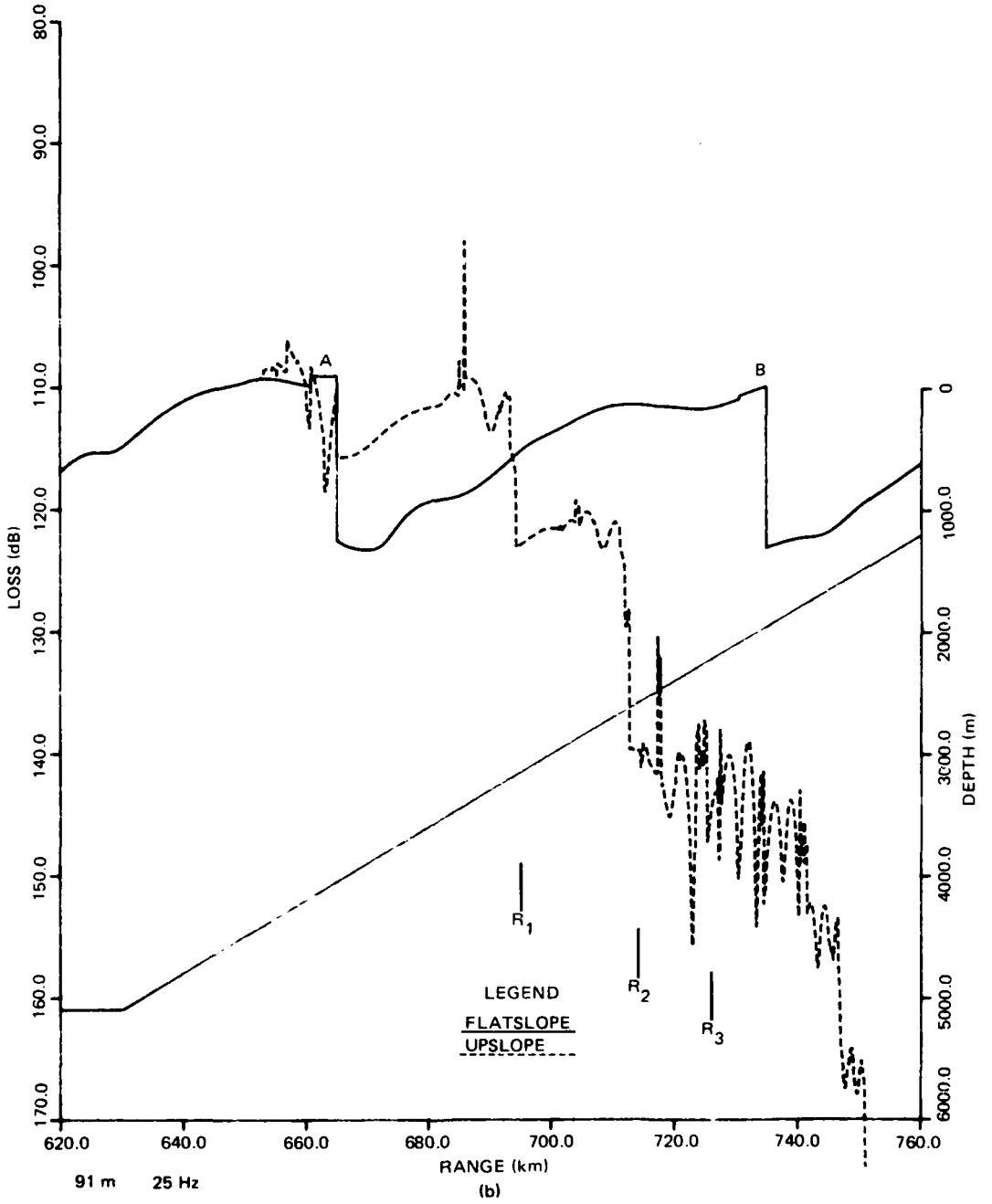

Figure 54. (Continued.)

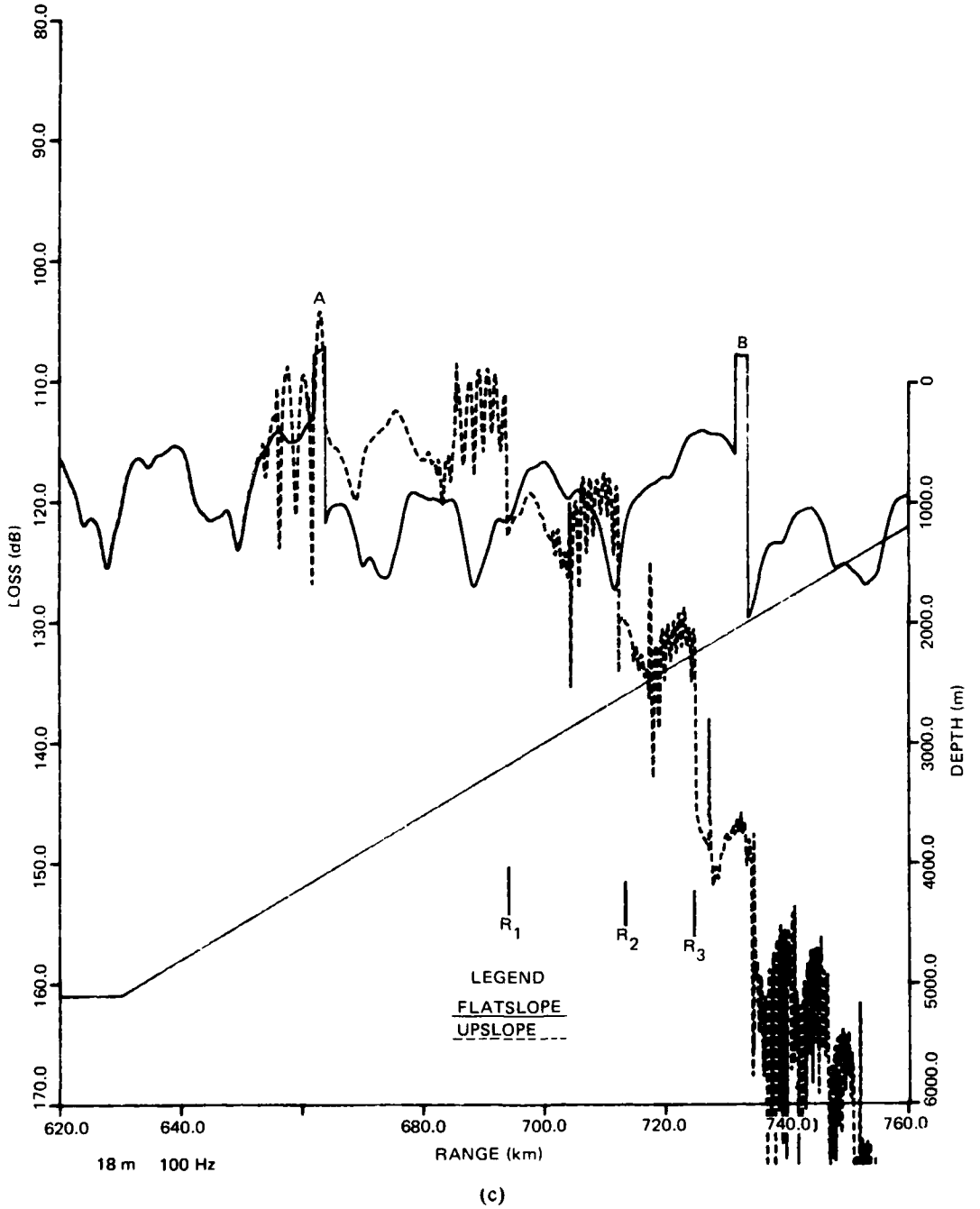

(c)

Figure 54. (Continued.)

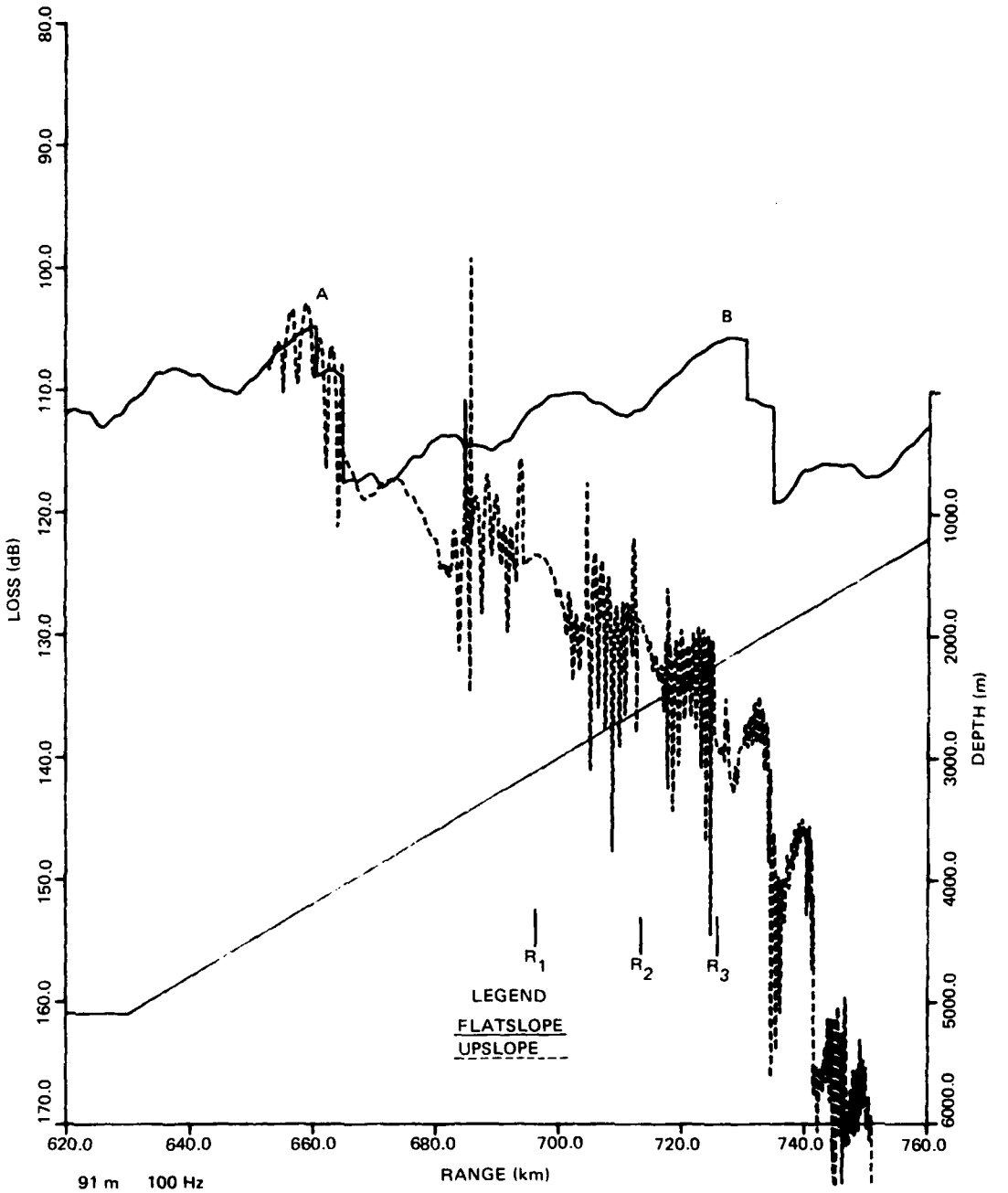

(d)

Figure 54. (Continued.)

The propagation loss structure has not yet been examined in complete detail. However, we have identified some of the salient features. Consider first the solid curve; ie, propagation for a flat bottom. Consider the low-loss pedestal labeled A. The two ranges which bound this pedestal are determined by the zero-degree ray at the source which also grazes the flat bathymetry. The far range of the pedestal occurs where this ray has grazed the bottom eight times after leaving the source and is headed downward at the near-surface receiver. The near range of the pedestal occurs for this same ray but is headed upward at the near-surface receiver. At rays shorter than the pedestal, the upgoing and downgoing ray paths cancel and are subject to the surface decoupling loss. The pedestal itself represents conditions of no decoupling loss because, over this range interval, there is no upward-headed arrival to cancel the dominant downward-headed arrival. At ranges beyond the pedestal, all arrivals must reflect at least nine times from the bottom. The propagation loss increases markedly here because there is one more bottom reflection and because the dominant arrivals are again subject to surface decoupling loss.

The pedestal labeled B is the counterpart of A, but with one more bottom reflection. The general trend of decreasing loss between the far range of pedestal A and the near range of pedestal B is caused by decreasing bottom loss as the bottom grazing angle is approached. Superimposed on this trend is a modulation produced by the coherent addition of ray arrivals.

Consider now the dashed curve of figure 54a. The range marked R_1 represents the range of the ray which has reflected nine times from the flat bottom and just grazes the bottom slope on the way upward from the ninth encounter with the flat bottom. Rays with slightly smaller grazing angle will reflect from the slope and also have ranges less than R_1. However, the surface decoupling loss is less for these rays than for the flat bottom because they form steeper angles at the receiver. This decreased decoupling loss more than affects the increased loss due to a reflection off the slope and the result is "slope enhancement."

We believe that range R_2 represents the range where this slope-grazing ray reflects off the slope once before encountering the receiver. Similarly, R_3 apparently represents the range where this slope-grazing ray reflects off the slope twice before encountering the receiver. The general trend toward increasing loss at ranges beyond R_1 is caused by increased bottom loss due to more reflections from the bottom slope and increased bottom loss due to successive steeper reflection angles off the slope. In this example, the maximum range of slope enhancement appears to be associated with the range R_2. The propagation loss for arrivals which have reflected more than twice off the slope is larger than that for a flat bottom.

Figure 54b is the counterpart of figure 54a but for a receiver depth of 91 m. There appears to be some slope enhancement out to range R_1. However, the propagation loss for arrivals which have reflected more than once off the slope is larger than that for a flat bottom. At a range interval centered at about 680 km, there is an enhancement of about 10 dB.

There are some vestigial remains of pedestals A and B for the flat-bottom evaluation. However, the small jump at the near range of the pedestals suggests that the surface decoupling effect is not nearly as important as for the shallow receiver in figure 54a. Note that the enhanced values at 680 km do not rise above the flat-bottom values just before pedestal A. Thus it is unlikely that any slope enhancement would be discerned in experimental data because the levels to not rise above shorter-range signals for a flat bottom as they do in figure 54a.

Figure 54c is the counterpart of figure 54a, but for a frequency of 100 Hz. Again, there appears to be some slope enhancement out to range R_1. However, the enhanced levels do not rise significantly above the general level of propagation loss for the flat bottom, and so would not likely be discerned in experimental data. The jump at the near range of pedestals A and B indicates that the surface decoupling plays a contributing role here. Note that the multipath phasing effects are much more pronounced at 100 Hz than at 25 Hz. The propagation losses of figure 54c display a much more rapid beat structure than in figure 54a or b. This is particularly true of the upslope result at ranges just short of R_1 and R_2, where reflection from the slope produces more multipaths than for the flat-bottom case.

Figure 54d is the counterpart of figure 54b for a frequency of 100 Hz. There is little evidence of slope enhancement here.

The results of figures 54a to d are in general qualitative agreement with the experimental results of figure 38. The greatest amount of slope enhancement is predicted for the shallow receiver at low frequency. This result and figure 54d confirms Bannister's (ref 48) conjecture that surface decoupling can play a major role in slope enhancement. Figure 54d has essentially no surface decoupling effect and also shows little evidence of slope enhancement.

Before leaving figures 54a to d, note that the general level of propagation losses for the flat-bottom case clearly shows the effect of surface decoupling. These levels are about 130 dB for figure 54a, 115 dB for figure 54b, 120 dB for figure 55c, and 110 dB for figure 54d. These results agree with the characteristic that the surface decoupling loss increases with increasing frequency and increasing receiver depth.

Figures 54a–d represent only the initial results of our investigation of slope enhancement with the model of section 7.2.2 We have been sponsored by TAEAS (NORDA Code 530) in FY 1982 to evaluate the critical parameters of slope enhancement. Present plans are to examine a variety of other parameters besides frequency and receiver depth. These include source depth, different slopes or bathymetric contours, and different bottom-loss characteristics. We have also determined that the relationship of the range of the bottom-grazing ray to the toe of the slope plays a role in the enhancement. If the ray reflects from the flat bottom near the toe, the result is quite different from when the ray reflects from the flat bottom a half-loop length before the toe of the slope. We expect that in some cases the surface decoupling mechanism will not play a critical role. The other conditions should provide other sets of control cases. The important thing is to have test cases which contain all the significant factors in slope enhancement.

Slope enhancement clearly represents an area where the models should be compared with theoretical test cases rather than comparison with experiment. Experimental data based on a sparse sampling of shots are inadequate. Moreover, the complication of multiple mechanisms makes a model evaluation based on experiment very difficult. In contrast with the theoretical test cases, each factor can be evaluated separately as well as in combination. Ultimately, we want to test models against experimental data. However these data need to be of much higher quality than presently available. High-density CW measurements rather than shots should be taken and the environment (sound speed, bathymetry, and bottom loss) should be measured as accurately as possible.

Before closing this section, we note belatedly that in the theoretical ray model we always make the source the fixed element with respect to the bathymetry while the range is calculated to a moving receiver depth. This configuration is the reciprocal of the usual experimental setup where the receiver is fixed while the source moves in range. This brings us next to the topic of reciprocity.

7.2.4 Reciprocity Considerations

For many cases of experimental interest, the receiver is fixed or relatively fixed while the source is moving. When there is a range-dependent environment, this configuration is very time-consuming to model directly. The reason is that, for each range point where output is desired, the description of the environment must be translated since the source moves with respect to the fixed environment. A standard procedure is to evaluate the field by making the source the fixed element and the receiver the moving element. One then applies the classic reciprocity formula

$$I_{mov} = I_{fix} (C_s/C_h)^2 \tag{67}$$

where I_{mov} is the intensity for the moving source, I_{fix} is the intensity for a fixed source and moving receiver, C_s is the sound speed at the moving source, and C_h is the sound speed at the fixed receiver.

Equation 67 is easily derived for a range-dependent environment from simple ray theory considerations.

During the development of the rigorous ray theory described in section 7.2.2 and the evaluations of section 7.2.3, we saw that there was an opportunity to verify directly whether equation 67 held for a range-dependent bathymetry. Our initial results suggested that equation 67 did not hold under these conditions.

This possibility was suggested at the Parabolic Equation Workshop, held at NORDA from 31 March to 3 April 1981, and created quite a controversy. Several participants cited various proofs that equation 67 also held for range-dependent environments, whereas D. Thomson of DREP cited reference 75 as demonstrating the contrary.

There was a suggestion by C. Spofford of SAI that we compare numerical results for reciprocal configurations of a simple geometry. We then devised a simple test case. Figure 55a presents the first geometry, while figure 55b presents the second (reciprocal?) geometry. The intensity from point 1 to point 2 of figure 55a was calculated from

$$I_1 = \frac{\cot\theta_1 \cot\theta_2}{C_{m1}\left|\frac{\partial R}{\partial C_{m1}}\right|_R} \frac{C_{m2}}{C_{m1}} \tag{68}$$

where C_{m1} and C_{m2} are the phase velocities before and after reflection, respectively. The intensity from point 2 to point 1 of figure 55b was calculated from

$$I_2 = \frac{\cot\theta_1 \cot\theta_2}{C_{m2}\left|\frac{\partial R}{\partial C_{m2}}\right|_R} \frac{C_{m1}}{C_{m2}} \quad . \tag{69}$$

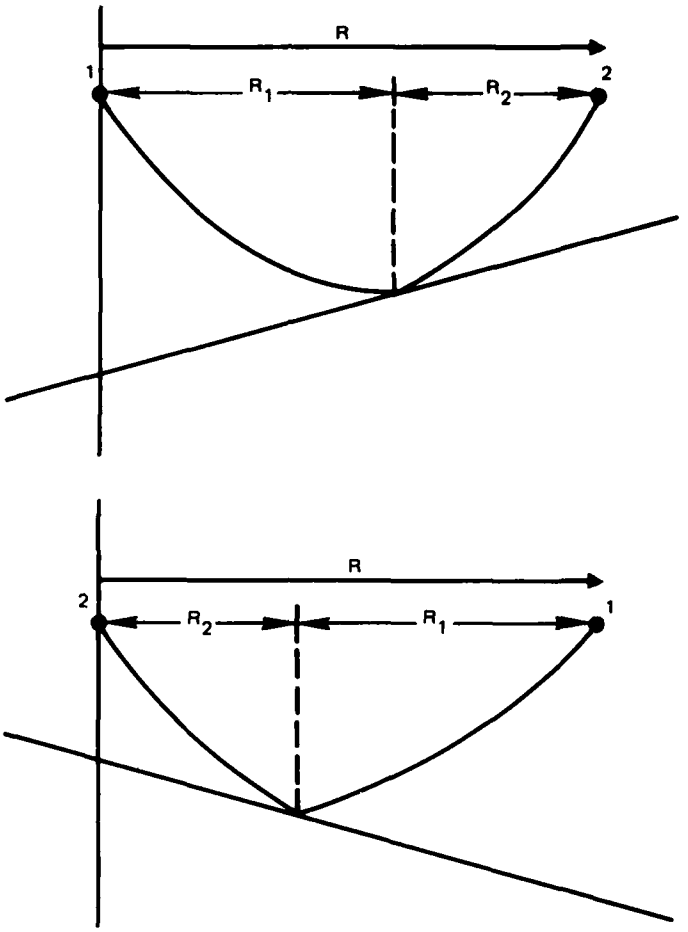

Figure 55a-b. Schematics illustrating a numerical reciprocity test: (a) upslope configuration; (b) reciprocal configuration.

Examination of the numerical results showed that

$$I_2 = I_1 (C_{m1}/C_{m2}) \tag{70}$$

and that

$$\frac{\partial R}{\partial C_{m2}} = \left(\frac{C_{m1}}{C_{m2}}\right)^2 \frac{\partial R}{\partial C_{m1}} \quad . \tag{71}$$

In addition, both $\partial R/\partial C_{m1}$ and $\partial R/\partial C_{m2}$ were independently checked by use of finite differences for adjacent ray parameters, ie, by $\Delta R/\Delta C_m$. Equations 70 and 71 were satisfied to five significant digits.

Equation 70 follows immediately from equations 68, 69, and 71. Our effort was then turned to a proof of equation 71 for the detailed theory outlined in section 7.2.2. With considerable effort, we were able to demonstrate that equation 72 held for this simple case. Furthermore, we could demonstrate that it also held for source and receiver at different depths and that the proof could be readily extended to arbitrary sound speed profile models and bottom profile models. The extension of the proof to muitiple reflections from the bottom was abandoned because it was incredibly difficult and involved. However, it was verified numerically for a two-bottom reflection version of figures 55a and b.

This work suggested that the generalization of equation 71 for the multiple bounce case was

$$\frac{\partial R}{\partial C_{mn}} \equiv \frac{\partial R}{\partial C_{mh}} = \left(\frac{C_{m1}}{C_{m2}}\right)^2 \left(\frac{C_{m2}}{C_{m3}}\right)^2 \cdots \left(\frac{C_{mn-1}}{C_{mn}}\right)^2 \frac{\partial R}{\partial C_{m1}} \equiv \left(\frac{C_{ms}}{C_{mh}}\right)^2 \frac{\partial R}{\partial C_{ms}} \tag{72}$$

where C_{ms} and C_{mh} are the phase velocities at source and receiver, respectively. Equation 72 holds for multiple reflections from any bottom profile and for any sound speed profile which depends only on depth.

Given the result of equation 72, it immediately follows that

$$I_{mov} = I_{fix}\left(\frac{C_s}{C_h}\right)^2 \frac{C_{mh}}{C_{ms}} \quad . \tag{73}$$

Equation 62 differs from the classic reciprocity result of equation 67 by the factor C_{mh}/C_{ms}. For single reflections, this term is less than 0.1 dB for typical continental slopes of -4° and 0.5 dB for typical volcanic seamount slopes of -14°. However, for multiple reflections it can build up to a substantial amount. The extreme case is for the vertical ray for a source above the slope. Here, C_{ms} is infinity and I_{mov} goes to zero.

Meanwhile, we obtained a copy of reference 75 and found that it investigated reciprocity from the standpoint of a differential equation approach to ray intensity. Reference 75 demonstrates that equation 67 does not hold for the case of a sloping bottom, but it does not give a simple answer as to what the relationship should be. We apprised MacKinnon of our results (ie, equations 72 and 73). Given the form of our result, he readily demonstrated that equations 72 and 73 held for multiple bottom reflections (reference 76).

Thus we were faced with a contradiction. Is the classic reciprocity relationship of equation 67 correct or is that of equation 73 correct? The answer to this dilemma was provided by Spofford (ref 77), who noted that our examples of figures 55a and 55b do not have the same environment in both directions. Equations 68 and 69 assume implicitly

75. MacKinnon, R. F., and M. Nell, Some Results on Ray-Acoustic Intensity Calculations, Defense Research Establishment Pacific technical memo 75-4, May 1975.
76. MacKinnon, R. F., private communication, May 1981.
77. Spofford, C., private communication, June 1981.

cylindrical symmetry about the source point. One must look at the three-dimensional environment of this assumption. This environment for figure 55a is an inverted cone with the source located above the apex and the bottom contour rising in all radial directions. However, the environment for figure 55b is an upright cone with the source located above the apex and the bottom contour falling in all radial directions. These are obviously not the same environment.

Furthermore, Spofford (ref 77) states that the classical reciprocity relationship of equation 67 holds. He believes that when the reciprocal formulation of equation 69 is corrected for symmetry about the receiver rather than about the source, this formulation, together with equation 72, will lead to equation 67. The exact form of this correction has not been established for the point source, and should be done so by someone well versed in the intricacies of three-dimensional ray theory.

However, at the suggestion of Dr. H. P. Bucker of NOSC, we have looked at a simpler problem which avoids the complication of a three-dimensional medium. Consider element 1 and 2 of figures 55a and 55b to be a line source and line receiver in a Cartesian coordinate system R, Z, y where the line source and receiver extend out of the plane of figure 55 in the direction y. The bottom is a planar surface in the y direction. The sound speed depends only on Z. Reasons for choosing this configuration are that the environment is now reciprocal and we do not have to deal with the coordinate y.

If we look at the geometry of a line source and line receiver for a flat bottom, we find that the intensity from point 1 to point 2 is

$$I_1 = \frac{1}{\left|\frac{\partial R}{\partial \theta_1}\right| \sin \theta_2} \tag{74}$$

and from point 2 to point 1 is

$$I_2 = \frac{1}{\left|\frac{\partial R}{\partial \theta_2}\right| \sin \theta_1} \tag{75}$$

The equivalents to these in terms of phase velocity when there are nonflat bottom reflections are

$$I_1 = \frac{\cot \theta_1 \cot \theta_2}{C_{m1}\left|\frac{\partial R}{\partial C_{m1}}\right|}\left(\frac{C_{m2}}{C_2}\right) \tag{76}$$

and

$$I_2 = \frac{\cot \theta_2 \cot \theta_1}{C_{m2}\left|\frac{\partial R}{\partial C_{m2}}\right|}\left(\frac{C_{m1}}{C_1}\right) \tag{77}$$

Thus from equations 76 and 77, it follows that

$$I_2 = I_1 \left(\frac{C_2}{C_1}\right)\left(\frac{C_{m1}}{C_{m2}}\right)^2 \frac{\partial R}{|\partial C_{m1}|} \Big/ \frac{\partial R}{|\partial C_{m2}|} \quad . \tag{78}$$

For the case of a flat bottom, $C_{m1} = C_{m2}$ and equation 78 clearly reduces to

$$I_{mov} = I_{fix}\,(C_s/C_h) \tag{79}$$

where the source is the moving element. However, if we substitute equation 72, which must hold for profiles with Z-dependence only, into equation 78 we find that the sloping bottom case also reduces to equation 79. The result is the same for the inclined plane as for the flat plane. Thus classical reciprocity holds for this case and Spofford (ref 77) appears to be correct in resolving our apparent contradiction to reciprocity. Spofford is also correct in "believing that equation 72 is probably correct." Indeed, equation 72 must hold for classical reciprocity to apply for the Cartesian problem just posed. There remains some question as to why the ratio (C_s/C_h) appears in equation 79 rather than the classical ratio $(C_s/C_h)^2$. We believe this to be a difference between the line source and point source formulation.

Thus it would appear that classical reciprocity holds for variable bathymetry. However, the modeling community is "not out of the woods yet." As Spofford points out, this investigation has raised questions as to the description of the azimuthal component of the bottom. Most propagation models (ray trace, PE, normal modes, etc) all assume radial symmetry about the source. This assumption may be very unrealistic when one critically examines the consequences for high-angle rays.

Consider, for example, the three-dimensional formulation of figure 55b with the source located above the apex of a cone. We believe that the ray intensity for $\theta_s = 90°$ is zero because this single ray is "split" into all azimuthal directions. However, for the three-dimensional formulation of figure 55a with the source located above the apex of an inverted cone, we believe that the ray intensity for $\theta_h = 90°$ is very large. This configuration needs to be investigated in detail. For steeper source angles, the ray will travel in the negative R direction after the last reflection; ie, $\theta_h > 90°$. A relative maximum in range is likely to be formed somewhere near the $\theta_h = 90°$ ray. However, we need more experience with rays traveling in the negative range direction before we know how caustics are formed for this configuration.

We recommend that some test cases be prepared which adequately address symmetry about the receiver, as compared with symmetry about the source. It is small comfort to know that classical reciprocity holds when models do not take into account the proper symmetry for the bottom contour. With some additional work, it would appear that ray formulations can be made. However, the problem of bottom symmetry about the receiver rather than the source will not be so easily treated for normal mode or PE models.

We hope that some of the remaining problems with reciprocity for a range-dependent bottom will be resolved and that the entire subject will be dealt with in future publications. We plan to publish our initial derivation of equation 71 and encourage MacKinnon (ref 76) and Spofford (ref 77) to publish their contributions as well.

7.2.5 Propagation Over a Sloping Bottom

This section describes some investigations of propagation over a sloping bottom by using a variety of wave theory approaches. These investigations suggest several test cases.

The work of reference 64 serves as a convenient starting place. Bradley presents an exact normal mode solution for a wedge-shaped duct in an isospeed water layer overlying a rigid bottom of constant slope. The solution involves the evaluation of an integral. The solution is split up into five cases corresponding to various asymptotic expansions for the Bessel and Hankel functions appearing in the integral. These correspond to five different physical regimes determined by the geometry of the source and receiver relative to each other and to the shoreline. Only the first term of the asymptotic expansions is used in the solution. Reference 64 does not present examples of the detailed evaluation of the modal field containing phasing effects. The examples employ methods which average out the range and angular fine structure, leaving a relatively simple dependence on range.

It is important to note here that Bradley does not assume radial symmetry of the bottom; ie, the bottom surface is not a cone but a plane. Thus this is a three-dimensional problem in which cross slope as well as up- or down-slope propagation is addressed.

Reference 78 applies an adiabatic approximation, which ignores mode coupling, to this wedge problem and compares the results of this approximation to the exact result of reference 64. Slopes of 0.01 and 0.2 (angles of 35' and 11°19') were examined. Graves concludes that the role of mode coupling appears only moderately significant even for the larger wedge angle cited.

Reference 70 applies the adiabatic approximation to a normal mode approach which allows the sound speed to vary in depth and range. This method was also applied to a depth-dependent sound speed profile and to a range-varying bathymetric profile corresponding to experimental conditions. At longer ranges, the experimental results showed losses considerably in excess of theoretical calculations. This discrepancy is attributed to the effect of mode coupling, which is ignored in the adiabatic approximation.

Reference 79 provides a very thorough treatment of coupled mode theory. Rutherford's chief concern is the application of coupled mode theory to the problem of variable boundaries, as contrasted with the application to range-dependent sound speed profiles by earlier investigators. He provides a very detailed analysis of the wedge-shaped ocean; ie, an isospeed water layer overlying a rigid bottom of constant slope. This work is also presented in reference 80, which is more readily available than reference 79. He concludes that the conventional theory of coupled normal modes developed for range-dependent sound speed profiles involves approximations which are inconsistent when applied to conditions of a range-dependent bottom profile. Furthermore, he develops first-order corrections to the conventional theory which are applicable to the range-dependent bottom profile. Rutherford compares results of adiabatic mode theory with conventional coupled mode theory as well as a coupled mode theory with first-order corrections. His results for

78. Graves, R. D., et al, Range-Dependent Normal Modes in Underwater Sound Propagation: Application to the Wedge-Shaped Ocean, J Acoust Soc Am 58, 1171-1177, Dec 1975.
79. Rutherford, S. R., An Examination of Coupled Mode Theory as Applied to Underwater Sound Propagation, Applied Research Laboratory TR 79-44, July 1979.
80. Rutherford, S. R., and K. E. Hawker, Consistent Coupled Mode Theory of Sound Propagation for a Class of Nonseparable Problems, J Acoust Soc Am 70, 554-564, Aug 1981.

a slope angle of 2.5° show reasonable agreement between adiabatic and corrected coupled mode theory. However, there does appear to be a serious problem with conventional coupled mode theory.

Reference 81 presents some interesting comparisons among various propagation models over a sloping bottom. Figure 56 is a schematic of the environmental profile. The water column is isospeed. However, the bottom is not rigid; it is an isospeed liquid half-space with a constant density and depth-independent absorption coefficient. Computations were made at 25 Hz for the SNAP normal mode model, which is based on the adiabatic approximation, and the PAREQ model, which is based on the parabolic equation method. Agreement between the methods was good for a 0.85° slope in both upslope and downslope configurations but not for the 8.5° slope. For the configuration of figure 56 at ranges beyond about 15 km, the SNAP losses were consistently high by about 7 dB. For a downslope configuration, the mean levels beyond about 15 km were in agreement with the PAREQ result, which oscillated about the SNAP result. Reference 81 attributes the differences to the fact that SNAP does not take into account mode coupling, whereas PAREQ does.

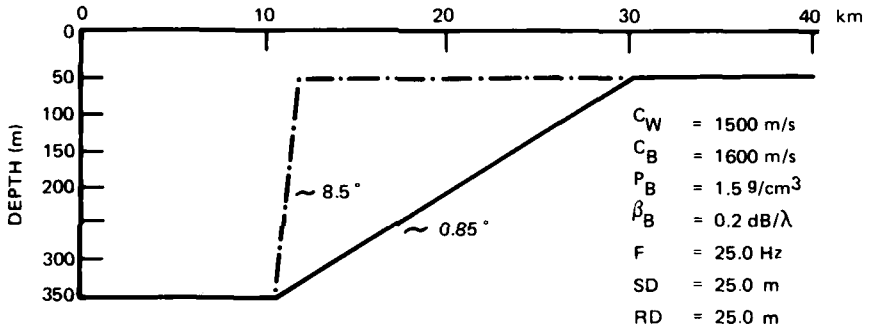

Figure 56. Upslope environmental model.

These results are also presented in reference 82, which compares them to the results of an implicit finite-difference (IFD) method. This method is an improvement to the standard PE method and uses a split-step Fourier algorithm. It has various advantages over PE, as discussed in reference 82. The PAREQ and IFD results for this problem are quite similar. Note that the upslope and downslope configurations of references 81 and 82 are reciprocal for the case of 0.85° slope. However, they are not reciprocal for the 8.5° slope. In the reciprocal case of figure 56, the toe of the slope is 30 km away from the source, whereas in the downslope case of references 81 and 82, the toe of the slope is slightly in excess of 10 km from the source. This aspect appears to have been overlooked and may be part of the reason that the upslope and downslope results are different.

81. Jensen, F., and W. A. Kuperman, Environmental Acoustical Modeling at Saclantcen, Saclantcen report SR-34, Nov 1979.

82. Lee, D. L., et al, Finite-Difference Solution to the Parabolic Wave Equation, J Acoust Soc Am 70, 795-800, Sep 1981.

Reference 81 also presents a propagation loss contour plot for the 0.85° slope of figure 56 determined by PAREQ. Of greatest interest are the contours which illustrate how energy penetrates into the bottom. These contours clearly demonstrate that energy propagating upslope does not leak into the bottom more or less monotonically with range. Rather, the penetration of energy into the upsloping bottom is characterized by patterns resembling beams. These beams appear to originate from positions that correspond, at least approximately, to those ranges for which the bathymetry shoals to the various mode cutoff depths. The first such beam is related to the cutoff depth of the highest-order mode, the second beam corresponds to the next-highest-order mode, and so on. This problem is significant to the underwater acoustics community from the standpoint of understanding the mechanism of upslope propagation for a lossy bottom. The results themselves are of more concern to the seismic community, which has an understandably keen interest in the coupling of waterborne energy into the Continental Shelf and vice versa.

Figure 57 presents a sloping bottom environment, which was test problem IV for the PE workshop held at NORDA on March 31-April 3, 1981. This problem appears similar to that of figure 56, but with some important differences. The acoustic frequency of both studies was 25 Hz. However, figure 57 represents a deep-water case while figure 56 is for shallow water. The sound speed of problem IV was depth-dependent. The bottom consisted of a liquid-absorbing sediment layer overlying a semi-infinite basement. The sound speed of this sediment layer was both range and depth-dependent.

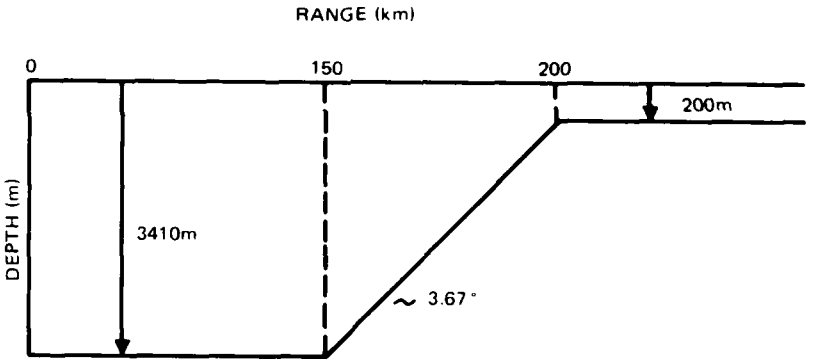

Figure 57. Schematic of the bathymetric profile for test problem IV of the PE Workshop.

Various implementations of PE were compared with each other. The results of these comparisons will be published in a Workshop Proceedings. White (ref 83) has compared these various implementations and his impression is that there is good agreement for the flat bottom regime, but there are also distinct differences once the full impact of the slope is felt. The adiabatic normal mode model, SNAP, of reference 81 has also been applied, but we must wait for the Proceedings to determine the agreement with the various PE implementations.

Before we make comments about the PE Workshop as it pertains to control models, we should set the Workshop goals in better perspective. First of all, the test problems were

83. White, D., private communication.

not intended to be controls in our sense. The test problems were to serve as a basis for comparison between a plethora of computer implementations of the parabolic equation and the idea of deriving a "state-of-the-art" model by combining attributes of the most promising of the PE models. One of the objectives of the workshop was to identify range-dependent environmental problems that could provide a set of benchmark test cases. We hope here to outline some test cases which will more than just test implementations of PE. Hopefully, our test case would help determine the inherent limitations of the PE as a general method.

The model of figure 57 was a good choice for comparing PE models. It contains range variability in the sound speed profiles, bathymetry, and bottom properties, and is designed to simulate a realistic ocean condition. However, it is this very complication which makes it premature as a test case in our sense.

One of the drawbacks of Workshop Problem IV was that there was no standard against which to judge the various PE implementations. Over the flat "bathymetry", good agreement was generally obtained between the PE implementations and between them and several normal mode approaches. However, what is "ground truth" in the slope region of figure 57? Does the best implementation of PE provide an accurate solution to this problem? The slope of 3.67° in figure 57 is close to a 4° slope, which is regarded as typical of continental shelves. What about a slope of 14°, typical of volcanic seamounts? Moreover, the problem involves not just the slope itself, but also the number of bottom reflections of significant arrivals, since the ray angle steepens by twice the bottom slope on each successive reflection. Concern is not limited to the effects of a shrinking channel, but the larger number of bottom interactions may also create some strain on adiabatic assumptions. From the standpoint of accuracy, which is better: PE or an adiabatic normal mode implementation? What about coupled mode theory? The work of reference 79 suggests that for range-dependent boundaries, adiabatic methods may be more accurate than conventional coupled methods. The model of figure 57 appears too complicated to address these questions properly.

What we suggest is the investigation of a number of successively more complicated controls. Whenever possible, the following models should be tested: "exact" solution, adiabatic mode theory, conventional coupled mode theory, coupled mode theory with corrections for variable boundary conditions, various implementations of the parabolic equation, and various ray theories. As the controls became more complicated, the "exact" solution may become more elusive. However, it is to be hoped that investigation of the simpler models will reveal secondary standards which can serve as reasonable ground truth for more complicated controls.

The wedge-shaped duct in an isospeed water layer overlying a rigid bottom of constant slope appears to be the simplest control environment. What appears desirable is a comparison of the results of the "exact" method of reference 64 with the various solutions of reference 80, which compares different approximations to each other but not against a rigorous standard. As we have seen, there are many studies available which cannot be readily compared because the conditions are different. For example, reference 78 addresses slopes of 35′ and 11°19′, while reference 80 addresses a slope of 2.5°. Moreover, the model of reference 80 assumes cylindrical symmetry (or a conical bottom), whereas the model of reference 64 is for a planar bottom. Furthermore, references 64 and 78 address downslope propagation, whereas reference 80 considers upslope propagation. Reference 64 also contains a ray theory solution. Thus comparisons of various ray theories and various mode

theories could be made. The original implementations of the PE model would not treat a rigid bottom. However, other implementations may be able to do so.

The next more complicated control environment is that of figure 56. This may not have an exact solution, but a wedge-shaped version may have. Since the problems encountered in shallow water may be entirely different than in deep water, a deep-water version is also recommended. The geometry of figure 57 appears suitable, but with isospeed water and bottom layers.

A systematic comparison between the results of various methods as a function of bottom slope and frequency should be made to establish a better feel for the conditions under which the various approaches are valid. These methods could be better or even worse than we estimate on the basis of various approximations. For example, our experience with ray theory is that it compares much better with normal mode theory than one predicts on the basis of approximations.

It would also be advisable to determine configurations which lead to a large slope enhancement and to test the various methods to determine whether they exhibit the correct response. As we have discussed in section 7.2.3, many receiver and frequency combinations display no or only a miniscule enhancement. Good comparisons between methods must be achieved for conditions in which the slope has a significant effect and does not merely produce a prosaic perturbation of the acoustic field.

Once secondary controls have been established with some feel for valid frequency and slope regimes, the control environment should be extended to the more complicated case such as test problem IV, with depth-dependent sound speeds in water and sediment and range-dependent properties in the sediment. It may be advisable to do this in several steps so as to evaluate potential difficulties separately. There are so many different factors involved that the reason for differences between various approaches would be difficult to determine unless the factors were tested separately.

A somewhat more difficult problem than the sloping bottom is propagation over a seamount or ridge. This topic has received enough consideration to warrant a special session and panel discussion of the Acoustical Society of America (ref 84). This problem could obviously profit from a series of control cases, but a specification of such cases appears premature at this time.

8.0 ADDITIONAL CONSIDERATIONS OF IMPORTANCE

This section presents various other areas where controls are necessary or useful. For the most part, these areas are only outlined, as a detailed treatment is beyond the scope of this report, which has been concerned mainly with test cases for the numerical evaluation of propagation loss. Section 8.1 points out desirable features of a good propagation model, which go well beyond propagation loss per se. Section 8.2 outlines propagation approaches in addition to the normal mode or ray theory approaches which have been the primary concern of this report. Section 8.3 outlines other models which may not fall under the classification of propagation but are closely related and are necessary from the standpoint of underwater acoustics.

84. Ebbeson, G. R., and H. Medwin, chairmen: Topographical Effects on Ocean Propagation, supplement 1, 69, S58-S60, spring 1981.

8.1 DESIRABLE PROPERTIES OF PROPAGATION MODELS

This section was originally prepared as an explanation of why such large effort has gone into modeling and why there are so many models in existence. It answers the question of why we cannot have one perfect model that does everything. However, it also serves as a guide to other factors which may profit from control cases.

8.1.1 General Requirements

1. Reasonable accuracy within some prescribed limits.
2. Fast program execution time or low cost.
3. Small program length and low storage requirements.
4. Varying degrees of automation of inputs, programs, and outputs.
5. Default provisions when input data are missing.
6. Interaction with operator.
7. Provision of new insights into the physical principles of propagation.
8. Accuracy sufficient to serve as a test case against which other models may be compared.
9. Notification to the operator when the model is being misapplied or the outputs are of questionable accuracy.
10. No arbitrary and significant changes to inputs to accommodate special algorithms.
11. Outputs verifiable with experimental data.
12. Adequate documentation.

This outline of general requirements is, for the most part, self-explanatory. This report has only addressed item 1. The remainder of the list does not require controls in our sense.

8.1.2 Inputs Treated

1. Dependence of sound speed on range.
2. Dependence of sound speed on three dimensions.
3. Sound speed modification for Earth's curvature.
4. Sound speed microstructure.
5. Internal waves.
6. Surface scattering or environmental inputs to evaluate same.
7. Temperature dependence of absorption at high frequencies.
8. Dependence of bathymetry on range.
9. Dependence of bathymetry on three dimensions.
10. Bathymetric microstructure.
11. Complex bottom reflection coefficients (bottom loss and phase shift).
12. Compressional sound speed, gradients, and absorption in sub-bottom.

13. Shear sound speed, gradients, and absorption in sub-bottom.
14. Density structure in sub-bottom.
15. Frequency.
16. Near-surface sources.
17. Near-bottom sources.
18. Moving sources (applies proper reciprocity relations).
19. Directional sources.
20. Transient sources.
21. Broadband sources.
22. Distributed (multipole) sources.
23. Confidence limits on inputs.

The input requirements on this outline do require controls. It is not adequate to determine that a model merely accepts or even requires these inputs. One must determine that the model treats the inputs properly rather than superficially. Most of these inputs have been already addressed in controls already presented. There are a few exceptions.

Item 3 relates to taking the effect of the Earth's curvature into account in propagation problems. The simplest approach is to modify the sound speed observations to correct for the Earth's sphericity and then use these modified sound speeds in the approach for a flat Earth. It is a fairly easy matter to prepare a test case to assure that a computer routine modifies the profiles correctly. The effect of the Earth's curvature is not trivial. It shortens convergence zone ranges by about 1% and can also have a significant effect on depth excess under conditions which are close to bottom limiting. In using a propagation program, one needs to know whether to input raw or modified sound speeds since some propagation programs treat this problem internally, either by profile modification methods or by some other method. A number of years ago, we had occasion to compare our ray theory results with corresponding results of FNWC for the same observed profile. We found that our group velocities (R/T) were consistently higher than the FNWC results. We found that whereas our method of modifying profiles gives ranges projected on the ocean surface, the FNWC model was giving ranges projected on the axis of the deep sound channel because of the manner in which the Earth's sphericity was treated.

Items 4, 5, and 10 are primarily inputs to statistical models of propagation loss, which are not addressed in this report.

Item 7 applies to higher frequencies roughly from 10 to 24 kHz. Here, the predominant loss mechanism is absorption in the water. Ray programs for these frequencies must evaluate the attenuation loss layer by layer since this loss depends strongly on temperature.

Item 23 is a recommendation for future models, although it might be difficult to implement. The idea is to place confidence limits on all environmental inputs, with the model making use of them as well as the mean values.

8.1.3 Output Requirements

1. Incoherent propagation loss.
2. Coherent propagation loss.
3. Phase of the resultant pressure.
4. Travel time structure of multipaths.
5. Phase relationship between multipaths.
6. Vertical arrival structure of multipaths.
7. Horizontal arrival structure of multipaths.
8. Doppler shifts for moving source, moving receiver, ocean currents, or ocean surface.
9. Dispersion (group velocity as a function of frequency).
10. Spatial coherence.
11. Temporal coherence.
12. Null points for multipath propagation.
13. Complex reflection coefficients at ocean bottom (when not given as an input).
14. Evaluation for multiple receiver depths.
15. Evaluation for near-surface receivers.
16. Evaluation for near-bottom receivers.
17. Evaluation for unevenly spaced range points.
18. Detailed evaluations for long-range window.
19. Evaluation to some maximum range.
20. Evaluation to some minimum range.
21. Evaluation for some maximum frequency.
22. Evaluation for some minimum frequency.
23. Evaluation of multiple frequencies.
24. Special plotting routines such as contouring amplitude and phase.
25. Confidence limits on outputs.
26. Corrections of echo-sounder depths to true bottom depth.
27. Statistical properties of propagation loss.
28. Scattering coefficients.

Some of these output requirements have been alluded to before. A number of others do not require further explanation. Those that may follow.

Item 12 refers to the fact that when contours of propagation loss are made in the range receiver plane, it is found that there are points where the intensity goes to zero. The contours of phase show a nonlinear behavior. Such contours are shown in figures 10 and 11

of reference 85. At this stage, there is no consensus as to the importance of this phenomenon. In the future, this output may be an important requirement.

Items 17 to 23 point up some output requirements that may exclude certain approaches or make them prohibitively expensive. In item 17, for example, some approaches require regular spacing of range or depth increments, whereas the problem of a drooping "horizontal" hydrophone array requires irregular spacing.

Item 18 refers to an advantage of the normal mode approach as compared to other approaches. One can evaluate the field in detail over some long-range window without having to make calculations at shorter ranges. For example, the PE method has to creep out from zero range even though our interest is only in some long-range segment.

Items 19 and 20 refer to range limitations on some models. Some models are too expensive to operate to the extremely long ranges. Other models such as normal modes cannot be used to evaluate fields at very close ranges because the solutions diverge.

Items 21 and 22 refer to frequency limitations. Typically, ray models work well at higher frequencies, whereas normal mode models work well at lower frequencies.

Item 25 is the output counterpart of item 23 of outline 8.1.2. Rather than a single output, it would be desirable to have confidence limits as well.

Item 26 is an output necessary in correcting echo-sounder depths, based on a sound speed of 4800 ft/s to the true bottom depth. This is usually a special program. It evaluates

$$\bar{C}_h = \int_{O_B}^{Z_B} \frac{dZ}{C(Z)} \Big/ Z_B \tag{80}$$

which represents the harmonic mean sound speed to the true bottom depth Z_B. The true depth is obtained from the echo sounder-depth, Z_S, from

$$Z_B = (\bar{C}_h / C_e)\, Z_S \tag{81}$$

where C_e is the sound speed assumed in the echo sounder. A simple test case can be constructed to test correction programs. This may appear trivial, but we have heard of well known investigators who have erroneously used the mean sound speed rather than the harmonic mean.

Item 27 refers to the statistical characteristics of propagation loss; ie, some measure of the fluctuation of propagation loss. This could be an output requirement of a propagation program. It is more likely to be handled in a complementary program, as outlined in section 8.3.

Item 28 is the evaluation of scattering coefficients. Here, we are referring to the reflection in the nonspecular as well as the more common specular direction.

85. Gordon, D. F., Multipath Interference Nulls in Long-Range, Low-Frequency, Acoustic Propagation by Normal Modes, J Acoust Soc Am 67, 106-120, Jan 1980.

8.1.4 Propagation Environments Treated

1. Direct field.
2. Surface ducts or depressed surface ducts.
3. Convergence zones.
4. Reliable acoustic paths.
5. RSR propagation.
6. SOFAR (near-axial) propagation.
7. Bottom-reflected paths.
8. Paths refracted in sub-bottom.
9. Shallow water.
10. Diffracted propagation into shadow zones.
11. Multiple ducts.
12. Convergence zones with small depth excess.
13. Up-, down-, and cross-slope propagation.
14. Multipath propagation from moving source or receiver.
15. Propagation through eddies.
16. Propagation across oceanic fronts.
17. Near-field effects.
18. Propagation under ice cover.
19. Nonlinear effects.
20. Surface (Stoneley) waves
21. Propagation into the Earth's crust.
22. Propagation over seamounts.
23. Diffraction around seamounts or islands.

This outline indicates the various types of environments that models must address. Most of these have been addressed by recommendation for specific control models.

8.2 APPROACHES TO EVALUATION OF ACOUSTIC FIELDS

1. Numerical solution of the time-dependent wave equation (ref 86).
2. Time-independent wave equation
   A. Fast field program (ref 87).
   B. Residue (normal mode) theory (ref 87).
   C. Adiabatic normal mode theory (ref 79).
   D. Coupled normal mode theory (ref 79).

86. Smith, M. C., Underwater Acoustic Propagation Prediction by the Alternating-Direction Implicit-Explicit Computational Method, J Acoust Soc Am 46, 233-237, July 1969.
87. DiNapoli, F. R., and R. L. Davenport, Computer Models of Underwater Acoustic Propagation, Naval Underwater Systems Center TR 5867, Jan 1980.

3. Parabolic equation
   A. Split-step algorithm (ref 87).
   B. Improved versions (ref 87, 88).
4. Eikonal equation
   A. Classical ray theory.
   B. Ray theory with corrections.
5. Radiation transport equation (ref 35).
6. Multipath expansion (ref 87).
7. Finite element method (ref 87).
8. Huygen's principle (ref 92).
9. Green's function solutions (ref 93).

This outline presents various approaches to the evaluation of acoustic fields. Those listed may not be primary references, but are convenient and, in turn, present other references. Our first inclination was to prepare a tree which would place these approaches in their proper descent from the wave equation. After a brief struggle, we abandoned the idea when we read the following on page 356 of reference 88: "the relationships are incestuous and the taxonomy complicated". This outline is not complete, but is comparable to similar listings by other investigators.

Item 1 represents solutions to the full-wave equation. The sound speed may vary with all three geometrical coordinates and with time as well. Reference 86 presents the solution of a simple example by using finite difference techniques. It finds the entire field as a function of time. This is the most versatile approach but is too time-consuming for present computer technology and exceeds by far our ability to describe the ocean environment.

Item 2 represents various solutions to the time-independent wave equation. In this method, the differential equation is converted to an integral representation. Method 2A solves this by direct integration, while method 2B uses contour integration with residues and branch line contributions. Methods 2A and 2B are for range-independent profiles. Methods 2C and 2D are extensions of method 2B to handle range-dependent environments.

Item 3 represents solutions to the parabolic equation, which is an approximation to the wave equation. The numerical solutions of this equation are marching solutions which progress from the source. In contrast, the solutions of approach 1 are much more difficult

88. Weston, D. E., and P. B. Rowlands, Guided Acoustic Waves in the Ocean, Rep Prog Phys, 42, 347-387, 1979.
89. Eby, E. S., Frenet Formulation of Three-Dimensional Ray Tracing, J Acoust Soc Am 42, 1287-1297, Dec 1967.
90. Eby, E. S., Geometric Theory of Ray Tracing, J Acoust Soc Am 47, 273-275, Jan 1970.
91. Spofford, C. W., private communication.
92. Baker, B. B., and E. T. Copson, The Mathematical Theory of Huygen's Principle, Oxford University Press, second edition, 1950.
93. Wood, D. H., Green's Functions for Unbounded Constant Gradient Media, J Acoust Soc Am 46, 1333-1339, Nov 1969.

because they require a simultaneous treatment of the entire environment; ie, the environment 100 km from the source has an effect, at least in theory, on the field 10 m from the source. Method 3A refers to the original split-step algorithm of Tappert, which employed fast Fourier transforms to achieve the solution. Method 3B refers to a host of fixes and improvements to method 3A. Many of these are listed in reference 88. Most of them are improvements on the differential equation approach, such as the use of finite differences in reference 82. However, reference 87 discusses converting the parabolic equation to an integral representation which could be integrated numerically. Moreover, there are normal mode solutions to the parabolic equation. These solutions might be useful as a control because then one could distinguish between errors introduced by the PE equation itself from errors introduced by the methods used to implement the equation.

Item 4 represents solutions to the eikonal equation which is again an approximation to the wave equation. A three-dimensional treatment of the eikonal equation is presented in reference 89, whereas a two-dimensional treatment has been alluded to already in reference 10. Note that Fermat's principle can be derived from the eikonal equation. Indeed, Fermat's principle appears to be more fundamental since it can be used to formulate ray paths as temporal geodesics (ref 90) in Riemannian spaces. For variation in one dimension, the eikonal equation reduces to Snell's law, with which one can derive the classical ray theory of approach 4A. However, one can derive the same results from the integral representation of the wave equation by saddle point methods. Approach 4B refers to ray theory with corrections. These various corrections have been discussed in detail. Note that the outline is deceiving, in that these corrections do not derive from the eikonal equation but stem from the wave equation itself. This illustrates, in part, Weston's comments (ref 88) on incestuous relationships and complicated taxonomies. Before leaving the subject of corrected ray theory, we have been mildly chided in the past for bolstering ray theory with a series of "Band-Aids." *We only wish to point out that now the PE approach has its own* fully developed suite of Band-Aids. The same holds true of range-dependent mode theory with its adiabatic approximation, coupled modes, corrections for nonflat boundaries, etc.

Item 5 represents solutions to the radiation transport equation. Our impression was that the transport equation appears in conjunction with the eikonal equation. According to Spofford, "the eikonal equation leads to the ray or ray-tracing equations and the transport equation is consistent with the computation of ray amplitude from ray-tube spreading." Viewed in this light, it would appear that the transport equation is superfluous because the ray tube spreading can be derived from the ray paths themselves. However, as previously discussed in reference 35, the transport equation makes use of a statistical treatment of scattering and of the stochastic part of sound speed profiles. Thus it appears that the transport equation can be important in its own right.

Item 6 represents multipath expansion approaches discussed in reference 87. These are hybrid models which use a combination of wave and ray theory. Reference 87 discusses approaches by Weinberg and Leiberger as examples of this method.

Item 7 refers to the finite element method, which does not pertain to a particular equation, as do items 1 through 6, but rather to a particular technique for solving partial differential equations. It is a popular method in other disciplines and has been applied to underwater acoustics, as described in reference 87.

We list item 8 for completeness. We know of two independent attempts to implement Huygen's principle in a computer routine to evaluate underwater acoustic fields. Neither attempt was successful for reasons which have not been completely resolved. The

relationship of this approach to others is not clear. No doubt, some of these problems could be thrashed out by plowing through reference 92 – a formidable task indeed. This approach appears to have received considerable attention in the evaluation of diffraction fields caused by various obstacles in a homogeneous medium. It is not clear that the method has any advantageous qualities when applied to diffraction fields caused by an inhomogeneous refractive medium.

Item 9 refers to an exact closed-form solution to the time-dependent wave equation for the case of an unbounded medium and a constant gradient medium. Solutions are given for point, line, and plane sources. This would appear to be a good test case for method 1A.

In passing, we made note of Wood's use of asymptotic series solutions in three dimensions which he has compared numerically with other ray methods (ref 94). This and the work of reference 5 introduced in section 1.2 appear to be a fertile source of control solutions.

The controls presented in this report have been limited primarily to methods 2B, 4A, and 4B because these are our areas of familiarity. Some others, such as method 2A, have provided excellent controls. Other approaches such as methods 2C, 2D, 3A, and 3B have been tested against each other but not against a more exact control. With such a control, these methods could be rigorously tested to the limits of their capability, as we have attempted to do with ray theory in section 4.1.1. Once this has been done successfully, we can have confidence in these methods serving as controls for more realistic environments than can be treated by exact methods.

8.3 COMPLIMENTARY AREAS OF MODELING

1. Reverberation fields and properties.
2. Noise fields and properties.
3. Statistical distributions of propagation loss, reverberation, and noise.
4. Evaluation of target strengths.
5. Simulation of signal processing.
6. Seismic propagation.
7. Interaction effects of multiple sources.
8. Field inversion.

This outline lists a number of modeling areas which are closely related to propagation. They could all profit from test cases, although at least some fall beyond the responsibility of the propagation modeler.

Item 1 refers to reverberation, which not only contains all the elements of propagation but also the problems of scattering and bistatic configurations of source and receiver.

Item 2 refers to noise, which again contains all elements of propagation as well as the radiation characteristics and geographical distribution of noise sources.

94. Wood, D. H., Parameterless Examples of Wave Propagation, J Acoustic Soc Am 73, 1727-1736, Dec 1973.

Item 3 refers to models which describe the statistical distribution of propagation loss, reverberation, or noise. Here, we are discussing appropriate theoretical models such as normal distributions, gamma distributions, etc, with appropriate estimates of statistical parameters.

Item 4 concerns an area which was removed from environmental acoustics a number of years ago. However, a good propagation model is of limited value in active sonar analyses if little is known about target strengths including azimuthal and vertical echo distributions.

The importance of item 5 has already been alluded to. The outputs of the propagation program must feed into the signal processing simulation, which in turn produces the end product. Again, this appears to be more the responsibility of signal processing personnel. The processing techniques which must be simulated are integration, filtering, array beam forming, and correlation.

Item 6 refers to seismic propagation models, which the underwater acoustic community may find useful. Perhaps we should pay more heed to the measurement and theory of shear waves. In the past, our interest in shear waves has been on the negative side; ie, these are mechanisms which increase bottom loss.

Item 7 is an area which lies in the domain of the transducer theory. What we have in mind are cases where we cannot evaluate fields by superposition of point sources. There may be cases where the transducer model and propagation model cannot be considered separately; ie, a strong interaction between the transducer and the medium.

Item 8 refers to a class of inversion problems. We are usually given the environment and need to model the acoustic field. The inversion problem is just the opposite. Given certain properties of the acoustic field, can we determine what the environment is?

9.0 POSTSCRIPT

What started out as a fairly modest effort of specifying a few controls has turned out to be a major project. Moreover, we have had to resist the impulse to include still more topics – not from the standpoint of interest or importance but because of marginal funding and other commitments.

Unfortunately, the scope of this effort has precluded the detailed investigation that might have cleared up many of the questions that have been raised and might have produced new control cases or exposed further gaps in our understanding. No doubt some of our more speculative considerations are wrong, since we have "let it all hang out" even if our ideas have been contrary to popular opinion. We would be only too glad to have any feedback which clears up our areas of concern and ignorance.

In retrospect, we were surprised by two apparently contradictory facts. We found that there were more inadequately investigated propagation environments than we had anticipated. On the other hand, we were pleasantly surprised to find the amount of effort that had gone into propagation problems as a whole.

It is also evident that this report is incomplete and should be updated in, say, another five years with perhaps a different format. We have obviously overlooked some important test cases and would appreciate having them pointed out to us. As an example, page 362 of reference 88 cites the work of Kuznetsov and Komissarova as giving an exact solution to

propagation in a wedge by using cylindrical polar coordinates in contrast to the Cartesian formulation of reference 64. This may well be the exact solution sought in the discussion of section 7.2.5.

We also hope that other investigators will look into some of the open problems posed in this report. As an example, we have followed our own advice and assigned the problem of section 4.4.2 to Dr E. P. McDaid under the NOSC New Professional Program. Reference 95 not only provides test cases, it demonstrates that mode attenuation does not increase monotonically with mode number; ie, the mode with smallest attenuation may not be mode 1. Indeed, for the limiting case of very high frequencies, the mode attenuation decreases monotonically with increasing mode number. Reference 95 then agrees with the speculation of section 4.2.2 that mode attenuation does not always increase with increasing mode number. It not only can form a relative minimum, as suggested in section 4.2.2, but this minimum can occur for an arbitrarily large mode number provided that the frequency is sufficiently high.

95. McDaid, E. P., Sound Propagation in a Stratified Ocean: Numerical Investigation of a Bilinear Sound Speed Profile with Two Negative Gradients, NOSC TN 961, Jan 1981.

REFERENCES

1. Pedersen, M. A., Acoustic Intensity Anomalies Introduced by Constant Velocity Gradients, J Acoust Soc Am 33, 465-474, Apr 1961.
2. Pedersen, M. A., and D. F. Gordon, Normal-Mode Theory Applied to Short-Range Propagation in an Underwater Acoustic Surface Duct, J Acoust Soc Am 37, 105-118, Jan 1965.
3. Spofford, C. W., A Synopsis of the AESD Workshop on Acoustic-Propagation Modeling by Non-Ray-Tracing Techniques, 22-25 May 1973, Washington, DC, Acoustic Environmental Support Detachment (AESD) TN-73-05, Nov 1973.
4. Blatstein, I. M., Evaluation of Methods for Comparing Propagation Models, J Acoust Soc Am 55S, S34 (A), Apr 1974.
5. Wood, D. H., Comparison of Models with Theoretical Examples, J Acoust Soc Am 55S, S44 (A), Apr 1974.
6. Pedersen, M. A., and D. F. Gordon, Comparison of Curvilinear and Linear Profile Approximations in the Calculation of Underwater Sound Intensities by Ray Theory, J Acoust Soc Am 41, 419-438, Feb 1967.
7. White, D., Velocity Profiles that Produce Acoustic Focal Points on an Axis of Minimum Velocity, J Acoust Soc Am 46, 1318-1332, Nov 1969.
8. Physics of Sound in the Sea, NAVMAT P-9675, Washington DC, 49, 1969.
9. Pedersen, M. A., Theory of the Axial Ray, J Acoust Soc Am 45, 157-176, Jan 1969.
10. White, D., Ray Theory for Wide Classes of Sound-Speed Profiles with Two-Dimensional Variation, J Acoust Soc Am 63, 405-419, Feb 1978.
11. Wolfe, P., private communications.
12. DeSanto, J. A., Ocean Acoustics, Springer-Verlag, 1979.
13. White, D., and M. A. Pedersen, Evaluation of Shadow Zone Fields by Uniform Asymptotics and Complex Rays, J Acoust Soc Am 69, 1029-1059, April 1981.
14. Blatstein, I. M., Comparison of Normal Mode Theory, Ray Theory, and Modified Ray Theory for Arbitrary Sound Velocity Profiles Resulting in Convergence Zones, Naval Ordnance Laboratory TR 74-95, Aug 1974.
15. Pedersen, M. A., et al, Comparison of Ray-Theory and Normal-Mode Results for Convergence Zones, Tenth International Congress on Acoustics, Sydney, Australia, Jul 1980.
16. Gordon, D. F., Underwater Sound Propagation Loss Program, Naval Ocean Systems Center TR 393, May 1979.
17. Murphy, E. L., and J. A. Davis, Modified Ray Theory for Bounded Media, J Acoust Soc Am 56, 1747-1760, Dec 1974.
18. Brekhovskikh, L. M., Waves in Layered Media, Academic, 474-492, 1960.
19. Sachs, D. A., and A. Silbiger, Focusing and Refraction of Harmonic Sound and Transient Pulses in Stratified Media, J Acous Soc Am 49, 824-84J, Mar 1971.
20. Holford, R. L., Modifications to Ray Theory Near Cusped Caustics, Continuation of LRAPP, Ref 7, Bell Telephone Labs, Whippany, NJ, Feb 1972 (unpublished).
21. Spofford, C. W., Implementation of Cusped Caustics in the FACT program, LRAPP Final Report, Ref 4, Bell Telephone Labs, Whippany, NJ, Apr 1973 (unpublished).
22. Orton, M., Underwater Sound Propagation in the Presence of Caustics Formed by Four-Ray Systems, Ocean Acoustics Program (ONR 486), Program Summary for FY-79, Nov 1979.

23. Pedersen, M. A., and D. White, Ray Theory for Sources and Receivers on an Axis of Minimum Velocity, J Acoust Soc Am 48, 1219-1248, Nov 1970.
24. Pedersen, M. A., and D. White, Ray Theory of the General Epstein Profile, J Acoust Soc Am 44, 765-786, Sep 1968.
25. Deavenport, R. L., A Normal Mode Theory of an Underwater Acoustic Duct by Means of Green's Function, Radio Science, vol 1, no. 6, Jun 1966.
26. Kerr, D. E., Propagation of Short Radio Waves, McGraw-Hill, NY, 140-174, 1951.
27. Marsh, H. W., Theory of the Anomalous Propagation of Acoustic Waves in the Ocean, Naval Underwater Sound Laboratory Report 111, 1950.
28. Pedersen, M. A., and D. F. Gordon, Theoretical Investigation of a Double Family of Normal Modes in an Underwater Acoustic Surface Duct, J Acoust Soc Am 47, 304-326, Jan 1970.
29. Pedersen, M. A., and D. F. Gordon, Normal-Mode and Ray Theory Applied to Underwater Acoustic Conditions of Extreme Downward Refraction, J Acoust Soc Am 51, 323-368, Jan 1972.
30. Au, W. W. L., An Investigation of a Double Family of Normal Modes in an Isovelocity Underwater Acoustic Surface Duct, J Acoust Soc Am 50, 286-299, Jul 1971.
31. Murphy, E., Supplement to Informal Notes on Surface Duct Propagation, prepared for Second Session of the International Workshop on Low Frequency Propagation and Noise, Monterey CA, Nov 1975 (unpublished).
32. Available to authorized requestors.
33. Anderson, E. R., and M. A. Pedersen, Surface-Duct Sonar Measurements (SUDS I 1972), Naval Undersea Center TP 463, Nov 1976.
34. Podeszwa, E. M., Sound Speed Profiles for the Norwegian Sea, Naval Underwater Systems Center, TD 6035, Jun 1979.
35. Wilson, H. L., and F. D. Tapport, Acoustic Propagation in Random Oceans Using the Radiation Transport Equation, J Acoust Soc Am 66, 256-274, Jul 1979.
36. Arase, T., Some Characteristics of Long-Range Explosive Sound Propagations, J Acoust Soc Am 31, 588-595, May 1959.
37. Tindle, C. T., and K. M. Guthrie, Rays as Interfering Modes in Underwater Acoustics, J Sound and Vibration 34, 291-295, 1974.
38. Podeszwa, E. M., Sound Speed Profile for the North Atlantic Ocean, Naval Underwater Systems Center TD 5447, Oct 1976.
39. Gordon, D. F., Normal Modes in a Pair of Ocean Acoustic Ducts, Royal Australian Navy Research Laboratory, AR-001-021, Sep 1978.
40. Available to authorized requestors.
41. Bucker, H. P., Normal-Mode Sound Propagation in Shallow Water, J Acoust Soc Am 36, 251-258, Feb 1964.
42. Available to authorized requestors.
43. Lee, P. C. Y., and S. S. Chen, Vibrations of Contoured and Partially Plated Contoured, Rectangular AT-Cut Quartz Plates, J Acoust Soc Am 46, 1193-1202, Nov 1969.
44. Smith, R. A., Wave Mechanics of Crystalline Solids, Chapman and Hall, London, 1961.
45. Gordon, D. F., and D. White, Bottom Interaction Represented by Impedance Conditions in Normal-Mode Calculations, Conference on Bottom-Interacting Ocean Acoustics, SACLANT ASW Centre, LaSpezia, Italy, Jun 1980.
46. Otsubo, H., et al, Normal-Mode Solution in the Ocean with Absorbing Bottom Sediments Which Have a Sound Speed Gradient, J Acoust Soc Japan (E) 1, 47-57, 1980.

47. Pedersen, M. A., et al, Low Frequency Propagation Effects for Sources or Receivers Near the Ocean Surface, Naval Undersea Surface, Naval Undersea Center TP 488, Sep 1975.
48. Bannister, R. W., and M. A. Pedersen, Low Frequency Surface Interference Effects in Long Range Sound Propagation, article submitted to J Acoust Soc Am 69, 76-83, Jan 1981.
49. Towne, D. H., and K. G. Wilson, Refraction and Diffraction of Explosive Pressure Pulses by Gradients in the Propagation Velocity, part II, Woods Hole Oceanog Inst, ref no 57-45, 1957.
50. White, D., Normal Mode Evaluation of FASOR Shallow Water Areas, unpublished.
51. Mitchell, S. K., and J. J. Lemmon, A Ray Theory Model of Acoustic Interaction with the Ocean Bottom, J Acoust Soc Am 66, 855-861, Sep 1979.
52. Vidmar, P. J., and T. L. Foreman, A Plane-Wave Reflection Loss Model Including Sediment Rigidity, J Acoust Soc Am 66, 1830-1835, Dec 1979.
53. Gupta, R. N., Reflection of Elastic Waves from a Linear Transition Layer, Bull Seism Soc Am 56, 511-526, 1966.
54. Vidmar, P. J., Ray Path Analysis of Sediment Shear Wave Effects on Bottom Reflection Loss, J Acoust Soc Am 68, 639-648, Aug 1980.
55. Vidmar, P. J., The Effect of Sediment Rigidity in Bottom Reflection Loss in a Typical Deep Sea Sediment, J Acoust Soc Am 68, 634-638, Aug 1980.
56. Hawker, K. E., The Influence of Stonely Waves on Plane Wave Reflection Coefficients: Characteristics of Bottom Reflection Loss, J Acoust Soc Am 64, 548-555, Aug 1978.
57. Rutherford, S. R., and K. E. Hawker, The Effects of Density Gradients on Bottom Reflection Loss for a Class of Marine Sediments, J Acoust Soc Am 63, 750-757, Mar 1978.
58. *White, D., and D. F. Gordon, Analysis of Shallow Water Sound Propagation by Normal* Mode Theory, J Acoust Soc Am (A) 60S, 34, Fall 1976.
59. Davis, J. A., Extended Modified Ray Theory Field in Bounded and Unbounded Inhomogeneous Media, J Acoust Soc Am 57, 276-286, Feb 1975.
60. White, D., private communication.
61. Murphy, E. L., Modified Ray Theory for the Two-Turning-Point Problem, J Acoust Soc Am 47, 899-908, Mar 1970.
62. Bucker, H. P., and H. E. Morris, Epstein Normal-Mode Model of a Surface Duct, J Acoust Soc Am 41, 1475-1478, Jun 1967.
63. Stickler, D. C., Normal-Mode Program with Both the Discrete and Branch Line Contributions, J Acoust Soc Am 57, 856-861.
64. Bradley, D., and A. A. Hudimac, The Propagation of Sound in a Wedge Shaped Shallow Water Duct, Naval Ordnance Laboratory TR 70-235, Nov 1970.
65. Stone, J. L., A Theoretical Analysis of Acoustic Wave Modes in Layered Liquids, Princeton Univ report no 9, contract N60NR-270 (1953).
66. Floyd, E. R., Modified Phase Integral Approximation for a More Rigorous Ray-Tracing Technique, J Acoust Soc Am 60, 801-809, Oct 1976.
67. Clark, J. G., et al, Multipath Acoustic Propagation with a Moving Source in a Bounded Deep Ocean Channel, J Acoust Soc Am 60, 1274-1284, Dec 1976.
68. Hawker, K. E., A Normal Mode Theory of Acoustic Doppler Effects in the Oceanic Waveguide, J Acoust Soc Am 65, 675-681, Mar 1979.
69. Warfield, J. T., and M. J. Jacobson, Acoustic Propagation in a Channel with Range Dependent Sound Speed, J Acoust Soc Am 45, 1145-1156, May 1969.

70. Nagl, A., et al, Adiabatic Mode Theory of Underwater Sound Propagation in a Range Dependent Environment, J Acoust Soc Am 63, 739-749.
71. Abramowitz, J., and I. A. Stegun, Handbook of Mathematical Functions, National Bureau of Standards Applied Mathematics Series: 55, June 1964.
72. Chwieroth, F. S., et al, Mode Coupling in a Sound Channel with Range-Dependent Parabolic Velocity Profile, J Acoust Soc Am 64, 1105-1112, Oct 1978.
73. Pedersen, M. A., and R. F. Hosmer, Combined Acoustic Propagation in Eastpac Region (Exercise CAPER): Initial Acoustic Analysis, NOSC TR-276, June 1978.
74. Tappert, F. D., private communication.
75. MacKinnon, R. F., and M. Nell, Some Results on Ray-Acoustic Intensity Calculations, Defense Research Establishment Pacific technical memo 75-4, May 1975.
76. MacKinnon, R. F., private communication, May 1981.
77. Spofford, C., private communication, June 1981.
78. Graves, R. D., et al, Range-Dependent Normal Modes in Underwater Sound Propagation: Application to the Wedge-Shaped Ocean, J Acoust Soc Am 58, 1171-1177, Dec 1975.
79. Rutherford, S. R., An Examination of Coupled Mode Theory as Applied to Underwater Sound Propagation, Applied Research Laboratory TR 79-44, July 1979.
80. Rutherford, S. R., and K. E. Hawker, Consistent Coupled Mode Theory of Sound Propagation for a Class of Nonseparable Problems, J Acoust Soc Am 70, 554-564, Aug 1981.
81. Jensen, F., and W. A. Kuperman, Environmental Acoustical Modeling at Saclantcen, Saclantcen report SR-34, Nov 1979.
82. Lee, D. L., et al, Finite-Difference Solution to the Parabolic Wave Equation, J Acoust Soc Am 70, 795-800, Sep 1981.
83. White, D., private communication.
84. Ebbeson, G. R., and H. Medwin, chairmen: Topographical Effects on Ocean Propagation, Supplement 1, 69, S58-S60, spring 1981.
85. Gordon, D. F., Multipath Interference Nulls in Long-Range, Low-Frequency, Acoustic Propagation by Normal Modes, J Acoust Soc Am 67, 106-120, Jan 1980.
86. Smith, M. C., Underwater Acoustic Propagation Prediction by the Alternating-Direction Implicit-Explicit Computational Method, J Acoust Soc Am 46, 233-237, July 1969.
87. DiNapoli, F. R., and R. L. Davenport, Computer Models of Underwater Acoustic Propagation, Naval Underwater Systems Center TR 5867, Jan 1980.
88. Weston, D. E., and P. B. Rowlands, Guided Acoustic Waves in the Ocean, Rep Prog Phys, 42, 347-387, 1979.
89. Eby, F. S., Frenet Formulation of Three-Dimensional Ray Tracing, J Acoust Soc Am 42, 1287-1297, Dec 1967.
90. Eby, F. S., Geometric Theory of Ray Tracing, J Acoust Soc Am 47, 273-275, Jan 1970
91. Spofford, C. W., private communication.
92. Baker, B. B., and E. T. Copson, The Mathematical Theory of Huygen's Principle, Oxford University Press, second edition, 1950.
93. Wood, D. H., Green's Functions for Unbounded Constant Gradient Media, J Acoust Soc Am 46, 1333-1339, Nov 1969.
94. Wood, D. H., Parameterless Examples of Wave Propagation, J Acoust Soc Am 54, 1727-1736, Dec 1973.
95. McDaid, E. P., Sound Propagation in a Stratified Ocean: Numerical Evaluation for a Bilinear Sound Speed Profile with Two Negative Gradients, NOSC TR

AD-A118 324 NAVAL OCEAN SYSTEMS CENTER SAN DIEGO CA F/G 17/1
USE OF THEORETICAL CONTROLS IN UNDERWATER ACOUSTIC MODEL EVALUA--ETC(U)
JAN 82 M A PEDERSEN, R W MCGIRR
UNCLASSIFIED NOSC/TR-758 NL

INITIAL DISTRIBUTION

CHIEF OF NAVAL OPERATIONS
WASHINGTON, DC 20350

NAVAL OCEANOGRAPHY COMMAND
NSTL STATION
BAY ST LOUIS, MS 39529
CODE N3

NAVAL OCEANOGRAPHIC OFFICE
NSTL STATION
BAY ST LOUIS, MS 39529
CODE 7300
CODE 9000

NAVAL OCEAN RESEARCH & DEVELOPMENT ACTIVITY
NSTL STATION
BAY ST LOUIS, MS 39529
CODE 100
CODE 110
CODE 115
CODE 300
CODE 320
CODE 323
CODE 500
CODE 520
CODE 522
CODE 530
CODE 531

NAVAL SEA SYSTEMS COMMAND
WASHINGTON, DC 20362
SEA 63D5
SEA 63R
SEA 63RA

NAVAL ELECTRONICS SYSTEMS COMMAND
WASHINGTON, DC 20360
ELEX 612

NAVAL SURFACE WEAPONS CENTER
WHITE OAK LABORATORY
SILVER SPRING, MD 20910

NAVAL AIR SYSTEMS COMMAND
WASHINGTON, DC 20361
NAIR 370
NAIR 954

NAVAL UNDERWATER SYSTEMS CENTER
NEW LONDON LABORATORY
NEW LONDON, CT 06320
CODE 10
CODE 3202
CODE 33
CODE 334

PROJECT MANAGER
ANTI-SUBMARINE WARFARE SYSTEM PROJECT
WASHINGTON, DC 20360
PM-4

FLEET NUMERICAL OCEANOGRAPHY CENTER
MONTEREY, CA 93940

OPERATIONAL TEST & EVALUATION FORCE
NAVAL BASE
NORFOLK, VA 23511

OFFICE OF NAVAL RESEARCH
WASHINGTON, DC 20037

OFFICE OF NAVAL RESEARCH
ARLINGTON, VA 22217

OFFICE OF NAVAL RESEARCH
BRANCH OFFICE
PASADENA, CA 91106

NAVAL RESEARCH LABORATORY
WASHINGTON, DC 20375
CODE 5101
CODE 5121

DEFENSE TECHNICAL INFORMATIOM CENTER
ALEXANDRIA, VA 22314

CATHOLIC UNIVERSITY
WASHINGTON, DC 20064
H. M. UBERALL

NEW YORK UNIVERSITY
251 MERCER STREET
NEW YORK, NY 10012
D. C. STICKLER

PENNSYLVANIA STATE UNIVERSITY
PO BOX 30
STATE COLLEGE, PA 16801
S. MCDANIEL

UNIVERSITY OF CALIFORNIA
SCRIPPS INSTITUTE OF OCEANOGRAPHY
SAN DIEGO, CA 92152
V. C. ANDERSON

UNIVERSITY OF MIAMI
4600 RICHENBACKER CAUSEWAY
MIAMI, FL 33149
F. TAPPERT

UNIVERSITY OF TEXAS
APPLIED RESEARCH LABORATORY
PO BOX 8029
AUSTIN, TX 78712
DR. K. HAWKER
DR. P. J. VIDMAR

BELL TELEPHONE LABORATORIES
WHIPPANY ROAD
WHIPPANY, NJ 07981
DR. R. L. HOLFORD

OCEAN DATA SYSTEMS, INC.
6000 EXECUTIVE BLVD
ROCKVILLE, MD 20852
G. V. JACOBS

OCEAN DATA SYSTEMS, INC.
3255 WING STREET, SUITE 550
SAN DIEGO, CA 92110
K. OSBORNE

PLANNING SYSTEMS, INC.
7900 WESTPARK DRIVE, SUITE 600
MCLEAN, VA 22102
DR. R. C. CAVANAGH

SCIENCE APPLICATIONS, INC.
PO BOX 1303
MCLEAN, VA 22102
C. W. SPOFFORD
W. D. KIRBY
H. J. VENNE, JR.